Mechanism and regulation of magnetosomal iron uptake and biomineralization in *Magnetospirillum gryphiswaldense*

Dissertation

der Fakultät für Biologie

der

Ludwig-Maximilians-Universität München

vorgelegt von

René Uebe

aus Stralsund

München

19.12.2011

Gutachter:

1. Prof. Dr. Dirk Schüler
2. Prof. Dr. Heinrich Jung

Tag der mündlichen Prüfung: 02.05.12

Publications and manuscripts originating from this thesis

CHAPTER 2

Uebe, R., Voigt, B., Schweder, T., Albrecht, D., Katzmann, E., Lang, C., Böttger, L., Matzanke, B. and Schüler, D. (2010). Deletion of a *fur*-like gene affects iron homeostasis and magnetosome formation in *Magnetospirillum gryphiswaldense*. *J. Bacteriol.* **192**: 4192-4204.

CHAPTER 3

Uebe, R., Junge, K., Henn, V., Poxleitner, G., Katzmann, E., Plitzko, J. M., Zarivach, R., Kasama, T., Wanner, G., Pósfai, M., Böttger, L., Matzanke, B. and Schüler, D. (2011). The cation diffusion facilitator proteins MamB and MamM of *Magnetospirillum gryphiswaldense* have distinct and complex functions, and are involved in magnetite biomineralization and magnetosome membrane assembly. *Mol. Microbiol.* **82**: 818-835.

CHAPTER 4

Uebe, R., Henn, V. and Schüler, D. (2012). The MagA protein of magnetospirilla is not involved in bacterial magnetite biomineralization. *J. Bacteriol.* **194**: 1018-1023

INDEX

ABBREVIATIONS

aa	Amino acid
ABC	ATP-binding cassette
CDF	Cation diffusion facilitator
CET	Cryo-electron tomography
CL	Cell lysate
CM	Cytoplasmic membrane
cp	Cytoplasm
CPA	Cation proton antiporter
Fur	Ferric uptake regulator
HtrA	High temperature requirement
Irr	Iron responsive regulator
MAI	Magnetosome island
MM	Magnetosome membrane
MP	Membrane protein
MRI	Magnetic resonance imaging
MTB	Magnetotactic bacteria
NF	Non-magnetic fraction
OATZ	Oxic-anoxic transition zone
OM	Outer membrane
PDZ	Protein domain also found in the proteins, PSD95, DlgA and Zo-1
pp	Periplasm
SD	Standard deviation
SDS-PAGE	Sodium dodecyl sulphate – polyacrylamide gel electrophoresis
SP	Soluble protein
TEM	Transmission electron microscopy
TMD	Transmembrane domain
TMH	Transmembrane helix
TPR	Tetra tricopeptid
TRIS	Tris(hydroxymethyl)aminomethane

SUMMARY

Magnetotactic bacteria have the ability to orient along geomagnetic field lines based on the formation of intracellular nanometer-sized, membrane-enclosed magnetic iron minerals called magnetosomes. The formation of these unique bacterial organelles involves several processes such as cytoplasmic membrane invagination and magnetosome vesicle formation, accumulation of large amounts of iron in the vesicles, and crystallization of magnetite. In this thesis several aspects of the magnetite biomineralization-related iron metabolism of *Magnetospirillum gryphiswaldense* were analyzed.

First the regulation of magnetite biomineralization and iron uptake was studied. A homologue of the ferric uptake regulator Fur, which was able to complement a *fur* mutant of *Escherichia coli*, was identified and analyzed. A *fur* deletion mutant biomineralized fewer and slightly smaller magnetite crystals than the wild type. Although the total cellular iron accumulation of the mutant was decreased, it exhibited an increased level of cytoplasmic iron, which was bound mostly to a ferritin-like metabolite that was found significantly increased in transmission Mössbauer spectra of the mutant. Growth of the *fur* mutant was impaired in the presence of the oxidant paraquat and under aerobic conditions. Using a Fur titration assay and proteomic analysis, constituents of the Fur regulon were identified. Whereas the expression of most known magnetosome genes was unaffected in the *fur* mutant, the abundance of 14 proteins was altered between the mutant and the wild type including five proteins that constitute putative iron uptake systems. This data demonstrated that Fur is a regulator involved in global iron homeostasis which also affected magnetite biomineralization, probably by integrating and balancing the competing demands of magnetite biomineralization with the biochemical iron requirement and intracellular iron homeostasis.

In the second part of this thesis, two cation diffusion facilitator family proteins, MamB and MamM, were analyzed. Whereas both proteins are essential for magnetite biomineralization, only deletion of *mamB* resulted in loss of magnetosome membrane vesicles. MamB stability depended on the presence of MamM by formation of a heterodimer complex. In addition, MamB was found to interact with several other proteins including the PDZ1 domain of MamE, a putative magnetosome associated protease. Whereas any modification of MamB resulted in loss of function, substitution of amino acids within MamM lead to increased formation of polycrystalline instead of single crystals formed in the wild type. A single amino acid substitution within MamM resulted in the formation of crystals consisting of the iron(III)

oxide hematite, which coexisted with crystals of the mixed-valence oxide magnetite. Together, the data indicated that MamM and MamB have complex functions, and are involved in the control of different key steps of magnetosome formation, which are linked by their direct interaction.

Finally, the role of the presumptive magnetosmal iron transporter MagA was reassessed in two magnetotactic bacteria of the genus *Magnetospirillum*. Previous studies claimed that *magA* encodes a magnetosomal ferrous iron transporter with a supposedly essential function for magnetosome formation in *Magnetospirillum magneticum*, and might cause magnetite biomineralization if expressed in mammalian cells. Targeted deletion in *Magnetospirillum magneticum* and *Magnetospirillum gryphiswaldense* revealed that *magA* is not involved in magnetosome formation in magnetotactic bacteria as previously supposed.

ZUSAMMENFASSUNG

Magnetotaktische Bakterien haben die Fähigkeit, sich mit Hilfe von Magnetosomen, membranumschlossenen magnetischen Eisenmineralnanopartikeln, entlang des Erdmagnetfeldes zu orientieren. Die Bildung dieser einzigartigen bakteriellen Organellen beruht auf der Abfolge verschiedener Teilschritte wie Einstülpung der cytoplasmatischen Membran, Bildung von Magnetosomenvesikeln, Aufnahme und Akkumulation von Eisen in diesen Vesikeln sowie die Biomineralisation von Magnetit. In der vorliegenden Arbeit wurden verschiedene Aspekte des Eisenmetabolism zur Magnetitbiomineralisation von *Magnetospirillum gryphiswaldense* untersucht.

Zuerst wurde die Regulation der Magnetitbiomineralisation und der Eisenaufnahme untersucht. Ein Homolog des Regulatorproteins Fur (Ferric uptake regulator), welches in der Lage war, eine *fur* Mutante von *Escherichia coli* zu transkomplementieren, wurde identifiziert und analysiert. Eine *fur* Deletionsmutante bildete weniger und kleinere Magnetitkristalle als der Wildtyp. Obwohl der intrazelluläre Eisengehalt der *fur* Mutante insgesamt niedriger war, ergaben Transmissions-Mößbauer-Spektroskopie und Eisenbestimmungen, dass der Gehalt an cytoplasmatischem Eisen in der *fur* Mutante erhöht und Eisen überwiegend an eine Ferritin-ähnliche Komponente gebunden war. Das Wachstum der *fur* Mutante war in Gegenwart des Oxidationsmittels Paraquat oder durch hohe Sauerstoffkonzentrationen stärker gehemmt. Mittels einer Fur-Titrationsanalyse sowie einer Proteomanalyse konnten einige Komponenten des Fur Regulons identifiziert werden. Während die Expression der meisten bekannten Magnetosomengene durch die Deletion von *fur* nicht beeinträchtigt war, zeigten 14 Proteine eine veränderte Häufigkeit zwischen dem Wildtyp und der *fur* Mutante, von denen fünf Proteine Bestandteil von Eisenaufnahmesystemen waren. Dies zeigte, dass Fur eine zentrale Rolle für die Eisenhomöostase spielt und wahrscheinlich über die Regulation und Balance des biochemischen und des magnetosomalen Eisenbedarfs indirekt Einfluss auf die Magnetitbiomineralisation hat.

Im zweiten Teil dieser Arbeit wurden die cation diffusion facilitator Proteine MamB und MamM analysiert. Während beide Proteine essenziell für die Magnetitbiomineralisation waren, führte nur die Deletion von *mamB* zu einem Verlust der Magnetosomenvesikel. Die Stabilität von MamB war abhängig von einer Interaktion mit MamM, wahrscheinlich über die Bildung eines Heterodimers. Darüber hinaus konnte gezeigt werden, dass MamB mit mehreren anderen Proteinen wie der PDZ1 Domäne von MamE, einer mutmaßlichen

Magnetosomen assoziierten Protease, interagiert. Während nahezu jede gerichtete Modifikation einen Funktionsverlust von MamB hervorrief, führte der Austausch von Aminosäuren bei MamM zu einer verstärkten Bildung von polykristallinen anstelle von monokristallinen Wildtyp-Magnetitpartikeln. Ein einzelner Aminosäureaustausch in MamM induzierte die Bildung von Partikeln des Eisen(III)-oxids Hämatit, welche mit Partikeln des gemischt-valenten Oxids Magnetit koexistierten. Diese Daten zeigen, dass MamB und MamM komplexe Funktionen haben, an der Regulation verschiedener Kernprozesse der Magnetitbiomineralisation beteiligt sind und diese durch die Bildung eines Heterodimers miteinander verknüpfen.

Im letzten Teil dieser Arbeit wurde die Bedeutung des mutmaßlichen magnetosomalen Eisentransporters MagA für die Magnetitbiomineralisation in zwei magnetotaktischen Bakterien der Gattung *Magnetospirillum* erneut untersucht. MagA wurde in älteren Studien als magnetosomaler Eisen(II)-transporter mit essentieller Funktion für die Biomineralisation von Magnetit in *Magnetospirillum magneticum* beschrieben. Darüber hinaus sollte eine Expression von *magA* in Säugetierzelllinien angeblich ausreichend sein, um die Bildung von Magnetitnanopartikeln zu induzieren. Durch Deletionsmutagenese in *Magnetospirillum magneticum* und *Magnetospirillum gryphiswaldense* konnte gezeigt werden, dass entgegen der Resultate früherer Studien *magA* nicht an der Biomineralisation von Magnetit in magnetotaktischen Bakterien beteiligt ist.

CHAPTER 1

Introduction

1.1 Importance of iron in organisms

Incorporation of metal ions into biological macromolecules is essential for virtually all organisms. Metal ions are part of approximately one-third of all proteins, where they provide catalytic, regulatory, or structural roles critical to protein function (Shi and Chance, 2011). Zinc, for example, the most abundant metal in cells, plays important roles for the function of more than 300 enzyme classes, in stabilizing the DNA double helix, and in control of gene expression (Shi *et al.*, 2005; Shi and Chance, 2011). Iron, the second most metal ion found in proteins (Shi *et al.*, 2005), plays important roles for fundamental biological processes like respiration, photosynthesis, N_2 fixation, methanogenesis, and DNA synthesis (Andrews *et al.*, 2003). In contrast to zinc, which is redox inactive and exists only in a single oxidation state, iron can exist in two different readily interconvertible oxidation states under physiological conditions. Thus, the biological function of iron is mainly based on its highly variable redox potential (from -300 to +700 mV), but also its variable geometries and spin states (Andrews *et al.*, 2003). However, the accumulation of iron also poses the risk for an increased formation of oxygen radicals via the Fenton reaction, which can cause damage of DNA, proteins, and membrane lipids (Imlay and Linn, 1988; Winterbourn, 1995). Hence, precise mechanisms are required to balance the uptake, metabolism, and storage of iron (Andrews *et al.*, 2003).

Although iron might cause toxic effects to cells, almost all organisms depend on iron as a protein cofactor. Only very few exceptions have been described, lactobacilli, for example, have been reported to show no iron requirements (Weinberg, 1997). It is believed that the iron abstinence of lactobacilli confers an ecological advantage in their natural environment, where they compete with pathogenic bacteria (Chung *et al.*, 1998). On the other extreme, magnetotactic bacteria (MTB) have an extremely high demand for iron. In addition to their biochemical iron requirement these bacteria accumulate large amounts of iron for the synthesis of magnetosomes, which consist of membrane-enclosed, nanometer-sized crystals of the magnetic iron minerals magnetite (Fe_3O_4) or greigite (Fe_3S_4) (Frankel *et al.*, 1979;

Farina *et al.*, 1990; Mann *et al.*, 1990).

1.2 Ecology and diversity of magnetotactic bacteria

Magnetotactic bacteria were discovered in the early 1960's by Salvatore Bellini, a medical doctor at the University of Pavia in Italy, because of their ability to accumulate at the edge of a water droplet that corresponded to the magnetic North of a local magnetic field (Bellini, 2009a; Bellini, 2009b). However, the mechanism of their response to magnetic fields remained elusive until the American microbiologist Richard P. Blakemore rediscovered magnetotactic (Blakemore, 1975). Blakemore (1975) suggested that iron-rich, intracellular magnetic inclusions of the MTB (i.e. the mineral cores of magnetosomes (Balkwill *et al.*, 1980)) serve as magnetic dipoles, and convey a magnetic moment upon the cell to orient them in magnetic fields. Further on, it was proposed that this passive alignment in the geomagnetic field, in combination with aerotaxis, increases the efficiency of MTB to find their growth-favoring zones at or in close proximity to the oxic anoxic transition zone (OATZ) of marine or fresh water sediments (Frankel *et al.*, 1997). Alternatively, it was also suggested that magnetosomes might simply serve as iron storage and detoxification compartments (Junge, 2008) or as redox batteries, in which magnetite becomes partially oxidized while MTB are in oxidizing environments and reduced back to magnetite while the MTB are in reducing environments (Vali and Kirschvink, 1991; Kopp and Kirschvink, 2008).

With respect to morphology, physiology, and phylogeny MTB are a heterogeneous group of microorganisms. Magnetotactic rods, cocci, spirilla, vibrios, ovoid cells, or even multicellular aggregates of magnetotactic bacteria (DeLong *et al.*, 1993; Spring *et al.*, 1993; Flies *et al.*, 2005; Amann *et al.*, 2007; Lefèvre *et al.*, 2009) were found to belong to a wide range of bacterial lineages including the α-, δ- and γ-subgroups of the proteobacteria, the phylum *Nitospirae* as well as the candidate division OP3 (Spring *et al.*, 1993; Jogler *et al.*, 2009a; Kolinko *et al.*, 2011; Lefèvre *et al.*, 2011). Despite their ubiquitous distribution, not much is known about the functional role of MTB in their habitats since only few studies have addressed their potential contribution to biogeochemical cycles. Two studies, for example, reported that MTB play an important role in the iron cycle because certain MTB constitute up to 10% of the total bacterial population and accumulate significant amounts of the available dissolved iron (up to 10^{-14} g Fe per cell) (Spring *et al.*, 1993; Simmons *et al.*, 2007). In addition to the iron cycle, it was speculated that MTB significantly contribute to the sulfur and carbon cycles in their environments, because many MTB are able to form large amounts

of storage granules composed of elemental sulfur or polyhydroxybutyrate granules (Flies *et al.*, 2005; Simmons *et al.*, 2007; Faivre and Schüler, 2008).

As a result of their lifestyle adapted to chemically stratified habitats, which is hard to mimic under laboratory conditions, only few MTB have been grown in axenic cultures. The majority of cultivable MTB is affiliated with the α-subgroup of the proteobacteria, including the best-characterized MTB *Magnetospirillum magneticum* and *Magnetospirillum gryphiswaldense* (Jogler and Schüler, 2009). *M. gryphiswaldense*, the model organism of this thesis and many other studies, was isolated in 1990 from the sediment of the eutrophic river Ryck near Greifswald (Schleifer *et al.*, 1991; Schüler and Köhler, 1992). Cells of *M. gryphiswaldense* are helical, bipolar monotrichously flagellated, typically 2 to 3 µm long and 0.5 to 0.8 µm in diameter. A single cell contains up to 114 magnetosomes, which are aligned in a single or two linear chains within the cytoplasm (FIG. 1-1) (Schüler, 2004; Scheffel *et al.*, 2006; Scheffel and Schüler, 2007; Katzmann *et al.*, 2010). Magnetosomes of *M. gryphiswaldense* consist of cubo-octahedral magnetite crystals with an average crystal diameter of 35 to 40 nm (Schüler, 2002; Scheffel *et al.*, 2008).

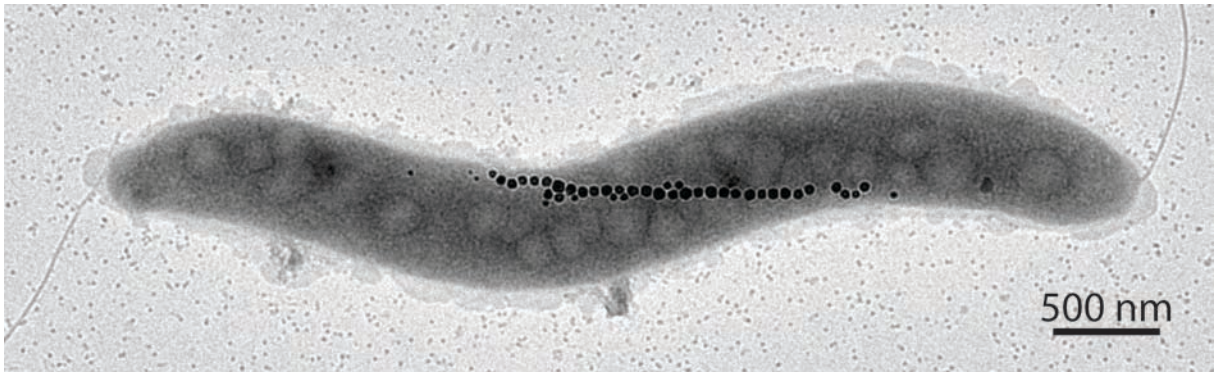

FIG. 1-1. Transmission electron micrograph of *M. gryphiswaldense* (micrograph by E. Katzmann). Electron dense particles at midcell are magnetite crystals in a chain-like arrangement.

M. gryphiswaldense is a microaerophilic organism and grows chemoorganoheterotrophically by use of different organic acids as electron donors, and oxygen or nitrate as terminal electron acceptors (Schüler, 1994). *M. gryphiswaldense* is less fastidious compared to other magnetotactic bacteria since it is more tolerant to oxygen (Heyen and Schüler, 2003). The recent development of techniques for its genetic manipulation such as DNA transfer via conjugation and the development of replicative as well as suicide vectors, in addition to the availability of a draft genome sequence have made *M. gryphiswaldense* a predestined model organism for the analysis of magnetosome biomineralization and magnetotaxis (Schultheiss and Schüler, 2003; Schultheiss *et al.*, 2004; Richter *et al.*, 2007; Ullrich and Schüler, 2010).

1.3 Iron metabolism of magnetotactic bacteria

Magnetotactic bacteria are able to accumulate large amounts of extracellular iron for the synthesis of intracellular magnetite or greigite crystals. The intracellular iron content of *M. gryphiswaldense*, for example, may account for up to 4% of the dry weight (Faivre and Schüler, 2008), which is over 150-times higher than the iron content of non-magnetic bacteria such as *Escherichia coli* (0.027% iron per dry weight (Abdul-Tehrani *et al.*, 1999)). Therefore, MTB were suggested to exhibit a different iron metabolism than non-magnetic bacteria (Xia *et al.*, 2007).

However, despite their large iron accumulation capacity, there is still no evidence for unique iron uptake systems in MTB. Cells of *M. gryphiswaldense* were found to incorporate extracellular ferrous iron by a slow, diffusion-like process (Schüler and Baeuerlein, 1996). Ferric iron on the other hand is incorporated very efficiently by a comparatively low-affinity, but high-velocity transport system that follows Michaelis-Menten kinetics (V_{max} = 0.86 nmol Fe min^{-1} (mg dry weight)$^{-1}$; K_m = 3 μM) (Schüler and Baeuerlein, 1996). Saturation of the ferric iron uptake was observed at an extracellular iron concentration of 20 μM (Schüler and Baeuerlein, 1996), which is consistent with the concentration of free iron in the natural habitat of magnetic bacteria (the OATZ) (Schüler, 1994; Flies *et al.*, 2005). Furthermore, it was shown that ferric iron incorporation was sensitive to 2,4-dinitrophenol and carbonylcyanide-*m*-chlorophenyl-hydrazone, indicating that ferric iron is taken up by an energy-dependent process (Schüler and Baeuerlein, 1996).

Bioinformatic reconstructions from the *M. gryphiswaldense* draft genome assembly revealed that iron uptake of *M. gryphiswaldense* proceeds by use of common iron uptake systems like two distinct FeoB ferrous iron uptake systems (Mgr1446 and ABL14106), a putative ATP-binding cassette (ABC) ferric iron transporter (Mgr0234-Mgr0236), and a putative ABC-type ferric siderophore transporter (Mgr0081-Mgr0083) (FIG. 1-2).

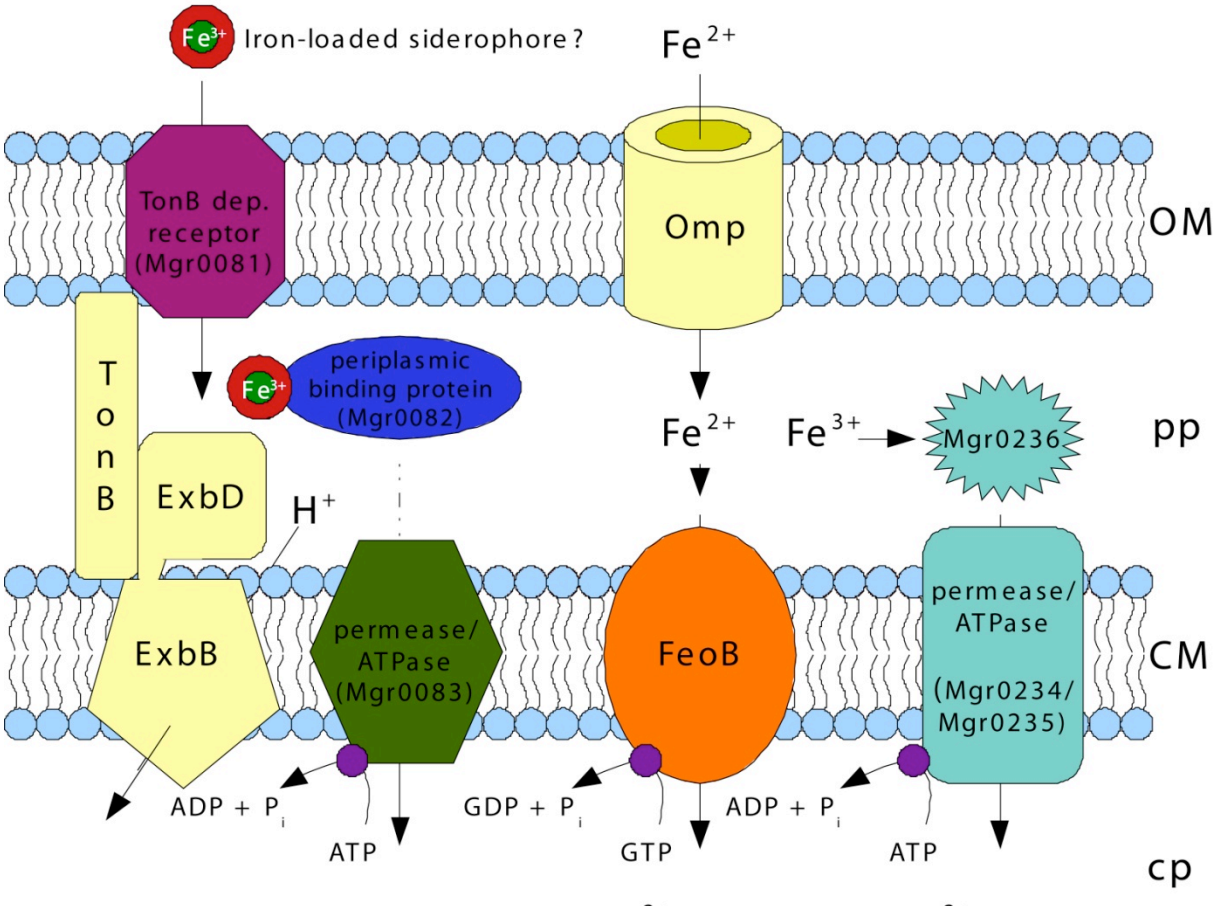

FIG. 1-2. Overview over iron uptake systems in *M. gryphiswaldense* reconstructed from the genome sequence (Uebe, this work). OM, outer membrane; pp, periplasm; CM, cytoplasmic membrane; cp, cytoplasm.

However, so far experimental evidence for an involvement in iron uptake was only reported for the FeoB1 uptake system (ABL14106). Compared to the wild type, a *M. gryphiswaldense feoB1* mutant showed a ~1.8-fold reduced uptake of ferrous iron, but still formed magnetite, although with decreased sizes (by 25%) and numbers (by 40%) (Rong *et al.*, 2008). Thus, it was concluded that the FeoB1 uptake system plays an accessory role in magnetite biomineralization (Rong *et al.*, 2008). Although the roles of the other putative iron uptake systems of *M. gryphiswaldense* have to be elucidated in future, the presence of an ABC-type ferric siderophore transport system remains peculiar since siderophore production and utilization by *M. gryphiswaldense* was not detectable yet (Schüler and Baeuerlein, 1996; Uebe *et al.*, 2010). In contrast, siderophore production and utilization has been reported for *M. magneticum*, *M. magnetotacticum*, and the magnetic vibrio MV-1 (Paoletti and Blakemore, 1986; Calugay *et al.*, 2003; Calugay *et al.*, 2004; Dubbels *et al.*, 2004; Calugay *et al.*, 2006). Nevertheless, it is still not clear if siderophore-mediated iron transport is also linked to magnetosome formation. In addition to the described iron uptake systems of *M. gryphiswaldense* other MTB also encode different iron uptake systems. *M. magneticum, M. magnetotacticum*, and the magnetic vibrio MV-1, for example, encode proteins that share

similarity to the *Saccharomyces cerevisiae* high-affinity iron uptake protein FTR1 (Dubbels *et al.*, 2004; Suzuki *et al.*, 2006). It was hypothesized that the activity of the putative FTR1-like iron permease from the magnetic vibrio MV-1 depends on the function of the periplasmic copper handling protein ChpA since several spontaneous *chpA* mutants showed a 20 to 80-fold decreased iron accumulation and were no longer able to biomineralize magnetite (Dubbels *et al.*, 2004). Biochemical analyses revealed that ChpA forms homodimers with an apparent subunit mass of about 19 kDa and binds one copper atom per dimer (Dubbels *et al.*, 2004). Given its periplasmic location and the fact that it binds copper, ChpA might provide copper to a copper-dependent Fe(II) oxidase similar to the multicopperoxidase FET3 of *S. cerevisiae*, which is required for the FTR1 mediated transport of ferric iron across the cell membrane (Dubbels *et al.*, 2004; Philpott and Protchenko, 2008).

The intracellular iron metabolism of MTB has been addressed in very few studies only. For example, it was suggested that the iron uptake of some MTB, including the magnetospirilla, is regulated by homologues of the transcriptional Ferric uptake regulator (Fur) since putative Fur binding sequences have been identified in the promoter regions of various genes implicated with iron uptake (Dubbels *et al.*, 2004; Rodionov *et al.*, 2006). Determination of the iron content of highly magnetic *M. gryphiswaldense* cells showed that magnetosome-bound iron constitutes up to 99% of the total cellular iron (Grünberg, unpublished results). In contrast, Mössbauer spectroscopic studies reported that magnetite contributes to only 70 to 80% of the intracellular iron in *M. magnetotacticum* and *M. gryphiswaldense* (Frankel *et al.*, 1983; Faivre *et al.*, 2007). Besides magnetite, these studies were also able to detect an octahedral ferrous iron metabolite in an oxygen environment as well as a high-density hydrous ferric oxide that exhibited ferritin-like Mössbauer spectra (Frankel *et al.*, 1983; Faivre *et al.*, 2007). In a more recent Mössbauer study on *M. gryphiswaldense* a fourth, previously unrecognized, iron metabolite with characteristics of a Fe_4-S_4 cluster was detected (Uebe *et al.*, 2011b). At the molecular level, however, these iron metabolites have not been characterized yet. Preliminary data exists only for the ferritin-like metabolite of *M. gryphiswaldense*, which has been shown to be a high-molecular-mass protein (M>100 kDa) composed of several 20 to 40 kDa subunits (Faivre *et al.*, 2007). Although this iron metabolite of *M. gryphiswaldense* exhibited Mössbauer characteristics of eukaryotic ferritins (Faivre *et al.*, 2007), genome analyses revealed that *Magnetospirillum* species encode for bacterioferritin (Bfr) only (Bertani *et al.*, 1997; Bertani *et al.*, 2001; Uebe, this work). Further analyses of the intracellular iron metabolism of *M. gryphiswaldense* and *M. magnetotacticum* have also shown that these MTB contain several proteins capable of

ferric iron reduction or oxidation of ferrous iron (Paoletti and Blakemore, 1988; Yamazaki *et al.*, 1995; Noguchi *et al.*, 1999; Xia *et al.*, 2007).

1.4 Magnetosomes and biomineralization of magnetite

1.4.1 Biomineralization of magnetite

The biomineralization of the mixed-valence iron oxide magnetite requires a strict control of the intracellular physico-chemical parameters since the formation of this mineral releases protons (equation 1) and its chemical stability is restricted to a relative narrow E_h- and pH-range (Bell *et al.*, 1987).

(eq. 1) $2\ Fe^{3+} + Fe^{2+} + 4\ H_2O \rightarrow Fe_3O_4 + 8\ H^+$ (Faivre *et al.*, 2005)

To achieve this control MTB have evolved small compartments, the magnetosome vesicles, which are formed by the magnetosome membrane (Gorby *et al.*, 1988). However, not much is known about the processes that lead to the formation of magnetite inside the vesicles. An oxygen isotope study, for example, showed that the oxygen atoms of magnetite are derived from water and not from molecular oxygen (Mandernack *et al.*, 1999). Early biochemical observations indicated that precipitation of magnetite involves formation of precursor minerals: (I) iron uptake into the cytoplasm and enzymatic reduction of ferric to ferrous iron, (II) formation of low density hydrous ferric oxides (e.g. α-FeOOH, γ-FeOOH) by oxidation, (III) formation of a ferrihydrite complex (γ-$FeO(OH)_2FeOH^+$) via dehydration, and (IV) reduction of one-third of the iron ions and further dehydration of ferrihydrite to magnetite (Frankel *et al.*, 1983). A more recent study, however, was unable to detect any mineral precursor (Faivre *et al.*, 2007). Therefore, a different model was suggested: (I) iron uptake and conversion into a ferrous high-spin species and a ferritin-like compound in/at the cytoplasmic membrane, (II) transport of both iron species to magnetosome vesicles via the periplasm, (III) release of Fe^{2+} and Fe^{3+} at the periplasm-magnetosome vesicle interface, and (IV) fast co-precipitation of Fe^{2+} and Fe^{3+} to form magnetite and eight protons without intermediate mineral precursors (Faivre *et al.*, 2007).

Using x-ray magnetic circular dichroism Staniland *et al.* (2007) observed hematite on the surface of immature magnetite crystals and hypothesized that hematite might be a precursor

mineral as proposed by Frankel *et al.* (1983). However, this has been questioned since a rapid conversion of the hematite hexagonal crystal structure to the cubic inverse spinel crystal structure of magnetite is likely not possible at ambient temperatures (Faivre and Schüler, 2008). As yet, no other mineral phase than magnetite was convincingly identified within magnetosomes, there is still no evidence for the formation of a magnetite precursor mineral phase (Faivre and Schüler, 2008). For comparison, several studies described the identification of greigite precursor minerals. Whereas Mann *et al.* (1990) detected non-magnetic pyrite (FeS_2), Farina *et al*. (1990) identified ferrimagnetic pyrrhotite (Fe_7S_8) in greigite producing MTB. In more recent studies the non-magnetic minerals mackinawite (tetragonal FeS) and sphalerite-type cubic FeS were observed (Pósfai *et al.*, 1998a; Pósfai *et al.*, 1998b). Most intriguingly it was also reported that magnetosomes which initially consisted of mackinawite spontaneously converted to greigite (Pósfai *et al.*, 1998a; Pósfai *et al.*, 1998b). Therefore, the following reaction scheme for greigite biomineralization was proposed:

cubic FeS → mackinawite (tetrag. FeS) → greigite (Fe_3S_4) (Pósfai *et al.*, 1998a; Pósfai *et al.*, 1998b).

Notably, the magnetosome mineral core of all cultivated MTB consists of magnetite. Several of these cultured MTB, including *M. gryphiswaldense*, continued to synthesize magnetite even under conditions which were thought to promote greigite formation (presence of S^{2-} and reducing environment) (Meldrum *et al.*, 1993a; Meldrum *et al.*, 1993b; Faivre, unpublished results). This indicates that the mineral type of the magnetosomes is species-specific. In addition to the mineral type MTB seem also to exert control about the crystal size and morphology since only crystals with a narrow size distribution and a specific crystal morphology could be observed within single MTB species (Sparks *et al.*, 1986; Bazylinski *et al.*, 1994; Devouard *et al.*, 1998; Bazylinski and Frankel, 2004; Arató *et al.*, 2005). Recently, it was described that the magnetite crystals of magnetosomes, in contrast to magnetite of Fe(III)-reducing bacteria, chemically synthesized magnetite or magnetite of geological origin, are composed of stoichiometric magnetite (Fischer *et al.*, 2011). Thus, MTB also seem to control the structural purity of the magnetic minerals, which in combination with the control of the magnetosome size and morphology is thought to achieve optimal magnetization of the magnetosomes (Fischer *et al.*, 2011).

Several studies observed that most magnetosomes contained only a single magnetite crystal, which suggests that nucleation of magnetite occurs at a single site within each magnetosome

vesicle (Devouard *et al.*, 1998; Faivre and Schüler, 2008). In some other biomineralization systems it was already shown that proteins with acidic domains/residues were able to complex positively charged ions, and thus helped to generate local supersaturating conditions for mineral nucleation (Belcher *et al.*, 1996; Kröger *et al.*, 1999). Consistent with this model, cryo-electron tomography and biochemical observations showed that small magnetite nuclei of magnetospirilla were always associated with the magnetosome membrane (Komeili *et al.*, 2006; Faivre *et al.*, 2007; Katzmann *et al.*, 2010). At the molecular level, however, it is still not clear how MTB achieve the nucleation control and how the magnetite crystals are attached to the magnetosome membrane.

1.4.2 Structure and composition of the magnetosome membrane

The intracellular biomineralization of magnetite takes place within preformed membrane compartments, the magnetosome vesicles (FIG. 1-3A) (Komeili *et al.*, 2004), which confer a spatial confinement for the biological control over physico-chemical conditions. The formation of these vesicles is a prerequisite for the biomineralization since mutant strains of *Magnetospirillum* species that lost the ability to form magnetosome vesicles were also unable to form magnetite (Murat *et al.*, 2010; Lohße *et al.*, 2011). Recently, it was shown by cryo-electron tomography that the magnetosome vesicles in magnetospirilla originate from the cytoplasmic membrane by invagination (FIG. 1-3B) (Komeili *et al.*, 2006; Katzmann *et al.*, 2010). Consistent with this observation, the lipid composition of the magnetosome membrane (MM) did not differ from the lipid composition of the cytoplasmic membrane (Gorby *et al.*, 1988; Grünberg *et al.*, 2004). The protein composition of the MM, however, was strikingly distinct from that of the cytoplasmic membrane (FIG. 1-3C) (Gorby *et al.*, 1988; Grünberg *et al.*, 2001; Grünberg *et al.*, 2004). The MM of *M. gryphiswaldense*, for example, was shown to contain a set of ~30 specific proteins present in different quantities (Grünberg *et al.*, 2004), which have been designated the magnetosome membrane proteins (Mam (Grünberg *et al.*, 2001)) and magnetic particle membrane-specific proteins (Mms (Okamura *et al.*, 2001)), respectively.

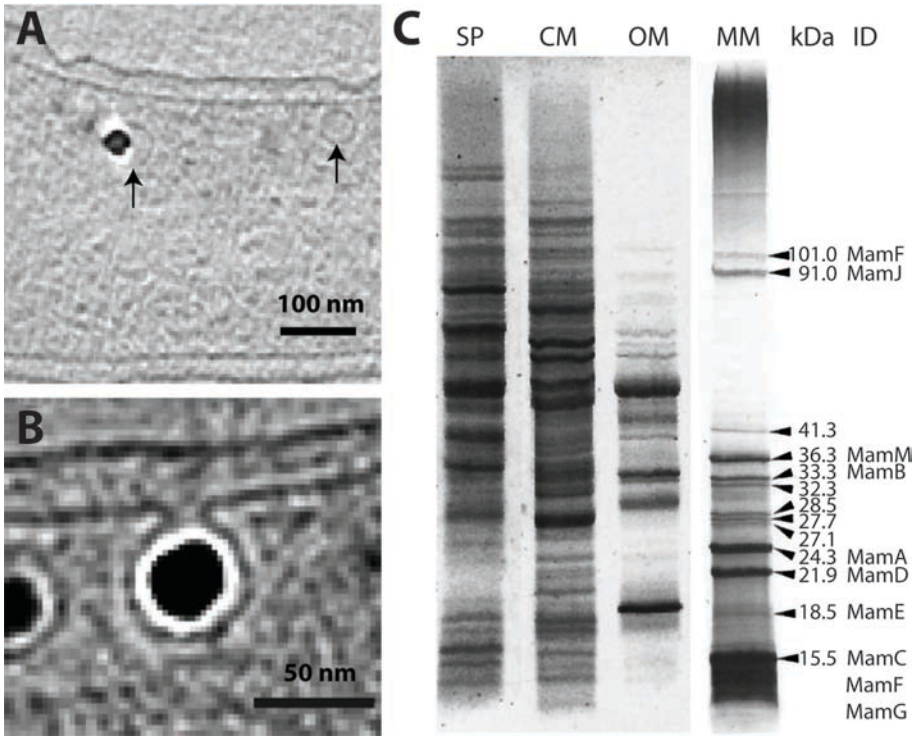

FIG. 1-3. A) Cryo-electron tomogram of *M. gryphiswaldense* (tomogram by E. Katzmann). Arrows represent positions of magnetosome vesicles. B) Cryo-electron tomogram of *M. magneticum* which shows that the magnetosome membrane is an invagination of the cytoplasmic membrane (Komeili *et al.*, 2006). C) Sodium dodecyl sulfate-polyacrylamid gel electrophoresis (SDS-PAGE) of MM-associated proteins from *M. gryphiswaldense* compared to soluble proteins (SP), cytoplasmic membrane proteins (CM) and outer membrane proteins (OM). The bands were visualized by staining with Coomassie blue. Arrowheads indicate the position, approximate molecular weight (in kDa) and the identity (ID) of several MM-specific proteins identified by amino-terminal protein sequence analysis (Grünberg *et al.*, 2001).

1.4.3 Genetics of magnetosome formation

Using a reverse genetics approach, Grünberg *et al*. (2001, 2004) showed that almost all magnetosome membrane-specific proteins were encoded by genes that are organized in four gene clusters (FIG. 1-4). These gene clusters are located close to each other within a 115 kb genomic region, which shares common characteristics of a genomic island similar to pathogenicity islands of pathogenic bacteria and was therefore termed the "magnetosome island" (MAI) (Ullrich *et al.*, 2005; Lohße *et al.*, 2011). Homologues of several genes encoded within the MAI of *M. gryphiswaldense* have subsequently also been found in all other analyzed MTB, including the uncultivated deep-branching nitrospira '*Candidatus* Magnetobacterium bavaricum' and a greigite producing multicellular δ-proteobacterium, which suggests a common origin of magnetosome formation (Jogler *et al.*, 2009a; Jogler *et al.*, 2009b; Abreu *et al.*, 2011; Jogler *et al.*, 2011).

The isolation of a spontaneous non-magnetic *M. gryphiswaldense* mutant mapped with a large deletion within the MAI showed that magnetosome formation is indeed dependent on

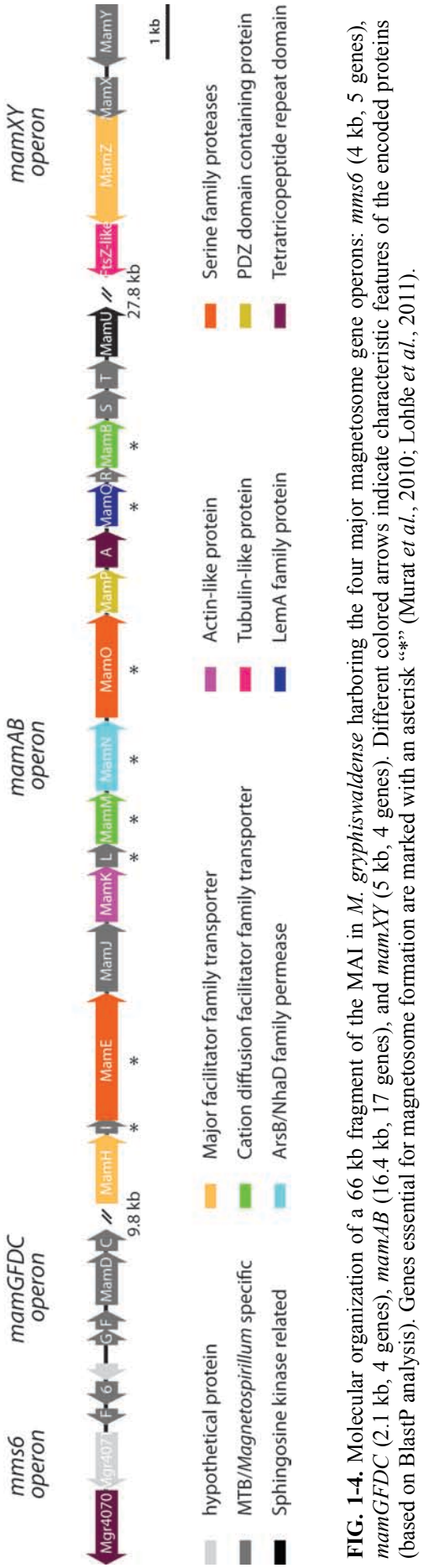

FIG. 1-4. Molecular organization of a 66 kb fragment of the MAI in *M. gryphiswaldense* harboring the four major magnetosome gene operons: *mms6* (4 kb, 5 genes), *mamGFDC* (2.1 kb, 4 genes), *mamAB* (16.4 kb, 17 genes), and *mamXY* (5 kb, 4 genes). Different colored arrows indicate characteristic features of the encoded proteins (based on BlastP analysis). Genes essential for magnetosome formation are marked with an asterisk "*" (Murat *et al.*, 2010; Lohße *et al.*, 2011).

the presence of proteins encoded within the MAI (Schübbe *et al.*, 2003). Directed deletion mutagenesis studies, however, revealed that magnetosome formation of *M. gryphiswaldense* and *M. magneticum* was only affected when at least one of the four magnetosome gene operons was deleted (FIG. 1-4) (Scheffel *et al.*, 2008; Murat *et al.*, 2010; Lohße *et al.*, 2011). Deletion of the entire *mamGFDC* operon in *M. gryphiswaldense*, for example, caused the formation of magnetosomes with a reduced magnetite crystal size (25% smaller) (Scheffel *et al.*, 2008). Thus, the MamGFDC proteins seem to be only involved in the regulation of the magnetite crystal size, although the MamGFDC proteins account for nearly 35% of all proteins associated with the magnetosome membrane (Scheffel *et al.*, 2008). More drastic effects were observed in a *M. gryphiswaldense mms6* operon mutant. This mutant strain produced smaller crystals that were scattered throughout the cell or aligned in irregular, widely spaced chains. Besides cubo-octahedral crystals also heterogeneous and aberrant crystal shapes were observed in the *mms6* operon mutant (Lohße *et al.*, 2011). From these results it was concluded that the proteins encoded within the *mms6* operon are likely involved in the control of crystal size, morphology, number, and alignment of magnetosomes (Lohße *et al.*, 2011). Also a *M. gryphiswaldense* deletion mutant of the entire *mamXY* operon was still

able to produce magnetosomes, although the intracellular localization of the magnetosome chain as well as magnetite crystallization were disturbed (Raschdorf, 2011). Therefore, the *mamXY* operon is assumed to regulate magnetite crystallization as well as the correct positioning of the magnetosome chain (Raschdorf, 2011). Only *M. gryphiswaldense* and *M. magneticum* mutants lacking the *mamAB* operon lost the ability to form magnetosomes (Murat *et al.*, 2010; Ullrich and Schüler, 2010; Lohße *et al.*, 2011). Thus, although each of the four magnetosome gene operons is required for the formation of wild type-like magnetosomes, only the *mamAB* operon is essential (Murat *et al.*, 2010; Lohße *et al.*, 2011).

Functions of individual genes and proteins of the *mamAB* operon

Despite recent progress in the genetic analysis of magnetosome formation, the underlying mechanisms are still poorly understood at the molecular level since only a few genes and proteins have been functionally characterized in detail.

The actin-like protein **MamK**, for example, was proposed to form a filamentous protein structure to which magnetosomes are attached to form magnetosome chains (Scheffel *et al.*, 2006). Consistent with this predicted function, filamentous protein structures were absent in a *mamK* mutant of *M. gryphiswaldense* (Katzmann *et al.*, 2010). However, the *mamK* deletion mutant also produced less magnetosomes, which were still aligned in short chains but aberrant intracellular localization, indicating that magnetite biomineralization is also disturbed and that magnetosome chain formation is more complex than initially expected (Katzmann *et al.*, 2010). Additionally, a more recent study showed that MamK is also required for the recruitment of the magnetosome chain to midcell and to the division site during cell division (Katzmann *et al.*, 2011). Deletion of ***mamJ*** in *M. gryphiswaldense* resulted in disruption of the magnetosome chain and agglomeration of magnetosomes. Based on two-hybrid interaction studies with MamK it was suggested that MamJ aligns the magnetosomes along the MamK filament (Scheffel *et al.*, 2006; Scheffel and Schüler, 2007). However, more recently it was reported that MamJ might be involved in the regulation of MamK-filament dynamics of *M. magneticum* (Draper *et al.*, 2011). **MamA**, a soluble tetratricopeptide repeat (TPR) domain-containing protein, is supposedly involved in the activation of magnetosome vesicles (Komeili *et al.*, 2004). A *M. magneticum mamA* deletion mutant, however, was still able to form wild type-like magnetosomes, although in slightly lower amounts (Komeili *et al.*, 2004). Recently, atomic force microscopy and resolution of the MamA crystal structure indicated that MamA might self-assemble through its TPR motifs to create a large

homooligomeric scaffold on the magnetosome surface, which can interact with other magnetosome-associated proteins (Yamamoto *et al.*, 2010; Zeytuni *et al.*, 2011). **MamO** and **MamE**, two putative proteases of the HtrA/DegP family essential for magnetite biomineralization, were also analyzed in detail. While MamE seems to be involved in targeting of magnetosome proteins to the MM as well as magnetite crystal maturation, the functional role of MamO remained elusive (Yang *et al.*, 2010; Quinlan *et al.*, 2011).

The functions of the other *mamAB* operon genes are largely unknown. However, based on protein similarity to known protein families of non-magnetotactic bacteria or characterization of mutant phenotypes putative functions have been proposed for some of these proteins. A ***mamN*** deletion mutant of *M. magneticum* was not able to biomineralize magnetite crystals, but still formed magnetosome vesicles and is therefore expected to be involved in the initiation of magnetite biomineralization (Murat *et al.*, 2010). Because of its similarity to proton translocating proteins, MamN was also suggested to be involved in pH-regulation of the magnetosome vesicle lumen (Faivre and Schüler, 2008). **MamQ** is a member of the LemA protein family. Although this family of proteins is widely distributed in bacteria, almost nothing is known about their putative functions. MamQ seems to be required for the biogenesis of the MM since deletion of *mamQ* in *M. magneticum* caused a loss of magnetite and magnetosome membrane formation (Murat *et al.*, 2010). Also **MamI** and **MamL**, two MTB-specific proteins, are required for the MM biogenesis. Deletion of either *mamI* or *mamL* abolished magnetite as well as magnetosome vesicle formation in *M. magneticum* (Murat *et al.*, 2010). **MamP**, a small PDZ domain containing protein, is suggested to be involved in the regulation of the magnetosome size in *M. magneticum* (Murat *et al.*, 2010). A similar function has been proposed for the MTB-specific protein **MamR** since the magnetosomes of a *M. magneticum mamR* deletion mutant were smaller than those of the wild type and even smaller than those of the *mamP* mutant strain (Murat *et al.*, 2010). According to the deletion mutant phenotypes of ***mamS*** and ***mamT***, which encode two further MTB-specific proteins, their gene products are involved in the regulation of crystal size and morphology. **MamU** shares significant similarity to sphingosine kinases and might therefore be involved in the lipid metabolism of magnetospirilla. Deletion of *mamU* in *M. magneticum*, however, caused no defects in magnetosome formation (Murat *et al.*, 2010). Also a ***mamH*** deletion mutant of *M. magneticum* was almost indistinguishable from wild type cells (Murat *et al.*, 2010). Thus, the function of the major facilitator superfamily (MFS) protein MamH remained unclear. ***mamM*** and ***mamB*** deletion mutants of *M. magneticum* were unable to biomineralize magnetite (Murat *et al.*, 2010). Although both genes encode proteins of the cation diffusion

facilitator (CDF) family, the phenotypes of the *mamM* and *mamB* deletion mutants are not congruent. Whereas the *mamB* deletion mutant strain lacked any intracellular membranes, the *mamM* mutant was still able to form empty magnetosome vesicles (Murat *et al.*, 2010). Thus, it was speculated that MamB is involved in magnetosome membrane biogenesis and MamM in the initiation of magnetite nucleation (Murat *et al.*, 2010).

1.4.4 Transport of iron into magnetosome vesicles

It has been suggested that iron concentrations of at least 30 mM are required for magnetite formation within magnetosome vesicles (Faivre and Schüler, 2008) because iron concentrations below 30 mM induced the formation of poorly crystalline iron oxides and other mineral phases like goethite instead of magnetite during abiotic magnetite syntheses (Faivre *et al.*, 2004). Accumulation of these millimolar amounts of iron in magnetosome vesicles from micromolar environmental concentrations is assumed to involve the uptake of iron into the cytoplasm by general iron uptake systems and subsequent iron transport into the magnetosome vesicles (Frankel *et al.*, 1983). The uptake of iron into magnetosome vesicles seems to be highly specific for iron since several studies reported that magnetite produced by MTB is completely free of impurities (Sparks *et al.*, 1990; Faivre and Schüler, 2008) or contains contaminating metal ions in significantly lower concentrations than abiotic magnetite (Towe and Moench, 1981; Thomas-Keprta *et al.*, 2000; Kopp and Kirschvink, 2008).

Initial genetic and biochemical studies proposed that MagA of *M. magneticum* functions as an essential magnetosome-directed iron transport protein (Nakamura *et al.*, 1995a; Nakamura *et al.*, 1995b) since MagA was shown to localize to the MM as well as to the cytoplasmic membrane and has an ATP-dependent ferrous iron transport activity (Nakamura *et al.*, 1995a; Nakamura *et al.*, 1995b). However, results of more recent studies raised several doubts about the localization of MagA in the MM as well as its essential role for magnetosome formation (Grünberg *et al.*, 2001; Grünberg *et al.*, 2004; Tanaka *et al.*, 2006; Lohße *et al.*, 2011; Uebe *et al.*, 2011a).

Although deletion mutagenesis of *mamM* and *mamB* in *M. magneticum* revealed that their gene products might have non-equivalent roles, MamM and MamB were suggested to transport ferrous iron ions into the magnetosome vesicles (Grünberg *et al.*, 2001; Nies, 2003; Grünberg *et al.*, 2004; Nies, 2011). These suggestions were based on the high abundance of MamM and MamB in the MM and their affiliation with the divalent metal ion transporting CDF family (Grünberg *et al.*, 2001; Grünberg *et al.*, 2004). Proteins of the ubiquitous CDF

family have been shown to exclusively export divalent metal cations including Zn^{2+}, Co^{2+}, Cd^{2+}, Mn^{2+}, Ni^{2+}, and Fe^{2+} from the cytoplasm out of the cell or into intracellular compartments using the proton motive force (Li and Kaplan, 1997; Nies, 2003; Grass *et al.*, 2005; Rosch *et al.*, 2009). Several studies showed that the metal export function of CDF proteins significantly contributes to the cellular metal ion homeostasis (Nies and Silver, 1995; Grass *et al.*, 2005; Montanini *et al.*, 2007). Recently, FieF (YiiP), a CDF protein from *E. coli* with significant similarity to the MamB and MamM, was shown to export iron and zinc over the cytoplasmic membrane (Grass *et al.*, 2005), which further supports the notion that MamB and MamM are involved in magnetosome-directed iron transport.

Most recently also the MFS proteins MamH and MamZ have been implicated with magnetosomal iron transport since co-deletion of *mamH* and *mamZ* in *M. gryphiswaldense* caused a drastic decrease in the amount of iron oxide particles, which also seemed to be less crystalline (Raschdorf, 2011). Because only the co-deletion of both genes resulted in the formation of poorly crystalline magnetosome mineral cores (Raschdorf, 2011), it was speculated that MamH and MamZ have redundant functions (Raschdorf, 2011). Proteins of the major facilitator superfamily are found in all domains of life and have been shown to transport various small solutes, including iron, in response to chemiosmotic gradients (Pao *et al.*, 1998). However, in contrast to members of the CDF family, MFS proteins have so far only been shown to be involved siderophore mediated transport of ferric iron ions (Lesuisse *et al.*, 1998).

Although, various proteins have been implicated with magnetosome-directed iron transport from the cytosol, the results of a recent Mössbauer spectrometric study on *M. gryphiswaldense* suggested a different iron uptake pathway for magnetite biomineralization (Faivre *et al.*, 2007). The authors proposed that iron for magnetite precipitation is accumulated in magnetosome vesicles by direct transport from the periplasm or that iron is processed throughout cell membranes directly to the MM without iron transport through the cytoplasm (Faivre *et al.*, 2007). These iron transport pathways would be possible as long as the magnetosome vesicles are permanently attached to the cytoplasmic membrane, as observed for *M. magneticum* (Komeili *et al.*, 2006). However, cryo-electron tomographic analyses and scanning electron microscopic analyses with a focused ion beam indicated that the MM of other MTB might not form a continuous structure with the cytoplasmic membrane (Scheffel *et al.*, 2006; Jogler *et al.*, 2011). Therefore, it was also suggested that magnetite crystal growth continues even after detachment of the vesicles from the cytoplasmic membrane due to high iron-load of the vesicles (Faivre *et al.*, 2007).

1.5 Regulation and dynamics of magnetosome formation

The biomineralization of magnetite by MTB requires anaerobic to microaerobic conditions as well as sufficient supply of iron (Faivre and Schüler, 2008). Magnetite formation by *M. gryphiswaldense* was limited by concentrations between 1 and 10 µM iron (Schüler and Baeuerlein, 1996), whereas iron concentrations below 1 µM prevented magnetite biomineralization (Faivre *et al.*, 2008). Biomineralization of magnetite was found close to saturation at 20 µM iron (Schüler and Baeuerlein, 1996), while higher iron concentrations increased the synthesis of magnetite crystals only slightly and were found to inhibit growth above 200 µM (Schüler and Baeuerlein, 1996) or 1 mM iron (Junge, 2008). The optimum oxygen supply for magnetite biomineralization was observed at a pO_2 of 0.25 mbar, whereas oxygen partial pressures above 20 mbar completely inhibited magnetite formation in *Magnetospirillum* strains (Heyen and Schüler, 2003). Notably, the synthesis of magnetite by abiotic processes also depends on very low oxygen concentrations to prevent oxidation of ferrous to ferric iron and formation of ferric iron minerals (maghemite, hematite, goethite) (Baumgartner and Faivre, 2011). However, it is still not clear if the inhibition of magnetite formation by oxygen in MTB is also caused by a disturbed stoichiometry between ferrous and ferric iron ions.

Due to their large iron accumulation and the risk of an increased formation of radical oxygen species via the Fenton reaction, MTB have a strong need to regulate and balance the iron uptake for magnetosome formation and biochemical requirements. However, only very few studies have addressed this question so far. Two studies investigated how the genes of the MAI are regulated. Whereas a global gene expression study with *M. magneticum* cells grown under different extracellular iron concentrations revealed no changes of the transcriptional level of most MAI genes (Suzuki *et al.*, 2006), Schübbe *et al.* (2006) showed that the genes of the *M. gryphiswaldense mamAB*, *mamGFDC*, and *mms6* operons are 2.5 to 137-fold down-regulated under iron-depleted as well as aerobic growth conditions. Bioinformatical analyses of the *M. magneticum* and *M. magnetotacticum* genome sequences suggested that the ferric uptake regulator (Fur) might be involved in the iron-responsive regulation of several magnetosome genes (Rodionov *et al.*, 2006). This hypothesis was further supported by the close linkage of a *fur* gene with magnetosome genes in a magnetosome island-like gene cluster of an uncultivated MTB (Jogler *et al.*, 2009b). In addition, it was reported that disruption of a *fur*-like gene in *M. gryphiswaldense* abolished magnetosome formation (Huang *et al.*, 2007). However, the results of this study have been questioned due to the

absence of complementation experiments, which are required because of the high frequency of spontaneous mutations (up to 10^{-2}) within the MAI of *M. gryphiswladense* (Ullrich *et al.*, 2005; Kolinko *et al.*, 2011a).

In apparent contrast to the transcriptional effects of iron depletion or oxygen presence on the magnetosome genes of *M. gryphiswaldense*, Western blot and proteomic analyses revealed almost no changes of the abundance of the proteins encoded within the magnetosome gene operons (Schübbe *et al.*, 2006; Uebe *et al.*, 2010). Additionally, cryo-electron tomographs of *M. magneticum* and *M. gryphiswaldense* showed that magnetosome vesicles are also present after repeated passages under iron-depleted or aerobic growth conditions (Komeili *et al.*, 2004; Komeili *et al.*, 2006; Katzmann, unpublished results). The presence of magnetosome vesicles even under magnetite-inhibiting conditions might be the prerequisite for rapid magnetite biomineralization after transfer to magnetite-inducing conditions. Two hours after iron addition to iron-starved cells of *M. magneticum* small magnetite crystals arranged in short chains were observed (Komeili *et al.*, 2004). In iron-starved *M. gryphiswaldense* small magnetite crystals were detectable by transmission electron microscopy approximately one hour after iron-induction (Faivre *et al.*, 2007). Using a more sensitive method (transmission Mössbauer spectroscopy) the authors detected the first magnetite signals already 20 min after iron-induction (Faivre *et al.*, 2007). In contrast, Schüler and Baeuerlein (1998) as well as Heyen and Schüler (2003) reported formation of small magnetite crystal immediately after iron induction. In a recent study it was even reported that only 15 min of iron-induction are sufficient for *M. gryphiswaldense* to form chains of mature magnetosomes (Staniland *et al.*, 2007). However, it was suggested that the differences between the results of previous studies and this study were caused by an inaccurate experimental setup applied in the latter study (Baumgartner and Faivre, 2011). Transfer of *M. gryphiswaldense* cells grown under iron-replete, aerobic conditions to iron-replete, microaerobic conditions resulted in the first response to external magnetic fields approximately 4 h after the transfer, suggesting that protein synthesis is required (Heyen and Schüler, 2003). More recent experiments, however, revealed first magnetite formation approximately 30 min after an oxygen-downshift (Y. Li, personal communication). Thus, although the underlying mechanisms might be distinct and are not understood yet, the induction of magnetite formation by addition of iron or oxygen downshift show the same dynamics.

1.6 Scope of this work

Magnetotactic bacteria accumulate large amounts of iron for the intracellular synthesis of magnetite crystals, which requires a strict control of the iron metabolism because of the potential risk of an increased formation of radical oxygen species. So far only very few studies have addressed iron homeostasis of magnetotactic bacteria. Several of them suggested that proteins of the Fur family play a central role in iron homeostasis and also magnetosome formation without providing experimental evidence (Rodionov *et al.*, 2006; Huang *et al.*, 2007; Jogler *et al.*, 2009b). In order to elucidate the contribution of Fur-like proteins to the iron homeostasis, in the **first part** of this thesis a detailed bioinformatical analysis of the putative constituents of iron-responsive regulators was applied. After identification of a putative genuine Fur, I specifically asked whether the Fur regulator might be involved in the formation of magnetosomes in *M. gryphiswaldense*.

Previous studies suggested that MamM and MamB are involved in magnetosome-directed iron transport from the cytoplasm (Grünberg *et al.*, 2001; Nies, 2003). Thus, in the **second part** of this thesis MamM and MamB were investigated with respect to their contribution to magnetosome-directed iron transport and magnetosome formation in *M. gryphiswaldense*.

Original findings suggested an essential role of MagA for magnetosome formation in *M. magneticum*, due to its presumptive magnetosome-directed iron transport activity (Matsunaga *et al.*, 1992; Nakamura *et al.*, 1995a; Nakamura *et al.*, 1995b; Smith *et al.*, 2006). However, more recent studies reported several conflicting results and, hence, raised doubts about the putative essential role of MagA for magnetosome formation (Grünberg *et al.*, 2001; Grünberg *et al.*, 2004; Tanaka *et al.*, 2006; Richter *et al.*, 2007; Lohße *et al.*, 2011). To resolve these conflicting results/observations, in the **third part** of this thesis, the role of MagA for magnetosome formation in *M. gryphiswaldense* and *M. magneticum* was elucidated by deletion mutagenesis.

1.7 References

Abdul-Tehrani, H., Hudson, A. J., Chang, Y. S., Timms, A. R., Hawkins, C., Williams, J. M., Harrison, P. M., Guest, J. R. and Andrews, S. C. (1999). Ferritin mutants of *Escherichia coli* are iron deficient and growth impaired, and *fur* mutants are iron deficient. *J. Bacteriol.* **181**: 1415-1428.

Abreu, F., Cantão, M. E., Nicolás, M. F., Barcellos, F. G., Morillo, V., Almeida, L. G. P., do Nascimento, F. F., Lefèvre, C. T., Bazylinski, D. A., R de Vasconcelos, A. T. and Lins, U. (2011). Common ancestry of iron oxide- and iron-sulfide-based biomineralization in magnetotactic bacteria. *ISME J.* **5**: 1634-1640.

Amann, R., Peplies, J. and Schüler, D. (2007). Diversity and taxonomy of magnetotactic bacteria. In: *Magnetoreception and magnetosomes in bacteria*. D. Schüler (ed.). Springer, Berlin, Heidelberg.

Andrews, S. C., Robinson, A. K. and Rodriguez-Quinones, F. (2003). Bacterial iron homeostasis. *FEMS Microbiol. Rev.* **27**: 215-237.

Arató, B., Szanyi, Z., Flies, C. B., Schüler, D., Frankel, R., Buseck, P. R. and Pósfai, M. (2005). Crystal-size and shape distributions of magnetite from uncultured magnetotactic bacteria as a potential biomarker. *Am. Mineral.* **90**: 1233-1241.

Balkwill, D., Maratea, D. and Blakemore, R. P. (1980). Ultrastructure of a magnetotactic spirillum. *J. Bacteriol.* **141**: 1399-1408.

Baumgartner, J. and Faivre, D. (2011). Magnetite biomineralization in bacteria. In: *Molecular biomineralization: Aquatic organisms forming extraordinary materials*. W. E. G. Müller (ed.). Springer, Heidelberg.

Bazylinski, D. and Frankel, R. (2004). Magnetosome formation in prokaryotes. *Nature Rev.* **2**: 217-230.

Bazylinski, D., Garratt-Reed, A. and Frankel, R. (1994). Electron-microscopic studies of magnetosomes in magnetotactic bacteria. *Microsc. Res. Tech.* **27**: 389-401.

Belcher, A. M., Wu, X. H., Christensen, R. J., Hansma, P. K., Stucky, G. D. and Morse, D. E. (1996). Control of crystal phase switching and orientation by soluble mollusc-shell proteins. *Nature* **381**: 56-58.

Bell, P. E., Mills, A. L. and Herman, J. S. (1987). Biogeochemical conditions favoring magnetite formation during anaerobic iron reduction. *Appl. Environ. Microbiol.* **53**: 2610-2616.

Bellini, S. (2009a). Further studies on "magnetosensitive bacteria". *Chinese Journal of Oceanology and Limnology* **27**: 6-12.

Bellini, S. (2009b). On a unique behavior of freshwater bacteria. *Chinese Journal of Oceanology and Limnology* **27**: 3-5.

Bertani, L. E., Huang, J. S., Weir, B. A. and Kirschvink, J. L. (1997). Evidence for two types of subunits in the bacterioferritin of Magnetospirillum magnetotacticum. *Gene* **201**: 31-36.

Bertani, L. E., Weko, J., Phillips, K. V., Gray, R. F. and Kirschvink, J. L. (2001). Physical and genetic characterization of the genome of Magnetospirillum magnetotacticum, strain MS-1. *Gene* **264**: 257-263.

Blakemore, R. P. (1975). Magnetotactic bacteria. *Science* **190**: 377-379.

Calugay, R. J., Miyashita, H., Okamura, Y. and Matsunaga, T. (2003). Siderophore production by the magnetic bacterium *Magnetospirillum magneticum* AMB-1. *FEMS Microbiol. Lett.* **218**: 371-375.

Calugay, R. J., Okamura, Y., Wahyudi, A. T., Takeyama, H. and Matsunaga, T. (2004). Siderophore production of a periplasmic transport binding protein kinase gene defective mutant of *Magnetospirillum magneticum* AMB-1. *Biochem. Biophys. Res. Commun.* **323**: 852-857.

Calugay, R. J., Takeyama, H., Mukoyama, D., Fukuda, Y., Suzuki, T., Kanoh, K. and Matsunaga, T. (2006). Catechol siderophore excretion by magnetotactic bacterium *Magnetospirillum magneticum* AMB-1. *J. Biosci. Bioeng.* **101**: 445-447.

Chung, K. T., Lu, Z. and Chou, M. W. (1998). Mechanism of inhibition of tannic acid and related compounds on the growth of intestinal bacteria. *Food Chem. Toxicol.* **36**: 1053-1060.

DeLong, E. F., Frankel, R. and Bazylinski, D. (1993). Multiple evolutionary origins of magnetotaxis in bacteria. *Science* **259**: 803-806.

Devouard, B., Posfai, M., Hua, X., Bazylinski, D., Frankel, R. and Buseck, P. (1998). Magnetite from magnetotactic bacteria; size distributions and twinning. *Am. Mineral.* **83**: 1387-1398.

Draper, O., Byrne, M. E., Li, Z., Keyhani, S., Barrozo, J. C., Jensen, G. and Komeili, A. (2011). MamK, a bacterial actin, forms dynamic filaments *in vivo* that are regulated by the acidic proteins MamJ and LimJ. *Mol. Microbiol.* **82**: 342–354.

Dubbels, B., DiSpirito, A., Morton, J., Semrau, J., Neto, J. and Bazylinski, D. (2004). Evidence for a copper-dependent iron transport system in the marine, magnetotactic bacterium strain MV-1. *Microbiology* **150**: 2921-2945.

Faivre, D., Agrinier, P., Menguy, N., Zuddas, P., Pachana, K., Gloter, A., Laval, J. and Guyot, F. (2004). Mineralogical and isotopic properties of inorganic nanocrystalline magnetites. *Geochim. Cosmochim. Acta* **68**: 4395-4403.

Faivre, D., Böttger, L. H., Matzanke, B. F. and Schüler, D. (2007). Intracellular magnetite biomineralization in bacteria proceeds by a distinct pathway involving membrane-bound ferritin and an iron(II) species. *Angew. Chem. Int. Ed. Engl.* **46**: 8495-8499.

Faivre, D., Menguy, N., Guyot, F., Lopez, O. and Zuddas, P. (2005). Morphology of nanomagnetite crystals: Implications for formation conditions. *Am. Mineral.* **90**: 1793-1800.

Faivre, D., Menguy, N., Posfai, M. and Schüler, D. (2008). Environmental parameters affect the physical properties of fast-growing magnetosomes. *Am. Mineral.* **93**: 463-469.

Faivre, D. and Schüler, D. (2008). Magnetotactic bacteria and magnetosomes. *Chem. Rev.* **108**: 4875-4898.

Farina, M., Esquivel, D. and Lins de Barros, H. (1990). Magnetic iron-sulphur crystals from a magnetotactic microorganism. *Nature* **343**: 256-258.

Fischer, A., Schmitz, M., Aichmayer, B., Fratzl, P. and Faivre, D. (2011). Structural purity of magnetite nanoparticles in magnetotactic bacteria. *J. R. Soc. Interface* **8**: 1011-1018.

Flies, C. B., Jonkers, H. M., de Beer, D., Bosselmann, K., Böttcher, M. E. and Schüler, D. (2005). Diversity and vertical distribution of magnetotactic bacteria along chemical gradients in freshwater microcosms. *FEMS Microbiol. Ecol.* **52**: 185-195.

Frankel, R., Papaefthymiou, G. C., Blakemore, R. P. and O'Brian, W. (1983). Fe_3O_4 precipitation in magnetotactic bacteria. *Biochim. Biophys. Acta* **763**: 147-159.

Frankel, R. B., Bazylinski, D. A., Johnson, M. S. and Taylor, B. L. (1997). Magneto-aerotaxis in marine coccoid bacteria. *Biophys. J.* **73**: 994-1000.

Frankel, R. B., Blakemore, R. P. and Wolfe, R. S. (1979). Magnetite in freshwater magnetotactic bacteria. *Science* **203**: 1355-1356.

Gorby, Y. A., Beveridge, T. J. and Blakemore, R. (1988). Characterization of the bacterial magnetosome membrane. *J. Bacteriol.* **170**: 834-841.

Grass, G., Otto, M., Fricke, B., Haney, C. J., Rensing, C., Nies, D. H. and Munkelt, D. (2005). FieF (YiiP) from *Escherichia coli* mediates decreased cellular accumulation of iron and relieves iron stress. *Arch. Microbiol.* **183**: 9-18.

Grünberg, K., Müller, E. C., Otto, A., Reszka, R., Linder, D., Kube, M., Reinhardt, R. and Schüler, D. (2004). Biochemical and proteomic analysis of the magnetosome membrane in *Magnetospirillum gryphiswaldense*. *Appl. Environ. Microbiol.* **70**: 1040-1050.

Grünberg, K., Wawer, C., Tebo, B. M. and Schüler, D. (2001). A large gene cluster encoding several magnetosome proteins is conserved in different species of magnetotactic bacteria. *Appl. Environ. Microbiol.* **67**: 4573-4582.

Heyen, U. and Schüler, D. (2003). Growth and magnetosome formation by microaerophilic *Magnetospirillum* strains in an oxygen-controlled fermentor. *Appl. Microbiol. Biotechnol.* **61**: 536-544.

Huang, Y., Zhang, W., Jiang, W., Rong, C. and Li, Y. (2007). Disruption of a *fur*-like gene inhibits magnetosome formation in *Magnetospirillum gryphiswaldense* MSR-1. *Biochemistry (Moscow)* **72**: 1247-1253.

Imlay, J. and Linn, S. (1988). DNA damage and oxygen radical toxicity. *Science* **240**: 1302-1309.

Jogler, C., Kube, M., Schübbe, S., Ullrich, S., Teeling, H., Bazylinski, D., Reinhardt, R. and Schüler, D. (2009a). Comparative analysis of magnetosome gene clusters in magnetotactic bacteria provides further evidence for horizontal gene transfer. *Environ. Microbiol.* **11**: 1267–1277.

Jogler, C., Lin, W., Meyerdierks, A., Kube, M., Katzmann, E., Flies, C., Pan, Y., Amann, R., Reinhardt, R. and Schüler, D. (2009b). Toward cloning of the magnetotactic metagenome: Identification of magnetosome island gene clusters in uncultivated magnetotactic bacteria from different aquatic sediments. *Appl. Environ. Microbiol.* **75**: 3972-3979.

Jogler, C. and Schüler, D. (2009). Genomics, genetics, and cell biology of magnetosome formation. *Annu. Rev. Microbiol.* **63**: 501-521.

Jogler, C., Wanner, G., Kolinko, S., Niebler, M., Amann, R., Petersen, N., Kube, M., Reinhardt, R. and Schüler, D. (2011). Conservation of proteobacterial magnetosome genes and structures in an uncultivated member of the deep-branching *Nitrospira* phylum. *Proc. Natl. Acad. Sci. U.S.A.* **108**: 1134-1139.

Junge, K. (2008). *Doctoral thesis*: Die Funktion der CDF-Transporter MamB und MamM beim magnetosomalen Eisentransport in *Magnetospirillum gryphiswaldense*. Universität Bremen, Bremen.

Katzmann, E., Müller, F. D., Lang, C., Messerer, M., Winklhofer, M., Plitzko, J. M. and Schüler, D. (2011). Magnetosome chains are recruited to cellular division sites and split by asymmetric septation. *Mol. Microbiol.* **doi: 10.1111/j.1365-2958.2011.07874.x**.

Katzmann, E., Scheffel, A., Gruska, M., Plitzko, J. M. and Schüler, D. (2010). Loss of the actin-like protein MamK has pleiotropic effects on magnetosome formation and chain assembly in *Magnetospirillum gryphiswaldense*. *Mol. Microbiol.* **77**: 208-224.

Kolinko, I., Jogler, C., Katzmann, E. and Schüler, D. (2011a). Frequent mutations within the genomic magnetosome island of *Magnetospirillum gryphiswaldense* are mediated by RecA. *J. Bacteriol.* **193**: 5328–5334.

Kolinko, S., Jogler, C., Katzmann, E., Wanner, G., Peplies, J. and Schüler, D. (2011b). Single-cell analysis reveals a novel uncultivated magnetotactic bacterium within the candidate division OP3. *Environ. Microbiol.* **doi: 10.1111/j.1462-2920.2011.02609.x.**

Komeili, A., Li, Z., Newman, D. K. and Jensen, G. J. (2006). Magnetosomes are cell membrane invaginations organized by the actin-like protein MamK. *Science* **311**: 242-245.

Komeili, A., Vali, H., Beveridge, T. J. and Newman, D. K. (2004). Magnetosome vesicles are present before magnetite formation, and MamA is required for their activation. *Proc. Natl. Acad. Sci. U.S.A.* **101**: 3839-3844.

Kopp, R. E. and Kirschvink, J. L. (2008). The identification and biogeochemical interpretation of fossil magnetotactic bacteria. *Earth-Science Reviews* **86**: 42-61.

Kröger, N., Deutzmann, R. and Sumper, M. (1999). Polycationic peptides from diatom biosilica that direct silica nanosphere formation. *Science* **286**: 1129-1132.

Lefèvre, C. T., Bernadac, A., Yu-Zhang, K., Pradel, N. and Wu, L.-F. (2009). Isolation and characterization of a magnetotactic bacterial culture from the Mediterranean Sea. *Environ. Microbiol.* **11**: 1646-1657.

Lefèvre, C. T., Viloria, N., Schmidt, M. L., Pósfai, M., Frankel, R. B. and Bazylinski, D. A. (2011). Novel magnetite-producing magnetotactic bacteria belonging to the gammaproteobacteria. *ISME J.* **21**: 97.

Lesuisse, E., Simon-Casteras, M. and Labbe, P. (1998). Siderophore-mediated iron uptake in *Saccharomyces cerevisiae*: the SIT1 gene encodes a ferrioxamine B permease that belongs to the major facilitator superfamily. *Microbiology* **144**: 3455-3462.

Li, L. and Kaplan, J. (1997). Characterization of two homologous yeast genes that encode mitochondrial iron transporters. *J. Biol. Chem.* **272**: 28485-28493.

Lohße, A., Ullrich, S., Katzmann, E., Borg, S., Wanner, G., Richter, M., Voigt, B., Schweder, T. and Schüler, D. (2011). Functional analysis of the magnetosome island in *Magnetospirillum gryphiswaldense*: The *mamAB* operon is sufficient for magnetite biomineralization. *PLoS One* **6**: e25561.

Mandernack, K. W., Bazylinski, D., Shanks, W. C. and Bullen, T. D. (1999). Oxygen and iron isotope studies of magnetite produced by magnetotactic bacteria. *Science* **285**: 1892-1896.

Mann, S., Sparks, N. H. C., Frankel, R., Bazlinski, D. A. and Jannasch, H. W. (1990). Biomineralization of ferrimagnetic greigite (Fe_3S_4) and iron pyrite (FeS_2) in a magnetotactic bacterium. *Nature* **343**: 258-261.

Matsunaga, T., Nakamura, C., Burgess, J. G. and Sode, K. (1992). Gene transfer in magnetic bacteria: transposon mutagenesis and cloning of genomic DNA fragments required for magnetosome synthesis. *J. Bacteriol.* **174**: 2748-2753.

Meldrum, F. C., Mann, S., Heywood, B. R., Frankel, R. and Bazylinski, D. (1993a). Electron-microscopy study of magnetosomes in 2 cultured vibrioid magnetotactic bacteria. *Proc. R. Soc. London, B* **251**: 237-242.

Meldrum, F. C., Mann, S., Heywood, B. R., Frankel, R. and Bazylinski, D. (1993b). Electron-microscopy study of magnetosomes in a cultured coccoid magnetotactic bacterium. *Proc. R. Soc. London, B* **251**: 231-236.

Montanini, B., Blaudez, D., Jeandroz, S., Sanders, D. and Chalot, M. (2007). Phylogenetic and functional analysis of the Cation Diffusion Facilitator (CDF) family: improved signature and prediction of substrate specificity. *BMC Genomics* **8**: 107.

Murat, D., Quinlan, A., Vali, H. and Komeili, A. (2010). Comprehensive genetic dissection of the magnetosome gene island reveals the step-wise assembly of a prokaryotic organelle. *Proc. Natl. Acad. Sci. U.S.A.* **107**: 5593-5598.

Nakamura, C., Burgess, J. G., Sode, K. and Matsunaga, T. (1995a). An iron-regulated gene, *magA*, encoding an iron transport protein of *Magnetospirillum* sp. strain AMB-1. *J. Biol. Chem.* **270**: 28392-28396.

Nakamura, C., Kikuchi, T., Burgess, J. G. and Matsunaga, T. (1995b). Iron-regulated expression and membrane localization of the MagA protein in *Magnetospirillum* sp. Strain AMB-1. *J. Biochem. (Tokyo)*. **118**: 23-27.

Nies, D. (2003). Efflux-mediated heavy metal resistance in prokaryotes. *FEMS Microbiol. Rev.* **27**: 313-339.

Nies, D. and Silver, S. (1995). Ion efflux systems involved in bacterial metal resistances. *J. Ind. Microbiol.* **14**: 186-199.

Nies, D. (2011). How iron is transported into magnetosomes. *Mol. Microbiol.* **82**(4): 792-796.

Noguchi, Y., Fujiwara, T., Yoshimatsu, K. and Fukumori, Y. (1999). Iron reductase for magnetite synthesis in the magnetotactic bacterium *Magnetospirillum magnetotacticum*. *J. Bacteriol.* **181**: 2142-2147.

Okamura, Y., Takeyama, H. and Matsunaga, T. (2001). A magnetosome-specific GTPase from the magnetic bacterium *Magnetospirillum magneticum* AMB-1. *J. Biol. Chem.* **276**: 48183-48188.

Pao, S. S., Paulsen, I. T. and Saier, M. H., Jr. (1998). Major facilitator superfamily. *Microbiol. Mol. Biol. Rev.* **62**: 1-34.

Paoletti, L. C. and Blakemore, R. P. (1986). Hydroxamate production by *Aquaspirillum magnetotacticum*. *J. Bacteriol.* **167**: 73-76.

Paoletti, L. C. and Blakemore, R. P. (1988). Iron reduction by *Aquaspirillum magnetotacticum*. *Curr. Microbiol.* **17**: 339-342.

Philpott, C. C. and Protchenko, O. (2008). Response to iron deprivation in *Saccharomyces cerevisiae*. *Eukaryotic Cell* **7**: 20-27.

Pósfai, M., Buseck, P. R., Bazylinski, D. and Frankel, R. (1998a). Iron sulfides from magnetotactic bacteria: Structure, composition, and phase transitions. *Am. Mineral.* **83**: 1469-1481.

Pósfai, M., Buseck, P. R., Bazylinski, D. and Frankel, R. (1998b). Reaction sequence of iron sulfide minerals in bacteria and their use as biomarkers. *Science* **280**: 880-883.

Quinlan, A., Murat, D., Vali, H. and Komeili, A. (2011). The HtrA/DegP family protease MamE is a bifunctional protein with roles in magnetosome protein localization and magnetite biomineralization. *Mol. Microbiol.* **80**: 1075–1087.

Raschdorf, O. (2011). *Diploma thesis*: Untersuchung der Funktion des *mamXY* Operons bei der Magnetosomenformation in *Magnetospirillum gryphiswaldense*. Ludwig-Maximilians-Universität, München.

Richter, M., Kube, M., Bazylinski, D., Lombardot, T., Glöckner, F., Reinhardt, R. and Schüler, D. (2007). Comparative genome analysis of four magnetotactic bacteria reveals a complex set of group-specific genes implicated in magnetosome biomineralization and function. *J. Bacteriol.* **189**: 4899-4910.

Rodionov, D., Gelfand, M., Todd, J., Curson, A. and Johnston, A. (2006). Computational reconstruction of iron- and manganese-responsive transcriptional networks in α-proteobacteria. *PLoS Comput. Biol.* **2**: 1568-1585.

Rong, C., Huang, Y., Zhang, W., Jiang, W., Li, Y. and Li, J. (2008). Ferrous iron transport protein B gene (*feoB1*) plays an accessory role in magnetosome formation in *Magnetospirillum gryphiswaldense* strain MSR-1. *Res. Microbiol.* **159**: 530-536.

Rosch, J. W., Gao, G., Ridout, G., Wang, Y.-D. and Tuomanen, E. I. (2009). Role of the manganese efflux system *mntE* for signalling and pathogenesis in *Streptococcus pneumoniae*. *Mol. Microbiol.* **72**: 12-25.

Scheffel, A., Gärdes, A., Grünberg, K., Wanner, G. and Schüler, D. (2008). The major magnetosome proteins MamGFDC are not essential for magnetite biomineralization in *Magnetospirillum gryphiswaldense* but regulate the size of magnetosome crystals. *J. Bacteriol.* **190**: 377-386.

Scheffel, A., Gruska, M., Faivre, D., Linaroudis, A., Graumann, P. L., Plitzko, J. and Schüler, D. (2006). An acidic protein aligns magnetosomes along a filamentous structure in magnetotactic bacteria. *Nature* **440**: 110-114.

Scheffel, A. and Schüler, D. (2007). The acidic repetitive domain of the *Magnetospirillum gryphiswaldense* MamJ protein displays hypervariability but is not required for magnetosome chain assembly. *J. Bacteriol.* **189**: 6437-6446.

Schleifer, K. H., Schüler, D., Spring, S., Weizenegger, M., Amann, R., Ludwig, W. and Köhler, M. (1991). The genus *Magnetospirillum* gen. nov., description of *Magnetospirillum gryphiswaldense* sp. nov. and transfer of *Aquaspirillum magnetotacticum* to *Magnetospirillum magnetotacticum* comb. nov. *Syst. Appl. Microbiol.* **14**: 379-385.

Schübbe, S., Kube, M., Scheffel, A., Wawer, C., Heyen, U., Meyerdierks, A., Madkour, M. H., Mayer, F., Reinhardt, R. and Schüler, D. (2003). Characterization of a spontaneous nonmagnetic mutant of *Magnetospirillum gryphiswaldense* reveals a large deletion comprising a putative magnetosome island. *J. Bacteriol.* **185**: 5779-5790.

Schübbe, S., Würdemann, C., Peplies, J., Heyen, U., Wawer, C., Glöckner, F. O. and Schüler, D. (2006). Transcriptional organization and regulation of magnetosome operons in *Magnetospirillum gryphiswaldense*. *Appl. Environ. Microbiol.* **72**: 5757-5765.

Schüler, D. (1994). *Doctoral thesis*: Isolierung und Charakterisierung magnetischer Bakterien - Untersuchungen zur Magnetitbiomineralisation in *Magnetospirillum gryphiswaldense*. Technische Universität, München.

Schüler, D. (2002). The biomineralisation of magnetosomes in *Magnetospirillum gryphiswaldense*. *Int. Microbiol.* **5**: 209-214.

Schüler, D. (2004). Molecular analysis of a subcellular compartment: The magnetosome membrane in *Magnetospirillum gryphiswaldense*. *Arch. Microbiol.* **181**: 1-7.

Schüler, D. and Baeuerlein, E. (1996). Iron-limited growth and kinetics of iron uptake in *Magnetospirilum gryphiswaldense*. *Arch. Microbiol.* **166**: 301-307.

Schüler, D. and Baeuerlein, E. (1998). Dynamics of iron uptake and Fe_3O_4 biomineralization during aerobic and microaerobic growth of *Magnetospirillum gryphiswaldense*. *J. Bacteriol.* **180**: 159-162.

Schüler, D. and Köhler, M. (1992). The isolation of a new magnetic spirillum. *Zentralbl. Mikrobiol.* **147**: 150-151.

Schultheiss, D., Kube, M. and Schüler, D. (2004). Inactivation of the flagellin gene *flaA* in *Magnetospirillum gryphiswaldense* results in nonmagnetotactic mutants lacking flagellar filaments. *Appl. Environ. Microbiol.* **70**: 3624-3631.

Schultheiss, D. and Schüler, D. (2003). Development of a genetic system for *Magnetospirillum gryphiswaldense*. *Arch. Microbiol.* **179**: 89-94.

Shi, W. and Chance, M. R. (2011). Metalloproteomics: forward and reverse approaches in metalloprotein structural and functional characterization. *Curr. Opin. Chem. Biol.* **15**: 144-148.

Shi, W., Zhan, C., Ignatov, A., Manjasetty, B. A., Marinkovic, N., Sullivan, M., Huang, R. and Chance, M. R. (2005). Metalloproteomics: High-throughput structural and functional annotation of proteins in structural genomics. *Structure* **13**: 1473-1486.

Simmons, S. L., Bazylinski, D. A. and Edwards, K. J. (2007). Population dynamics of marine magnetotactic bacteria in a meromictic salt pond described with qPCR. *Environ. Microbiol.* **9**: 2162-2174.

Smith, M. J., Sheehan, P. E., Perry, L. L., O'Connor, K., Csonka, L. N., Applegate, B. M. and Whitman, L. J. (2006). Quantifying the magnetic advantage in magnetotaxis. *Biophys. J.* **91**: 1098-1107.

Sparks, N. H. C., Courtaux, L., Mann, S. and Board, R. G. (1986). Magnetotactic bacteria are widely distributed in sediments in the UK. *FEMS Microbiol. Lett.* **37**: 305-308.

Sparks, N. H. C., Mann, S., Bazylinski, D. A., Lovley, D. R., Jannasch, H. W. and Frankel, R. B. (1990). Structure and morphology of magnetite anaerobically-produced by a marine magnetotactic bacterium and a dissimilatory iron-reducing bacterium. *Earth Planet. Sci. Lett.* **98**: 14-22.

Spring, S., Amann, R., Ludwig, W., Schleifer, K., van Gemerden, H. and Petersen, N. (1993). Dominating role of an unusual magnetotactic bacterium in the microaerobic zone of a freshwater sediment. *Appl. Environ. Microbiol.* **50**: 2397-2403.

Staniland, S., Ward, B., Harrison, A., Van der Laan, G. and Telling, N. (2007). Rapid magnetosome formation shown by real-time x-ray magnetic circular dichroism. *Proc. Natl. Acad. Sci. U.S.A.* **104**: 19524-19528.

Suzuki, T., Okamura, Y., Calugay, R. J., Takeyama, H. and Matsunaga, T. (2006). Global gene expression analysis of iron-inducible genes in *Magnetospirillum magneticum* AMB-1. *J. Bacteriol.* **188**: 2275-2279.

Tanaka, M., Okamura, Y., Arakaki, A., Tanaka, T., Takeyama, H. and Matsunaga, T. (2006). Origin of magnetosome membrane: Proteomic analysis of magnetosome membrane and comparison with cytoplasmic membrane. *Proteomics* **6**: 5234-5247.

Thomas-Keprta, K. L., Bazlinski, D. A., Kirschvink, J. L., Clemett, S. J., McKay, D. S., Wentworth, S. J., Vali, H., Gibson Jr., E. K. and Romanek, C. S. (2000). Elongated prismatic crystals in AL84001 carbonate globules : Potential Martian Magnetofossils. *Geochim. Cosmochim. Acta* **64**: 4049-4081.

Towe, K. and Moench, T. (1981). Electron-optical characterization of bacterial magnetite. *Earth Plan. Sci. Lett.* **52**: 213-220.

Uebe, R., Henn, V. and Schüler, D. (2011a). The MagA protein of magnetospirilla is not involved in bacterial magnetite biomineralization. *J. Bacteriol.* In press.

Uebe, R., Junge, K., Henn, V., Poxleitner, G., Katzmann, E., Plitzko, J. M., Zarivach, R., Kasama, T., Wanner, G., Pósfai, M., Böttger, L., Matzanke, B. and Schüler, D. (2011b). The cation diffusion facilitator proteins MamB and MamM of *Magnetospirillum gryphiswaldense* have distinct and complex functions, and are

involved in magnetite biomineralization and magnetosome membrane assembly. *Mol. Microbiol.* **82**: 818–835.

Uebe, R., Voigt, B., Schweder, T., Albrecht, D., Katzmann, E., Lang, C., Böttger, L., Matzanke, B. and Schüler, D. (2010). Deletion of a *fur*-like gene affects iron homeostasis and magnetosome formation in *Magnetospirillum gryphiswaldense*. *J. Bacteriol.* **192**: 4192-4204.

Ullrich, S., Kube, M., Schübbe, S., Reinhardt, R. and Schüler, D. (2005). A hypervariable 130-kilobase genomic region of *Magnetospirillum gryphiswaldense* comprises a magnetosome island which undergoes frequent rearrangements during stationary growth. *J. Bacteriol.* **187**: 7176-7184.

Ullrich, S. and Schüler, D. (2010). Cre-*lox*-based method for generation of large deletions within the genomic magnetosome island of *Magnetospirillum gryphiswaldense*. *Appl. Environ. Microbiol.* **76**: 2439-2444.

Vali, H. and Kirschvink, J. L. (1991). Observations of magnetosome organization, surface structure, and iron biomineralization of undescribed magnetic bacteria: evolutionary speculations. In: *Iron biominerals*. R. B. Frankel and R. P. Blakemore (ed.). Plenum Press, New York.

Weinberg, E. D. (1997). The *Lactobacillus* anomaly: total iron abstinence. *Perspect. Biol. Med.* **40**: 578-583.

Winterbourn, C. C. (1995). Toxicity of iron and hydrogen peroxide: the Fenton reaction. *Toxicol. Lett.* **82-83**: 969-974.

Xia, M., Wei, J., Lei, Y. and Ying, L. (2007). A novel ferric reductase purified from *Magnetospirillum gryphiswaldense* MSR-1. *Curr. Microbiol.* **55**: 71-75.

Yamamoto, D., Taoka, A., Uchihashi, T., Sasaki, H., Watanabe, H., Ando, T. and Fukumori, Y. (2010). Visualization and structural analysis of the bacterial magnetic organelle magnetosome using atomic force microscopy. *Proc. Natl. Acad. Sci. U.S.A.* **107**: 9382-9387.

Yamazaki, T., Oyanagi, H., Fujiwara, T. and Fukumori, Y. (1995). Nitrite reductase from the magnetotactic bacterium *Magnetospirillum magnetotacticum* - a novel cytochrome cd_1 with Fe(II): nitrite oxidoreductase activity. *Eur. J. Biochem.* **233**: 665-671.

Yang, W., Li, R., Peng, T., Zhang, Y., Jiang, W., Li, Y. and Li, J. (2010). *mamO* and *mamE* genes are essential for magnetosome crystal biomineralization in *Magnetospirillum gryphiswaldense* MSR-1. *Res. Microbiol.* **161**: 701-705.

Zeytuni, N., Ozyamak, E., Ben-Harush, K., Davidov, G., Levin, M., Gat, Y., Moyal, T., Brik, A., Komeili, A. and Zarivach, R. (2011). Self-recognition mechanism of MamA, a magnetosome-associated TPR-containing protein, promotes complex assembly. *Proc. Natl. Acad. Sci. U.S.A.* **108**: E480-E487.

CHAPTER 2

Deletion of a *fur*-like gene affects iron homeostasis and magnetosome formation in *Magnetospirillum gryphiswaldense*

2.1 Abstract

Magnetotactic bacteria synthesize specific organelles, the magnetosomes, which are membrane-enveloped crystals of the magnetic mineral magnetite (Fe_3O_4). The biomineralization of magnetite involves the uptake and intracellular accumulation of large amounts of iron. However, it is not clear how iron uptake and biomineralization are regulated and balanced with the biochemical iron requirement and intracellular homeostasis. In this study, we identified and analyzed a homologue of the ferric uptake regulator Fur in *Magnetospirillum gryphiswaldense*, which was able to complement a *fur* mutant of *Escherichia coli*. A *fur* deletion mutant of *M. gryphiswaldense* biomineralized fewer and slightly smaller magnetite crystals than did the wild type. Although the total cellular iron accumulation of the mutant was decreased due to reduced magnetite biomineralization, it exhibited an increased level of free intracellular iron, which was bound mostly to a ferritin-like metabolite that was found significantly increased in Mössbauer spectra of the mutant. Compared to that of the wild type, growth of the *fur* mutant was impaired in the presence of paraquat and under aerobic conditions. Using a Fur titration assay and proteomic analysis, we identified constituents of the Fur regulon. Whereas the expression of most known magnetosome genes was unaffected in the *fur* mutant, we identified 14 proteins whose expression was altered between the mutant and the wild type, including five proteins whose genes constitute putative iron uptake systems. Our data demonstrate that Fur is a regulator involved in global iron homeostasis, which also affects magnetite biomineralization, probably by balancing the competing demands for biochemical iron supply and magnetite biomineralization.

2.2 Introduction

Iron is an essential element for almost all bacteria, since iron-loaded metalloenzymes are integral parts of important biological pathways and processes like respiration, photosynthesis, N_2 fixation, methanogenesis, and DNA synthesis (Andrews *et al.*, 2003). Beside being indispensable, iron can be toxic in excess due to its ability to catalyze the production of highly deleterious oxygen species via the Fenton reaction (Winterbourn, 1995). Therefore, bacteria have to control their intracellular iron concentration in response to external iron availability. Iron homeostasis is typically controlled by iron-responsive transcriptional regulators, such as the ferric uptake regulator (Fur), which is the global regulator of iron metabolism in *Escherichia coli* (McHugh *et al.*, 2003). Fur serves as a sensor of intracellular iron concentration, and the regulation of gene expression by Fur proceeds via binding of a Fe^{2+}-bound Fur dimer to an operator site in the promoter region of the regulated genes, thereby repressing transcription. In *E. coli*, this operator site consists of a 19-bp palindromic consensus sequence termed the "iron box" (de Lorenzo *et al.*, 1987). Since Fur homologues can be found in a variety of Gram-negative and Gram-positive bacteria, a general mechanism for iron-responsive regulation has been suggested (Escolar *et al.*, 1999). However, work with other bacteria showed deviations from the classical model of Fur with respect to metal selectivity and biological functions. For example, several members of the Fur family of metalloregulators exhibit functional specialization (Lee and Helmann, 2007), including responsiveness to zinc (Zur (Patzer and Hantke, 1998)), nickel (Nur (Ahn *et al.*, 2006)), manganese (Mur (Platero *et al.*, 2004)), peroxide (PerR (Bsat *et al.*, 1998)), and heme (Irr (Yang *et al.*, 2006)). Several bacteria possess global iron regulators that share no homology to regulators of the Fur family, including DtxR-like transcriptional regulators (IdeR) (Tao *et al.*, 1994) and the RirA protein (Todd *et al.*, 2005). Some alphaproteobacteria, which comprise the majority of cultivated magnetotactic bacteria (MTB), differ considerably from well-studied systems like *E. coli* or *Pseudomonas aeruginosa* with respect to the regulation of their iron metabolism (Rudolph *et al.*, 2006; Johnston *et al.*, 2007).

In addition to their biochemical iron requirement, MTB accumulate large amounts of iron for the synthesis of magnetosomes, which are specific intracellular organelles for magnetic navigation that are aligned in chains (Jogler and Schüler, 2009). Individual magnetosome crystals are composed of magnetite (Fe_3O_4) and enveloped by the magnetosome membrane (MM), which invaginates from the cytoplasmic membrane (Komeili *et al.*, 2006; Katzmann *et al.*, 2010) and consists of phospholipids and a set of specific proteins (Grünberg *et al.*, 2004).

The biomineralization of magnetosomes involves the uptake of large amounts of iron that may account for up to 4% of dry weight, its intracellular sequestration and crystallization (Faivre and Schüler, 2008). Although of central interest for the understanding of magnetite biomineralization, only few studies have addressed its connection with general iron metabolism and homeostasis of MTB. Early studies in the alphaproteobacterium *Magnetospirillum gryphiswaldense* demonstrated that magnetite biomineralization is tightly coupled to iron uptake (Baeuerlein and Schüler, 1995), which proceeds by a fast, energy-dependent mechanism (Schüler and Baeuerlein, 1996; Schüler and Baeuerlein, 1998). Recently, Rong *et al.* (2008) showed that the disruption of the ferrous iron transporter FeoB1 leads to a reduction of magnetosome size and number in *M. gryphiswaldense*, which suggested a link between general iron metabolism and magnetosome biomineralization, although distinct pathways for magnetite formation and biochemical iron uptake were suggested by Faivre *et al.* (2007).

Due to the toxicity of iron, there is a strong need for MTB to sustain a strict iron homeostasis. However, it is not clear how iron uptake and storage are regulated and balanced with the biochemical iron requirement and biomineralization. In *M. gryphiswaldense*, transcription of several magnetosome genes (*mamGFDC* and *mms6*) was increased in the presence of iron (Schübbe *et al.*, 2006), indicating a regulatory effect of iron at the transcription level. Using a bioinformatic approach, Rodionov *et al.* predicted regulons of the putative iron-responsive regulators Fur and Irr in *M. magneticum* and *M. magnetotacticum* (Rodionov *et al.*, 2006). In contrast to other alphaproteobacteria, such as the *Rhizobiaceae*, in these MTB a generic Fur protein was predicted to be the major global iron-responsive regulator, whereas Irr seems to have limited importance, regulating just single genes (Rodionov *et al.*, 2006). However, an extension of the Fur regulon of other alphaproteobacteria was noted in *M. magneticum* and *M. magnetotacticum*, where in addition to multiple iron uptake genes, candidate Fur sites were observed upstream of genes related to magnetosome formation, such as *mamGFDC* and *mms6*. The hypothesis that Fur might be involved in the regulation of magnetosome biomineralization was further substantiated by the observed colocalization of *fur* homologues with magnetosome genes in *M. magneticum* and *M. magnetotacticum* as well as some uncultivated MTB (Jogler *et al.*, 2009). However, despite these indications for a putative role of Fur in controlling both iron homeostasis and magnetite synthesis, the mode of predicted iron regulation has remained unknown, since experimental analysis has been hampered by difficulties in genetic analysis of MTB.

In this study, we started to investigate components of general iron metabolism and their contribution to magnetite biomineralization in *M. gryphiswaldense* by the deletion of an identified *fur*-like gene. Subsequent analysis of intracellular iron metabolites and expression profiles in mutant and wild-type (WT) cells demonstrates that Fur is a global iron-responsive regulator in *M. gryphiswaldense* that also affects magnetosome biomineralization.

2.3 Materials and Methods

2.3.1 Bacterial strains and growth conditions

Bacterial strains and plasmids are described in Table 2-1.

Table 2-1. Bacterial strains and plasmids used in this study

Strain or plasmid	Important feature(s)	Source or reference
Strains		
E. coli		
DH5α	F' Φ80d*lac* ΔM15 Δ(*lacZYA-argF*)U169 *deo*R *rec*A1 *end*A1	Invitrogen
BW29427	*thrB1004 pro thi rpsL hsdS lacZ*ΔM15 RP4-1360 Δ(*araBAD*)567 Δ*dapA1341::[erm pir* (wt)]	Datsenko, K. and Wanner B. L. (unpublished)
H1717	*fhuF*::lp*lac*Mu53	(Hantke, 1987)
H1780	*fiu*::lp*lac*Mu53 *fur*	(Hantke, 1987)
M. gryphiswaldense		
R3/S1	Wild type, but Rif^r Sm^r	(Schultheiss *et al.*, 2005)
MSR1-B	Spontaneous non magnetic mutant of MSR-1	(Schübbe *et al.*, 2003)
RU-1	R3/S1+ Δ*fur*	This study
M. magneticum		
AMB-1	Wild type	(Kawaguchi *et al.*, 1992)
Plasmids		
pGEM-T easy	Cloning vector; Amp^r	Promega
pGEMPmamDC	pGEM-T easy + P_{mamDC}	This study
pGEMPmamAB	pGEM-T easy + P_{mamAB}	This study
pGEMPmms16	pGEM-T easy + P_{mms16}	This study
pGEMPrplK	pGEM-T easy + P_{rplK}	This study
pGEMPfhuF	pGEM-T easy + P_{fhuF}	This study
pGEMPmgr4079	pGEM-T easy + $P_{mgr4079}$	This study
pGEMfurup	pGEM-T easy + *fur* 2 kb upstream region	This study
pGEMfurdown	pGEM-T easy + *fur* 2 kb downstream region	This study
pJET1.2/blunt	Cloning vector; Amp^r	Fermentas
pJETEcfur	pJET1.2/blunt + *fur* from *E. coli*	This study
pJETamb1009	pJET1.2/blunt + *amb1009* from *M. magneticum*	This study
pJETamb4460	pJET1.2/blunt + *amb4460* from *M. magneticum*	This study
pJETmgr1314	pJET1.2/blunt + *mgr1314* from *M. gryphiswaldense*	This study
pBBR1MCS-2	Mobilizable broad-host-range vector; Km^r	(Kovach *et al.*, 1995)
pBBR1MCS-2fur	pBBR1MCS-2 containing *fur*	This study
pBBR1MCS-5	Mobilizable broad-host-range vector; Gm^r	(Kovach *et al.*, 1995)
pBBRPtet	Mobilizable broad-host-range vector; Km^r, + P*tet*	Lang, C. (unpublished)
pBBR1MCS-5Ptet	Mobilizable broad-host-range vector; Gm^r, + P*tet*	This study
pBBR1MCS-5Ptet/Ecfur	pBBR1MCS5Ptet with *fur* from pJETEcfur	This study
pBBR1MCS-5Ptet/amb1009	pBBR1MCS5Ptet with *fur* from pJETamb1009	This study
pBBR1MCS-5Ptet/amb4460	pBBR1MCS5Ptet with *fur* from pJETamb4460	This study
pBBR1MCS-5Ptet/mgr1314	pBBR1MCS5Ptet with *fur* from pJETmgr1314	This study
pCM184	Broad-host-range allelic exchange vector	(Marx and Lidstrom, 2002)
pCM184furup	pCM184 with 2 kb fragment from pGEMfurup	This study
pCM184Δfur	pCM184furup with 2 kb fragment from pGEMfurdown	This study

E. coli strains were routinely grown in lysogeny broth (LB) (Bertani, 1951) supplemented with gentamycin (15 µg ml^{-1}), kanamycin (25 µg ml^{-1}), or ampicillin (50 µg ml^{-1}) at 37°C with vigorous shaking (200 rpm). For cultivation of strain BW29427, LB was supplemented with DL-α,ε-diaminopimelic acid to 1 mM. *M. gryphiswaldense* strains were grown in modified flask standard medium (FSM) with 50 µM ferric citrate (Heyen and Schüler, 2003) or in low-iron medium (LIM) (Faivre *et al.*, 2008) supplemented with 10 µM iron chelator 2,2'-dipyridyl, unless specified otherwise. Cultivation was carried out at 30°C with moderate agitation (120 rpm) under aerobic, microaerobic, or anaerobic conditions in 1-liter flasks containing 100 ml medium. For aerobic cultivation, cells were incubated in free gas exchange with air. To generate microaerobic conditions, flasks were sealed before autoclaving with butyl-rubber stoppers under a microaerobic gas mixture containing 2% O_2 and 98% N_2. For anaerobic conditions, O_2 was omitted from the gas mixture. When necessary, media were supplemented with kanamycin (5 µg ml^{-1}).

2.3.2 Molecular and genetic techniques

Unless specified otherwise, molecular techniques were performed using standard protocols (Sambrook and Russel, 2001). DNA was sequenced using BigDye terminator v3.1 chemistry on an ABI 3700 capillary sequencer (Applied Biosystems, Darmstadt, Germany). Sequence data were analyzed using 4Peaks software (http://mekentosj.com/4peaks). All oligonucleotide primers (Table S2-1) were purchased from Sigma-Aldrich (Steinheim, Germany).

2.3.3 Isolation of total RNA and qualitative reverse transcriptase-PCR (RT-PCR)

For isolation of total cellular RNA, *M. gryphiswaldense* was grown in 100 ml LIM under microaerobic and anaerobic conditions as well as in FSM supplemented with 100 µM $FeCl_2$ or $MnCl_2$ under microaerobic conditions to mid-logarithmic growth phase. Cells were harvested and washed in 1 ml of phosphate-buffered saline (150 mM NaCl, 10 mM sodium phosphate, pH 7), and total RNA was isolated using an RNeasy Mini kit (Qiagen) according to the manufacturer's instructions. Isolated RNA was incubated with 10 U of RNase-free DNase I (MBI Fermentas, St. Leon Roth, Germany) for 30 min at 37°C and quantified by spectrophotometric measurements using an ND-1000 spectrophotometer (NanoDrop

Technologies, DE). cDNA was synthesized from RNA templates using random hexamer primers (Roche) and RevertAid H Minus M-MuLV reverse transcriptase (Fermentas) according to the manufacturer's instructions. Transcription of *fur* was monitored by PCR using the primers mgr1314fwRT and mgr1314revRT (see Table S1 in the supplemental material).

2.3.4 Fur Titration Assay (FURTA)

Putative promoter regions P_{mamDC}, P_{mamAB}, P_{mms16}, $P_{mgr4079}$, and P_{rplK} were PCR amplified with *Taq* polymerase (Fermentas) from genomic DNA of *M. gryphiswaldense* R3/S1. The Fur-regulated promoter P_{fhuF} was amplified from whole cells of *E. coli* DH5α. The resulting PCR fragments were 200 to 400 bp long and included the intergenic region upstream from the start codon to the next open reading frame. The PCR products were cloned into pGEM-T Easy, sequenced, and transformed into *E. coli* H1717. For examination of Fur regulation, plasmid-carrying *E. coli* H1717 strains were streaked on MacConkey lactose agar supplemented with ampicillin and 100 μM 2,2'-dipyridyl or 30 μM $FeCl_3$ and cultivated overnight at 37°C.

2.3.5 Heterologous transcomplemention of an *E. coli fur* mutant

For expression of Fur-like proteins, a 1.9-kb NcoI/SacI fragment from pBBR1Ptet bearing an anhydrotetracycline-inducible promoter was inserted into pBBR1MCS-5, which had been cut with the same restriction enzymes to generate pBBR1MCS-5Ptet. *fur*-like genes from *M. gryphiswaldense* and *M. magneticum* as well as *fur* from *E. coli* were PCR amplified with *Taq* polymerase (Fermentas) using primers adding an NdeI restriction site on the 5' end and a SacI restriction site on the 3' end of the corresponding gene (see Table S1 in the supplemental material). PCR products were ligated into a pJET1.2/blunt cloning vector using a CloneJET PCR cloning kit (Fermentas) according to the manufacturer's recommendations. Subsequently, the genes were cloned into pBBR1MCS-5Ptet using the restriction sites NdeI and SacI. The resulting plasmids were transformed into strain H1780. For transcomplementation analysis, plasmid-carrying strains were grown in LB supplemented with gentamicin under iron-replete (100 μM $FeCl_2$) and iron-depleted (200 μM 2,2'-dipyridyl) conditions to early log phase, induced by the addition of anhydrotetracycline at a final

concentration of 100 ng/ml, and incubated for another 2 to 3 h at 37°C. Determination of ß-galactosidase activity was carried out as described previously (Miller, 1972).

2.3.6 Generation of a *fur* deletion strain

A two-step, *cre-lox*-based method was used to generate an unmarked deletion of *fur* (Marx and Lidstrom, 2002). For the generation of an unmarked *M. gryphiswaldense fur* mutant, 2-kb fragments of the up- and downstream regions of Mg*fur* (*M. gryphiswaldense* Mgr1314; see Results) were amplified by PCR using Phusion polymerase (NEB) (for primers, see Table S1 in the supplemental material), cloned into pGEM-T Easy, and sequenced. Vector pGEMfurup was digested with MunI and NotI. The resulting 2-kb fragment was inserted into MunI/NotI-digested pCM184 to yield pCM184furup. Subsequently, pGEMfurdown and pCM184furup were digested with AgeI. The resulting 2-kb fragment from pGEMfurdown was then ligated into pCM184furup to yield pCM184Δfur. After verification of the correct orientation of the deletion construct by PCR, pCM184Δfur was transferred to *M. gryphiswaldense* R3/S1 by conjugation as described previously (Schultheiss and Schüler, 2003). Putative kanamycin-resistant *fur* mutants were isolated on LIM agar after incubation for 10 days at 30°C and 1% O_2 and analyzed by PCR. Correct genomic recombination could be verified in four of six candidate mutants by Southern blot analysis (see FIG. S1 in the supplemental material). One of them was subjected to conjugation with pCM157, a plasmid coding for Cre recombinase. After two passages in FSM, we found two clones that were no longer kanamycin resistant, due to the excision of the *loxP* site-flanked kanamycin resistance marker by Cre recombinase. One clone was cured from the *cre* expression plasmid pCM157 by repeated passaging in fresh FSM and was designated RU-1.

2.3.7 Analytical methods

Iron concentrations were determined by a modified version (Viollier *et al.*, 2000) of the ferrozine assay (Stookey, 1970) or by using a flame atomic absorption spectrometer (FAAS) (model AA240; Varian). For determination of iron content, cell pellets were washed in 20 mM Tris-HCl, 5 mM EDTA, pH 7.4, and digested as described previously (Heyen and Schüler, 2003). Transmission electron microscopy (TEM) analyses were performed as described previously (Jogler *et al.*, 2009). Siderophore production was monitored by a modified chrome azurol S (CAS) agar plate assay (Milagres *et al.*, 1999), and culture

supernatants were measured using a CAS decoloration assay as previously described (Schwyn and Neilands, 1987). Protein concentrations were measured with a bicinchoninic protein quantification kit (Sigma, Munich, Germany) according to the manufacturer's instructions. The average magnetic orientation of cell suspensions (C_{mag}) was assayed as previously described (Schüler *et al.*, 1995). Briefly, cells were aligned at different angles relative to a light beam by means of an external magnetic field. The ratio of the resulting maximum and minimum scattering intensities (C_{mag}) is correlated with the average number of magnetic particles and can be used for a qualitative assessment of magnetite formation.

2.3.8 Transmission Mössbauer Spectroscopy (TMS)

For the determination of intracellular iron metabolites, microaerobic precultures (100 ml) of *M. gryphiswaldense* WT and RU-1 were grown in iron-replete FSM. The *fur* mutant was alternatively precultured in LIM supplemented with 10 µM 2,2'-dipyridyl. After three passages in the corresponding medium, all cultures were transferred to fresh FSM. RU-1 was grown in microaerophilic 1-liter batch cultures supplemented with a mixture of 20 µM $^{57}Fe(citrate)_2$ and 20 µM $^{56}Fe(citrate)_2$. Cells of *M. gryphiswaldense* WT were incubated with 20 µM $^{57}Fe(citrate)_2$ in an oxystat fermentor under defined microaerophilic conditions using a modified protocol of large-scale cultivation of *M. gryphiswaldense* (Heyen and Schüler, 2003).

For TMS, cells were harvested by centrifugation at 4,700 rpm and 4°C. Pellets were washed, weighed, transferred into Delrin Mössbauer sample holders, frozen in liquid nitrogen, and kept at this temperature until measurement. TMS was performed in constant acceleration mode. The spectrometer was calibrated against α-iron at room temperature. Samples were measured in a continuous-flow cryostat (Oxford Instruments) above the Verwey transition of magnetite at 130 K. The ^{57}Co source exhibiting an activity of 0.19 GBq was sealed in an Rh matrix at room temperature and was mounted on a constant velocity drive. The detector consisted of a proportional counter filled with argon-methane (90:10). Spectral data were buffered in a multichannel analyzer and transferred to a personal computer for further analysis by employing the Vinda program on an Excel 2003 platform. Spectra were analyzed by least-square fits of Lorentzian line shapes to the experimental data (Gunnlaugsson, 2006).

2.3.9 Cell fractionation and preparation of protein extracts

For proteomic analysis, *M. gryphiswaldense* R3/S1 and RU-1 were grown in 100 ml iron-rich FSM (50 µM ferric citrate) or iron-depleted LIM plus 10 µM 2,2'-dipyridyl (<1 µM iron) under anaerobic conditions to log phase in nine parallels. All parallels of each condition were pooled, and cells were pelleted at 9,200 x *g*, washed (20 mM Tris-HCl, pH 7.4, 5 mM EDTA), and resuspended into ice-cold 20 mM Tris-HCl, 1 mM EDTA, 0.1 mM phenylmethylsulfonyl fluoride, pH 7.4. Cell suspensions were lysed by three passages through a French press, and cellular debris was removed by low-speed centrifugation. Cleared cell lysates were subjected for 30 min to centrifugation at 265,000 x *g* to separate cellular membranes, magnetosomes, and empty magnetosome vesicles from the soluble protein fraction (Grünberg *et al.*, 2001). Pelleted membrane proteins were resuspended in 20 mM Tris-HCl, 1 mM EDTA, 0.1 mM phenylmethylsulfonyl fluoride, pH 7.4, 1% (w/v) sodium dodecyl sulfate (SDS). Nonmagnetic fractions were prepared by subjecting cell extracts to magnetic columns and sucrose cushion centrifugation using a protocol for the isolation of magnetosomes as described previously (Grünberg *et al.*, 2001), but omitting EDTA from buffers. All protein fractions were stored at –80°C until analysis.

2.3.10 2-D gel electrophoresis

For isoelectric focusing (IEF), protein extracts from the soluble fraction (500 µg protein) were loaded onto commercially available immobilized pH gradient (IPG) strips (pH 3-10 NL; Amersham Biosciences) according to the method of Büttner et al. (Büttner *et al.*, 2001). In the second dimension, polyacrylamide gels of 12.5% acrylamide and 2.6% bisacrylamide were used. The resulting two-dimensional (2D) gels were stained with colloidal Coomassie brilliant blue (CBB) as described previously (Voigt *et al.*, 2004).

2.3.11 Protein digestion, mass spectrometry and data analysis

Spots were cut from the 2D gels and transferred into microtiter plates. Proteins were tryptically digested using an Ettan spot handling workstation (GE Healthcare). Mass spectra of the protein fragments were measured by matrix-assisted laser desorption ionization-time of flight tandem mass spectrometry (MALDI-TOF-MS-MS) using a proteome analyzer 4800 (Applied Biosystems). The parameters for the measurements were set as described previously (Voigt *et al.*, 2006), except that the signal-to-noise ratio for the TOF-TOF measurements was

raised to 10. Proteins were identified by searching an *M. gryphiswaldense* databank with the Mascot search engine (search parameters are described in reference (Voigt *et al.*, 2006)). Differentially expressed proteins on the 2D gels were analyzed with Delta 2D software (Decodon, Greifswald, Germany) (Voigt *et al.*, 2006). For analysis of membrane proteins, 1D gel lanes were manually cut into 10 equal slices and the slices were digested with trypsin. Liquid chromatography (LC)-coupled mass spectrometry was performed as described previously (Wolff *et al.*, 2008). Ratios of identified peptide ion abundances higher than +2 or smaller than –2 were set as a threshold indicating significant changes.

2.3.12 Bioinformatics

The protein sequences of *E. coli* Fur (NCBI accession no. AP_001321.1), *Corynebacterium diphtheriae* DtxR (NCBI accession no. AAA23302.1), and *Rhizobium leguminosarum* RirA (NCBI accession no. YP_766387.1) were used as a query in BLAST searches of the genomes of *M. gryphiswaldense* WT, *M. magneticum* AMB-1, and *M. magnetotacticum* MS-1 using the BLASTP algorithm 2.2.16 (Altschul *et al.*, 1997) with a cutoff E value of $1e^{-05}$ or an amino acid similarity of >30%. Sequence alignments and construction of similarity trees were performed using MEGA4 software (Tamura *et al.*, 2007). Sequences were aligned by ClustalW (default settings), and similarity trees were constructed using the minimal evolution (ME) method (Rzhetsky and Nei, 1992). Fur-like proteins with NCBI accession numbers ZP_00208795.1, ZP_00052390.2, and ZP_00209401.1 present in the genome assembly of *M. magnetotacticum* MS-1 (NCBI accession no. AAAP00000000) were omitted from analyses, since the whole-genome sequence contigs on which the three proteins are found share no homology to other *Magnetospirillum* sequences but have almost 100% identity to *Methylobacterium* species or 80% identity to *Xylanimonas cellulosilytica* DSM 15894 and thus are likely to represent contaminations.

2.4 Results

2.4.1 Identification of a putative *fur* gene

Using *Corynebacterium diphtheriae* DtxR (NCBI accession no. AAA23302.1) and *R. leguminosarum* RirA (NCBI accession no. YP_766387.1) as queries in BLASTP analysis, we failed to detect homologs of the diphtheria toxin repressor family (DtxR) or the rhizobial iron regulator RirA in the genome of *M. gryphiswaldense*. However, BLASTP searches with *E. coli* Fur (NCBI accession no. AP_001321.1) yielded five hits with significant similarities (>30%) (see Table S2-2 in the supplemental material). Closer inspection of the five candidate Fur proteins revealed that they fall into three different subfamilies of the Fur superfamily (FIG. 2-1).

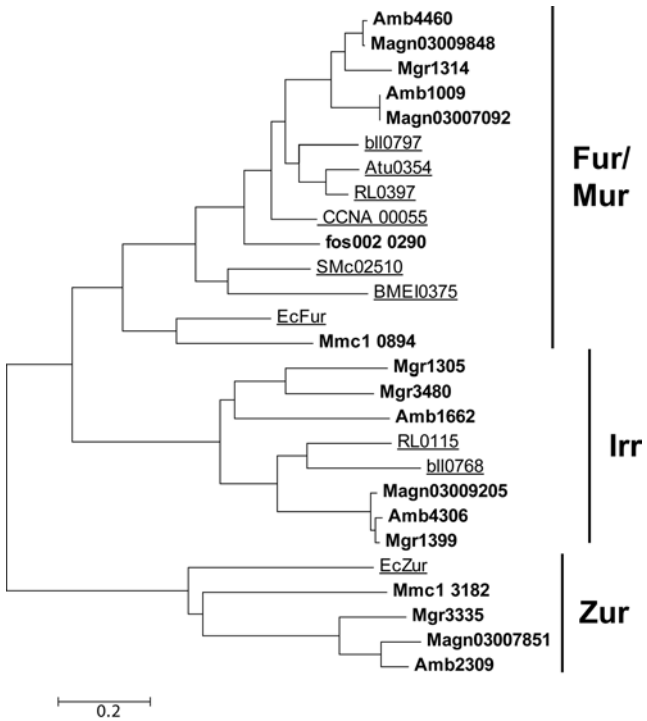

FIG. 2-1. Similarity tree of alphaproteobacterial and *E. coli* Fur-like proteins. Sequences are designated by locus tags. Fur-like proteins of MTB are shown in bold. Proteins that have been characterized experimentally are underlined. Locus tags refer to *M. gryphiswaldense* (Mgr1305, Mgr1314, Mgr1399, Mgr3335, and Mgr3480), *M. magneticum* (Amb1009, Amb1662, Amb2309, Amb4306, and Amb4460), *M. magnetotacticum* (Magn03007092, Magn03007851, Magn03009848, and Magn03009205), *Bradyrhizobium japonicum* (bll0768 and bll0797), *Agrobacterium tumefaciens* (Atu0354), *Rhizobium leguminosarum* (RL0115 and RL0397), *Caulobacter crescentus* (CCNA_00055), uncultured MTB (fos002_0290), *Sinorhizobium meliloti* (SMc02510), *Brucella melitensis* (BMEI0375), *E. coli* (EcFur and EcZur), and *Magnetococcus* sp. (Mmc1_0894 and Mmc1_3182). A more extended tree showing characterized and noncharacterized Fur-like proteins is shown in FIG. S2 in the supplemental material.

Three proteins (Mgr1305, Mgr1399, and Mgr3480) are more closely related to the Irr subfamily (Small *et al.*, 2009), whereas one protein (Mgr3335) belongs to the Zur family of putative Zn regulators (Althaus *et al.*, 1999). One single protein, Mgr1314, referred to herein

as *Mg*Fur, belongs to the Fur/Mur subfamily, which comprises genuine iron- and manganese-responsive regulators (Rodionov *et al.*, 2006). *Mgfur* is part of a putative polycistronic operon and is flanked upstream by a gene encoding a putative transcriptional regulator of the Ros/MucR family (Mgr1313) and downstream by a gene encoding a putative hemolysin-like protein (Mgr1315), as well as 13 additional genes that are transcribed in the same direction. *Mgfur* encodes a protein of 143 amino acid residues containing the highly conserved putative regulatory Fe-sensing site (i.e., S1) (Pohl *et al.*, 2003), consisting of amino acid residues H91, D93, E112, and H129, and the highly conserved structural Zn-binding site (i.e., S2), consisting of residues H37, E85, H94, and E105. RT-PCR analysis revealed that *Mgfur* was transcribed under all tested (i.e., iron-replete and -depleted) conditions (data not shown).

We found that, within the genus *Magnetospirillum*, Fur is well conserved with respect to sequence (see Table S3 in the supplemental material) as well as its genomic localization within a highly conserved 11-kb region. However, while *Mgfur* is present in a single copy in *M. gryphiswaldense*, a second copy (with 79% identity to Amb4460 and 73% identity to *Mg*Fur at the amino acid level) is present in the genomes of the closely related species *M. magneticum* and *M. magnetotacticum*. Notably, in the latter strains the second ortholog is associated with a partial duplication of the *mamAB* operon (region R9 (Murat *et al.*, 2010)), a 7-kb region which is absent from the genome of *M. gryphiswaldense*.

2.4.2 *Mg*Fur transcomplements an *E. coli fur* mutation

To test whether *Mg*Fur is a genuine iron-responsive regulator, the reporter strain *E. coli* H1780 was transcomplemented with pBBR1MCS-5Ptet, pBBR1MCS-5Ptet/amb1009, pBBR1MCS- 5Ptet/amb4460, pBBR1MCS-5Ptet/mgr1314, and pBBR1MCS-5Ptet/Ecfur, containing *fur* orthologs of *M. magneticum*, *M. gryphiswaldense*, and *E. coli* as a positive control. This strain harbors a *lacZ* reporter gene under the control of the promoter of the iron-regulated outer membrane protein gene *fiu*. Due to an undefined mutation of native *fur*, ß-galactosidase is constitutively expressed unless strain H1780 is transformed with plasmids containing a functional *fur* gene. Plasmids were transferred into *E. coli* H1780, and transformed strains were grown under iron-replete and iron-depleted conditions. ß-Galactosidase activities showed that *Mg*Fur and Fur proteins of *M. magneticum* AMB-1 and *E. coli* (*Ec*Fur) were able to bind to the *fiu* promoter and repress *lacZ* expression to similar extents under iron-replete conditions (FIG. 2-2).

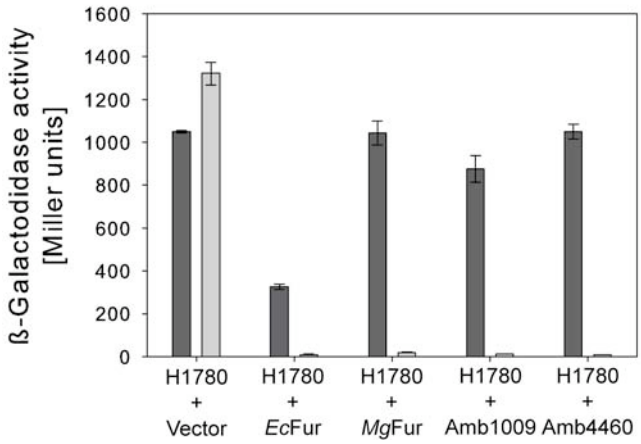

FIG. 2-2. ß-Galactosidase activities of the *fiu-lacZ* fusion strain H1780 harboring the indicated plasmids and grown in LB under iron-limiting (200 µM 2,2'-dipyridyl) (black bars) and iron-sufficient (100 µM $FeCl_3$) (gray bars) conditions. The assays were performed in triplicate, and values are expressed as the means, with standard deviations displayed as error bars.

ß-Galactosidase activity was highest under iron-depleted conditions in all tested strains, indicating that binding of Fur to the *fiu* promoter was iron dependent. Strain H1780 (pBBR1MCS-5Ptet/Ecfur) showed intermediate ß-galactosidase activities in the absence of iron, indicating that *Ec*Fur is able to repress *lacZ* expression without iron, similarly to results observed previously in several studies using high-copy-number plasmids for the expression of *Ec*Fur (Lowe *et al.*, 2001; Parker *et al.*, 2005). Regulation of *lacZ* in strain H1780 carrying an empty vector was the same irrespective of iron concentration, as ß-galactosidase activities were equally high under iron-replete and iron-depleted conditions. These results suggested that *Mg*Fur is functional in *E. coli*.

2.4.3 Generation and analysis of a *M. gryphiswaldense fur* mutant

To analyze whether *Mg*Fur has iron-responsive regulatory functions in *M. gryphiswaldense* as well and to clarify the role of Fur in the biomineralization of magnetosomes, an unmarked *fur* mutant strain of *M. gryphiswaldense* was constructed by a *cre-lox*-based method (Marx and Lidstrom, 2002), resulting in an unmarked in-frame deletion of *fur*. TEM analysis showed that the *fur* mutant strain RU-1 was still able to produce magnetosomes, although with diameters (28.6 ± 9.1 nm) and in numbers (40 ± 14.3 per cell) significantly reduced compared to those for the WT (46 ± 16.1 magnetosomes per cell and 30.6 nm ± 9.0 nm in diameter) (Mann-Whitney test; $P \leq 0.003$) (FIG. 2-3).

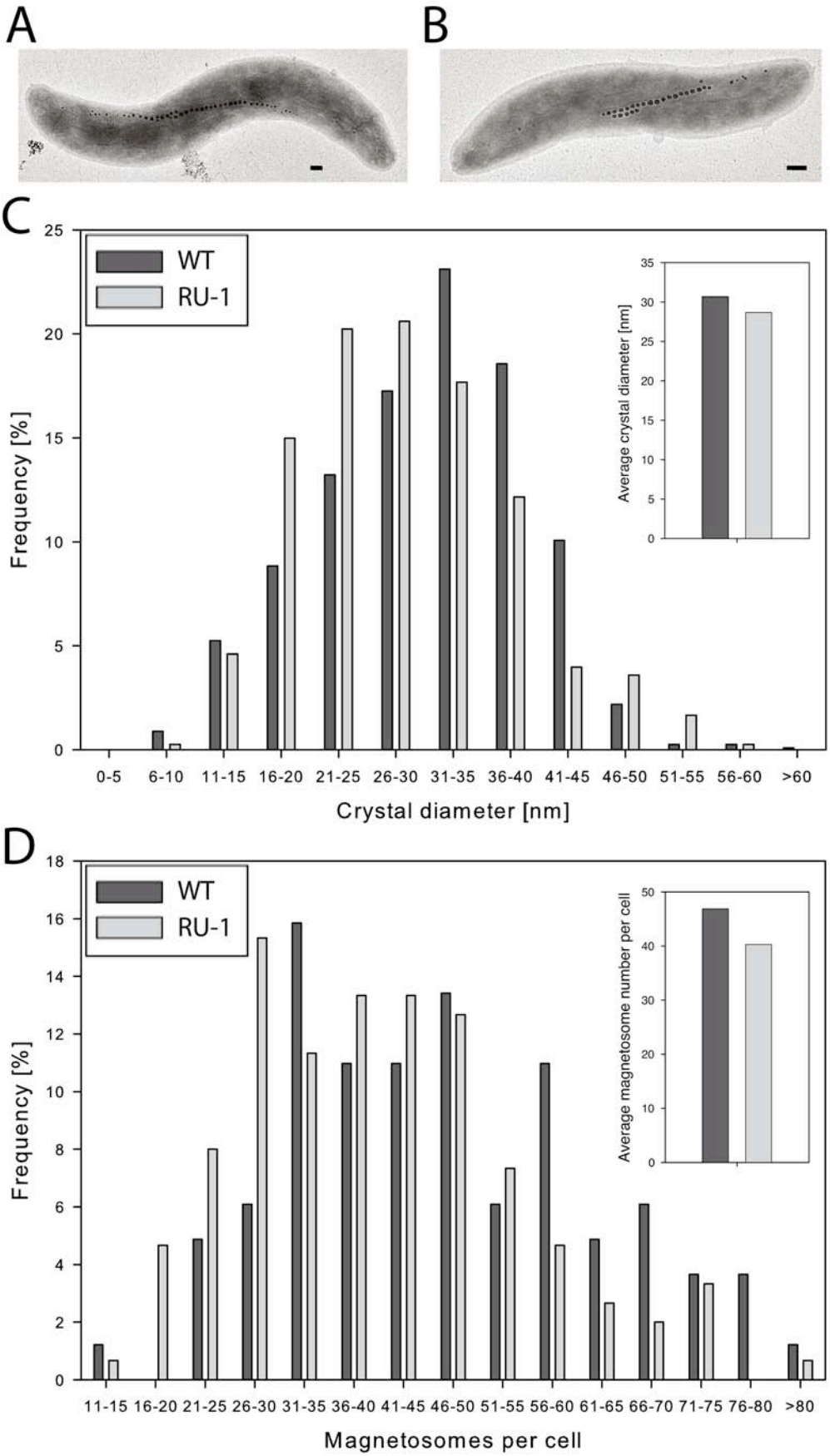

FIG. 2-3. Transmission electron micrographs of the WT (A) and RU-1 (B). Bar, 100 nm. (C) Magnetite crystal size distribution determined from 200 cells by TEM. (D) Distribution of magnetosome number per cell.

For further characterization, both strains were iron deprived by three passages in LIM supplemented with 10 µM 2,2'-dipyridyl, a medium supporting growth but not magnetite synthesis, until cellular magnetism was no longer detectable and subsequently inoculated into fresh LIM containing different iron concentrations to reinduce magnetite biomineralization. Under aerobic and anaerobic growth conditions, growth rates of the *fur* mutant were slightly lower than those of the WT, whereas under microaerobic conditions, RU-1 showed growth rates similar to those of the WT at all tested iron concentrations (Table 2-2).

Table 2-2. Growth rate (h^{-1}) and doubling time (in h) of WT and RU-1 grown under different oxygen and iron concentrations[a]

Strain	Parameter	Result[a] under the following culture conditions				
		2% O2 and:			0% O2 and	21% O2 and
		5 µM Fe citrate	50 µM Fe citrate	250 µM Fe citrate	50 µM Fe citrate	50 µM Fe citrate
WT	µ (h^{-1})	0.169 (± 0.010)	0.162 (± 0.001)	0.165 (± 0.010)	0.148 (± 0.015)	0.121 (± 0.013)
	t_D (h)	4.10 (± 0,24)	4.29 (± 0.02)	4.19 (± 0.26)	4.68 (± 0.68)	5.73 (± 0.60)
RU-1	µ (h^{-1})	0.167 (± 0.003)	0.158 (± 0.001)	0.149 (± 0.019)	0.124 (± 0.003)	0.090 (± 0.002)
	t_D (h)	4.16 (± 0.07)	4.40 (± 0.00)	4.64 (± 0.59)	5.60 (± 0.14)	7.70 (± 0.17)

[a] Values are the sample means of at least replicate cultures. Sample standard deviations are in parentheses

However, magnetosome formation in RU-1 became detectable by C_{mag} only about 3 h after that in the WT (FIG. 2-4B). This delay was also observed with increased extracellular concentrations of ferric citrate (250 µM) (FIG. 2-4D). When RU-1 was cultured under anaerobic conditions, no difference in time course of magnetite formation was observed (FIG. 2-4E). In addition, the maximal C_{mag} values that were reached by RU-1 were significantly smaller than those reached by the WT. These differences were most pronounced (RU-1 C_{mag} reached only 40% of WT C_{mag}) at low iron concentrations (5 µM). Although C_{mag} values of the *fur* mutant increased with extracellular iron concentration to up to 85% of the WT value with 250 µM ferric citrate and under anaerobic conditions, they never did reach WT levels under any condition tested (FIG. 2-4F).

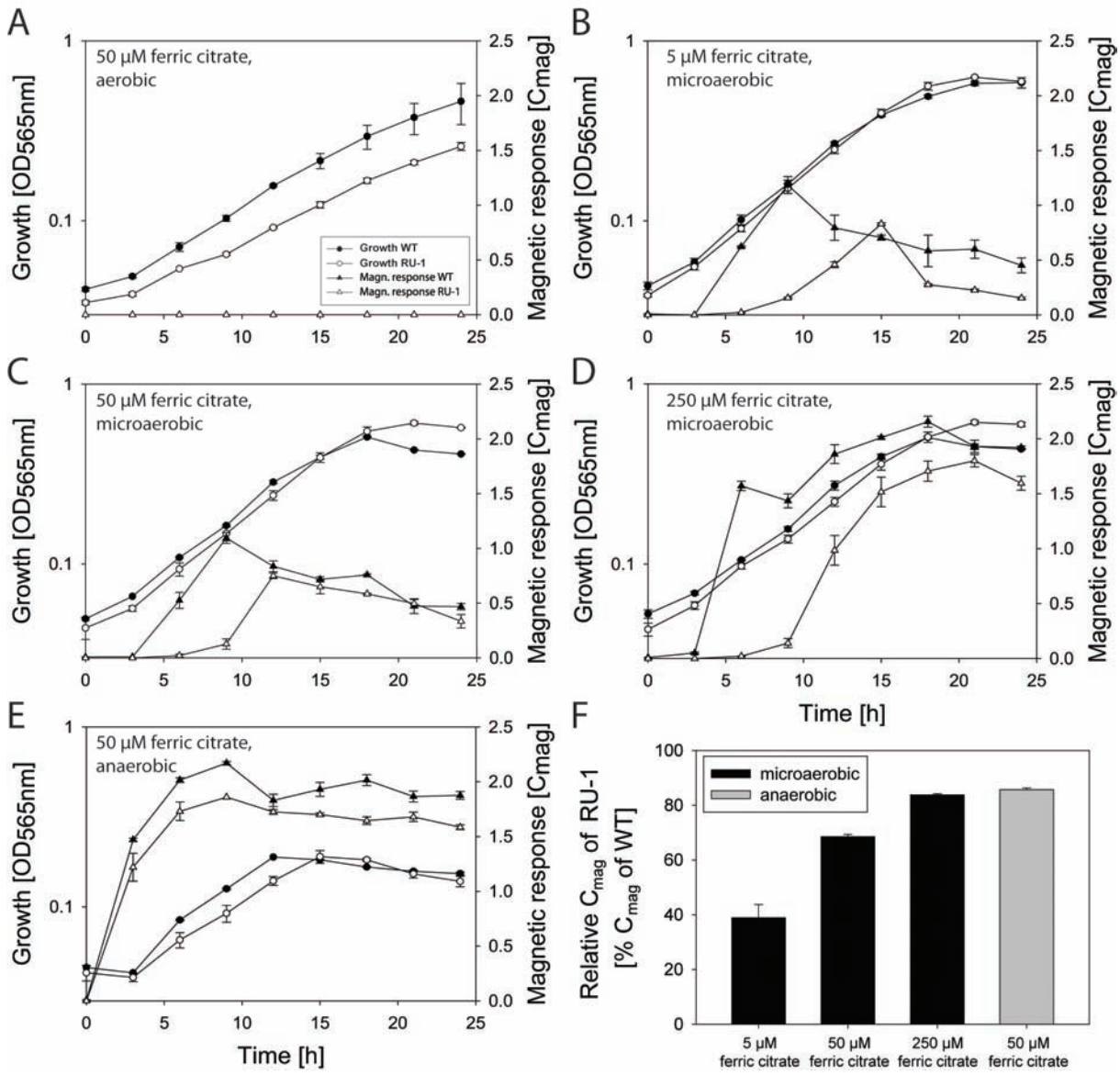

FIG. 2-4. (A to E) Levels of growth (optical density [OD] at 565 nm) and magnetic response (C_{mag}) of the WT and RU-1 grown under different conditions. (F) Relative maximal C_{mag} of RU-1 grown in LIM, determined from results shown in panels B to E. Data are from representative experiments done in duplicate. The entire experiment was repeated three times, with comparable results. Values are given as means ± standard deviations.

Consistent with TEM and C_{mag} data, the total intracellular iron content after microaerobic growth with 50 µM iron was also reduced in the *fur* mutant by 50% compared to the level for the WT (FIG. 2-5A). Transcomplementation of the *fur* mutant by a WT *fur* allele on pBBR1MCS-2fur resulted in partial restoration of the WT iron content (see FIG. S2-3 in the supplemental material).

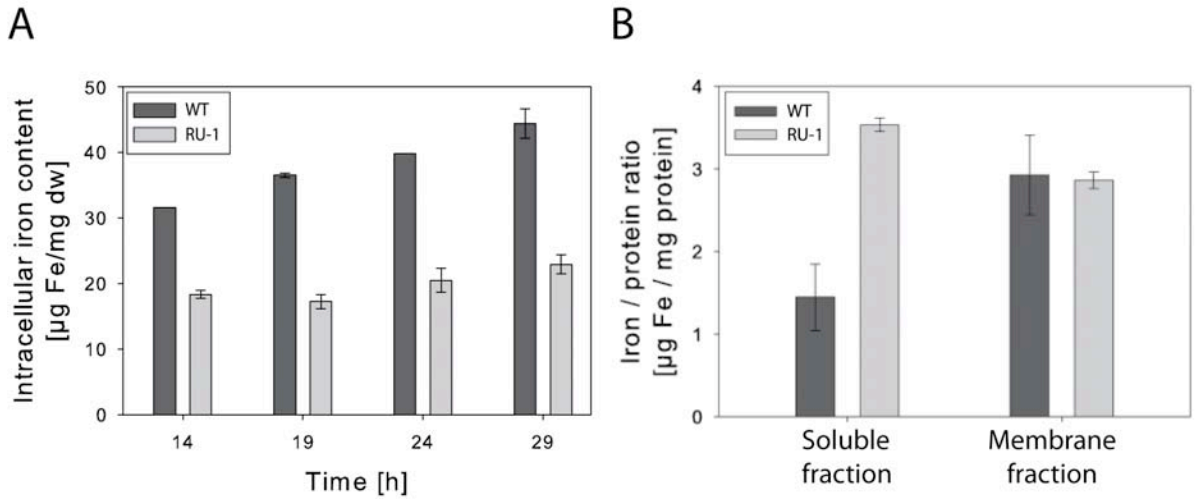

FIG. 2-5. (A) Time courses of total intracellular iron content of the WT and RU-1 during growth in FSM under microaerobic conditions. Values are given as means ± standard deviations (SD) from three independent replicates. (B) Iron-to-protein ratios of WT and RU-1 nonmagnetic cytoplasmic and membrane-enriched protein fractions. Values are given as means ± SD from two independent replicates.

Unlike in other *Magnetospirillum* species (Paoletti and Blakemore, 1986; Calugay *et al.*, 2003), no siderophores could be detected in *M. gryphiswaldense* under any tested condition in previous studies. However, although there is no clear genomic indication of siderophore synthesis, we cannot entirely exclude the possibility of the synthesis and use of primary catecholate-like metabolites as siderophores under some unspecified conditions, as described for *M. magneticum* (Calugay *et al.*, 2006). Since *fur* mutants of several other bacteria (e.g. *Pseudomonas aeruginosa* and *Shewanella oneidensis*) showed increased or constitutive production of siderophores (Prince *et al.*, 1993; Thompson *et al.*, 2002), we reassessed siderophore production using the CAS decoloration assay with supernatants from cultures grown under different iron concentrations and a modified plate growth CAS assay. However, again we were unable to detect siderophore production either in the *fur* mutant or in the WT (data not shown).

As *fur* mutants of *E. coli* are known to be susceptible to higher iron concentrations than the WT (Touati *et al.*, 1995), we also checked for increased sensitivity of *M. gryphiswaldense* RU-1 to various metals (Fe, Mn, and Co) at different concentrations. Dose-response assays under microaerobic conditions revealed identical growth yields for the WT and RU-1 between 0 and 500 µM iron as well as 0 and 2 mM manganese (see FIG. S2-4A and B in the supplemental material). Only at very high concentrations of iron (>1,000 µM) and manganese (>3 mM) was growth of RU-1 increasingly inhibited relative to that of the WT. No differences with respect to growth yield could be observed in the presence of Co (5 to 100 µM) (data not shown). These data indicate a different role for *Mg*Fur than for *Ec*Fur.

Since growth of *M. gryphiswaldense* RU-1 was impaired under aerobic conditions, we also compared the sensitivities of the WT and RU-1 strains against the superoxide-producing agent paraquat (Bus *et al.*, 1974). Growth in the presence of 5 μM paraquat resulted in growth yields of the WT being reduced by 40%, whereas growth of RU-1 was inhibited by 60% (see FIG. S2-4C in the supplemental material). At higher paraquat concentrations, both strains were equally inhibited. These results suggest that *Mg*Fur might be involved in the oxidative stress response of *M. gryphiswaldense*.

2.4.4 Mössbauer spectroscopic analysis of RU-1 reveals a large pool of iron bound to a ferritin-like component

Previous Mössbauer experiments revealed that the intracellular iron pool of the WT grown under microaerobic conditions comprises mainly magnetite, a ferritin-like component, and a ferrous high-spin component (Faivre *et al.*, 2007). Here, we performed a comparative determination of intracellular iron metabolites and their contributions in *M. gryphiswaldense* WT and RU-1 by using transmission Mössbauer spectroscopy (TMS) analyses. Prior to TMS analyses, cultures of *M. gryphiswaldense* WT and RU-1 were passaged three times under microaerobic, iron-replete conditions. To study iron metabolites in iron-induced cells, an additional culture of RU-1 was passaged three times under microaerobic, iron-depleted conditions (RU-1 –Fe) until no magnetism was observed by C_{mag} measurements. After three passages, all cultures were transferred to fresh FSM supplemented with 40 μM $^{57}Fe(citrate)_2$ (WT) or a mixture of 20 μM $^{57}Fe(citrate)_2$ and 20 μM $^{56}Fe(citrate)_2$ (RU-1) and cultivated under microaerobic conditions.

Mössbauer spectra are characterized by three different parameters: the isomer shift, δ; the quadrupole splitting, ΔE_Q; and the magnetic hyperfine field, $B_{HF.}$ The isomer shift, δ, which originates from the electric monopole interaction between the nucleus and the electronic shell, is a measure of the degree of covalent bonding of the iron atom with a ligand and is also an attribute for the oxidation state of the iron atom. The quadrupole splitting, ΔE_Q, originates from the electric quadrupole interaction between the nucleus and the electronic shell and is a measure for the symmetry of the metal chelate and for the covalent distribution of ligand-metal bonding. The magnetic hyperfine field, B_{HF}, is a result of magnetic dipole interaction between the nucleus and electrons and generates six-line or even more complicated spectra. Whole-cell, late-log Mössbauer analyses revealed the presence of metabolites showing characteristics of a ferrous iron high-spin metabolite, ferric iron bound to a ferritin-like

metabolite, and magnetite in both strains under all tested conditions (see FIG. S2-5 in the supplemental material). However, the relative contributions of the metabolites differed between the WT and the *fur* mutant strain (Table 2-3).

Table 2-3. Mössbauer parameters of *M. gryphiswaldense* WT and RU-1

Metabolite	Parameter	Result for strain		
		WT	RU-1 +Fe	RU-1 -Fe
Ferritin-like metabolite	δ [mms^{-1}]	0.45	0.45	0.46
	ΔE_Q [mms^{-1}]	0.76	0.67	0.70
	Contribution [%]	50.4	75.8	89.5
	[% x g^{-1}][a]	23.3	38.3	32.6
Ferrous high-spin metabolite	δ [mms^{-1}]	1.27	1.28	1.28
	ΔE_Q [mms^{-1}]	2.81	2.85	2.90
	Contribution [%]	0.35	2	1.6
	[% x g^{-1}]	0.16	1	0.6
Magnetite -site A	δ [mms^{-1}]	0.37	0.32	0.32
	ΔE_Q [mms^{-1}]	0	0	0
	Contribution [%]	16.4	7.4	3
	[% x g^{-1}]	7.6	3.7	1.1
	B_{hf} [T]	49.1	48.4	48.9
Magnetite-site B	δ [mms^{-1}]	0.75	0.82	0.82
	ΔE_Q [mms^{-1}]	0	0	0
	Contribution [%]	32.8	14.8	5.9
	[% x g^{-1}]	15.2	7.5	2.1
	B_{hf} [T]	47.1	46.9	45
Ferritin-like metabolite/ magnetite	FMR	1.02	3.41	10.1

[a] Relative contribution normalized by sample mass.

Whereas ferritin-like metabolite (50.4%) and magnetite (49.2%) contributed almost equally to the intracellular iron pool of the WT, the most abundant iron species found in RU-1 (75.8% for RU-1 +Fe and 89.5% for RU-1 –Fe) exhibited Mössbauer parameters similar to those of ferritins. Magnetite accounted for only 22.2% (+Fe) and 8.9% (–Fe) of the intracellular iron pool of RU-1, confirming the reduced magnetite biomineralization in the *fur* mutant observed by TEM. In all samples, only a small relative contribution came from a ferrous iron high-spin, ferrochelatin-like iron species also found in many bacterial and fungal systems (Böhnke and Matzanke, 1995). However, while in the WT the ferrous iron high-spin metabolite contributed only 0.35% to the intracellular iron pool, in RU-1 this metabolite was increased to 2% (RU-1 +Fe) and 1.6% (RU-1 –Fe).

Since the contribution ratio of ferritin-like iron to magnetite (FMR) was changed from 1.02 in the WT to 3.4 and 10.1 in the *fur* mutant, these data suggested that an increased amount of

iron was bound to proteins in RU-1. To test this assumption, we analyzed the iron-to-protein ratios of nonmagnetic cell fractions of the WT and RU-1 grown to late log phase under microaerobic conditions. The iron-protein ratio of the membrane fraction was 3 µg Fe mg protein^{-1} for both strains. However, in the soluble fraction, the iron-protein ratio of the WT was only 1.44 µg Fe mg protein^{-1}, whereas in the *fur* mutant, the iron-protein ratio was increased more than 2-fold (3.53 µg Fe mg protein^{-1}) (FIG. 2-5B), which was consistent with the estimations derived from TMS analysis.

2.4.5 Analyis of the putative Fur regulon

To analyze putative targets of Fur, we performed a Fur titration assay (FURTA) (Stojiljkovic *et al.*, 1994). In a FURTA, high-copy-number plasmids carrying promoters with putative Fur-binding elements are introduced into *E. coli* H1717, a strain carrying a *lacZ* reporter construct under the control of the Fur-regulated promoter *fhuF*. If plasmids contain sequences capable of binding Fur, a titration of the repressor will occur, leading to expression of the *lacZ* reporter. *E. coli* strain H1717 was transformed with the high-copy-number plasmid pGEM-T Easy or pGEM-T Easy promoter construct from *M. gryphiswaldense*, including putative promoter regions of *mamDC*, *mamAB*, *mms16* (*apdA*), *mgr4079*, and *rplK* as well as the promoter P_{fhuF} of *E. coli*. P_{fhuF} and P_{rplK} served as controls, whereas P_{mamDC} and P_{mamAB} have been shown to be iron regulated (Schübbe *et al.*, 2006). In addition, P_{mamDC} of *M. magneticum* and *M. magnetotacticum* was previously predicted *in silico* to be Fur regulated (Rodionov *et al.*, 2006). All strains formed pink colonies on iron-depleted MacConkey lactose agar (see FIG. S2-6 in the supplemental material), showing high ß-galactosidase activities, since *Ec*Fur does not repress the *fhuF* promoter in the absence of available iron. Strains harboring the plasmids pGEMPfhuF (positive control) and pGEMPmamDC also formed pink colonies on agar plates supplemented with 30 µM $FeCl_3$, suggesting that Fur was titrated out by Fur binding sequences within the tested promoters. All other strains formed white or only slightly pinkish colonies on iron-replete agar plates, indicating that Fur represses the expression of *lacZ* in the presence of iron. These data also demonstrated that Fur is involved in the transcriptional regulation of at least some magnetosome genes.

2.4.6 Proteomic analysis of the Fur regulon

To identify other putative constituents of the Fur regulon in addition to the tested targets, we performed a proteome-wide analysis of cytoplasmic and membrane-enriched protein fractions of the WT and the *fur* mutant grown under iron-replete and under iron-depleted conditions. In total, 719 proteins were identified in the membrane-enriched fractions by 1D LC-MS-MS analysis, and 735 spots were detected on 2D gels of the cytoplasmic fractions (see FIG. S2-7 in the supplemental material). By use of 1D LC-MS-MS proteomic analysis, 23 proteins whose genes are part of a 130-kb genomic magnetosome island (MAI), harboring most magnetosome genes (Ullrich *et al.*, 2005), were identified. Eighteen of these identified genes are part of the *mam* and *mms* operons encoding magnetosome proteins. Analysis of the expression data revealed almost no differences in expression level of these identified MAI proteins between the WT and RU-1 (see Table S2-4 in the supplemental material). The only exception was Mms6, a protein that was reported to affect magnetite crystal formation *in vitro* (Arakaki *et al.*, 2003), which showed an expression level reduced by 55% in RU-1 under iron-replete conditions compared to that for the WT. Mgr4109, a putative type I secretion system ATPase encoded within the MAI, was detected in RU-1 but not in the WT.

Significant changes in expression levels were observed for 14 proteins encoded outside the MAI (Table 2-4), of which 12 were upregulated in RU-1 and two were upregulated in the WT under iron-depleted and iron-replete conditions. Five of the proteins with altered expression levels are components of putative iron uptake systems, comprising all iron uptake systems predicted from the genome of *M. gryphiswaldense* (R. Uebe, unpublished data).

Table 2-4. Proteins that are differentially expressed between the WT and RU-1 under different growth conditions (–Fe and +Fe), as identified by LC-MS-MS[a]

Expression level in RU-1 vs. WT	NCBI accession no. or locus tag	Protein identification/function	Molecular size (kDa)	No. of peptide ions				Relative expression level in RU-1	
				WT		RU-1			
				-Fe	+Fe	-Fe	+Fe	RU-1 -Fe / WT -Fe	RU-1 +Fe / WT +Fe
Upregulated	**MGR0081**	**TonB-dependent outer membrane receptor**	**72**	**ND[b]**	**ND**	**17**	**23**	**Unique**	**Unique**
	MGR0236	**bacterial extracellular solute-binding protein**	**36**	**12**	**ND**	**25**	**13**	**2.08**	**Unique**
	MGR0237	PAS:GGDEF	76	ND	ND	10	13	Unique	Unique
	MGR0662	hypothetical protein	32	ND	ND	10	12	Unique	Unique
	MGR0705	conserved hypothetical protein	11	ND	ND	19	14	Unique	Unique
	MGR0706	conserved hypothetical protein	12	11	ND	26	28	2.36	Unique
	MGR0707	conserved hypothetical protein	12	ND	ND	17	14	Unique	Unique
	MGR1021	periplasmic trypsin-like serine protease	56	ND	ND	11	12	Unique	Unique
	MGR1446	**FeoB2**	**83**	**10**	**ND**	**53**	**50**	**5.30**	**Unique**
	MGR1447	**FeoA2**	**9**	**13**	**11**	**31**	**34**	**2.38**	**3.09**
	MGR1593	transcriptional regulator ArsR family	20	ND	ND	14	13	Unique	unique
	MGR4109	HlyB type I secretion system ATPase	81	ND	ND	11	11	Unique	unique
Downregulated	MGR0698	CydA cytochrome d ubiquinol oxidase subunit 1	58	10	11	ND	ND	Unique (WT)	Unique (WT)
	ABL14106	**Feo B1**	**76**	**40**	**50**	**ND**	**10**	**Unique (WT)**	**-5.00**

[a] Characteristics of proteins with putative relation to iron metabolism are shown in bold.
[b] ND, not detected

Mgr0236, a putative bacterial extracellular binding protein that displays 59.8% similarity to the periplasmic ferric iron binding protein FutA2 (Badarau *et al.*, 2008), showed a 2-fold-increased expression in RU-1 versus in the WT under iron-depleted conditions. Under iron-replete conditions, Mgr0236 was repressed in the WT but was still detectable in the *fur* mutant, as was also observed by 2D gel analysis (data not shown). Interestingly, *mgr0236* is highly similar to *mgr4079*, a pseudogene copy of *mgr0236*, which encodes a protein truncated by the first 60 amino acids (82.7% similarity to Mgr0236) and which is located within the MAI of *M. gryphiswaldense*. Mgr0081, a TonB-dependent outer membrane receptor putatively involved in the uptake of iron-siderophore complexes, was detected in RU-1 but not in the WT. The ferrous iron transport system FeoAB2 (Mgr1447 and Mgr1446) was expressed in a 2-fold-larger amount in RU-1 than in the WT. In addition to these iron transport systems, other proteins putatively involved in metal metabolism showed different expression levels between RU-1 and the WT. This included a transcriptional regulator of the metal-binding ArsR family that was detectable in RU-1 but not in the WT. Three highly basic proteins, whose genes are colocalized with a putative heavy-metal-transporting P-type ATPase, also showed an increased expression level in the *fur* mutant. Other proteins that showed differential expression had no obvious relation to metal metabolism (Mgr0237, Mgr0662, Mgr1021, and Mgr4109).

The genome of M. *gryphiswaldense* encodes a second copy of the Feo iron uptake system, designated *feoAB1*, which was previously shown to have an accessory role in magnetite biomineralization (Rong *et al.*, 2008). Under iron-depleted and -replete conditions, the second Feo system is expressed in smaller amounts in the *fur* mutant than in the WT. The iron-containing protein CydA, a cytochrome oxidase, was also expressed at higher levels in the WT than in RU-1, since it was detected only in the WT.

2.5 Discussion

We identified and analyzed the genuine Fur-like iron regulator *Mg*Fur (Mgr1314), which is one of five predicted proteins of the Fur superfamily in *M. gryphiswaldense*, with four of them (including *Mg*Fur) being putative iron-responsive transcriptional regulators. This number is notably high compared to those for the genomes of other bacteria of the alphaproteobacterial clade, which contain between zero (e.g., *Rickettsia* and *Ehrlichia* species) and three (e.g., *Bradyrhizobium japonicum*) genes encoding iron-responsive regulators (Rodionov *et al.*, 2006).The multitude of putative iron regulators may either reflect the need for very strict iron homeostasis in *M. gryphiswaldense* and indicate particularly fine-tuned and versatile iron regulation or simply represent functional redundancy.

The colocalization of *fur* homologues with magnetosome genes in several cultivated and uncultivated MTB (Jogler *et al.*, 2009), as well as the identification of putative Fur binding sites within the promoter regions of two magnetosome operons (Rodionov *et al.*, 2006), suggested a close link between Fur and the regulation of biomineralization. However, our data indicate that *Mg*Fur is not essential for magnetite synthesis, as the *fur* mutant was still able to produce functional magnetite crystals, albeit fewer and smaller than those produced by the WT. The reduction of total iron accumulation by 50% in RU-1 was due to the lower content of magnetite as shown by Mössbauer (TMS) analysis and iron measurements. On the other hand, these analyses also revealed that, compared to the WT, in which iron is deposited mainly as magnetite, in RU-1 the largest proportion of bulk intracellular iron is bound to proteins in the nonmagnetic fraction, as indicated by a 2.4-fold-increased iron-to-protein ratio of the nonmagnetic fraction. In particular, the intracellular iron in RU-1 was bound mostly to an as-yet-unidentified ferritin-like metabolite, which appears to be upregulated in the mutant compared to the level in the wild type when incubated under identical conditions, based on previous analyses (Faivre *et al.*, 2007). A similar effect was observed in a *fur* mutant of *Helicobacter pylori* (Bereswill *et al.*, 2000), where a deregulation of the iron storage protein ferritin (Pfr) was observed, leading to higher expression rates of Pfr. In contrast, in an *E. coli fur* mutant, ferritin-bound iron was decreased, resulting in 2.5-fold-lower intracellular iron contents (Abdul-Tehrani *et al.*, 1999), whereas relative intracellular levels of ferrous iron were substantially increased, as detected by TMS (B. Matzanke, unpublished data). Thus, although *Mg*Fur was able to substitute for *Ec*Fur in *E. coli* in an iron-dependent manner, our observations argue for a somewhat distinct regulatory role in *M. gryphiswaldense*.

Although levels of intracellular ferrous iron detectable by TMS were relatively low in both *M. gryphiswaldense* WT and RU-1 compared to observations in *E. coli*, we found that ferrous iron signals were significantly increased in TMS of *M. gryphiswaldense* RU-1. The increase in protein-bound iron, and in particular the increased proportion of free ferrous iron, might explain the observed sensitivity of RU-1 against O_2- and paraquat-induced oxidative stress, since ferrous iron promotes the generation of radical oxygen species via the Fenton reaction (Winterbourn, 1995), and we did not observe any changes in expression levels of proteins of the oxidative stress response. Unexpectedly, the *fur* mutant was also growth impaired under anaerobic conditions, indicating that the increased intracellular iron concentration interferes with enzymes of the anaerobic metabolism.

Although putative Fur binding sites within the promoter regions of magnetosome operons were predicted *in silico* (Rodionov *et al.*, 2006) and in part also experimentally confirmed in this study, proteomic analyses revealed that the expression levels of most detected magnetosomal proteins were unaffected by the deletion of *fur*. The only exception is the magnetosome protein Mms6, which showed a decreased expression in RU-1 grown under iron-sufficient conditions. Therefore, we cannot entirely exclude the possibility that the magnetosomal *mamDC* promoter exhibits some unspecific affinity to *Ec*Fur. Differential expression patterns were observed for several proteins putatively involved in iron uptake for general iron metabolism, indicating an important role of Fur in iron homeostasis of *M. gryphiswaldense*. Remarkably, Mgr0532 and Mgr0533, representing putative bacterioferritins, did not exhibit differential expression in RU-1 versus the WT, suggesting that they are not identical with the ferritin-like constituent that caused an increased signal in TMS. However, it cannot be excluded that the increased ferritin-like pool is a result of increased iron binding to bacterioferritin due to higher intracellular iron concentrations. In summary, the proteomic approach revealed only 14 proteins whose expression was significantly altered between the WT and RU-1. This is consistent with observations of several *fur* mutants, where Fur plays only a minor role in iron homeostasis (van Vliet *et al.*, 1998; Parker *et al.*, 2005; da Silva Neto *et al.*, 2009), compared to the large Fur regulon of *E. coli*, in which up to 100 genes are down- or upregulated by the direct or indirect effect of Fur (Hantke, 2001; McHugh *et al.*, 2003). In several alphaproteobacteria, proteins other than Fur, such as RirA (Todd *et al.*, 2005; Viguier *et al.*, 2005) and Irr (Small *et al.*, 2009), have taken over the function of a global iron-responsive regulator. By genome analysis of *M. gryphiswaldense*, we also identified three proteins (Mgr1305, Mgr1399, and Mgr3480) within the Fur superfamily, which are more closely related to the Irr subfamily (Small *et al.*,

2009) (FIG. 1). It seems possible that these Irr-like proteins are also involved in more complex regulatory networks overlapping the *Mg*Fur regulon. A recent study addressed the function of a presumptive Fur-like protein of *M. gryphiswaldense* (Mgr1399), which, however, was assigned as Irr-like in our study. Supposedly, deletion of Mgr1399 resulted in a nonnmagnetic phenotype (Huang *et al.*, 2007). However, in the absence of transcomplementation experiments these results are not conclusive, given the high genetic instability of the magnetic phenotype that gives rise to frequent spontaneous mutations within the MAI of *M. gryphiswaldense* (Ullrich *et al.*, 2005). Therefore, future work is required to study the contribution of the Irr-like proteins to iron homeostasis in more detail.

In conclusion, our data demonstrate that *Mg*Fur is involved in iron homeostasis and, to a lesser extent, also affects magnetite biomineralization. Since most magnetosome proteins exhibited similar levels of expression between the WT and RU-1, the reduced magnetite synthesis most likely is caused by indirect consequences of the deregulated phenotype. For example, it could be that the increased uptake of iron into the cytoplasm and its subsequent sequestration by cytoplasmic proteins lead to a decreased pool of iron available for magnetite biomineralization in the *fur* mutants, whereas in the WT, *Mg*Fur might be involved in balancing the competing demands for biochemical iron supply and magnetite biomineralization (Faivre *et al.*, 2007). A possible explanation for the observed delay of magnetite synthesis in iron-induced cells grown under microaerobic, but not anaerobic, conditions might be that the increased pool of cytoplasmic iron-binding proteins has to be saturated before iron becomes available for magnetite biomineralization. However, further studies including the identification and biochemical characterization of individual iron-sequestering cellular constituents are required to provide deeper insights into the regulation of biomineralization.

2.6 Acknowlegments

This work was supported by the Deutsche Forschungsgemeinschaft (Schu 1080/6-2). We thank Klaus Hantke, University of Tübingen, and Gregor Grass, University of Halle, for their gift of strains *E. coli* H1717 and *E. coli* H1780. We thank Anna Pollithy for help with cloning.

2.7 References

Abdul-Tehrani, H., Hudson, A. J., Chang, Y. S., Timms, A. R., Hawkins, C., Williams, J. M., Harrison, P. M., Guest, J. R. and Andrews, S. C. (1999). Ferritin mutants of *Escherichia coli* are iron deficient and growth impaired, and *fur* mutants are iron deficient. *J. Bacteriol.* **181**: 1415-1428.

Ahn, B.-E., Cha, J., Lee, E.-J., Han, A.-R., Thompson, C. and Roe, J.-H. (2006). Nur, a nickel-responsive regulator of the Fur family, regulates superoxide dismutases and nickel transport in *Streptomyces coelicolor*. *Mol. Microbiol.* **59**: 1848 - 1858.

Althaus, E. W., Outten, C. E., Olson, K. E., Cao, H. and O'Halloran, T. V. (1999). The ferric uptake regulation (Fur) repressor is a zinc metalloprotein. *Biochemistry (Mosc).* **38**: 6559-6569.

Altschul, S., Madden, T., Schaffer, A., Zhang, J., Zhang, Z., Miller, W. and Lipman, D. (1997). Gapped BLAST and PSI-BLAST: a new generation of protein database search programs. *Nucleic Acids Res.* **25**: 3389-3402.

Andrews, S. C., Robinson, A. K. and Rodriguez-Quinones, F. (2003). Bacterial iron homeostasis. *FEMS Microbiol. Rev.* **27**: 215-237.

Arakaki, A., Webbs, J. and Matsunaga, T. (2003). A novel protein tightly bound to bacterial magnetite particles in *Magnetospirillum magnetotacticum strain* AMB-1. *J. Biol. Chem.* **278**: 8745-8750.

Badarau, A., Firbank, S. J., Waldron, K. J., Yanagisawa, S., Robinson, N. J., Banfield, M. J. and Dennison, C. (2008). FutA2 is a ferric binding protein from *Synechocystis* PCC 6803. *J. Biol. Chem.* **283**: 12520-12527.

Baeuerlein, E. and Schüler, D. (1995). Biomineralisation: Iron transport and magnetite crystal formation in *Magnetospirillum gryphiswaldense*. *J. Inorg. Biochem.* **59**: 107.

Bereswill, S., Greiner, S., van Vliet, A. H. M., Waidner, B., Fassbinder, F., Schiltz, E., Kusters, J. G. and Kist, M. (2000). Regulation of ferritin-mediated cytoplasmic iron storage by the ferric uptake regulator homolog (Fur) of *Helicobacter pylori*. *J. Bacteriol.* **182**: 5948-5953.

Bertani, G. (1951). Studies on lysogenesis I.: The mode of phage liberation by lysogenic *Escherichia coli*. *J. Bacteriol.* **62**: 293-300.

Böhnke, R. and Matzanke, B. F. (1995). The mobile ferrous iron pool in *Escherichia coli* is bound to a phosphorylated sugar derivative. *Biometals* **8**: 223-230.

Bsat, N., Herbig, A., Casillas-Martinez, L., Setlow, P. and Helmann, J. D. (1998). *Bacillus subtilis* contains multiple Fur homologues: identification of the iron uptake (Fur) and peroxide regulon (PerR) repressors. *Mol. Microbiol.* **29**: 189-198.

Bus, J. S., Aust, S. D. and Gibson, J. E. (1974). Superoxide- and singlet oxygen-catalyzed lipid peroxidation as a possible mechanism for paraquat (methyl viologen) toxicity. *Biochem. Biophys. Res. Commun.* **58**: 749-755.

Büttner, K., Bernhardt, J., Scharf, C., Schmid, R., Mäder, U., Eymann, C., Antelmann, H., Völker, A., Völker, U. and Hecker, M. (2001). A comprehensive two-dimensional map of cytosolic proteins of *Bacillus subtilis*. *Electrophoresis* **22**: 2908-2935.

Calugay, R. J., Miyashita, H., Okamura, Y. and Matsunaga, T. (2003). Siderophore production by the magnetic bacterium *Magnetospirillum magneticum* AMB-1. *FEMS Microbiol. Let.* **218**: 371-375.

Calugay, R. J., Takeyama, H., Mukoyama, D., Fukuda, Y., Suzuki, T., Kanoh, K. and Matsunaga, T. (2006). Catechol siderophore excretion by magnetotactic bacterium *Magnetospirillum magneticum* AMB-1. *J. Biosci. Bioeng.* **101**: 445-447.

da Silva Neto, J. F., Braz, V. S., Italiani, V. C. S. and Marques, M. V. (2009). Fur controls iron homeostasis and oxidative stress defense in the oligotrophic alpha-proteobacterium *Caulobacter crescentus*. *Nucl. Acids Res.* **37**: 4812-4825.

de Lorenzo, V., Wee, S., Herrero, M. and Neilands, J. B. (1987). Operator sequences of the aerobactin operon of plasmid ColV-K30 binding the ferric uptake regulation (*fur*) repressor. *J. Bacteriol.* **169**: 2624-2630.

Escolar, L., Perez-Martin, J. and de Lorenzo, V. (1999). Opening the iron box: transcriptional metalloregulation by the Fur protein. *J. Bacteriol.* **181**: 6223-6229.

Faivre, D., Böttger, L. H., Matzanke, B. F. and Schüler, D. (2007). Intracellular magnetite biomineralization in bacteria proceeds by a distinct pathway involving membrane-bound ferritin and an iron(II) species. *Angew. Chem. Int. Ed. Engl.* **46**: 8495-8499.

Faivre, D., Menguy, N., Posfai, M. and Schüler, D. (2008). Environmental parameters affect the physical properties of fast-growing magnetosomes. *Am. Mineral.* **93**: 463-469.

Faivre, D. and Schüler, D. (2008). Magnetotactic bacteria and magnetosomes. *Chem. Rev.* **108**: 4875-4898.

Grünberg, K., Müller, E. C., Otto, A., Reszka, R., Linder, D., Kube, M., Reinhardt, R. and Schüler, D. (2004). Biochemical and proteomic analysis of the magnetosome

membrane in *Magnetospirillum gryphiswaldense*. *Appl. Environ. Microbiol.* **70**: 1040-1050.

Grünberg, K., Wawer, C., Tebo, B. M. and Schüler, D. (2001). A large gene cluster encoding several magnetosome proteins is conserved in different species of magnetotactic bacteria. *Appl. Environ. Microbiol.* **67**: 4573-4582.

Gunnlaugsson, H. (2006). A simple model to extract hyperfine interaction distributions from Mössbauer spectra. *Hyperfine Interact.* **167**: 851-854.

Hantke, K. (1987). Selection procedure for deregulated iron transport mutants (*fur*) in *Escherichia coli* K 12: fur not only affects iron metabolism. *Mol. Gen. Genet.* **210**: 135-139.

Hantke, K. (2001). Iron and metal regulation in bacteria. *Curr. Opin. Microbiol.* **4**: 172-177.

Heyen, U. and Schüler, D. (2003). Growth and magnetosome formation by microaerophilic *Magnetospirillum* strains in an oxygen-controlled fermentor. *Appl. Microbiol. Biotechnol.* **61**: 536-544.

Huang, Y., Zhang, W., Jiang, W., Rong, C. and Li, Y. (2007). Disruption of a *fur*-like gene inhibits magnetosome formation in *Magnetospirillum gryphiswaldense* MSR-1. *Biochemistry (Moscow)* **72**: 1247-1253.

Jogler, C., Lin, W., Meyerdierks, A., Kube, M., Katzmann, E., Flies, C., Pan, Y., Amann, R., Reinhardt, R. and Schüler, D. (2009). Toward cloning of the magnetotactic metagenome: Identification of magnetosome island gene clusters in uncultivated magnetotactic bacteria from different aquatic sediments. *Appl. Environ. Microbiol.* **75**: 3972-3979.

Jogler, C. and Schüler, D. (2009). Genomics, genetics, and cell biology of magnetosome formation. *Annu. Rev. Microbiol.* **63**: 501-521.

Johnston, A., Todd, J., Curson, A., Lei, S., Nikolaidou-Katsaridou, N., Gelfand, M. and Rodionov, D. (2007). Living without Fur: the subtlety and complexity of iron-responsive gene regulation in the symbiotic bacterium *Rhizobium* and other α-proteobacteria. *Biometals* **20**: 501-511.

Katzmann, E., Scheffel, A., Gruska, M., Plitzko, J. M. and Schüler, D. (2010). Loss of the actin-like protein MamK has pleiotropic effects on magnetosome formation and chain assembly in *Magnetospirillum gryphiswaldense*. *Mol. Microbiol.* **77**: 208-224.

Kawaguchi, R., Burgess, J. and Matsunaga, T. (1992). Phylogeny and 16S rRNA sequence of *Magnetospirillum* sp. AMB-1, an aerobic magnetic bacterium. *Nucl. Acid Res.* **20**: 1140.

Komeili, A., Li, Z., Newman, D. K. and Jensen, G. J. (2006). Magnetosomes are cell membrane invaginations organized by the actin-like protein MamK. *Science* **311**: 242-245.

Kovach, M. E., Elzer, P. H., Hill, D. S., Robertson, G. T., Farris, M. A., Roop, R. M. and Peterson, K. M. (1995). Four new derivatives of the broad-host-range cloning vector pBBR1MCS, carrying different antibiotic-resistance cassettes. *Gene* **166**: 175-176.

Lee, J. and Helmann, J. (2007). Functional specialization within the Fur family of metalloregulators. *Biometals* **20**: 485-499.

Lowe, C. A., Asghar, A. H., Shalom, G., Shaw, J. G. and Thomas, M. S. (2001). The *Burkholderia cepacia fur* gene: co-localization with *omlA* and absence of regulation by iron. *Microbiology* **147**: 1303-1314.

Marx, C. and Lidstrom, M. (2002). Broad-Host-Range *cre-lox* system for antibiotic marker recycling in gram-negative bacteria. *Biotechniques* **33**: 1062-1067.

McHugh, J. P., Rodriguez-Quinones, F., Abdul-Tehrani, H., Svistunenko, D. A., Poole, R. K., Cooper, C. E. and Andrews, S. C. (2003). Global iron-dependent gene regulation in *Escherichia coli*. *J. Biol. Chem.* **278**: 29478-29486.

Milagres, A. M. F., Machuca, A. and Napoleao, D. (1999). Detection of siderophore production from several fungi and bacteria by a modification of chrome azurol S (CAS) agar plate assay. *J. Microbiol. Meth.* **37**: 1-6.

Miller, J. H. (1972). *Experiments in Molecular Genetics.* Cold Spring Harbor Laboratory Press, Cold Spring Harbor, New York.

Murat, D., Quinlan, A., Vali, H. and Komeili, A. (2010). Comprehensive genetic dissection of the magnetosome gene island reveals the step-wise assembly of a prokaryotic organelle. *Proc. Natl. Acad. Sci. USA* **107**: 5593-5598.

Paoletti, L. C. and Blakemore, R. P. (1986). Hydroxamate production by *Aquaspirillum magnetotacticum*. *J. Bacteriol.* **167**: 73-76.

Parker, D., Kennan, R. M., Myers, G. S., Paulsen, I. T. and Rood, J. I. (2005). Identification of a *Dichelobacter nodosus* ferric uptake regulator and determination of its regulatory targets. *J. Bacteriol.* **187**: 366-375.

Patzer, S. I. and Hantke, K. (1998). The ZnuABC high-affinity zinc uptake system and its regulator Zur in *Escherichia coli*. *Mol. Microbiol.* **28**: 1199-1210.

Platero, R., Peixoto, L., O'Brian, M. R. and Fabiano, E. (2004). Fur is involved in manganese-dependent regulation of *mntA* (*sitA*) expression in *Sinorhizobium meliloti*. *Appl. Environ. Microbiol.* **70**: 4349-4355.

Pohl, E., Haller, J. C., Mijovilovich, A., Meyer-Klaucke, W., Garman, E. and Vasil, M. L. (2003). Architecture of a protein central to iron homeostasis: crystal structure and spectroscopic analysis of the ferric uptake regulator. *Mol. Microbiol.* **47**: 903-915.

Prince, R. W., Cox, C. D. and Vasil, M. L. (1993). Coordinate regulation of siderophore and exotoxin A production: molecular cloning and sequencing of the *Pseudomonas aeruginosa fur* gene. *J. Bacteriol.* **175**: 2589-2598.

Rodionov, D., Gelfand, M., Todd, J., Curson, A. and Johnston, A. (2006). Computational reconstruction of iron- and manganese-responsive transcriptional networks in α-proteobacteria. *PLoS Comput. Biol.* **2**: 1568-1585.

Rong, C., Huang, Y., Zhang, W., Jiang, W., Li, Y. and Li, J. (2008). Ferrous iron transport protein B gene (*feoB1*) plays an accessory role in magnetosome formation in *Magnetospirillum gryphiswaldense* strain MSR-1. *Res. Microbiol.* **159**: 530-536.

Rudolph, G., Hennecke, H. and Fischer, H.-M. (2006). Beyond the Fur paradigm: iron-controlled gene expression in rhizobia. *FEMS Microbiol. Rev.* **30**: 631-648.

Rzhetsky, A. and Nei, M. (1992). A simple method for estimating and testing minimum-evolution trees. *Mol. Biol. Evol.* **9**: 945-967.

Sambrook, J. and Russel, D. (2001). *Molecular cloning: A laboratory manual*. Cold Spring Harbor Laboratory Press, Cold Spring Harbor, New York.

Schübbe, S., Kube, M., Scheffel, A., Wawer, C., Heyen, U., Meyerdierks, A., Madkour, M. H., Mayer, F., Reinhardt, R. and Schüler, D. (2003). Characterization of a spontaneous nonmagnetic mutant of *Magnetospirillum gryphiswaldense* reveals a large deletion comprising a putative magnetosome island. *J. Bacteriol.* **185**: 5779-5790.

Schübbe, S., Würdemann, C., Peplies, J., Heyen, U., Wawer, C., Glöckner, F. O. and Schüler, D. (2006). Transcriptional organization and regulation of magnetosome operons in *Magnetospirillum gryphiswaldense*. *Appl. Environ. Microbiol.* **72**: 5757-5765.

Schüler, D. and Baeuerlein, E. (1996). Iron-limited growth and kinetics of iron uptake in *Magnetospirilum gryphiswaldense*. *Arch. Microbiol.* **166**: 301-307.

Schüler, D. and Baeuerlein, E. (1998). Dynamics of iron uptake and Fe_3O_4 biomineralization during aerobic and microaerobic growth of *Magnetospirillum gryphiswaldense*. *J. Bacteriol.* **180**: 159-162.

Schüler, D., Uhl, R. and Baeuerlein, E. (1995). A simple light scattering method to assay magnetism in *Magnetospirillum gryphiswaldense*. *FEMS Microbiol. Lett.* **132**: 139-145.

Schultheiss, D., Handrick, R., Jendrossek, D., Hanzlik, M. and Schüler, D. (2005). The presumptive magnetosome protein Mms16 is a poly(3-hydroxybutyrate) granule-bound protein (phasin) in *Magnetospirillum gryphiswaldense*. *J. Bacteriol.* **187**: 2416-2425.

Schultheiss, D. and Schüler, D. (2003). Development of a genetic system for *Magnetospirillum gryphiswaldense*. *Arch. Microbiol.* **179**: 89-94.

Schwyn, B. and Neilands, J. B. (1987). Universal chemical assay for the detection and determination of siderophores. *Anal. Biochem.* **160**: 47-56.

Small, S. K., Puri, S., Sangwan, I. and O'Brian, M. R. (2009). Positive control of ferric siderophore receptor gene expression by the Irr protein in *Bradyrhizobium japonicum*. *J. Bacteriol.* **191**: 1361-1368.

Stojiljkovic, I., Bäumler, A. J. and Hantke, K. (1994). Fur regulon in gram-negative bacteria : Identification and characterization of new iron-regulated *Escherichia coli* genes by a Fur titration assay. *J. Mol. Biol.* **236**: 531-545.

Stookey, L. L. (1970). Ferrozine - a new spectrophotometric reagent for iron. *Anal. Chem.* **42**: 779-781.

Tamura, K., Dudley, J., Nei, M. and Kumar, S. (2007). MEGA4: Molecular evolutionary genetics analysis (MEGA) software version 4.0. *Mol. Biol. Evol.* **24**: 1596-1599.

Tao, X., Schiering, N., Zeng, H.-y., Ringe, D. and Murphy, J. R. (1994). Iron, DtxR, and the regulation of diphtheria toxin expression. *Mol. Microbiol.* **14**: 191-197.

Thompson, D. K., Beliaev, A. S., Giometti, C. S., Tollaksen, S. L., Khare, T., Lies, D. P., Nealson, K. H., Lim, H., Yates, J., Brandt, C. C., Tiedje, J. M. and Zhou, J. (2002). Transcriptional and proteomic analysis of a ferric uptake regulator (Fur) mutant of *Shewanella oneidensis*: Possible involvement of Fur in energy metabolism, transcriptional regulation, and oxidative stress. *Appl. Environ. Microbiol.* **68**: 881-892.

Todd, J. D., Sawers, G. and Johnston, A. W. B. (2005). Proteomic analysis reveals the wide-ranging effects of the novel, iron-responsive regulator RirA in *Rhizobium leguminosarum* bv. *viciae*. *Mol. Gen. Genom.* **273**: 197-206.

Touati, D., Jacques, M., Tardat, B., Bouchard, L. and Despied, S. (1995). Lethal oxidative damage and mutagenesis are generated by iron in Δf*ur* mutants of *Escherichia coli*: protective role of superoxide dismutase. *J. Bacteriol.* **177**: 2305-2314.

Ullrich, S., Kube, M., Schübbe, S., Reinhardt, R. and Schüler, D. (2005). A hypervariable 130-kilobase genomic region of *Magnetospirillum gryphiswaldense* comprises a magnetosome island which undergoes frequent rearrangements during stationary growth. *J. Bacteriol.* **187**: 7176-7184.

van Vliet, A. H. M., Wooldridge, K. G. and Ketley, J. M. (1998). Iron-responsive gene regulation in a *Campylobacter jejuni fur* mutant. *J. Bacteriol.* **180**: 5291-5298.

Viguier, C., O'Cuiv, P., Clarke, P. and O'Connell, M. (2005). RirA is the iron response regulator of the rhizobactin 1021 biosynthesis and transport genes in *Sinorhizobium meliloti* 2011. *FEMS Microbiol. Lett.* **246**: 235-242.

Viollier, E., Inglett, P. W., Hunter, K., Roychoudhury, A. N. and Van Cappellen, P. (2000). The ferrozine method revisited: Fe(II)/Fe(III) determination in natural waters. *Appl. Geochem.* **15**: 785-790.

Voigt, B., Schweder, T., Becher, D., Ehrenreich, A., Gottschalk, G., Feesche, J., Maurer, K.-H. and Hecker, M. (2004). A proteomic view of cell physiology of *Bacillus licheniformis*. *Proteomics* **4**: 1465-1490.

Voigt, B., Schweder, T., Sibbald, M. J. J. B., Albrecht, D., Ehrenreich, A., Bernhardt, J., Feesche, J., Maurer, K.-H., Gottschalk, G., Dijl, J. M. v. and Hecker, M. (2006). The extracellular proteome of *Bacillus licheniformis* grown in different media and under different nutrient starvation conditions. *Proteomics* **6**: 268-281.

Winterbourn, C. C. (1995). Toxicity of iron and hydrogen peroxide: the Fenton reaction. *Toxicol. Lett.* **82-83**: 969-974.

Wolff, S., Hahne, H., Hecker, M. and Becher, D. (2008). Complementary analysis of the vegetative membrane proteome of the human pathogen *Staphylococcus aureus*. *Mol. Cell. Proteomics* **7**: 1460-1468.

Yang, J., Sangwan, I., Lindemann, A., Hauser, F., Hennecke, H., Fischer, H.-M. and O'Brian, M. R. (2006). *Bradyrhizobium japonicum* senses iron through the status of haem to regulate iron homeostasis and metabolism. *Mol. Microbiol.* **60**: 427-437.

2.8 Supplemental material

Table S2-1. Oligonucleotides used in this study.

Primer	Nucleotide sequence (5'-3')[a]
mgr1314fwRT	ATGGTTTCGCGTATTGAACAGC
mgr1314revRT	CTATTTGTCGTCGGAATCACCG
mgr1314up_fw	CAATTGCGCATGACCGAATTCGCCCCG
mgr1314up_rev	GCGGCCGCAATACGCGAAACCATGGC
mgr1314do_fw	ACCGGTTTGATTCCGACGACAAATAG
mgr1314do_rev	ACCGGTCCAGTTCGGAAAATACCTTC
mgr1314fw	CATATGGTTTCGCGTATTGAACAGC
mgr1314rev	GAGCTCCTATTTGTCGTCGGAATCAC
mgr1314_del_fw	CAATTACGCCGCGCATCG
mgr1314_del_rev	AGCCGCCTCGACCTCGTT
mgr1314_probe_fw	TCGCCCCCAATTACGCCGCG
mgr1314 _probe_rev	CGCTCGGCGCCTCTTCATAGCGG
PfhuFfw	GGGCCCGATTTCATCTCTTTCATT
PfhuFrev	CCATGGTCGGGATAGTAATCTAAATGATAAT
Pmms16fw	CTCGAGGAGCCTCTCCATTAAACAATG
Pmms16rev	CATATGCTTGAATTCCTCCAACCGGGGGTATG
PrplKfw	AAGCTTGGCATCAAGGTTTCGGAAG
PrplKrev	CATATGTTTACCCTACCTCTGGTCG
Pmgr4079fw	CATATGCTGGCCCTCACCCGCTGA
Pmgr4079rev	CTCGAGGCCGCCAGCTTCTGTCCT
PmamDCrev	CATATGCTGATCTCCGGCAAGTGTATG
PmamDCfw	CTCGAGCAATGACCACCACCACCTTA AAC
PmamABfw	CTCGAGATGGCGCAAAGATGTGACGT C
PmamABrev	CATATGTCCCGTCACAATTCACCTCC
amb1009fw	CATATGATTTCTCGAATCGAACAACG
amb1009rev	GAGCTCTCAGTCGGCGGTTTCGTC
amb4460fw	CATATGATTTCACGCATCGAGCAAC
amb4460rev	GAGCTCCTATTTCTCTTCCGGTTTATCA
Ecfurfw	CATATGACTGATAACAATACCGCC
Ecfurrev	GAGCTCTTATTTGCCTTCGTGCGC

[a] Underlining indicates restriction site used for cloning purposes

Table S2-2. Identified Fur-like proteins of *M. gryphiswaldense* and similarity (%) to homologues. Locus tags refer to *M. magneticum* AMB-1 (Amb prefix), *M. magnetotacticum* MS-1 (Magn prefix), *Magnetococcus* sp. MC-1 (Mmc1 prefix), *Desulfovibrio magneticus* RS-1 (DMR prefix) and to an uncultured MTB (fos002_0290).

Protein	Similarity to *Ec*Fur	Best hit outside MTB	Similarity to MTB homologues	
		Locus tag / organism / similarity	Locus tag	Similarity
Mgr1314	50%	Rru_A3767 / *Rhodospirillum rubrum* ATCC 11170 / 80%	Amb4460	91%
			Amb1009	86%
			Magn03009848	91%
			Magn03007092	86%
			fos002_0290	64%
			Mmc1_0894	44%
			DMR_43000	47%
			DMR_04370	43%
			DMR_19790	41%
Mgr1305	33%	*rpsP* / alpha proteobacterium BAL199 / 52%	-	-
Mgr1399	37%	RC1_2944 / *Rhodospirillum centenum* SW / 76%	Amb4306	89%
			Magn03009205	90%
Mgr3480	34%	Atu0153 / *Agrobacterium tumefaciens* str. C58 / 65%	Amb1662	62%
Mgr3335	30%	MELB17_01720 / *Marinobacter sp.* ELB17 / 59%	Amb2309	75%
			Magn03007851	68%
			Mmc1_3182	50%
			DMR_26810	33%

Table S2-3. Similarity (%) between *E. coli*, *M. gryphiswaldense* (locus tags with Mgr prefix) and *M. magneticum* (locus tags with Amb prefix) Fur and Fur-like proteins. Numbers in brackets indicate similarity to the Fur domain of Amb4306.

No.	Locus tag	% similarity											
		1	2	3	4	5	6	7	8	9	10	11	12
1	EcFur	100											
2	Mgr1314	49.7	100										
3	Mgr1305	33.3	28.4	100									
4	Mgr1399	37.2	37.1	53.1	100								
5	Mgr3480	34.2	34.7	66.9	63.8	100							
6	Mgr3335	29.5	33.1	26.3	23.1	24.5	100						
7	Amb1009	52.3	86	33.3	38.9	37.1	31.6	100					
8	Amb4460	51.7	90.9	30.4	34.4	38.9	38.9	87.4	100				
9	Amb1662	36.2	35.4	55.4	52.4	61.6	32.7	38.6	37.2	100			
10	Amb4306	19.9 (39.9)	19.5 (38.9)	26.9 (51.4)	47.6 (88.5)	32.5 (67.2)	13.1 (24.4)	19.6 (40.1)	17.1 (38.2)	26.2 (51.8)	100 (47.6)		
11	Amb2309	35.5	29.4	26.7	27.3	28	75.2	30	30.6	32.1	11.6 (25.5)	100	
12	EcZur						37.4					39.1	100

Table S2-4. Expression levels of MAI proteins identified by LC-MS/MS

Locus tag	Protein identification / function	Molecular size (kDa)	No. of predited TMDs[a] TMHMM / Sosui	No. of peptide ions				Relative expression level in RU-1	
				WT		RU-1			
				-Fe	+Fe	-Fe	+Fe	RU-1 –Fe / WT -Fe	RU-1 +Fe / WT +Fe
MGR4022	TPR-like protein	50	0	10	ND[b]	11	11	1.10	Unique
MGR4041	Conserved hypothetical protein	9	0	ND	ND	11	ND	Unique	-
MGR4072	MmsF	14	3 / 2	17	15	12	13	-1.42	-1.15
MGR4073	Mms6	13	1	17	56	11	24	-1.55	-2.33
MGR4076	MamF	12	3	16	14	15	15	-1.07	1.07
MGR4077	MamD	30	1 / 0	37	19	31	19	-1.19	1.00
MGR4078	MamC	12	2	170	188	224	174	1.32	-1.08
MGR4091	MamE	78	1	75	51	82	52	1.09	1.02
MGR4092	MamJ	44	0	19	18	17	18	-1.12	1.00
MGR4093	MamK	39	0	31	27	25	20	-1.24	-1.35
MGR4095	MamM	34	3 / 6	15	12	14	17	-1.07	1.42
MGR4097	MamO	65	8 / 10	34	37	36	34	1.06	-1.09
MGR4099	MamA	24	0	26	26	23	27	-1.13	1.04
MGR4100	MamQ	30	1	16	16	16	15	1.00	-1.07
MGR4101	MamR	8	0	23	20	23	22	1.00	1.10
MGR4102	MamB	32	3 / 4	12	13	11	14	-1.09	1.08
MGR4103	MamS	19	1 / 2	16	19	14	17	-1.14	-1.12
MGR4104	MamT	19	1	15	13	14	15	-1.07	1.15
MGR4109	HlyB (Type I secretion system ATPase)	81	5 / 6	ND	ND	11	11	Unique	Unique
MGR4115	Hypothetical protein	12	0	ND	13	13	ND	Unique	Unique (WT)
MGR4147	ftsZ like protein	34	0	12	11	13	13	1.08	1.18
MGR4150	MamY	41	1 / 2	17	16	17	14	1.00	-1.14
MGR4191	Adenine phosphoribosyltransferase	20	0	10	12	10	11	1.00	-1.09

[a] TMDs, transmembrane domains
[b] ND, not detected

Table S2-5. Putative Fur-box sequences identified by similarity to predicted Fur-box sequences of *M. magneticum* (Rodionov *et al.*, 2006) and their relative position to the startcodon of differentially expressed genes in RU-1.

NCBI accession no. or locus tag	Protein identification / function	Putative Fur-box sequence	Position
MGR0081	**TonB-dependent outer membrane receptor**	**GTTGAGAGTGCGACGCATT**	**-80**
MGR0236	**Bacterial extracellular solute-binding protein**	**CATGCAAATCACTCGCATA**	**-36**
MGR0237	PAS:GGDEF		
MGR0662	Hypothetical protein	AAAGCGAGCTTCCCGCTGG	-59
MGR0705	Conserved hypothetical protein		
MGR0706	Conserved hypothetical protein	TTTGATAGTGATTTGCGTT	-90
MGR0707	Conserved hypothetical protein		
MGR1021	Periplasmic trypsin-like serine protease	-	-
MGR1446	**Feo B2**	**GGTGATAACCAATCGCGAC**	**-96**
MGR1447	**Feo A2**		
MGR1593	Transcriptional regulator ArsR family	GATGGCAAGGGGTTTTTAT	-101
MGR4109	HlyB type I secretion system ATPase	TTTGACGCGTGTATGCATC	-90
MGR0698	CydA cytochrome d ubiquinol oxidase subunit 1	GGTGCGGGGCAGTCGCCAG	-142
ABL14106	**Feo B1**	**ATCGCAACTCATTCGCAAT**	**-64**

[a] Proteins with putative relation to iron metabolism are shown in bold.

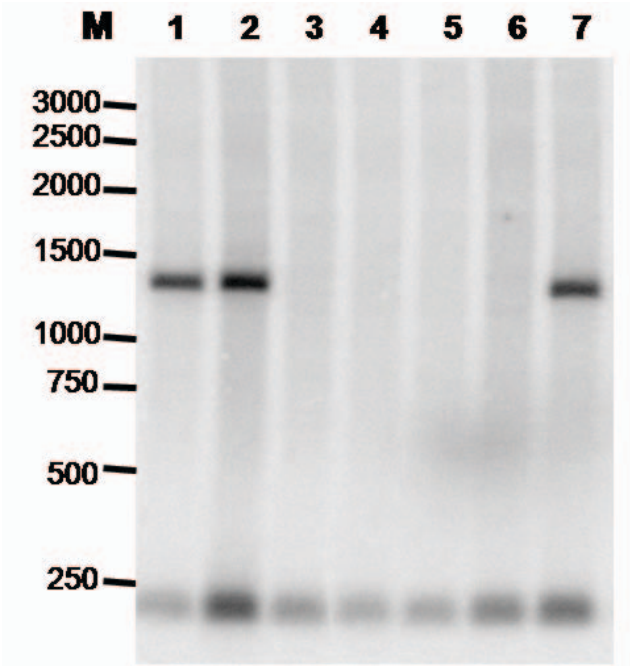

FIG. S2-1. Confirmation of *fur* deletion by Southern blot analysis of NcoI-digested WT (lane 1) and putative *fur* mutant (lane 2-7) genomic DNA. The blot was hybridized with a probe overlapping the NcoI restriction site. Digestion of WT should result in a 208 bp band and a 1362 bp fragment, whereas digestion of genomic DNA from *fur*⁻ clones should result in a fragment of 208 bp. Lane M, molecular weight marker (bp).

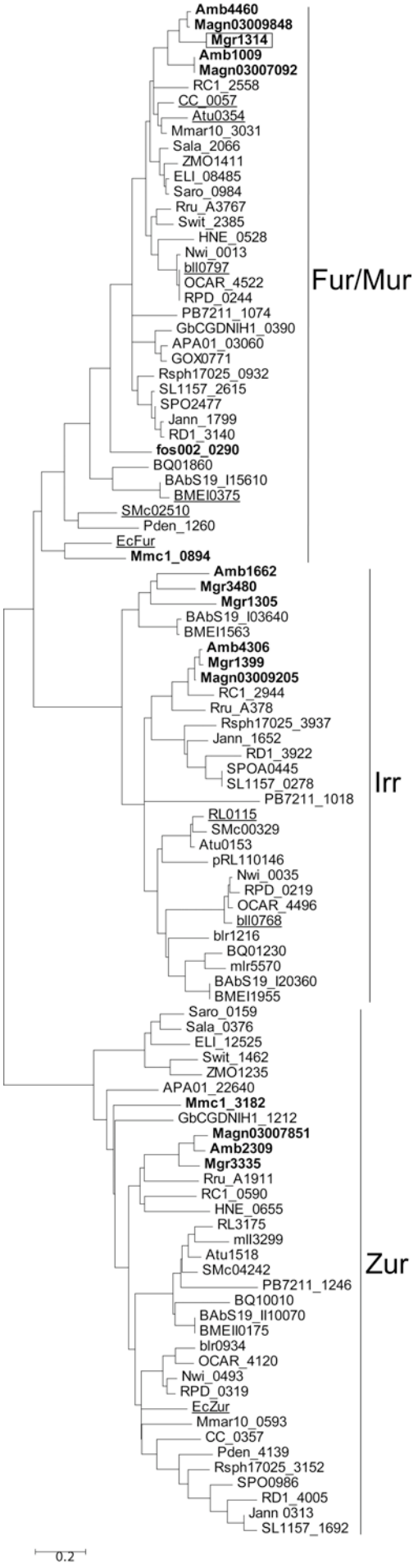

FIG. S2-2. Similarity tree of α-proteobacterial and *E. coli* Fur-like proteins. Sequences are designated by locus tag accession numbers. Fur-like proteins of MTB are shown in bold. Proteins that have been characterized experimentally are underlined. MgFur is boxed.

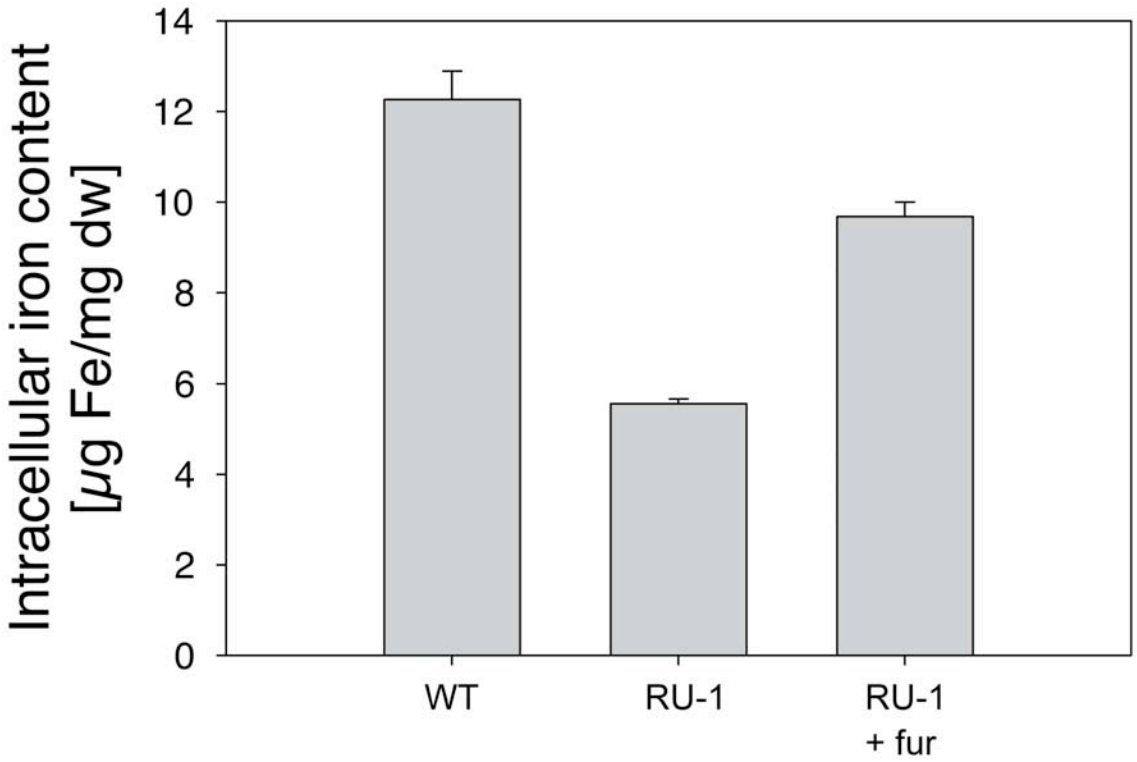

FIG. S2-3. Intracellular iron content of WT, RU-1 and RU-1 transcomplemented with pBBR1MCS-2fur grown in FSM under microaerobic conditions. Values are given as means ± SD of three independent replicates.

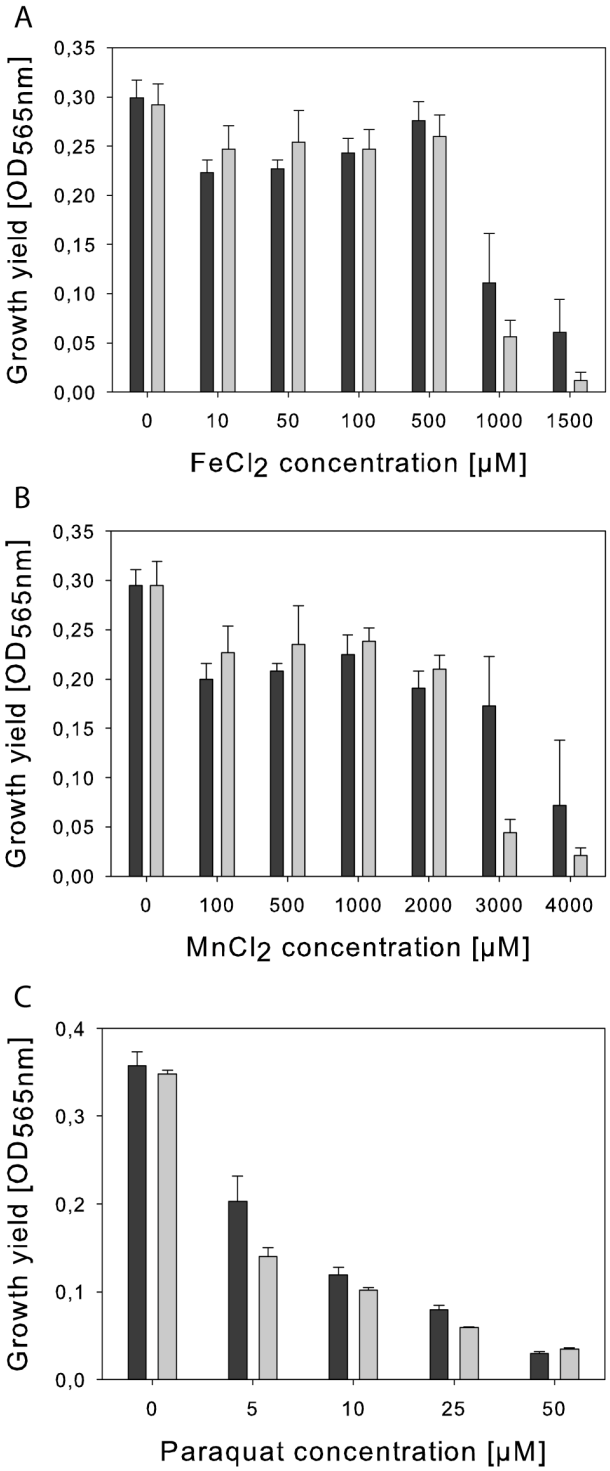

FIG. S2-4. Growth yield of WT and RU-1 after 24 h growth at 30 °C at different concentrations of iron (A), manganese (B), and paraquat (C). Values are given as means ± SD of three independent replicates.

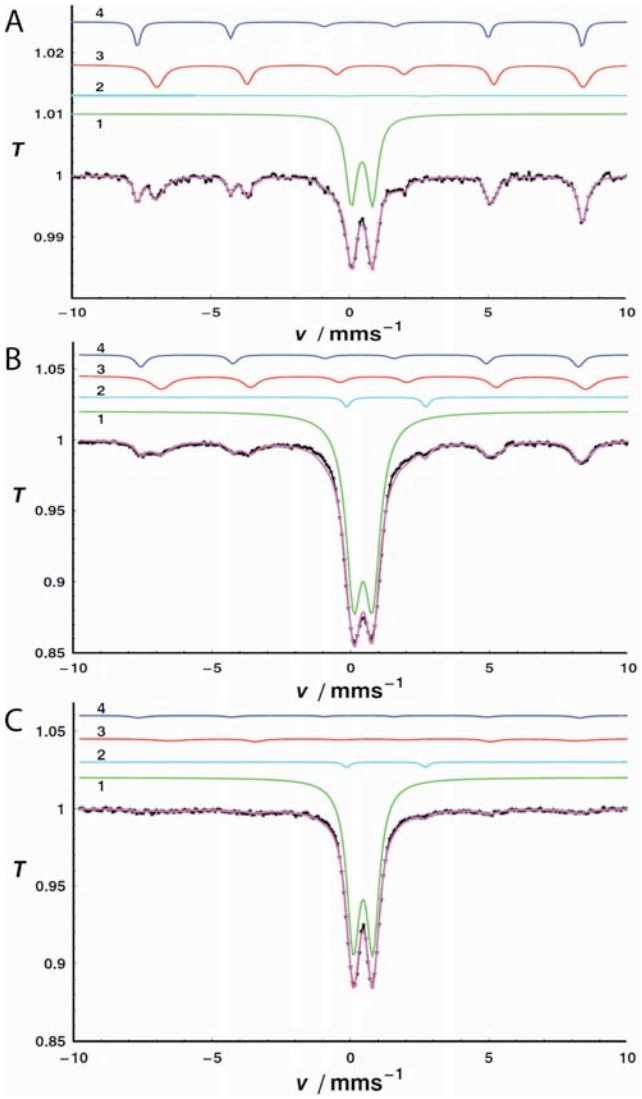

FIG. S2-5. Whole-cell transmission Mössbauer spectra of (A) WT, (B) RU-1 +Fe and (C) RU-1 –Fe. Precultures of (A) and (B) were grown in iron replete media. Precultures of (C) were kept in low iron media. Subspectrum 1 corresponds to a ferritin-like component characterized by a temperature-dependent doublet exhibiting an unusually low isomer shift for an oxo mineral; species 2 shows an isomer shift and quadrupole splitting typical for high spin ferrous iron in an octahedral oxygen ligand sphere. Subspectra (3) and (4) represent two magnetically split sextets attributed to magnetite A and magnetite B, respectively.

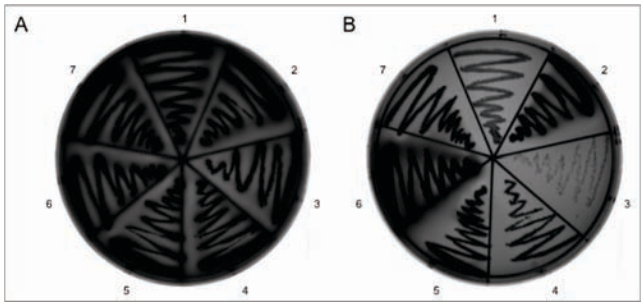

FIG. S2-6. FURTA assay with *E. coli* H1717 carrying (1) pGEM, (2) pGEMPfhuF, (3) pGEMPmgr4079, (4) pGEMPrplK, (5) pGEMPmms16, (6) pGEMPmamDC and (7) pGEMPmamAB streaked on (A) iron-depleted MacConkey (100 μM 2,2'-dipyridyl) and (B) iron-replete MacConkey (30 μM $FeCl_3$)

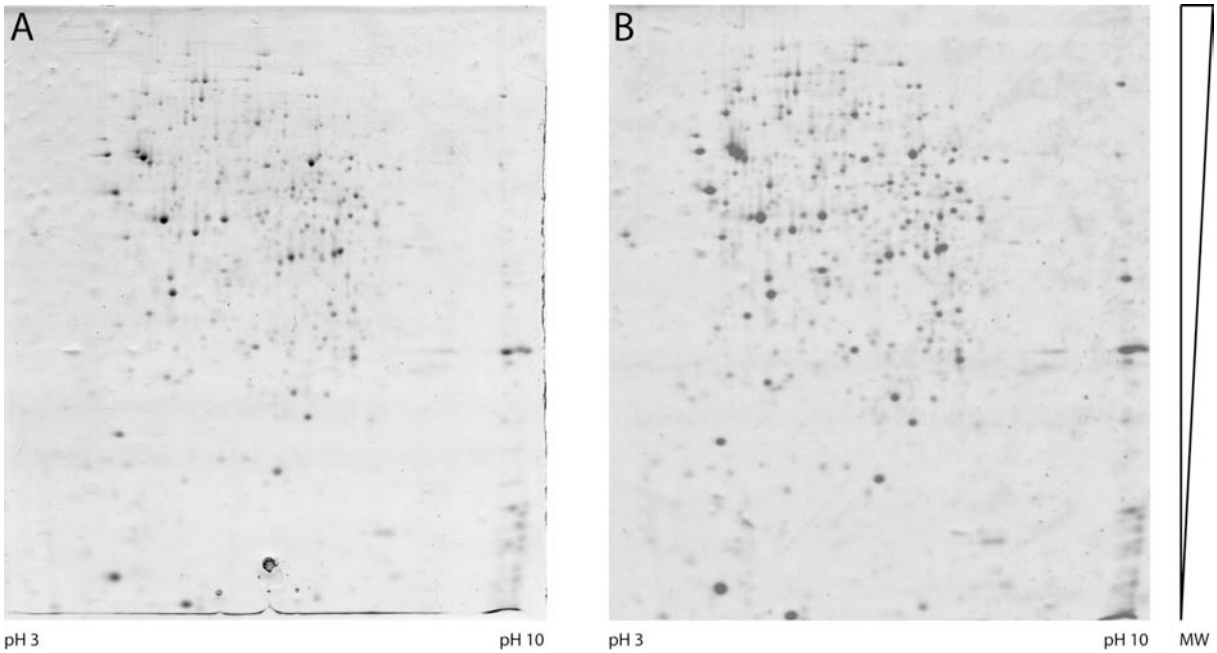

FIG. S2-7. Coomassie silver blue stained 2D-gels of soluble protein fractions obtained from A) WT and B) RU-1 after growth under iron-deplete conditions.

FIG. S2-8. Putative Fur-box consensus sequence of *M. gryphiswaldense* Fur regulated genes *feoAB1, feoAB2, mgr0081 and mgr0236* derived from homology search with Fur-box sequences of *M. magneticum* (Rodionov *et al.*, 2006).

2.9 References

Rodionov, D., Gelfand, M., Todd, J., Curson, A. and Johnston, A. (2006). Computational reconstruction of iron- and manganese-responsive transcriptional networks in α-proteobacteria. *PLoS Comput. Biol.* **2**: 1568-1585.

CHAPTER 3

The cation diffusion facilitator proteins MamB and MamM of *Magnetospirillum gryphiswaldense* have distinct and complex functions, and are involved in magnetite biomineralization and magnetosome membrane assembly

3.1 Abstract

Magnetotactic bacteria form chains of intracellular membrane-enclosed, nanometre-sized magnetite crystals for navigation along the earth's magnetic field. The assembly of these prokaryotic organelles requires several specific polypeptides. Among the most abundant proteins associated with the magnetosome membrane of *Magnetospirillum gryphiswaldense* are MamB and MamM, which were implicated in magnetosomal iron transport because of their similarity to the cation diffusion facilitator family. Here we demonstrate that MamB and MamM are multifunctional proteins involved in several steps of magnetosome formation. Whereas both proteins were essential for magnetite biomineralization, only deletion of *mamB* resulted in loss of magnetosome membrane vesicles. MamB stability depended on the presence of MamM by formation of a heterodimer complex. In addition, MamB was found to interact with several other proteins including the PDZ1 domain of MamE. Whereas any genetic modification of MamB resulted in loss of function, site-specific mutagenesis within MamM lead to increased formation of polycrystalline magnetite particles. A single amino acid substitution within MamM resulted in crystals consisting of hematite, which coexisted with magnetite crystals. Together our data indicate that MamM and MamB have complex functions, and are involved in the control of different key steps of magnetosome formation, which are linked by their direct interaction.

3.2 Introduction

Magnetotactic bacteria (MTB) use the earth's magnetic field for navigation to find growth-favouring microoxic zones within stratified sediments. This ability is based on the formation of unique intracellular organelles called magnetosomes. In the α-proteobacterial *Magnetospirillum* species individual magnetosomes consist of single-domain magnetite (Fe_3O_4) crystals and are enveloped by a magnetosome membrane (MM) that invaginates from the cytoplasmic membrane (Komeili *et al.*, 2006; Katzmann *et al.*, 2010). The magnetosome membrane contains a set of specific proteins that are involved in the uptake and intracellular sequestration of iron, crystallization of magnetite, as well as in the assembly and intracellular positioning of magnetosome chains (Grünberg *et al.*, 2001; Grünberg *et al.*, 2004; Komeili *et al.*, 2006; Scheffel *et al.*, 2006; Katzmann *et al.*, 2010). Most genes encoding the magnetosome membrane specific proteins are clustered within a genomic magnetosome island (Schübbe *et al.*, 2003; Ullrich *et al.*, 2005). This ~130 kb genomic region comprises the *mamAB*, *mamGFDC*, *mamXY*, and *mms6* gene operons that encode all known magnetosome membrane proteins. Whereas a large proportion of the magnetosome island genes is involved in the regulation of crystal size and morphology (Scheffel *et al.*, 2008; Ding *et al.*, 2010; Murat *et al.*, 2010; Tanaka *et al.*, 2011), only deletion of the 16 kb large *mamAB* gene cluster, which in *Magnetospirillum gryphiswaldense* comprises 17 co-transcribed genes, resulted in the loss of the ability to form any magnetosome-like structures (Murat *et al.*, 2010; Ullrich and Schüler, 2010). Through genetic dissection of the *mamAB* operon of *Magnetospirillum magneticum* AMB-1 eight genes were shown to be essential for magnetite biomineralization (Murat *et al.*, 2010). Whereas *mamE*, *mamM*, *mamN* and *mamO* deletion mutants did no longer produce magnetite crystals but were still able to form magnetosome membrane vesicles, no vesicles were observed in deletion mutants of *mamI*, *mamL*, *mamQ* and *mamB* (Murat *et al.*, 2010). However, still little is known about the molecular mechanisms of magnetosome membrane and magnetite formation. So far, only two of the essential proteins MamO and MamE, belonging to the family of putative HtrA/DegP family proteases, were analyzed in detail. While two distinct functions, targeting of magnetosome proteins to the magnetosome membrane and magnetite crystal maturation, have been assigned to MamE (Quinlan *et al.*, 2011), the functional role of MamO remained unclear (Yang *et al.*, 2010; Quinlan *et al.*, 2011).

Although other essential Mam proteins have not yet been analyzed in detail, putative functions were suggested for some of them because of homology to known protein families.

For example MamM and MamB, two of the most abundant magnetosome proteins, were suggested to have a role in magnetosome-directed iron transport because of their homology to the cation diffusion facilitator (CDF) family (Grünberg *et al.*, 2001; Nies, 2003; Grünberg *et al.*, 2004). CDF proteins are found in all domains of life and have been shown to contribute to metal ion homeostasis (Paulsen and Saier, 1997). Members of the CDF family generally transport divalent transition metal cations, including Zn^{2+}, Co^{2+}, Cd^{2+}, Mn^{2+}, Ni^{2+} and Fe^{2+} from the cytoplasm into intracellular compartments or into the periplasmic or extracellular space using the proton motive force (Nies, 2003; Grass *et al.*, 2005; Rosch *et al.*, 2009). Despite an unusual degree of size variation (300-750 aa residues) and sequence divergence, most members have a common architecture. With few exceptions CDF proteins are predicted to have a cytoplasmic N-terminus followed by six transmembrane-spanning helices and a cytoplasmic C-terminal tail (Paulsen and Saier, 1997). While transmembrane domains (TMD) are the most conserved regions of CDF family proteins, the carboxy-terminal domain (CTD) shows a high degree of sequence variability. At the structural level, however, the CTDs are notably conserved (Cherezov *et al.*, 2008; Higuchi *et al.*, 2009). Bioinformatic analyses revealed that the CDF family groups into three substrate-specific phylogenetic branches: (1) Zn-CDF, (2) Fe/Zn-CDF as well as (3) Mn-CDF (Montanini *et al.*, 2007). The majority of characterized CDF proteins belong to the Zn-CDF group, whereas the best-characterized member, FieF (YiiP), belongs to the subgroup of putative Fe/Zn-transporter. The X-ray structure of a FieF homodimer was resolved in a zinc-bound state, and three zinc-binding sites have been identified (Lu *et al.*, 2009). Four residues of the transmembrane helices (TMH) 2 and 5 form site A, a tetrahedral Zn^{2+} binding site located within the TMD that is believed to be the active site for zinc transport (Lu and Fu, 2007). Site B, the function of which remained unclear, is located in a cytoplasmic loop between transmembrane helix two and three. Four additional zinc cations are coordinated in site C and are stabilizing homodimer interactions at the CTD-CTD interface.

In the present study the functions of MamM and MamB of *M. gryphiswaldense* MSR-1 (MSR-1) were analyzed by deletion as well as site-directed mutagenesis. Besides further support for an iron-transporting function of MamM, we demonstrate that MamM is also involved in crystallization initiation and regulation of proper localization of other magnetosome proteins, such as MamC-GFP. Expression analyses, co-purification and a two-hybrid screening assay furthermore indicate an interaction between the two CDF family proteins MamM and MamB, which is required for the stabilization of MamB.

3.3 Results

3.3.1 MamM and MamB are highly conserved in all MTB

Analyses of sequenced MTB genomes as well as metagenomic sequences revealed that orthologues of *mamB* and *mamM* are present in the magnetosome islands of all MTB and that MamM and MamB are among the most highly conserved magnetosome proteins (Table S3-1). In eight of nine analyzed MTB sequences *mamM* and *mamB* were located within *mamAB*-like gene clusters, of which *mamM* was located upstream of *mamB* in seven gene clusters. Phylogenetic analyses showed that beside MamB (Montanini *et al.*, 2007), also MamM and MamV, a third putative CDF transporter exclusively found in the *mamAB* operons of *M. magneticum* AMB-1 and *Magnetospirillum magnetotacticum* MS-1, are members of the Fe/Zn-subfamily (FIG. S3-1A). MamB, MamM and MamV form a distinct coherent branch within this CDF subfamily (FIG. S3-1B), and are therefore designated as MTB-CDF. However, between each other the MTB-CDF proteins show a relatively high degree of sequence divergence (Table S3-1). With sizes of 318 aa and 297 aa MamM and MamB are within the size range of typical prokaryotic CDF members (Paulsen and Saier, 1997). Depending on the particular algorithm, MamB and MamM have three to six predicted transmembrane helices (Table S3-2).

3.3.2 Δ*mamM* and Δ*mamB* mutants are non-magnetic but have distinct phenotypes

Magnetospirillum gryphiswaldense Δ*mamB* and Δ*mamM* unmarked, in-frame deletion strains were constructed by a Cre/*loxP*-based method (Scheffel *et al.*, 2008). Both strains showed no growth defects compared to the wild type (data not shown), but were devoid of any electron-dense particles as shown by TEM (FIG. S3-2). Consistent with the lack of magnetite crystals, the intracellular iron content of Δ*mamB* and Δ*mamM* after microaerobic cultivation with 50 μM iron was reduced to 3.3 and 1.4 μM Fe g^{-1} dry weight (dw), respectively, compared to 60 μM Fe g^{-1} dw in the wild type. In addition, transmission Mössbauer spectra of MSR-1, strain MSR-1B, a spontaneous non-magnetic mutant lacking large parts of the magnetosome island (Schübbe *et al.*, 2003), Δ*mam*B and Δ*mamM* were recorded at 77 K and 4.2 K. Based on the Mössbauer parameters [isomer shift (δ), quadrupole splitting (ΔE_Q) and hyperfine field (Bhf)] four different Mössbauer species were identified

(Matzanke, 1991; Schünemann and Winkler, 2000; Matzanke, 2005) in spectra of MSR-1: magnetite (accounts to ~50% of the total cellular ^{57}Fe), a ferritin-like species (25% of the accumulated ^{57}Fe), an octahedral ferrous iron metabolite in an oxygen environment $[FeO_6X_n]^{n-10}$ (8.5% of the accumulated ^{57}Fe) and a putative Fe_4S_4-cluster (17% of the accumulated ^{57}Fe; Table 3-1; FIG. S3-3).

Table 3-1. Mössbauer parameters of iron metabolites in *M. gryphiswaldense* MSR-1, Δ*mamM,* Δ*mamB* and strain MSR-1B obtained from *in situ* spectra by least squares fit analysis. Spectra were taken at various temperatures in order to show magnetic splitting and to check second order Doppler shift. Spectra are depicted in FIG. S3-3.

Strain	Temperature [K]	ferritin-like					4Fe-4S			
		δ [mm s^{-1}]	ΔEq [mm s^{-1}]	Γ [mm s^{-1}]	Area [%]	Bhf [T]	δ [mm s^{-1}]	ΔEq [mm s^{-1}]	Γ [mm s^{-1}]	Area [%]
MSR-1	130	0.45	0.67	0.44	30.36	---	0.42	1.16	0.40	19.58
	77	0.46	0.64	0.43	27.25	---	0.45	1.09	0.39	16.80
	4.2	0.46	0.00	---	28.89	47.79	0.46	1.13	0.61	14.70
Δ*mamM*	77	0.46	0.72	0.43	54.50	---	0.45	1.21	0.36	32.54
	4.2	0.46	0.00	---	54.58	47.09	0.46	1.20	0.52	30.89
Δ*mamB*	77	0.46	0.71	0.42	55.00	---	0.46	1.20	0.36	33.53
	4.2	0.46	0.00	---	54.67	46.52	0.46	1.19	0.52	31.62
	2	0.46	0.00	---	55.41	46.47	0.46	1.20	0.51	30.79
MSR-1B	180	0.43	0.67	0.44	52.78	---	0.40	1.13	0.42	38.20
	150	0.44	0.68	0.43	52.78	---	0.41	1.17	0.40	38.20
	130	0.45	0.67	0.42	52.33	---	0.43	1.16	0.39	38.84
	110	0.45	0.69	0.44	52.78	---	0.43	1.17	0.39	38.20
	90	0.46	0.68	0.44	52.78	---	0.44	1.16	0.40	38.20
	80	0.46	0.69	0.45	52.78	---	0.45	1.18	0.40	38.20
	77	0.46	0.62	0.37	52.78	---	0.45	1.09	0.43	38.20
	4.2	0.46	0.00	---	52.78	47.50	0.46	1.19	0.62	38.20

Strain	Temperature [K]	$[Fe^{2+}O_6X_n]^{n-10}$				magnetite
		δ [mm s^{-1}]	ΔEq [mm s^{-1}]	Γ [mm s^{-1}]	Area [%]	Area [%]
MSR-1	130	1.33	2.79	0.77	7.57	42.49
	77	1.37	2.89	0.61	7.37	48.58
	4.2	1.39	2.99	0.79	8.82	47.60
Δ*mamM*	77	1.37	2.83	0.58	12.96	---
	4.2	1.39	2.90	0.70	14.53	---
Δ*mamB*	77	1.37	2.92	0.58	11.47	---
	4.2	1.39	2.95	0.80	13.72	---
	2	1.39	2.92	0.76	13.80	---
MSR-1B	180	1.30	2.61	0.41	8.97	---
	150	1.32	2.65	0.41	8.97	---
	130	1.35	2.76	0.47	8.84	---
	110	1.34	2.74	0.45	8.97	---
	90	1.36	2.75	0.44	8.97	---
	80	1.36	2.78	0.46	8.97	---
	77	1.37	2.87	0.32	8.97	---
	4.2	1.39	3.03	0.51	8.97	---

However, all three mutant strains lacked magnetite, whereas the other three iron species were also present: an octahedral ferrous iron metabolite in an oxygen environment $[FeO_6X_n]^{n-10}$ (~ 11% of the accumulated ^{57}Fe) , a ferritin-like species (~ 60% of the accumulated ^{57}Fe) and a putative Fe_4S_4-cluster (25 – 28% of the accumulated ^{57}Fe). Therefore, MamB and MamM seem to have magnetosome-specific functions, but are not involved in cytoplasmic iron accumulation.

Similar to findings in a *mamB* deletion mutant of *M. magneticum* AMB-1 (Murat *et al.*, 2010) cryo-electron tomographic analyses revealed that *M. gryphiswaldense* Δ*mamB* lacks any intracellular membranes (FIG. 3-1).

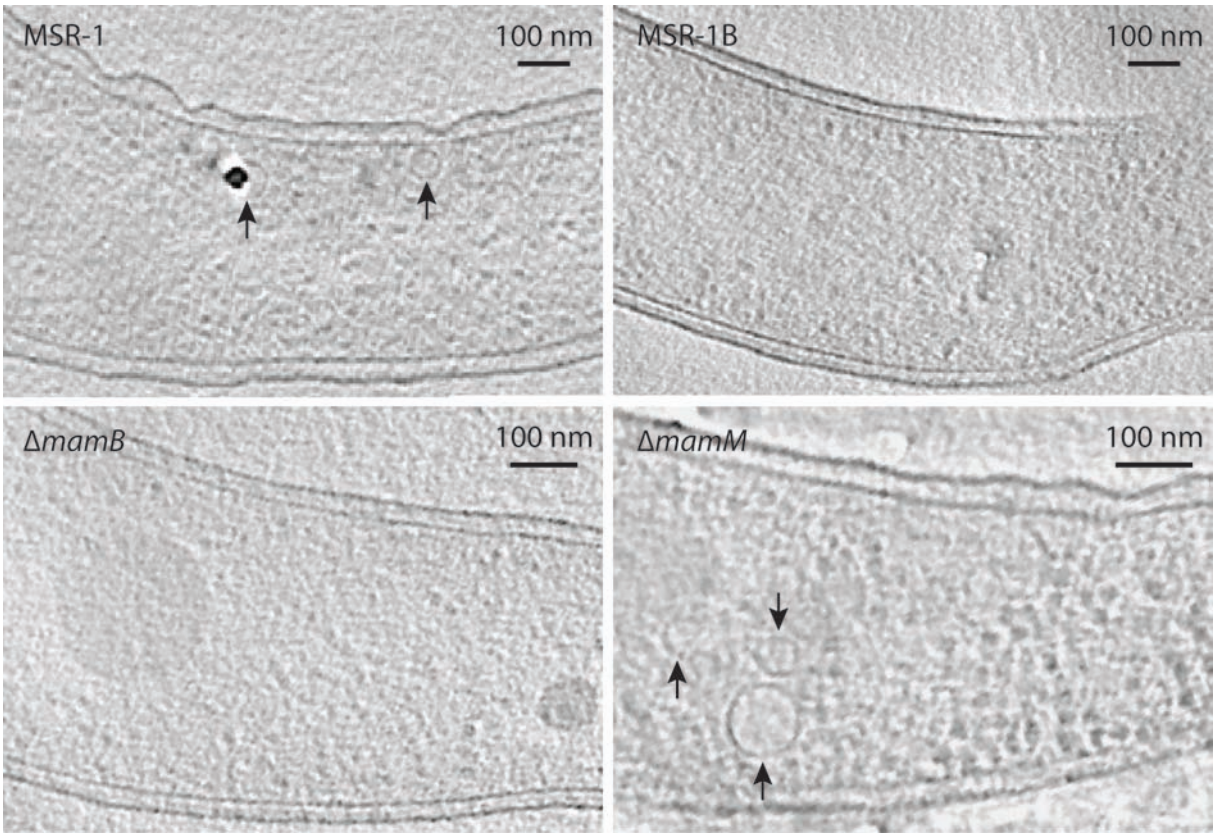

FIG. 3-1. x,y-slices of tomograms of *M. gryphiswaldense* strains MSR-1, MSR-1B, Δ*mamB* and Δ*mamM*. Arrows represent positions of magnetosome vesicles.

Whereas vesicles were clearly visible in MSR-1 and Δ*mamM*, vesicles were also not found in cryo-electron tomograms of MSR-1B (FIG. 3-1).

Complementation of Δ*mamM* and Δ*mamB* with wild type alleles restored the ability of both mutants to form magnetite crystals (FIG. S3-2). Transcomplementation of Δ*mamM* with pRU1-mamMwt restored the magnetic response to $C_{mag} = 0.92$ (± 0.114), whereas a magnetic response of $C_{mag} = 0.617$ (± 0.102) was observed when Δ*mamB* was transcomplemented with pRU1-mamBwt.

In trans expression of *mamB* in Δ*mamM* by pRU1-mamBwt and expression of *mamM* in Δ*mamB* by pRU1-mamMwt did not restore magnetite formation in the mutants, suggesting that MamB and MamM cannot compensate for each other.
Whereas the MamB orthologue of the related strain *M. magneticum* MS-1 restored magnetite formation to the same level as the native MgMamB, MamB orthologues of *Magnetococcus* sp. MC-1, the magnetic vibrio strain MV-1 or from the fosmid clone Fos001 were not able to transcomplement the Δ*mamB* mutant. This indicates that the MamB orthologues from remotely related MTB are either not expressed, functionally distinct, or MamB function depends on highly specific protein-protein interactions.

3.3.3 MamM is required for stability of MamB

Total membrane extracts of Δ*mamM* and Δ*mamB* were analyzed by Western blot. Immunodetection of MamM revealed equal amounts of MamM in MSR-1, Δ*mamB* and Δ*mamM* (pRU1-mamMwt), and confirmed its absence in Δ*mamM* (FIG. 3-2A). However, in Δ*mamM* also the amount of MamB was substantially reduced, since only a very faint MamB band was detected in the membrane fraction of Δ*mamM* (FIG. 3-2A). Although Δ*mamM* could be transcomplemented expression of *mamA*, located 4.1 kb downstream of *mamM*, but 1.8 kb upstream of *mamB*, was tested. Since the expression level of *mamA* was similar in all tested strains, polar effects caused by deletion of *mamM* could be excluded (FIG. 3-2A). However, transcomplementation of Δ*mamM* with pRU1-mamMwt also restored the MamB amount within Δ*mamM* membrane fractions back to wild type levels (FIG. 3-2A). These results suggest that stablility of MamB depends on the presence of MamM.

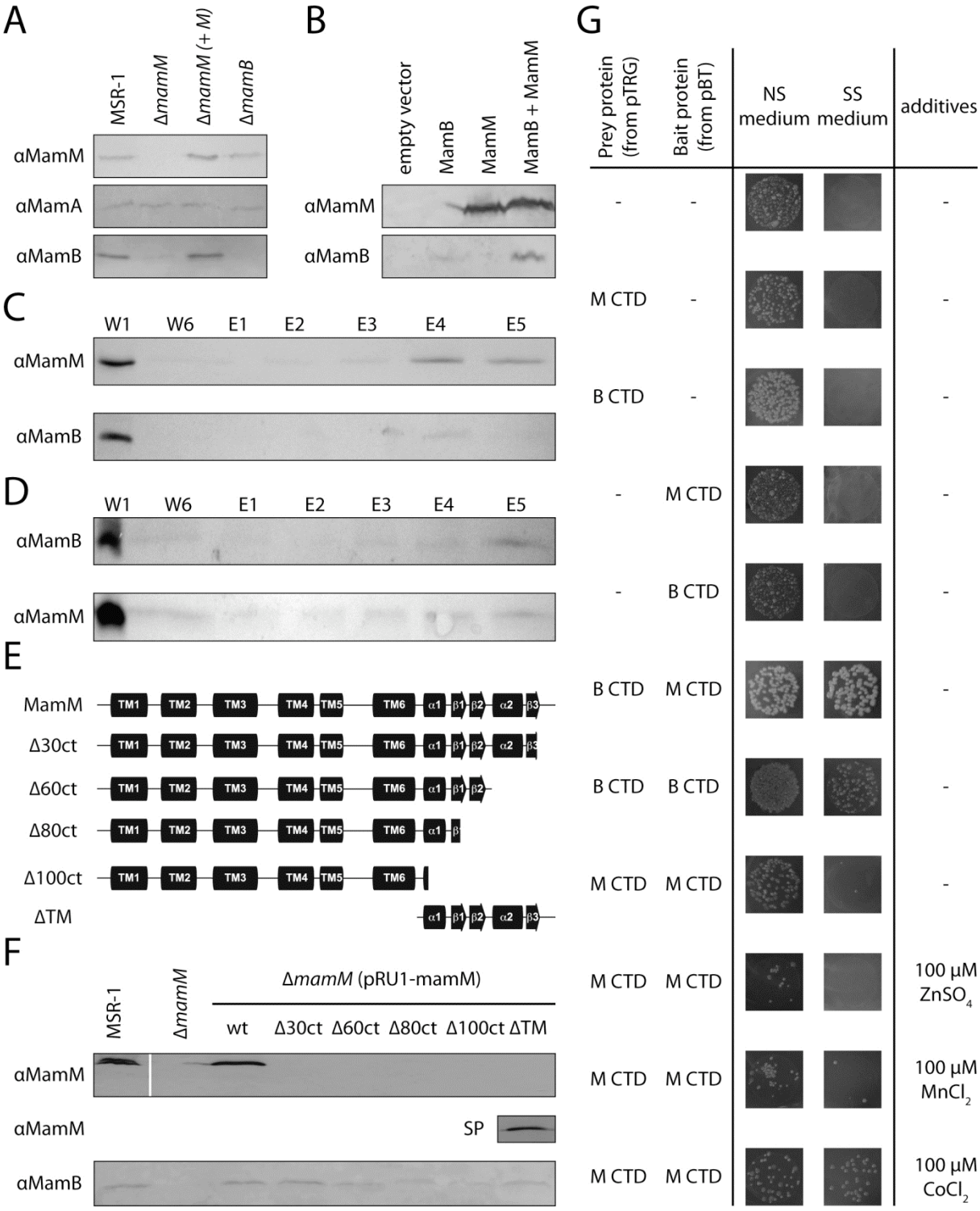

FIG 3-2. MamM stabilizes MamB by direct interaction. A) MamM, MamA and MamB immunodetection in total membrane fractions of *M. gryphiswaldense* MSR-1, Δ*mamM*, Δ*mamM* (pRU1-mamMwt) and Δ*mamB*. B) Immunodetection of MamM (top) and MamB (bottom) in crude extracts of *A. tumefaciens* C58 containing an empty vector or expressing MamB (B), MamM (M) or MamB + MamM (M+B). C) Strep-Tactin affinity chromatographic purification of MamM-Strep (top) and co-elution of untagged MamB (bottom). D) Strep-Tactin affinity chromatographic purification of MamB-Strep (top) and co-elution of untagged MamM (bottom); W1 and W6, washing fractions 1 and 6; E1 to E5, elution fractions 1 to 5, respectively. Co-elution of untagged MamM with MamB-Strep was additionally confirmed by co-expression in *E. coli* (FIG. S3-4). E) Overview of truncation constructs used for transcomplementation of Δ*mamM* and schematic representation of secondary structure elements. See FIG. S3-5A for 3D model representation of the deletions. F) Transcomplemetation of Δ*mamM* with MamM proteins shown in (E) and immunodetection of MamM (top) and MamB (bottom) proteins in total membrane fractions of *M. gryphiswaldense* MSR-1, Δ*mamM* and transcomplemented Δ*mamM* strains (top).

C-terminal truncated mutant proteins MamM Δ30ct to MamM Δ100ct lack the epitope recognized by the MamM-antibody. The N-terminal truncated protein MamM ΔTM lacking all transmembrane spanning helices was only detectable in the soluble protein fraction (SP, middle). G) Two-hybrid analysis of the interaction between MamB CTD (B CTD) and MamM CTD (M CTD) shown by growth of the two-hybrid validation *E. coli* strain spotted onto selective and nonselective screening medium after co-transformation with different prey (derivatives of pTRG) and bait (derivatives of pBT) expression vectors. Colony growth on nonselective screening (NS) medium verifies that co-transformation was successful, whereas on selective screening (SS) medium, colonies can grow only in the case of an interaction between bait and prey fusion proteins.

Next, it was tested if MamM alone is sufficient for the observed stabilization or if further magnetosome proteins are required. Therefore, *mamB* or *mamM* or both were expressed in the related α-proteobacterium *Agrobacterium tumefaciens* C58. Western blot analyses showed that *mamM* was highly expressed, independently of the co-expression of *mamB*. However, stability of MamB depended on the presence of MamM (FIG. 3-2B), since the amount of MamB was substantially reduced in the absence of MamM. The dependence of *mamB* expression on the coexpression of *mamM* was also observed upon overexpression of *mamM* and *mamB* in *Escherichia coli* (data not shown). These data clearly demonstrate that solely MamM is required for MamB stabilization.

To analyse, whether the stabilizing effect of MamM relies on a direct interaction between MamM and MamB co-purification experiments were performed. Therefore either MamB or MamM were labelled at the C-terminal end with a StrepII-tag and expressed in the corresponding deletion mutants *in trans*. After cell disruption, fractionation and solubilization, both Strep-tagged proteins could be affinity-purified using Strep-Tactin sepharose (FIG. 3-2C and D). However, also unlabelled MamM was detected in purified MamB-Strep extracts, as well as unlabelled MamB in purified MamM-Strep extracts. No band corresponding to the size of MamB was copurified when MamM-Strep was expressed in Δ*mamB* (data not shown). These data indicated that MamM and MamB physically interact with each other.

To identify the domains mediating the MamB-MamM interaction, gradually truncated MamM proteins were expressed *in trans* in the Δ*mamM* background (FIG. 3-2E). As monitored by C_{mag} measurements, magnetite formation of Δ*mamM* was only restored when the C-terminal truncated protein MamM Δ30ct was expressed. All other *mamM* mutants expressing proteins with increasingly larger C-terminal deletions failed to restore magnetite formation. Complementation experiments with N-terminally truncated MamM proteins also failed to restore the magnetic response of Δ*mamM*. However, as most MamM N-terminal truncations were not or only weakly expressed, they were not considered for further analysis except for MamM ΔTM.

In contrast to restoration of magnetite formation the ability to stabilize MamB did not require large parts of the MamM C-terminus: whereas MamM Δ30ct restored MamB expression to a

wild type-like level, deletion of 60 aa (MamM Δ60ct) reduced MamB expression, although expression level was still higher than in the untransformed Δ*mamM* mutant (FIG. 3-2F). MamB expression was further decreased when 80 (MamM Δ80ct) or 100 aa (MamM Δ100ct) were deleted, but MamB expression was still above the MamB expression level of Δ*mamM*. A slight increase in the MamB amount compared to the MamB levels of MamM Δ80ct and MamM Δ100ct transcomplemented Δ*mamM* was observed when only the soluble C-terminal domain of MamM was expressed (MamM ΔTM). These results indicated that the MamM C-terminal domain is required for MamB stabilization, but is not sufficient to restore MamB expression to wild type levels when expressed alone.

To seek further evidence for a direct interaction between MamB and MamM C-terminal domains, the BacterioMatch II bacterial two-hybrid system (Stratagene) was used. Interactions between a bait λcI-fusion protein encoded on a recombinant pBT and a prey RNAPα-fusion protein produced by a recombinant pTRG were monitored by growth of *E. coli* reporter strain co-transformants on selective medium containing 2.5 mM 3-amino-1,2,4-triazole (3-AT). To test for C-terminal interactions between MamM and MamB the C-terminal domains of MamB or MamM were fused to λcI on pBT and to the RNAPα subunit on pTRG. Whereas control co-transformations (pBT + pTRG, pBT-mamBCTD + pTRG, pBT-mamMCTD + pTRG, pBT + pTRG-mamBCTD and pBT + pTRG-mamMCTD) did not result in detectable growth on selective screening medium, co-transformation with pBT-mamMCTD and pTRG-mamBCTD yielded equal colony numbers on non-selective and selective screening medium (FIG. 3-2G). However, co-transformation of the *E. coli* validation reporter strain with pBT-mamBCTD and pTRG-mamBCTD also resulted in a significant number of colonies on selective screening medium, indicating a self-interaction of MamB. Interestingly, co-transformations with pBT-mamMCTD and pTRG-mamMCTD resulted in detectable growth on selective screening medium only when the medium was supplemented with metal ions, suggesting that the interaction between two protomers of the MamMCTD may depend on the presence of metal ions (FIG. 3-2G).

3.3.4 MamB participates in multiple protein-protein interactions

Multiple sequence alignments of all MamB and MamM homologues showed that in close proximity to the N-terminus a unique CxxC sequence motif was present in all MTB-CDF orthologues (FIG. S3-6A). In addition, a third cysteine residue conserved in all MTB-CDF was found at position 138 of MamB, and at position 139 of MamM. Since similar

residues were absent from CDF proteins of non-magnetotactic organisms, a specific function in magnetosome synthesis for these residues was assumed. Surprisingly, replacement of single or all conserved cysteine residues by serine/alanine within MamM did not affect the ability of the mutated proteins to transcomplement Δ*mamM* to the same level as the wild type allele (FIG. S3-6B). Within MamB, however, exchange of any of the three conserved cysteines by serine/alanine completely abolished its ability to transcomplement Δ*mamB* (FIG. S3-6C). Western blot analyses confirmed that all mutated proteins were expressed at wild type level. Thus the MTB-CDF specific cysteine residues are essential for MamB function, but had no detectable function in MamM.

One possible function of cysteine residues within CDF proteins is the formation of intermolecular disulphide bridges for oligomer assembly, as described for the plant CDF transporter MTP1 (Blaudez *et al.*, 2003). To test if the cysteine residues C6, C9 or C138/139 of MamB and MamM are also involved in disulphide bridge formation, band patterns of wild type proteins in total membrane fractions of MSR-1 after non-reducing SDS-PAGE were investigated. Analysis of MamM revealed no clear evidence for the formation of intermolecular disulphide bridges, since immunodetection of MamM yielded a band at the expected size of a MamM monomer as well as a smear migrating on top of the non-reducing SDS-PAGE gel (FIG. S3-7A). In similar experiments with MamB, however, four high molecular bands at sizes of approximately 62 kDa, 78 kDa, 80 kDa and 114 kDa representing putative oligomers of MamB were observed. No band at the expected size of a MamB monomer was observed unless dithiothreitol (DTT) as a reducing agent was included into the sample buffer (FIG. S3-7B). Interestingly, an identical MamB-band pattern after non-reducing SDS-PAGE was observed when membrane extracts of Δ*mamM* were analyzed (data not shown). Therefore, MamB is likely to form oligomers that are sensitive to DTT, independently of its interaction with MamM. To further investigate MamB oligomer formation the MamB cysteine exchange mutants were included into the analyses. Whereas all putative oligomer bands found in the wild type were also observed in membrane extracts of Δ*mamB* expressing MamB C6S, MamB C9S or MamB C6,9S; oligomer bands with sizes of 62 and 114 kDa were lacking in membrane extracts of Δ*mamB* (pRU1-mamBC138A) (FIG. 3-3). However, an additional band corresponding to the size of a MamB monomer was detectable, indicating that the exchange of C138A partially inhibits MamB-oligomer formation.

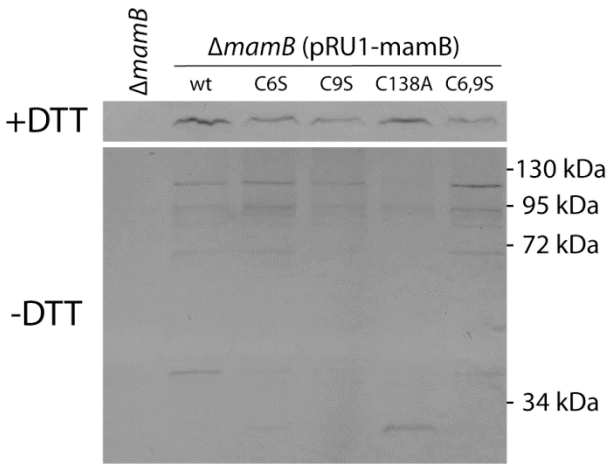

FIG 3-3. Immunodetection of MamB wild type and mutant proteins in total membrane fractions of Δ*mamB* and transcomplemented Δ*mamB* strains after reducing SDS-PAGE (+DTT, upper panel) or non-reducing SDS-PAGE (-DTT, lower panel). Molecular weight markers are shown at right.

Hints for additional putative protein-protein interactions were obtained using bioinformatic screens for functional sites/motifs within MamB and MamM (Prosite, Motif Scan, ELM server). Analyses by the ELM server (Puntervoll *et al.*, 2003) revealed the presence of eleven internal putative PDZ class III binding-motifs within MamB and MamM and one class II binding-motif at the very C-terminal end of MamB (Table S3-3). PDZ domains are small protein-protein interaction modules organizing protein networks on membranes (Fanning and Anderson, 1999), which have been extensively studied in eukaryotes, but are also present in bacterial proteins (Ponting, 1997). Analyses of protein domain architectures of all MSR-1 proteins using SMART (Schultz *et al.*, 1998) revealed the presence of ten putative PDZ domains within seven protein sequences, including the two magnetosome membrane proteins MamE and MamP. As most PDZ domains recognize the very carboxy-terminal ends of their target proteins (Jelen *et al.*, 2003), removal of the MamB and MamM C-terminal ends should affect their ability to transcomplement the corresponding mutants if these proteins are interaction partner of PDZ domains. Therefore complementation analyses with Δ*mamB* expressing MamBwt and mutated MamB proteins carrying deletions of five or ten C-terminal amino acids (MamB Δ5ct and MamB Δ10ct) were performed. Since MamM carries a longer C-terminal end, the *mamM* mutant was transcomplemented with wild type or mutant proteins carrying deletions of ten and thirty amino acids. Whereas the C-terminal deletions did not affect the ability of MamM to restore the magnetic response of Δ*mamM* (FIG. 3-4A), a gradual decrease of the magnetic response with Δ*mamB* expressing progressively truncated MamB proteins was observed (FIG. 3-4B). Thus, these results hint towards a putative interaction of MamB with PDZ domain containing proteins.

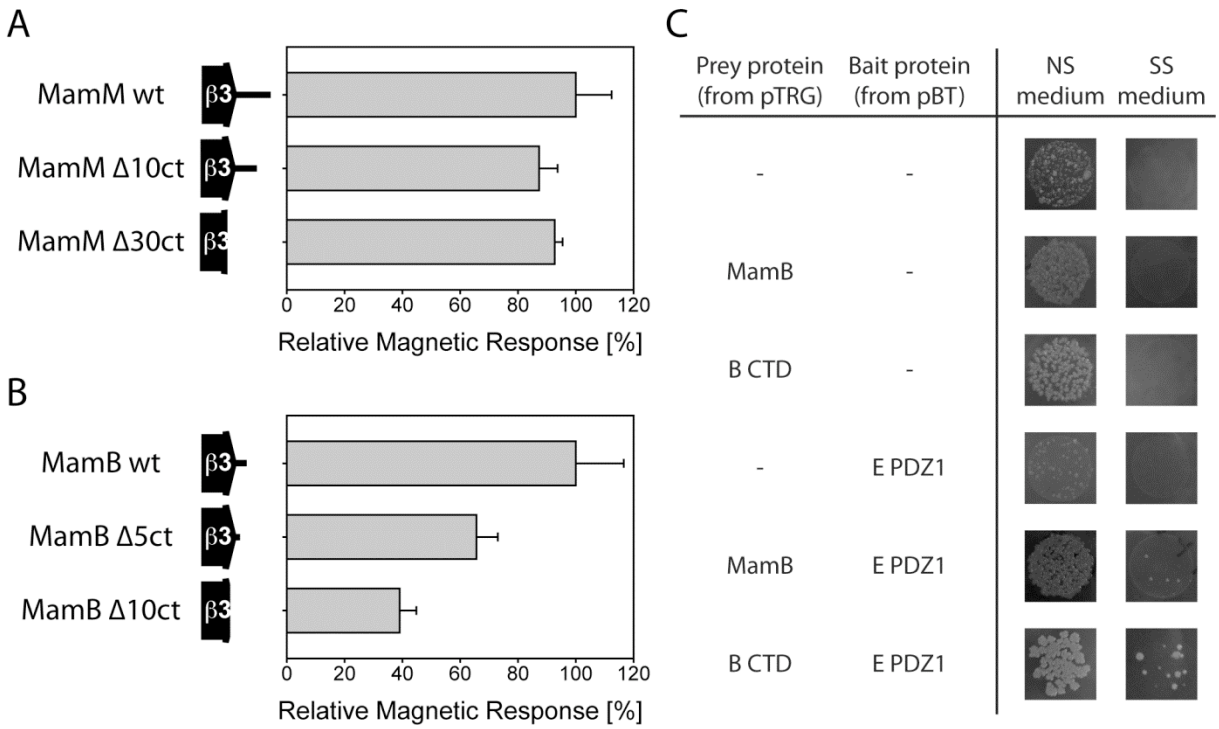

FIG 3-4. A) Magnetic response of Δ*mamM* expressing MamM Δ10ct and MamM Δ30ct relative to Δ*mamM* (pRU1-mamMwt). The assays were performed in triplicate with three independent transconjugants, and values are expressed as means, with standard deviations displayed as error bars. B) Magnetic response of Δ*mamB* expressing MamB Δ5ct and MamM Δ10ct relative to Δ*mamB* (pRU1-mamBwt). The assays were performed in triplicate with three independent transconjugants, and values are expressed as means, with standard deviations displayed as error bars. C) Two-hybrid analysis of the interaction between MamB, the MamB CTD (B CTD) and the MamE PDZ1 (E PDZ1) domain shown by growth of the *E. coli* two-hybrid validation strain spotted onto selective and nonselective screening medium after co-transformation with different prey (derivatives of pTRG) and bait (derivatives of pBT) expression vectors. Colony growth on nonselective screening (NS) medium verifies that co-transformation was successful, whereas on selective screening (SS) medium, colonies can grow only in the case of an interaction between bait and prey fusion proteins.

To directly test for interactions between MamB and PDZ domains the BacterioMatch II bacterial two-hybrid screen was used as described above. MamB as well as its C-terminal domain were fused to the RNA polymerase α-subunit (in pTRG) and the PDZ domains of MamE as well as MamP were fused to the λcI-repressor (in pBT). Growth on selective screening medium was only observed when co-transformations with pBT-mamEPDZ1 and pTRG-mamB or pTRG-mamBCTD were performed, suggesting an interaction of the PDZ1 domain of MamE with the C-terminal domain of MamB (FIG. 3-4C).

3.3.5 MamM and MamB are targeted to the magnetosome as well as to the cytoplasmic membrane

In previous studies MamM and MamB were co-purified with magnetite crystals, demonstrating that both proteins are directly associated with the magnetosome membrane

(Grünberg *et al.*, 2001). However, it remained unclear if MamB and MamM are exclusively targeted to the magnetosome membrane. To analyse the subcellular localization of MamM and MamB different cell fractions of MSR-1 were separated by SDS-gel electrophoresis, blotted and probed with anti-MamM and anti-MamB antibodies. MamB was present in all membrane containing cell fractions, but not detectable in the soluble protein fraction. Despite detection of a faint MamM band in the soluble protein fraction the cell lysate and total membrane fractions revealed much stronger MamM signals. Strongest MamM signals, however, were detected in the magnetosome membrane fraction. Although MamB was partially degraded during magnetosome membrane preparation, the magnetosome membrane fraction also revealed the strongest MamB signals. Interestingly, MamM and MamB signals were also detectable in the non-magnetic membrane fraction (FIG. 3-5A), suggesting that the localization of both MTB-CDF proteins is not restricted to the magnetosome membrane.

Consistent with Western blot results, a C-terminal MamM-GFP fusion expressed *in trans* in MSR-1 localized along the cytoplasmic membrane as well as in a straight line running through the centre of the cell resembling a chain-like organization (FIG. 3-5B). When MamM-GFP was expressed in Δ*mamJ*, in addition to a fluorescence signal around the cell a single bright fluorescent focus appeared within the cell, consistent with magnetosome localization of Δ*mamJ* cells (Scheffel *et al.*, 2006) (FIG. 3-5B). *In trans* expression of a C-terminal MamB-GFP fusion in MSR-1 resulted in several different localization patterns, including one to three bright foci distributed through the cell, as well as patchy membrane localization. However, in 20% of the MSR-1 (pRU1-mamBGFP) population MamB-GFP fluorescence signals were also observed as a bright chain-like structure at midcell (FIG. 3-5C).

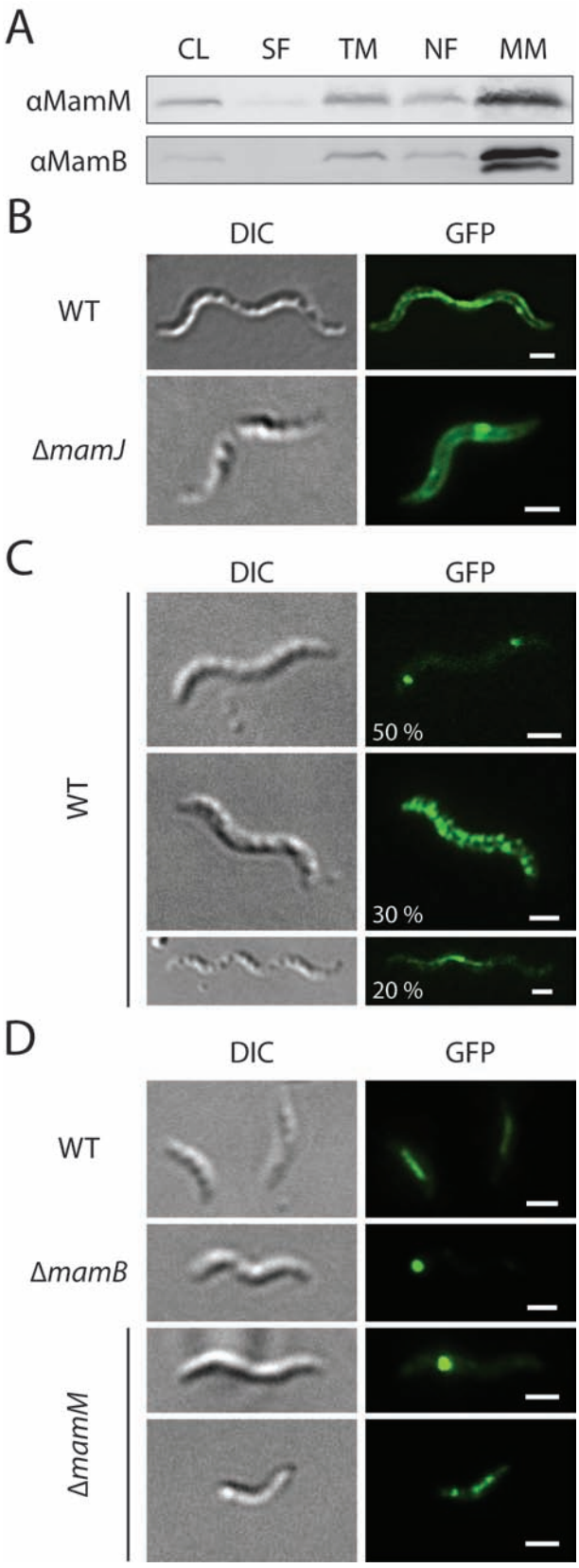

FIG 3-5. A) Immunodetection of MamM (top) and MamB (bottom) in cell lysate (CL), soluble (SF), total membrane (TM), non-magnetic (NF) and magnetosome membrane (MM) protein fractions of MSR-1. B) Representative fluorescence micrographs of MSR-1 and Δ*mamJ* expressing MamM-GFP. C) Representative fluorescence micrographs of MSR-1 expressing MamB-GFP. Values in the lower left corner indicate the % distribution of the corresponding localization pattern. D) Representative fluorescence micrographs of MSR-1, Δ*mamB* and Δ*mamM* expressing MamC-GFP. ≥500 cells were examined. Scale bars, 1 μm.

3.3.6 Localization of MamC-GFP is altered in Δ*mamM* and Δ*mamB*

The *in vivo* localization of MamC-GFP, a marker for magnetosome chain localization (Lang and Schüler, 2008; Quinlan *et al.*, 2011), was analyzed in Δ*mamM* and Δ*mamB*. Whereas MamC-GFP mainly localized as a filament-like structure centered at midcell in MSR-1 (pCL6) (FIG. 3-5D), this wild type-like localization was never observed in Δ*mamB* (pCL6). Here only one to three, fluorescent foci without a clear intracellular localization were observed (FIG. 3-5D). In a Δ*mamM* (pCL6) strain, the MamC-GFP fluorescence signals also mainly appeared as one or multiple, fluorescent foci without specific localization. However, in ~2% of the Δ*mamM* (pCL6) population the arrangement of the fluorescent foci was reminiscent of short or fragmented magnetosome chains (FIG. 3-5D).

3.3.7 MamM is involved in the control of magnetite nucleation and crystal growth

We performed a series of site-directed mutagenesis experiments to exchange amino acids, which, according to a protein alignment with the related protein FieF (FIG. 3-6A), corresponded to the putative active site (metal binding 'site A'). The ability of the mutant MamM or MamB proteins to restore magnetite formation in Δ*mamM* or Δ*mamB in trans*, respectively, was monitored by determination of the magnetic response (C_{mag}).

Whereas the wild type alleles restored magnetite biomineralization as described above, no magnetic response was observed when *mamB* mutant alleles (H46A, D50A, D158A) were expressed in Δ*mamB*. Even a replacement of the conserved aspartate 50 by glutamate (D50E) did not restore magnetite crystallization. In contrast, all tested mutant alleles of MamM (Y46H, Y46D, D50A, H155A, H159A) restored magnetic response of Δ*mamM*. However, the magnetic response of Δ*mamM* expressing *mamM* mutant alleles was not restored to the same level as with the wild type allele. Whereas an exchange of tyrosine 46 to histidine (Y46H, C_{mag} = 0.82) restored the magnetic response of Δ*mamM* to 90% of the wild type allele, replacement of tyrosine 46 with aspartate reduced magnetic response to only ~1% of the wild type level (C_{mag} = 0.01). Intermediate magnetic responses were detected in Δ*mamM* mutants expressing MamM D50A (C_{mag} = 0.46; 50% of wild type allele), MamM H155A (C_{mag} = 0.59; 65% of wild type allele) and MamM D159A (C_{mag} = 0.52; 56% of wild type allele) (Table S3-4).

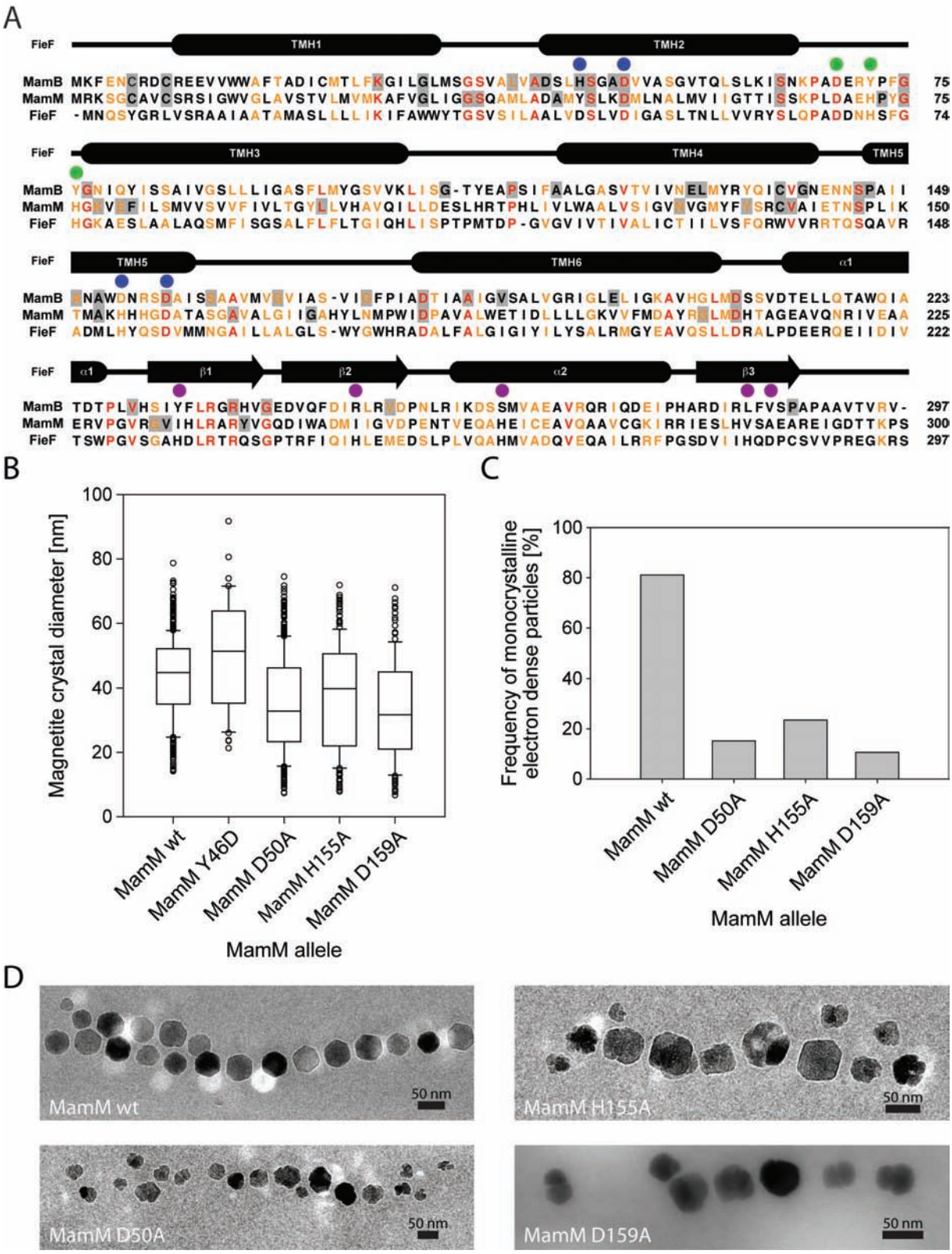

FIG 3-6. A) ClustalW sequence alignment between MamB, MamM and FieF with schematic representation of FieF secondary structure according to (Lu *et al.*, 2009). Conserved residues are shown in red and homologous residues in orange. Gray boxes indicate conserved residues within MamB or MamM homologues. FieF metal binding sites A, B and C are indicated by blue, green and purple dots, respectively. See also FIG. S3-5 for 3D model representation of MamB and MamM. B) Box plot showing magnetite crystal size distribution of Δ*mamM* strains expressing different MamM proteins grown at 1% O_2 for 72 h at 23°C. C) Frequency of monocrystalline electron-dense particles determined from 132 (MamM wt), 92 (MamM D50A), 85 (MamM H155A) and 66 (MamM D159A) particles shown in (B). D) Representative TEM micrographs of electron dense particles from Δ*mamM* strains expressing MamM wt, MamM D50A, MamM H155A and MamM D159A shown in (C).

Whereas the wild type alleles restored magnetite biomineralization as described above, no magnetic response was observed when *mamB* mutant alleles (H46A, D50A, D158A) were expressed in Δ*mamB*. Even a replacement of the conserved aspartate 50 by glutamate (D50E) did not restore magnetite crystallization. In contrast, all tested mutant alleles of MamM (Y46H, Y46D, D50A, H155A, H159A) restored magnetic response of Δ*mamM*. However, the magnetic response of Δ*mamM* expressing *mamM* mutant alleles was not restored to the same level as with the wild type allele. Whereas an exchange of tyrosine 46 to histidine (Y46H, C_{mag} = 0.82) restored the magnetic response of Δ*mamM* to 90% of the wild type allele, replacement of tyrosine 46 with aspartate reduced magnetic response to only ~1% of the wild type level (C_{mag} = 0.01). Intermediate magnetic responses were detected in Δ*mamM* mutants expressing MamM D50A (C_{mag} = 0.46; 50% of wild type allele), MamM H155A (C_{mag} = 0.59; 65% of wild type allele) and MamM D159A (C_{mag} = 0.52; 56% of wild type allele) (Table S4).

Electron microscopy of the strains expressing the different MamM mutant proteins revealed that the proportion of cells devoid of any magnetite particles was increased compared to the strain transcomplemented with the wild type allele. Around 20% of the cells did not contain any electron dense particles when the native MamM was expressed, whereas expression of MamM D50A resulted in approximately 33% empty cells. The proportion of empty cells was even higher when MamM H155A (48%), MamM D159A (51%), and MamM Y46D (81%) mutant proteins were expressed in Δ*mamM*. However, also the size of the magnetite crystals was affected by the aa exchanges (FIG. 3-6B). On average the wild type MamM transcomplemented strain produced magnetite crystals with a diameter of 43 nm (±12.5 nm), but diameters of crystals in MamM D50A, MamM H155A and MamM D159A transcomplemented strains were significantly decreased to 35 nm (±14.8 nm), 37.9 nm (±16.3 nm) and 33.3 nm (±15.5 nm), respectively (FIG. S3-8). In addition, the particle size distribution of Δ*mamM* (pRU1-mamMD50A), Δ*mamM* (pRU1-mamMH155A) and Δ*mamM* (pRU1-mamMD159A) was bimodal, with maxima within the wild type range (40 to 50 nm) as well as within the superparamagnetic size range (15 to 25 nm) (FIG. S3-8). Strain Δ*mamM* (pRU1-mamMY46D) also showed a bimodal crystal size distribution, but notably, besides a small population of crystals with diameters between 25 and 30 nm, the majority of crystals had diameters between 50 and 55 nm, which was larger than the crystals of Δ*mamM* (pRU1-mamMwt) as also indicated by an increased average crystal diameter of 50.6 nm (±17.3 nm).

Also the magnetosome shape was markedly affected by expression of MamM D50A, MamM H155A or MamM D159A in Δ*mamM*. In Δ*mamM* (pRU1-mamMwt) most particles

were cubo-octahedral magnetite single crystals (FIG. 3-6C and D). In contrast, almost all particles of the strains expressing mutated MamM proteins appeared as polycrystalline aggregates of at least two crystals (FIG. 3-6C and D).

To analyse effects on crystal formation in more detail biomineralization after induction of crystal formation by addition of iron to iron-starved cells was studied. Whereas the magnetic response of Δ*mamM* (pRU1-mamMwt) was C_{mag} = 0.7, cultures of Δ*mamM* (pRU1-mamMD50A) still showed no magnetic response 17 h after iron induction. However, in TEM micrographs of Δ*mamM* (pRU1-mamMD50A) small electron dense particles (mean diameter = 14.5 nm) were already visible in approximately 30% of the cells, whereas particles with an average diameter of 22.5 nm were present in 55% of Δ*mamM* (pRU1-MamMwt). Most particles of Δ*mamM* (pRU1-MamMwt) were cubo-octahedral single crystals. However, the majority of particles in Δ*mamM* (pRU1-mamMD50A) appeared to be poorly crystalline and composed of multiple grains (FIG. 3-7A and B). Since Δ*mamM* (pRU1-mamMD50A) showed no magnetic response and the electron dense particles exhibited a poorly organized distribution, the elemental composition of these particles was analyzed by energy-filtered transmission electron microscopy. As shown in FIG. 3-7C all particles were composed of iron and oxygen, indicating that the particles were composed of iron oxides. However, characterization of the particles by high-resolution TEM (HRTEM) revealed that the lattice fringes of several small, irregular particles were clearly distinct from magnetite and most likely corresponded to hematite (FIG. 3-7D). In contrast to these small and irregular particles, lattice fringes of larger particles clearly corresponded to those of magnetite (FIG. 3-7E). Thus, a single amino acid exchange within MamM caused the formation of a mineral phase distinct from magnetite in a fraction of particles.

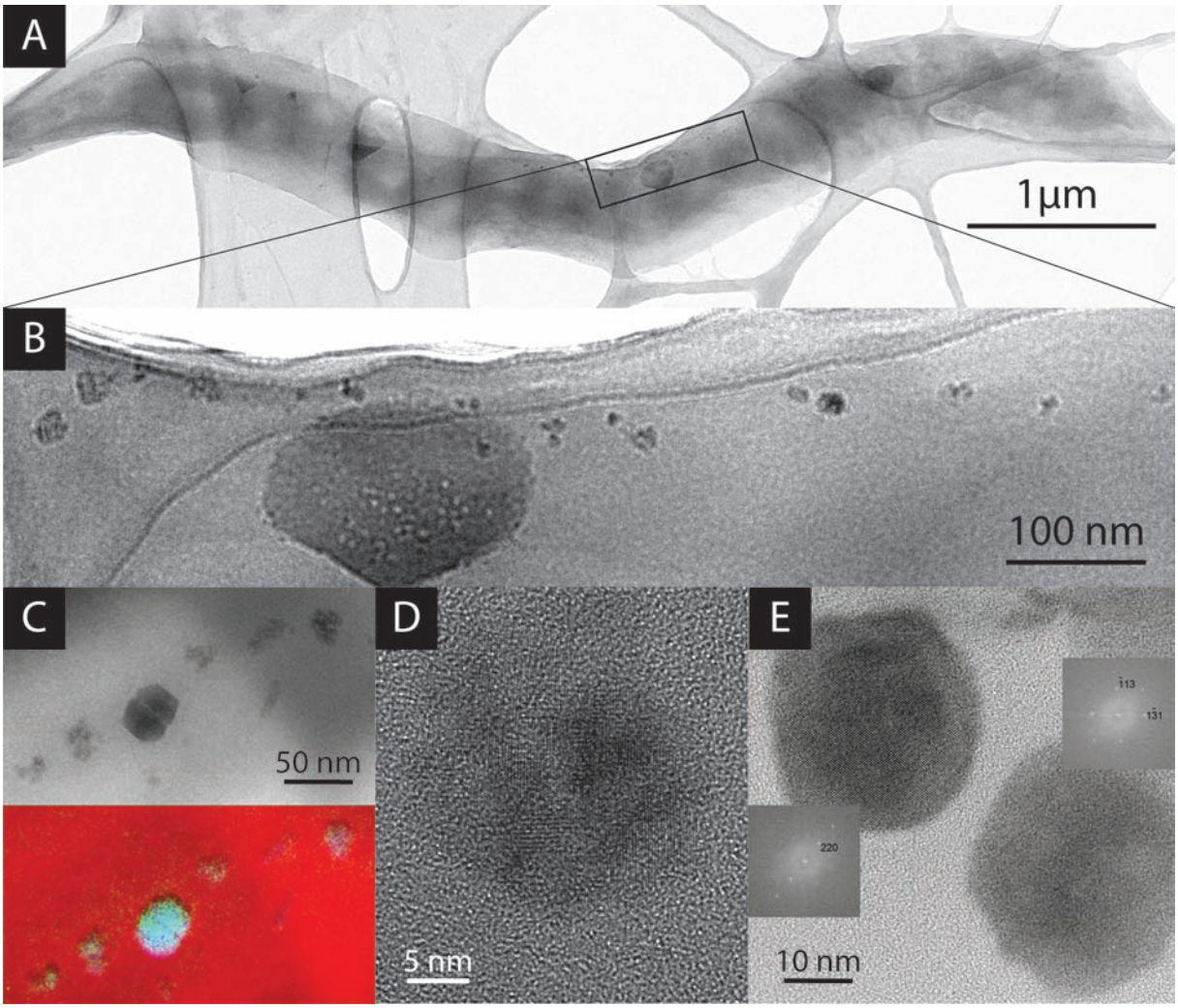

FIG 3-7. Formation of magnetite particles is delayed in Δ*mamM* (pRU1-mamMD50A). A) Representative TEM micrograph of Δ*mamM* (pRU1-mamMD50A) 17 h after iron induction. B) Magnification of the boxed area in A) showing small poorly crystalline and poorly organized electron dense particles at midcell. C) TEM micrograph showing a twinned magnetite magnetosome and several poorly crystallized particles (top) and composite of energy-filtered images obtained from the same area (bottom). Carbon, iron and oxygen are indicated by red, blue and green colors, respectively. D) HRTEM micrograph of a small electron dense particle with lattice fringes corresponding to hematite [121]. E) HRTEM micrograph showing larger magnetite particles. The crystal on the left side is not in a zone-axis orientation, while the one on the right is in [125] orientation.

3.4 Discussion

Previous studies suggested that magnetosome-directed iron transport might be driven by the CDF family proteins MamB and MamM (Grünberg *et al.*, 2004; Faivre *et al.*, 2008). Results of our study are still consistent with an iron-transporting function of both proteins, since MamB as well as MamM belong to the Fe/Zn-subfamily of CDF transporter, and deletion of either *mamB* or *mamM* resulted in the loss of magnetite biomineralization. In addition, Mössbauer spectroscopy indicated that both proteins have magnetosome-specific functions and are not involved in cytoplasmic iron accumulation. However, the lack of magnetosome membrane vesicles in Δ*mamB*, but not in Δ*mamM* argues against equivalent functions of both MTB-CDF proteins. Consistent with different phenotypes of the mutants, MamB and MamM cannot functionally compensate each other, thus verifying that MamB and MamM have distinct functions. In agreement with these findings a *mamB* mutant in *M. magneticum* AMB-1 was also lacking magnetosome membrane vesicles, whereas vesicles were still formed in a *mamM* mutant strain (Murat *et al.*, 2010).

We found several indications that MamB and MamM interact with each other, although MamB and MamM seem to be involved in different steps of magnetosome formation. Stable expression of MamB depended on the presence of MamM as shown by decreased MamB levels in Δ*mamM*. Simultaneous expression of MamB and MamM in heterologous hosts confirmed that stable MamB expression depended on coexpression of MamM independent of the presence of other magnetosome-specific factors. In addition, co-purification of untagged MamB or MamM with MamM-Strep and MamB-Strep fusion proteins, respectively, showed that MamB and MamM physically interact with each other. Hence, MamM might protect MamB from proteolytic degradation when both proteins form a complex, while MamB is degraded in the absence of MamM. Similar observations were made when SecY (Akiyama *et al.*, 1996) or the ATP synthase subunit a (Kihara *et al.*, 1995) were expressed in excess to their interacting subunits. Both unbound proteins are degraded by the membrane integrated FtsH protease when they are not protected by interacting subunits to avoid deleterious effects. Alternatively, MamM might be directly involved in the correct folding of MamB. Although the exact mechanism for the MamB stabilization remains to be established, MamB-stabilization involves the cytoplasmic carboxy-terminal domains of MamM and MamB. Expression of truncated MamM proteins in Δ*mamM* resulted in reduced MamB expression levels when more than 30 aa were removed from the C-terminal end assuming a stabilizing function of the C-terminus, which was consistent with results of the bacterial two-hybrid

assay. Though important for the stabilization of MamB, the CTD of MamM alone is not sufficient to increase MamB expression to wild type levels. Therefore, further domains have to be involved in the MamB-MamM interaction. This is consistent with the mode of interaction between two FieF protomers (Lu and Fu, 2007). Besides intense interaction at the FieF CTD-CTD interface, an intracellular loop between TMH2 and TMH3 is involved in dimerization contacts (Lu and Fu, 2007). In addition, salt bridges are formed between the N-terminal part of TMH3 and a cytoplasmic loop that connects the TMD to the CTD (Lu *et al.*, 2009). Based on this model, our data hint toward the formation of a MamB-MamM heterodimer. Although Haney *et al.* (2005) initially proposed that CDF family proteins might generally form homodimers, in addition to this study there is increasing evidence for heterodimer formation within this protein family (Ellis *et al.*, 2005; Ishihara *et al.*, 2006).

Nevertheless, the existence of a heterodimer of MamB and MamM alone was still not sufficient to explain the observed difference of the Δ*mamB* and Δ*mamM* phenotypes, since loss of either component within a functional MamBM-heterodimer should lead to similar phenotypes. However, the ability of the Δ*mamM* mutant to still form magnetosome membrane vesicles and the formation of disulphide-linked MamB oligomers in Δ*mamM* in conjunction with the observed self-interaction of the MamB or MamM CTDs in bacterial two-hybrid screens imply that both proteins also form homodimers. Although already suggested by several studies (Murgia *et al.*, 1999; Blaudez *et al.*, 2003), this is the first experimental evidence for CDF proteins that can either act in homo- or heterodimeric complexes. However, we cannot completely rule out the possibility that the observed interaction between MamM and MamB depends on an interaction between a MamB homodimer and a homodimer of MamM.

Our results further suggest that MamB might be involved in an additional extensive protein-protein interaction network. It forms intermolecular disulphide bridges via a putatively membrane embedded cysteine residue C138. Similar observations were made in a study addressing the function of the poplar CDF transporter MTP1 (Blaudez *et al.*, 2003). However, mutational analyses of this protein failed to assign a specific cysteine residue to the observed disulphide bond formation (Montanini *et al.*, 2007). In contrast to MTP1, the observed DTT-sensitive MamB complexes have molecular masses that only partially match homomeric MamB assemblies (the 62 kDa band approximately corresponds to a MamB dimer), indicating that MamB might also undergo heteromeric interactions (bands at ~78 kDa, ~80 kDa and ~114 kDa). Future identification of these interaction partners will be fundamental for the understanding of MamB function, since exchange of the residue responsible for

intermolecular disulphide bridge formation (C138A) not only blocks MamB oligomerization, but also magnetosome formation. Moreover, bioinformatic analyses predicted multiple putative PDZ domain binding motifs within MamB. The results of the bacterial two-hybrid experiments indicate that the magnetosome protein MamE might interact with the MamB carboxy-terminal domain via its PDZ1 domain. Although further experiments are required to confirm the MamB-MamE interaction and colocalization of the interacting domains, the reduced magnetic response of MamB C-terminal truncation mutants might be attributed to a reduced interaction with MamE, as most PDZ domains mediate protein-protein interactions by binding of target polypeptides at their carboxy-terminal end (Fanning and Anderson, 1996). In addition, the localization of MamB with GFP fused to its C-terminus seemed to be impaired since only a minor fraction of cells showed a MamB-localization corresponding to the results of the MamB-immunodetection in the cytoplasmic membrane and the magnetosome membrane. Interestingly, MamE was previously shown to be required for proper localization of MamC-GFP, MamA-GFP and MamJ-GFP in the closely related *M. magneticum* strain AMB-1 (Murat *et al.*, 2010; Quinlan *et al.*, 2011); however, no evidence of a direct interaction with one of these proteins was shown. Although the functional role of a MamB-MamE interaction remains ambiguous, one might speculate that MamE, like MamB, is involved in magnetosome membrane vesicle formation, since Murat and colleagues described that the so far only proteins essential for magnetosome membrane vesicle formation, MamI, MamL, MamQ and MamB alone are not sufficient for vesicle formation (Murat *et al.*, 2010). This hypothesis is further supported by findings of Quinlan *et al.* (2011), where co-deletion of *mamE* and *limE*, a *mamE*-like gene, in *M. magneticum* AMB-1 leads to mislocalization of GFP-MamI, a protein that is essential for vesicle formation. An additional hint for a putative role of MamE in vesicle formation is the similar MamC-GFP localization pattern between *M. gryphiswaldense* Δ*mamB* observed in this study, and *M. magneticum* ΔR9Δ*mamE* (Quinlan *et al.*, 2011). However, MamC-GFP localization was also affected by the deletion of *mamM*. Since cryo-electron tomographic analyses showed that Δ*mamM* is able to form empty magnetosome vesicles, which are aligned along the MamK-filaments, the observed MamC-GFP localization pattern might have been caused by a reduced number of vesicles due to degradation of MamB in the absence of MamM.

Besides stabilization of MamB, MamM is also directly involved in the regulation of crystal growth. Substitution of amino acids within the membrane embedded putative metal binding site A against alanine resulted in significantly increased amounts of small crystals (20 – 25 nm) within the superparamagnetic size range. Interestingly, magnetosomes with a similar

bimodal size distribution were observed in *M. magneticum* ΔR9Δ*mamE* expressing a heme-defective MamE (Quinlan *et al.*, 2011). However, despite this similarity it is unlikely that MamE and MamM act at the same stage of magnetosome formation. Whereas MamE was shown to be involved in protein sorting and regulation of crystal growth (Quinlan *et al.*, 2011), our data show that MamM is already involved at the step of nucleation initiation, since amino acid substitutions within the putative active site of MamM drastically increased the number of polycrystalline magnetite particles. These observed effects of the amino acid substitutions within MamM on the magnetosome crystal size and morphology might be the result of a reduced iron transport rate into the magnetosome vesicles, which in turn cause reduced iron concentrations within magnetosome vesicles. Consistent with this assumption is the delay in the formation of electron-dense particles in iron-induction experiments observed for Δ*mamM* (pRU1-mamMD50A). Also the observation of poorly crystalline iron-oxide particles during the iron-induction experiment supports that exchange of MamM D50A leads to reduced iron concentrations within magnetosome vesicles, since reduction of the iron concentration during abiotic magnetite crystallization also results in the formation of poorly crystallized iron oxides, iron hydroxides as well as the iron mineral goethite (Faivre *et al.*, 2004). Intriguingly, substitution of D50 by alanine within MamM also resulted in the appearance of small and poorly crystalline particles, which were composed of hematite (α-Fe_2O_3). Since larger magnetite magnetosomes were also observed it might be suggested that hematite is a precursor mineral of magnetite as discussed previously (Staniland *et al.*, 2007). However, the solid-state transformation of hematite into magnetite involves extensive rearrangements of the crystal structure and requires strong reductants or very high temperatures under abiotic conditions (Watanabe *et al.*, 1996; Kashiwaya *et al.*, 2007). Therefore, it seems more likely that the expression of mutated MamM proteins led to conditions disfavouring the formation of magnetite. Decreased transport rates, for example, could also lead to an increased pH within the magnetosome vesicles since CDF transporter generally employ an H^+-antiport mechanism. Previous studies showed that magnetite is only stable in a pH range from ~7 to 14, whereas hematite depending on the redox potential is stable from pH ~1 to 14 (Bell *et al.*, 1987). As an alternative explanation, the formation of the ferric iron mineral hematite could also be the consequence of a reduced influx of ferrous iron into the magnetosome vesicles, which is consistent with a model discussed for abiotic magnetite formation. According to this model in a first step a ferric oxide or hydroxide and in a second step magnetite is formed through reaction of ferrous iron with the ferric oxide/hydroxide (Jolivet *et al.*, 1992; Faivre *et al.*, 2004). Although these data suggest an

iron-transporting role of MamM, direct confirmation for iron transport is still missing because all our attempts to demonstrate MamM transport activities by *in vitro* (e.g. reconstituted proteoliposomes) or *in vivo* (e.g. serial dilution spot assays) methods failed because of technical challenges (data not shown). However, in contrast to usual bacterial CDF transporter, the transport activity of MamM needs to be regulated directly at the magnetosome membrane, since MamM also localizes to the cytoplasmic membrane. Thus, a simple transport mechanism in response to available ferrous iron would be detrimental for magnetosome formation. Therefore, it might be necessary to identify further proteins interacting with MamM. One possible interaction would be an iron-delivering metal-chaperone, which was also suggested for FieF (Lu and Fu, 2007).

Contrary to *mamM*, mutational analysis of *mamB* revealed almost no information about putative functions, since almost every mutation entirely abolished functionality. Thus, MamB appears to be a highly specialized protein in which even minor deviations from the wild type structure were not tolerated. It therefore remains incomprehensible how a putative metal-transporting protein is involved in magnetosome membrane vesicle formation.

In conclusion our data provided functional insights into how the two main processes of magnetosome formation, magnetosome membrane vesicle formation and initiation of magnetite formation, are linked to each other via the two CDF transporter MamM and MamB. We further provided evidence that MamB is integrated into an intense protein interaction network essential for magnetosome formation. We additionally showed that MamE is a putative interaction partner of MamB and might therefore be also necessary for magnetosome vesicle formation.

3.5 Experimental procedures

3.5.1 Bacterial strains and growth conditions

Bacterial strains and plasmids used in this study are listed in Table S3-5. *A. tumefaciens* and *E. coli* strains were routinely grown in lysogeny broth (LB) supplemented with kanamycin (25 µg ml^{-1}), gentamycin (50 µg ml^{-1}) or ampicillin (50 µg ml^{-1}). For growth of *E. coli* BW29427 LB was supplemented with 1 mM DL-α,ε-diaminopimelic acid. Cultivation of *A. tumefaciens* strains was carried out at 30°C and cultivation of *E. coli* strain at 37°C. *M. gryphiswaldense* strains were cultivated as described (Uebe *et al.*, 2010). When necessary, media were supplemented with kanamycin (5 µg ml^{-1}). For iron induction experiments *M. gryphiswaldense* strains were iron-starved by three microaerobic passages under iron-limited conditions (low-iron medium (Faivre *et al.*, 2008) supplemented with 10 µM 2,2'-dipyridyl) until no magnetic response was detectable (C_{mag} = 0) and no electron dense particles were visible by TEM. Subsequently strains were transferred into fresh flask standard medium (FSM) medium containing 50 µM ferric citrate, grown under microaerobic conditions for 17 h, harvested and analyzed.

3.5.2 Molecular and genetic techniques

Molecular techniques were performed using standard protocols (Sambrook and Russel, 2001). DNA was sequenced using BigDye terminator v3.1 chemistry on an ABI 3700 capillary sequencer (Applied Biosystems, Darmstadt, Germany). Sequence data were analyzed using 4Peaks software (http://mekentosj.com/4peaks). All oligonucleotide primers (Table S3-6) were purchased from Sigma-Aldrich (Steinheim, Germany).

3.5.3 Generation of unmarked deletion mutants

A two step, Cre-*lox*-based method for antibiotic marker recycling in gram-negative bacteria (Scheffel *et al.*, 2008) was used to generate unmarked, in-frame deletion mutants of *mamM* and *mamB*. For construction of the deletion vectors, 1.5 to 2 kb fragments of the up- und downstream flanking regions of *mamM* and *mamB* were amplified by PCR using Phusion polymerase (NEB; primers Table S6), cloned into pGEM-Teasy and sequenced. The 5' and

3' fragments were excised from pGEM with the indicated restriction enzymes and introduced into the corresponding restriction sites of pCM184 to create pCM184ΔmamM and pCM184ΔmamB, respectively.

Plasmids pCM184ΔmamM and pCM184ΔmamB were introduced into MSR-1 by conjugation using *E. coli* BW29427 as donor strain as described earlier (Schultheiss and Schüler, 2003). Counterselection of recombinant MSR-1 against *E. coli* was performed on FSM agar with kanamycin (5 μg ml^{-1}). Double-crossover events were distinguished from single-crossover events by replica plating on FSM agar containing kanamycin/ampicillin or kanamycin, respectively.

E. coli BW29427 was used as a donor strain to transfer the helper plasmid pCM157 into the kanamycin-marked deletion mutants *M. gryphiswaldense* (Δ*mamM*::Km) and *M. gryphiswaldense* (Δ*mamB*::Km) by conjugation. Exconjugants were selected on FSM agar containing tetracycline and passaged several times in 10 ml microaerobic liquid medium to allow expression of the Cre recombinase. After four passages the kanamycin cassette was excised by specific recombination of the two *loxP* sites flanking the kanamycin resistance marker. The resulting mutants were confirmed by PCR and sequencing, cured from pCM157 by repeated passages in fresh FSM medium and termed Δ*mamM* and Δ*mamB*, respectively.

3.5.4 Complementation of Δ*mamM* and Δ*mamB*

Complementation *in trans* was mainly carried out with pRU1 a P_{mamAB} containing derivative of the broad host range plasmid pBBR1MCS-2. For the construction of pRU1 the lac promoter of pBBR1MCS-2 was replaced against a NsiI/KpnI-digested 200 bp PCR fragment containing the intergenic region between *mgr4088* and *mamH* by digestion with NsiI and KpnI. For transcomplemetation assays *mamM* and *mamB* genes of MSR-1 were cloned into pRU1 to yield pRU1-mamMwt and pRU1-mamBwt. Both plasmids were subsequently used as templates for site-directed mutagenesis using the Phusion® Site-Directed Mutagenesis Kit (NEB) and mutagenesis primer (Table S3-6). For transcomplemetation assays *mamM* and *mamB* containing pRU1-derivatives were transferred to Δ*mamM* or Δ*mamB* mutants by conjugation, respectively.

3.5.5 Construction of GFP fusion proteins and fluorescence microscopy

mamM and *mamB* were amplified using primers as described and inserted into the restriction sites NdeI and XhoI of pCL5 (Lang and Schüler, 2008), resulting in C-terminal GFP fusion vectors pCL5-mamM and pCL5-mamB. The mamB-GFP fusion was then amplified using primers mamB(wt)_for/M13f, digested with KpnI/SacI and inserted into the corresponding restriction sites of pRU1 to generate pRU1-mamBGFP.
M. gryphiswaldense strains bearing pCL5-mamM, pRU1-mamBGFP or pCL6 were grown in 3-ml FSM in 6-well plates to stationary phase at 30°C and 2% O_2 without agitation. Cells were washed with phosphate-buffered saline (pH 7.4), immobilized on agarose pads (FSM salts in H_2O, supplemented with 1% agarose), and imaged with an Olympus BX81 microscope equipped with a 100 UPLSAPO100XO objective (numerical aperture of 1.40) and a Hamamatsu Orca AG camera. Images were captured and analyzed using Olympus cell software.

3.5.6 Cellular fractionation, electrophoresis and immunological detection

For expression analyses *M. gryphiswaldense* strains were grown in 200 ml FSM medium under microaerobic conditions to stationary phase, harvested by centrifugation at 9,200 x *g*, washed (20 mM Tris-HCl, pH 7.4, 5 mM EDTA) and resuspended into ice-cold 20 mM Tris-HCl, 1 mM EDTA, 0.1 mM phenylmethylsulfonyl fluoride (PMSF), pH 7.4. Cell suspensions were lysed by three passages through French press, and cellular debris was removed by low-speed centrifugation. Cleared cell lysates were subjected for 30 min to centrifugation at 265,000 x *g* to separate cellular membranes and magnetosomes from the soluble protein fraction. Pelleted membrane proteins were resuspended in 20 mM Tris-HCl, 1 mM EDTA, 0.1 mM PMSF, pH 7.4, 1% sodium dodecyl sulfate (SDS). For fractionation of the magnetosome membrane and non-magnetic membrane fraction the method of (Lang and Schüler, 2008) was applied. After French press treatment and low-speed centrifugation cleared cell lysates were passed through a MACS magnetic-separation column placed between Sm-Co magnets (Miltenyi, Germany) to separate magnetosomes from the non-magnetic cell fraction. The column bound magnetosomes were first washed with 50 ml of 10 mM HEPES, 1 mM EDTA, pH 7.4, followed by 50 ml of high salt buffer (10 mM HEPES, 200 mM NaCl, 1 mM EDTA, pH 7.4), and water before the magnetic field was removed and

the magnetosomes were eluted in 10 mM HEPES, 1 mM EDTA, pH 7.4. Subsequently, the magnetosomes were centrifuged through an 8-ml sucrose cushion (60% [wt/wt] in 10 mM HEPES, 1 mM EDTA, pH 7.4) at 200,000 x *g* for 90 min. Due to their high specific density, magnetosomes sediment at the bottom of the tube, whereas other cellular constituents are retained by the sucrose cushion. Finally, the magnetosomes were resuspended in 1 ml of 10 mM HEPES, 1 mM EDTA, pH 7.4. The non-magnetic cell fraction, which was not retained by the magnetic column, was subjected to centrifugation at 4,000 x *g* for 60 min to remove residual cell debris. The supernatant was subjected to 30 min of centrifugation at 265,000 x *g* to separate the cellular membranes from the soluble proteins. The sedimented membrane fraction was resuspended (10 mM HEPES, 1 mM EDTA, 1% SDS, pH 7.4) and centrifuged a second time at 265,000 x *g* for 30 min. The resulting supernatant contained the non-magnetic membrane fraction.

Protein concentrations were determined with a BCA-Protein Micro assay kit (Pierce) according to the manufacturer's instructions. For one-dimensional SDS-PAGE the procedure of Laemmli (Laemmli, 1970) was used. Protein samples from different cellular fractions were resuspended in electrophoresis sample buffer (62.5 mM Tris-HCl, pH 6.8, 0.1 M DTT, 1.6% SDS, 5% glycerol, 0.002% bromophenol blue), or sample buffer lacking DTT and denatured at 95°C for 5 min. Twenty micrograms of protein were loaded onto gels unless specified otherwise. For Western blot analyses, 12% (w/v) gels were used, and following electrophoresis, proteins were transferred onto nitrocellulose membranes (Protran, Whatman) by electroblotting. The membranes were blocked for 2 h at room temperature (5% skim milk in Tris-buffered saline (TBS)) and subsequently incubated for 1 h in TBS with anti-MamM (purchased from Pineda Antibody Service, Berlin, Germany), anti-MamB (purchased from Pineda Antibody Service, Berlin, Germany) or anti-MamA (Taoka *et al.*, 2006) antibodies at 1:2,000; 1:1,000 and 1:5,000 dilutions, respectively. Membranes were washed several times with Tween-Tris-buffered saline (TTBS) and TBS before incubation with an alkaline phosphatase-labeled goat anti-rabbit immunoglobulin G antibody (Santa Cruz, Biotechnology, Inc.) at 1:2,000 dilution in TBS. After incubation at room temperature for 45 min, membranes were washed with TBS, and a BCIP (5-bromo-4-chloro-3-indolylphosphate)/nitroblue tetrazolium detection reagent (Roche Diagnostics, Mannheim, Germany) was used for detection.

3.5.7 Heterologous expression of *mamM* and *mamB*

For heterologous expression of MamB in *A. tumefaciens mamB* was PCR-amplified using the primer pair mamB(wt)_for/mamBTand_rw and subcloned into pGEM-Teasy. The resulting vector pGEM-mamBTand was digested with restrictions enzymes KpnI/BamHI and a 900 bp fragment containing *mamB* was inserted into the corresponding restriction sites of pBBR1MCS-5 to yield the final MamB expression vector pBBR1MCS-5-mamB. For single expression of MamM, *mamM* was amplified using the primer pair mamM(wt)_for/rev. The resulting PCR product was digested with KpnI and SacI and inserted into the corresponding restriction sites of pBBR1MCS-5 resulting in pBBR1MCS-5-mamM. For simultaneous expression of MamB and MamM a transcriptional fusion of *mamB* and *mamM* was generated by insertion of *mamM* into pBBR1MCS-5-mamB. Therefore *mamM* was amplified with mamMTandRBS_fw and mamM(wt)_rev and ligated into pGEM-Teasy. The vector pGEM-mamMTand was subsequently digested with BamHI/SacI and the *mamM*-containing fragment was inserted into the BamHI/SacI restriction sites of pBBR1MCS-5-mamB to generate the co-expression vector pBBR1MCS-5-mamBM.
The final plasmids were transferred to *A. tumefaciens* C58 by conjugation as described above for *M. gryphiswaldense*.

3.5.8 Co-elution assay

To investigate direct protein-protein interaction between MamM and MamB co-elution assays were performed by taking advantage of the StrepII tag fused to the C-terminus of MamB or MamM. 1% (w/v) n-dodecyl-ß-maltoside solubilized membrane protein extracts containing Strep-tagged proteins were applied to a Strep-Tactin superflow column (IBA Tagnology, Göttingen, Germany) with a column volume of 0.5 ml, followed by purification according to the manufacturer's instructions. Control experiments were performed under the same conditions with unlabelled proteins as well as MamM-Strep expressed in Δ*mamB*.

3.5.9 Bacterial two-hybrid assay

Protein-protein interactions were investigated using the BacterioMatch II two-hybrid system vector kit and the BacterioMatch II validation reporter strain according to the manufacturer's instructions with a minor modification as described (Scheffel and Schüler, 2007).

For construction of bait (pTRG) and prey (pBT) expression vectors, full-length *mamM*, full-length *mamB*, and partial *mamM* (MCTD: 211-318), *mamB* (BCTD: 209-297), *mamP* (PPDZ: 82-188) and *mamE* (EPDZ1: 551-663; EPDZ2: 677-772) sequences were inserted into BamHI/XhoI restriction sites of pTRG or pBT*, a pBT-derivative in which the BamHI and XhoI sites have been separated by primer mediated insertion of nine nucleotides.

3.5.10 Analytical methods

Imaging of cells by transmission electron microscopy and cryo-electron tomography was performed as previously described (Katzmann *et al.*, 2010). Energy-filtered TEM was performed using a Gatan Imaging Filter on a JEOL 3010 microscope. High-resolution TEM was carried out using an image spherical aberration corrected FEI Titan 80-300 TEM, operated at 80 kV to reduce specimen damage from electron beam irradiation.

The average magnetic orientation of cell suspensions (C_{mag}) was assayed as described (Schüler *et al.*, 1995).

For Transmission Mössbauer Spectroscopy (TMS) on whole cells, *M. gryphiswaldense* strains MSR1, Δ*mamM*, Δ*mamB* and MSR1-B were grown in microaerophilic 1.5-L batch cultures supplemented with 40 μM $^{57}Fe(citrate)_2$. Cells were harvested by centrifugation at 9,258 x *g*, 4°C. Pellets were washed, weighed, transferred into Delrin® Mössbauer sample holders, frozen in liquid nitrogen, and kept at this temperature until measurement except for overnight transport on dry ice. Mössbauer spectra were recorded in the horizontal transmission geometry using a constant acceleration spectrometer operated in conjunction with a 512-channel analyzer in the time-scale mode. The detector consisted of a proportional counter filled with argon-methane (9:1). The source was at room temperature and consisted of 1.4 GBq [^{57}Co] diffused in Rh foil (WissEl). The spectrometer was calibrated against α-iron at room temperature (RT). For measurements at 77 K, samples were placed in a continuous-flow cryostat (Oxford Instruments). For measurements at 4.2 K a helium bath cryostat

(MD306, Oxford Instruments) was employed. Spectral data were transferred from the multi-channel analyzer to PC for further analysis employing the Vinda program (Gunnlaugsson, 1999) on an Excel 2003® platform. Isomer shift δ, quadrupole splitting ΔE_Q, B_{hf} and percentage of the total absorption area were obtained by least-squares fits of Lorentzian lines to the experimental spectra. All values are rounded to last given digit. The isomers shifts (δ), the quadrupole splitting (ΔE_Q) and the line width (Γ) are given in mm s^{-1}. The relative area is given in parts per hundreds.

3.5.11 Bioinformatic analysis

Sequence alignments and construction of similarity trees were performed using MEGA4 software (Tamura *et al.*, 2007). Sequences were aligned by ClustalW (default settings) and similarity trees were constructed using the Neighbor-Joining (NJ) method and the bootstrap (1000 replicates) phylogeny tests as described (Montanini *et al.*, 2007).

3.6 Acknowledgements

We thank Felix Froese, Anja Lindemann and Anna Pollithy for their valuable input into this work. We are very thankful to Prof. Y. Fukumori (Kanazawa University, Japan) for his kind gift of the anti-MamA (Mam22) antibody. This project was funded by the Deutsche Forschungsgemeinschaft (DFG Ma 916/21-1, Schu 1080/6-2 and 13-1).

3.7 References

Akiyama, Y., Kihara, A. and Ito, K. (1996). Subunit a of proton ATPase F_0 sector is a substrate of the FtsH protease in *Escherichia coli*. *FEBS Lett.* **399**: 26-28.

Bell, P. E., Mills, A. L. and Herman, J. S. (1987). Biogeochemical conditions favoring magnetite formation during anaerobic iron reduction. *Appl. Environ. Microbiol.* **53**: 2610-2616.

Blaudez, D., Kohler, A., Martin, F., Sanders, D. and Chalot, M. (2003). Poplar metal tolerance protein 1 confers zinc tolerance and is an oligomeric vacuolar zinc transporter with an essential leucine zipper motif. *Plant Cell* **15**: 2911-2928.

Cherezov, V., Höfer, N., Szebenyi, D. M. E., Kolaj, O., Wall, J. G., Gillilan, R., Srinivasan, V., Jaroniec, C. P. and Caffrey, M. (2008). Insights into the mode of action of a putative zinc transporter CzrB in *Thermus thermophilus*. *Structure* **16**: 1378-1388.

Ding, Y., Li, J., Liu, J., Yang, J., Jiang, W., Tian, J., Li, Y., Pan, Y. and Li, J. (2010). Deletion of the *ftsZ*-like gene results in the production of superparamagnetic magnetite magnetosomes in *Magnetospirillum gryphiswaldense*. *J. Bacteriol.* **192**: 1097-1105.

Ellis, C. D., MacDiarmid, C. W. and Eide, D. J. (2005). Heteromeric protein complexes mediate zinc transport into the secretory pathway of eukaryotic cells. *J. Biol. Chem.* **280**: 28811-28818.

Faivre, D., Agrinier, P., Menguy, N., Zuddas, P., Pachana, K., Gloter, A., Laval, J. and Guyot, F. (2004). Mineralogical and isotopic properties of inorganic nanocrystalline magnetites. *Geochim. Cosmochim. Acta* **68**: 4395-4403.

Faivre, D., Menguy, N., Posfai, M. and Schüler, D. (2008). Environmental parameters affect the physical properties of fast-growing magnetosomes. *Am. Mineral.* **93**: 463-469.

Fanning, A. S. and Anderson, J. M. (1996). Protein protein interactions: PDZ domain networks. *Curr. Biol.* **6**: 1385-1388.

Fanning, A. S. and Anderson, J. M. (1999). PDZ domains: fundamental building blocks in the organization of protein complexes at the plasma membrane. *J. Clin. Invest.* **103**: 767-772.

Grass, G., Otto, M., Fricke, B., Haney, C. J., Rensing, C., Nies, D. H. and Munkelt, D. (2005). FieF (YiiP) from *Escherichia coli* mediates decreased cellular accumulation of iron and relieves iron stress. *Arch. Microbiol.* **183**: 9-18.

Grünberg, K., Müller, E. C., Otto, A., Reszka, R., Linder, D., Kube, M., Reinhardt, R. and Schüler, D. (2004). Biochemical and proteomic analysis of the magnetosome membrane in *Magnetospirillum gryphiswaldense*. *Appl. Environ. Microbiol.* **70**: 1040-1050.

Grünberg, K., Wawer, C., Tebo, B. M. and Schüler, D. (2001). A large gene cluster encoding several magnetosome proteins is conserved in different species of magnetotactic bacteria. *Appl. Environ. Microbiol.* **67**: 4573-4582.

Gunnlaugsson, H. (1999). "Vinda - Plugin for the microsoft excel program designed for the analysis of Mössbauer spectra." from http://users-phys.au.dk/hpg/vinda.htm.

Haney, C. J., Grass, G., Franke, S. and Rensing, C. (2005). New developments in the understanding of the cation diffusion facilitator family. *J. Ind. Microbiol. Biotechnol.* **32**: 215-226.

Higuchi, T., Hattori, M., Tanaka, Y., Ishitani, R. and Nureki, O. (2009). Crystal structure of the cytosolic domain of the cation diffusion facilitator family protein. *Proteins: Struct., Funct., Bioinf.* **76**: 768-771.

Ishihara, K., Yamazaki, T., Ishida, Y., Suzuki, T., Oda, K., Nagao, M., Yamaguchi-Iwai, Y. and Kambe, T. (2006). Zinc transport complexes contribute to the homeostatic maintenance of secretory pathway function in vertebrate cells. *J. Biol. Chem.* **281**: 17743-17750.

Jelen, F., Oleksy, A., Smietana, K. and Otlewski, J. (2003). PDZ domains - common players in the cell signaling. *Acta Biochim. Pol.* **50**: 985-1017.

Jolivet, J. P., Belleville, P., Tronc, E. and Livage, J. (1992). Influence of Fe(II) on the formation of the spinel iron oxide in alkaline medium. *Clays Clay Miner.* **40**: 531-539.

Kashiwaya, Y., Yamaguchi, Y., Kinoshita, H. and Ishii, K. (2007). In situ observation of reduction behavior of hematite with solid carbon and crystallographic orientation between hematite and magnetite. *ISIJ Int.* **47**: 226-233.

Katzmann, E., Scheffel, A., Gruska, M., Plitzko, J. M. and Schüler, D. (2010). Loss of the actin-like protein MamK has pleiotropic effects on magnetosome formation and chain assembly in *Magnetospirillum gryphiswaldense*. *Mol. Microbiol.* **77**: 208-224.

Kihara, A., Akiyama, Y. and Ito, K. (1995). FtsH is required for proteolytic elimination of uncomplexed forms of SecY, an essential protein translocase subunit. *Proceedings of the National Academy of Sciences* **92**: 4532-4536.

Komeili, A., Li, Z., Newman, D. K. and Jensen, G. J. (2006). Magnetosomes are cell membrane invaginations organized by the actin-like protein MamK. *Science* **311**: 242-245.

Laemmli, U. K. (1970). Cleavage of structural proteins during the assembly of the head of bacteriophage T4. *Nature* **227**: 680-685.

Lang, C. and Schüler, D. (2008). Expression of green fluorescent protein fused to magnetosome proteins in microaerophilic magnetotactic bacteria. *Appl. Environ. Microbiol.* **74**: 4944-4953.

Lu, M., Chai, J. and Fu, D. (2009). Structural basis for autoregulation of the zinc transporter YiiP. *Nat. Struct. Mol. Biol.* **16**: 1063-1067.

Lu, M. and Fu, D. (2007). Structure of the zinc transporter YiiP. *Science* **317**: 1746-1748.

Matzanke, B. (1991). Structures, coordination chemistry and functions of microbial iron chelates. In: *Handbook of microbial iron chelates*. G. Winkelmann (ed.). CRC Press, Boca Raton.

Matzanke, B. (2005). Iron transport: Siderophores. In: *Encyclopedia of inorganic chemistry*. R. B. King (ed.). John Wiley & Sons, Chichester.

Montanini, B., Blaudez, D., Jeandroz, S., Sanders, D. and Chalot, M. (2007). Phylogenetic and functional analysis of the Cation Diffusion Facilitator (CDF) family: improved signature and prediction of substrate specificity. *BMC Genomics* **8**: 107.

Murat, D., Quinlan, A., Vali, H. and Komeili, A. (2010). Comprehensive genetic dissection of the magnetosome gene island reveals the step-wise assembly of a prokaryotic organelle. *Proc. Natl. Acad. Sci. U.S.A.* **107**: 5593-5598.

Murgia, C., Vespignani, I., Cerase, J., Nobili, F. and Perozzi, G. (1999). Cloning, expression, and vesicular localization of zinc transporter Dri 27/ZnT4 in intestinal tissue and cells. *Am. J. Physiol. Gastrointest. Liver Physiol.* **277**: G1231-G1239.

Nies, D. (2003). Efflux-mediated heavy metal resistance in prokaryotes. *FEMS Microbiol. Rev.* **27**: 313-339.

Paulsen, I. and Saier, M. (1997). A novel family of ubiquitous heavy metal ion transport proteins. *J. Membr. Biol.* **156**: 99-103.

Ponting, C. P. (1997). Evidence for PDZ domains in bacteria, yeast, and plants. *Protein Sci.* **6**: 464-468.

Puntervoll, P., Linding, R., Gemünd, C., Chabanis-Davidson, S., Mattingsdal, M., Cameron, S., Martin, D. M. A., Ausiello, G., Brannetti, B., Costantini, A., Ferrè, F., Maselli, V., Via, A., Cesareni, G., Diella, F., Superti-Furga, G., Wyrwicz, L.,

Ramu, C., McGuigan, C., Gudavalli, R., Letunic, I., Bork, P., Rychlewski, L., Küster, B., Helmer-Citterich, M., Hunter, W. N., Aasland, R. and Gibson, T. J. (2003). ELM server: a new resource for investigating short functional sites in modular eukaryotic proteins. *Nucleic Acids Res.* **31**: 3625-3630.

Quinlan, A., Murat, D., Vali, H. and Komeili, A. (2011). The HtrA/DegP family protease MamE is a bifunctional protein with roles in magnetosome protein localization and magnetite biomineralization. *Mol. Microbiol.* **80**: 1075–1087.

Rosch, J. W., Gao, G., Ridout, G., Wang, Y.-D. and Tuomanen, E. I. (2009). Role of the manganese efflux system *mntE* for signalling and pathogenesis in *Streptococcus pneumoniae*. *Mol. Microbiol.* **72**: 12-25.

Sambrook, J. and Russel, D. (2001). *Molecular cloning: A laboratory manual*. Cold Spring Harbor Laboratory Press, Cold Spring Harbor, New York.

Scheffel, A., Gärdes, A., Grünberg, K., Wanner, G. and Schüler, D. (2008). The major magnetosome proteins MamGFDC are not essential for magnetite biomineralization in *Magnetospirillum gryphiswaldense* but regulate the size of magnetosome crystals. *J. Bacteriol.* **190**: 377-386.

Scheffel, A., Gruska, M., Faivre, D., Linaroudis, A., Graumann, P. L., Plitzko, J. and Schüler, D. (2006). An acidic protein aligns magnetosomes along a filamentous structure in magnetotactic bacteria. *Nature* **440**: 110-114.

Scheffel, A. and Schüler, D. (2007). The acidic repetitive domain of the *Magnetospirillum gryphiswaldense* MamJ protein displays hypervariability but is not required for magnetosome chain assembly. *J. Bacteriol.* **189**: 6437-6446.

Schübbe, S., Kube, M., Scheffel, A., Wawer, C., Heyen, U., Meyerdierks, A., Madkour, M. H., Mayer, F., Reinhardt, R. and Schüler, D. (2003). Characterization of a spontaneous nonmagnetic mutant of *Magnetospirillum gryphiswaldense* reveals a large deletion comprising a putative magnetosome island. *J. Bacteriol.* **185**: 5779-5790.

Schüler, D., Uhl, R. and Baeuerlein, E. (1995). A simple light scattering method to assay magnetism in *Magnetospirillum gryphiswaldense*. *FEMS Microbiol. Lett.* **132**: 139-145.

Schultheiss, D. and Schüler, D. (2003). Development of a genetic system for *Magnetospirillum gryphiswaldense*. *Arch. Microbiol.* **179**: 89-94.

Schultz, J., Milpetz, F., Bork, P. and Ponting, C. P. (1998). SMART, a simple modular architecture research tool: Identification of signaling domains. *Proc. Natl. Acad. Sci. U.S.A.* **95**: 5857-5864.

Schünemann, V. and Winkler, H. (2000). Structure and dynamics of biomolecules studied by Mössbauer spectroscopy. *Rep. Prog. Phys.* **63**: 263-353.

Staniland, S., Ward, B., Harrison, A., Van der Laan, G. and Telling, N. (2007). Rapid magnetosome formation shown by real-time x-ray magnetic circular dichroism. *Proc. Natl. Acad. Sci. U.S.A.* **104**: 19524-19528.

Tamura, K., Dudley, J., Nei, M. and Kumar, S. (2007). MEGA4: Molecular evolutionary genetics analysis (MEGA) software version 4.0. *Mol. Biol. Evol.* **24**: 1596-1599.

Tanaka, M., Mazuyama, E., Arakaki, A. and Matsunaga, T. (2011). Mms6 protein regulates crystal morphology during nano-sized magnetite biomineralization *in vivo*. *J. Biol. Chem.* **286**: 6386-6392.

Taoka, A., Asada, R., Sasaki, H., Anzawa, K., Wu, L. and Fukumori, Y. (2006). Spatial localizations of Mam22 and Mam12 in the magnetosomes of *Magnetospirillum magnetotacticum*. *J. Bacteriol.* **188**: 3805-3812.

Uebe, R., Voigt, B., Schweder, T., Albrecht, D., Katzmann, E., Lang, C., Böttger, L., Matzanke, B. and Schüler, D. (2010). Deletion of a *fur*-like gene affects iron homeostasis and magnetosome formation in *Magnetospirillum gryphiswaldense*. *J. Bacteriol.* **192**: 4192-4204.

Ullrich, S., Kube, M., Schübbe, S., Reinhardt, R. and Schüler, D. (2005). A hypervariable 130-kilobase genomic region of *Magnetospirillum gryphiswaldense* comprises a magnetosome island which undergoes frequent rearrangements during stationary growth. *J. Bacteriol.* **187**: 7176-7184.

Ullrich, S. and Schüler, D. (2010). Cre-*lox*-based method for generation of large deletions within the genomic magnetosome island of *Magnetospirillum gryphiswaldense*. *Appl. Environ. Microbiol.* **76**: 2439-2444.

Watanabe, Y., Takemura, S., Yoshiaki, K. and Kuniyoshi, I. (1996). Reduction of hematite to magnetite induced by hydrogen ion implantation. *J. Phys. D: Appl. Phys.* **29**: 8.

Yang, W., Li, R., Peng, T., Zhang, Y., Jiang, W., Li, Y. and Li, J. (2010). *mamO* and *mamE* genes are essential for magnetosome crystal biomineralization in *Magnetospirillum gryphiswaldense* MSR-1. *Res. Microbiol.* **161**: 701-705.

3.8 Supplementary information

3.8.1 Experimental procedures

Co-elution of MamM with MamB-Strep after co-expression of mamB-strep and mamM in Escherichia coli

For simultaneous overexpression of *mamB-strep* and *mamM* a transcriptional gene fusion of *mamB-strep* and *mamM* was generated and inserted into pET51b(+) to yield pET51-mamBStrep-mamM. The co-expression vector was transformed to *E. coli* Rosetta(DE3). The resulting strain was cultivated in LB at 37°C and 180 rpm and overexpression of *mamB-strep* and *mamM* was induced by addition of 0.4 mM isopropyl-ß-thiogalactopyranosid. Three hours after induction cells were harvested, washed (100 mM Tris-HCl, protease inhibitor cocktail (Thermo Fisher Scientific), pH 8) and subjected to cell lysis by sonication. Cell debris was removed by centrifugation at 9,200 x *g*, 4°C for 30 min. To separate the membrane fraction from soluble proteins the supernatant was centrifuged for 30 min at 265,000 x *g*. The pellet was resuspended in 100 mM Tris-HCl, 1% (w/v) n-dodecyl-ß-maltoside and incubated for 1 h at 4°C followed by centrifugation for 30 min at 265,000 x *g*. The resulting supernatant was used for the co-elutuion assay as described.

3D homology modeling

3D homology-modeling was performed by SWISS-MODEL (Arnold *et al.*, 2006) in the automatic modeling mode with the FieF structure as template (PDB code: 3H90).

3.8.2 Supplementary figures

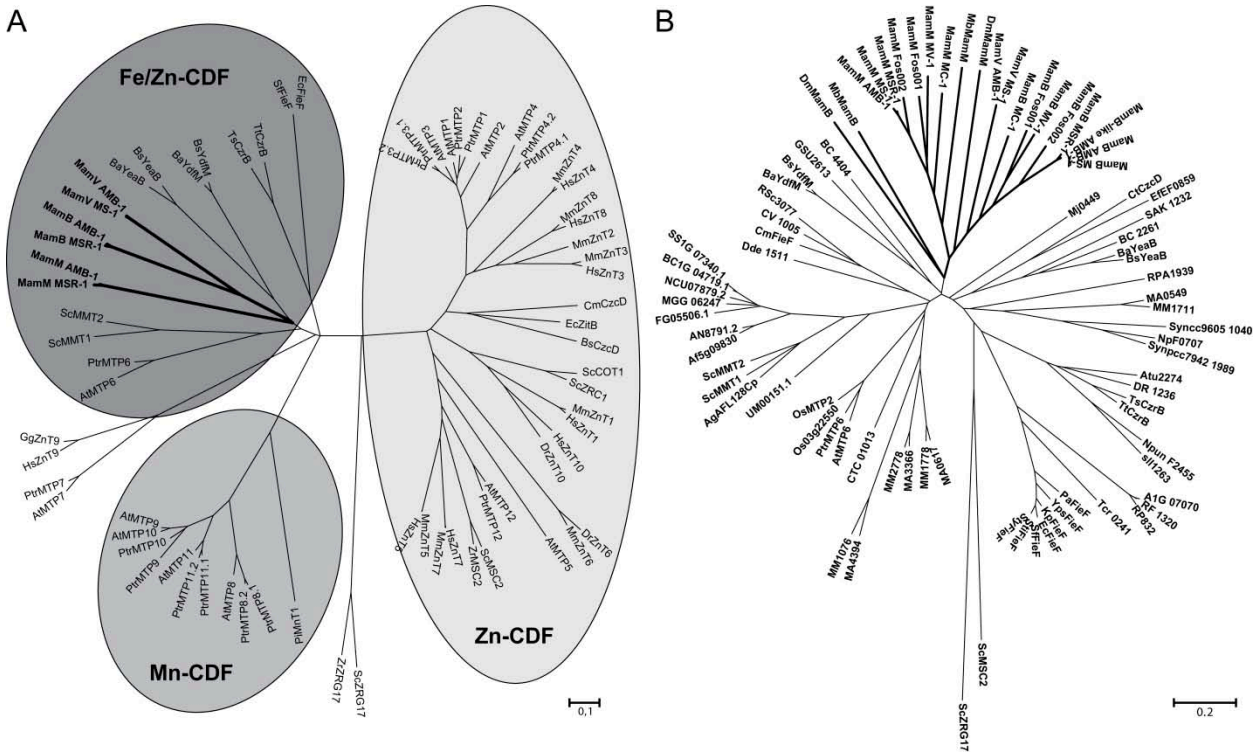

FIG. S3-1. A) Phylogenetic tree of the CDF family and grouping of MTB-CDF proteins. CDF subfamilies representing different metal specifities are highlighted by colored circles: light gray for zinc, dark gray for iron/zinc and intermediate gray for manganese (Montanini *et al.*, 2007). Representative MTB-CDF proteins are represented by bold lines and letters. The scale bar indicates an evolutionary distance of 0.1 amino acid substitution per site. B) Detailed phylogenetic tree of the Fe/Zn-subfamily of CDF transporters. MTB-CDF proteins are shown in bold. The scale bar indicates an evolutionary distance of 0.2 amino acid substitution per site. Accession numbers of proteins used to generate the trees are given in Table S3-7.

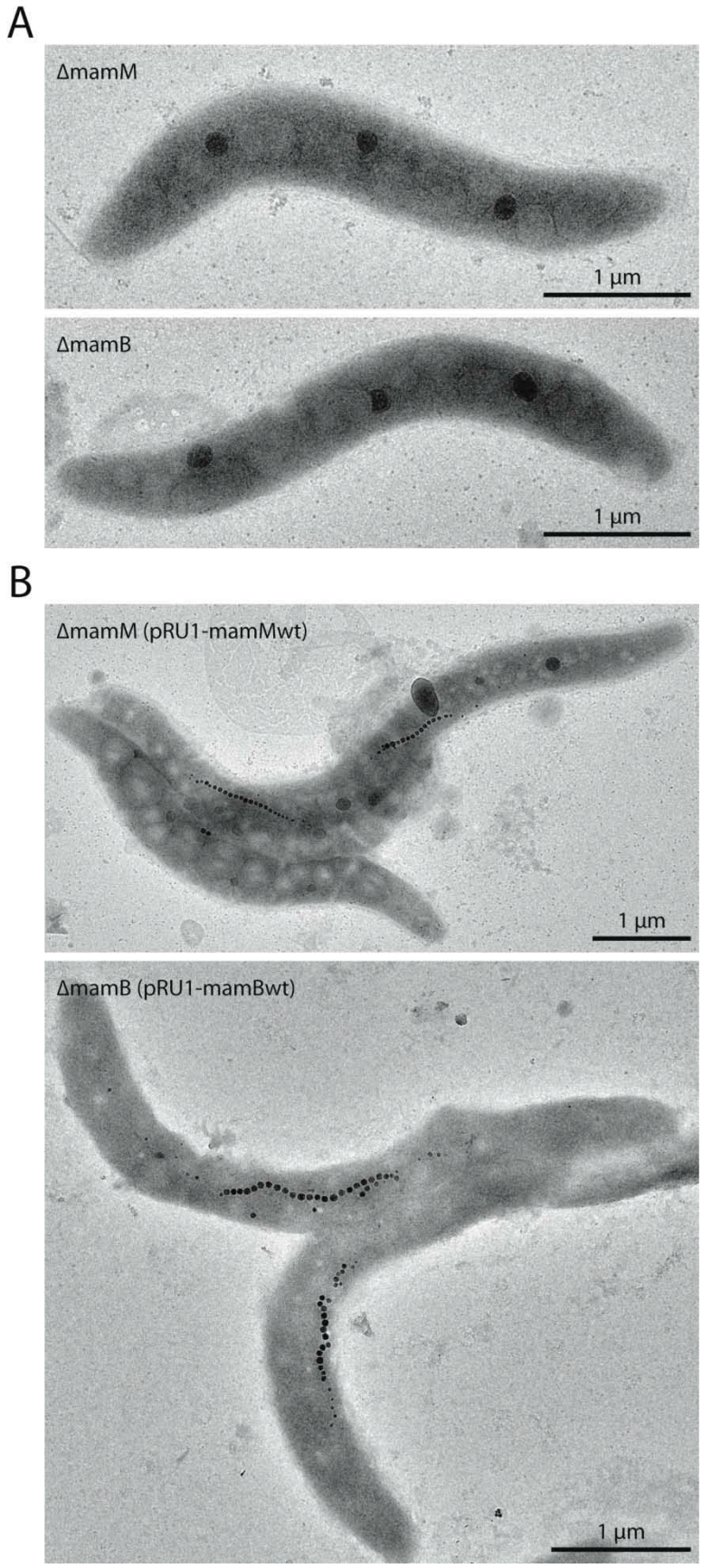

FIG. S3-2. TEM micrographs of *M. gryphiswaldense* mutants Δ*mamM* and Δ*mamB* and (A) untranscomplemented (B) transcomplemented.

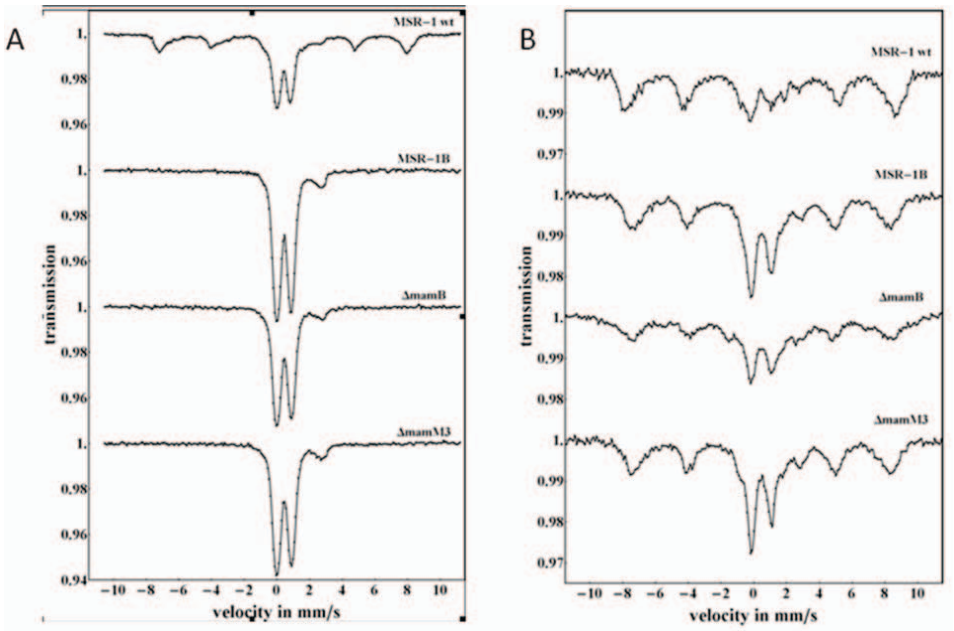

C

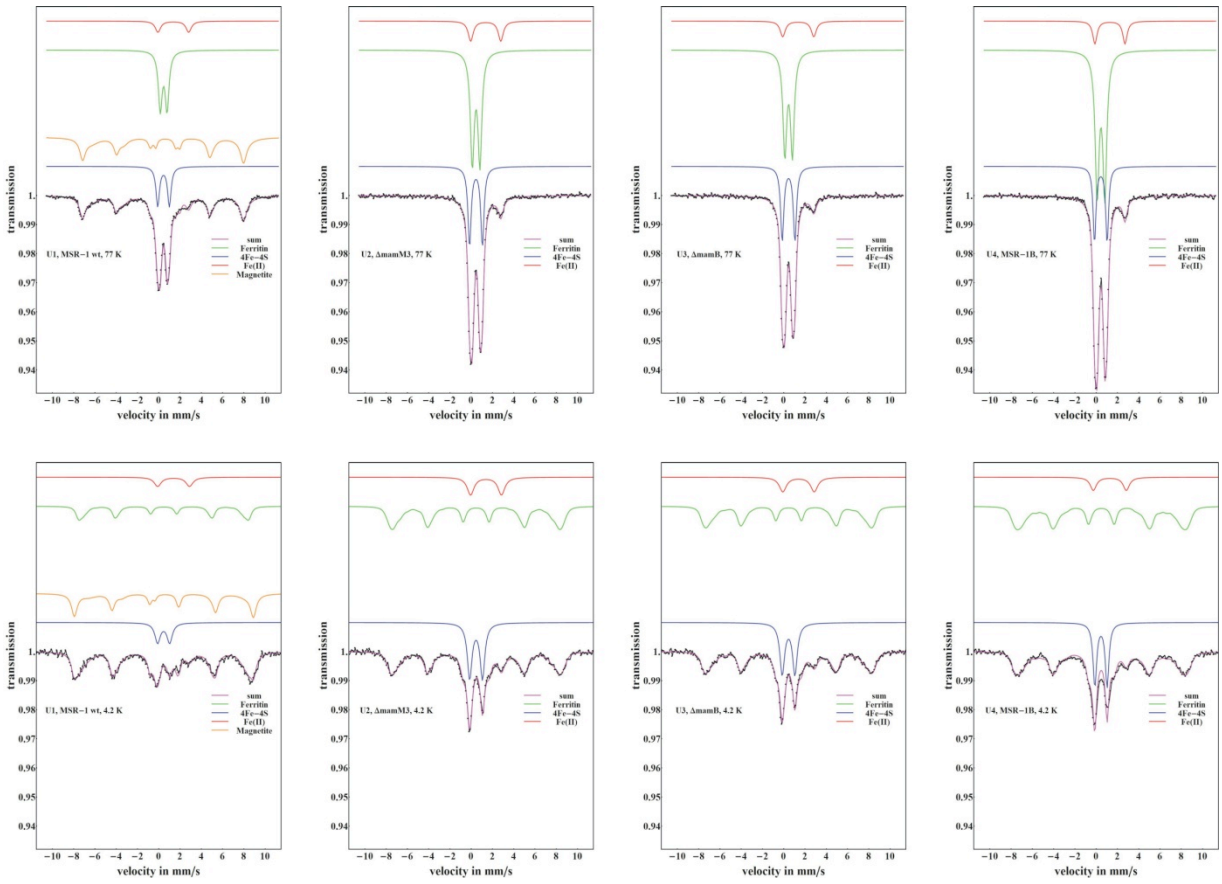

FIG S3-3. Transmission Mössbauer spectra of whole cells of *M. gryphiswaldense* MSR-1, MSR-1B, Δ*mamB* and Δ*mamM* at 77 K (A) and 4.2 K (B). C) Least squares fits of Lorentzian lines to experimental data of MSR-1, MSR-1B, Δ*mamB* and Δ*mamM* at 77 K and 4.2 K.

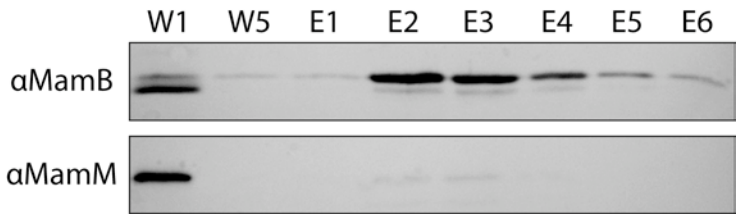

FIG. S3-4. Strep-Tactin affinity chromatographic purification of MamB-Strep (top) and co-elution of untagged MamM (bottom) in solubilized membrane fractions of *E. coli* Rosetta (DE3) (pET51-mamBStrep-mamM). W1 and W5, washing fractions 1and 5; E1 to E6, elution fractions 1 to 6, respectively.

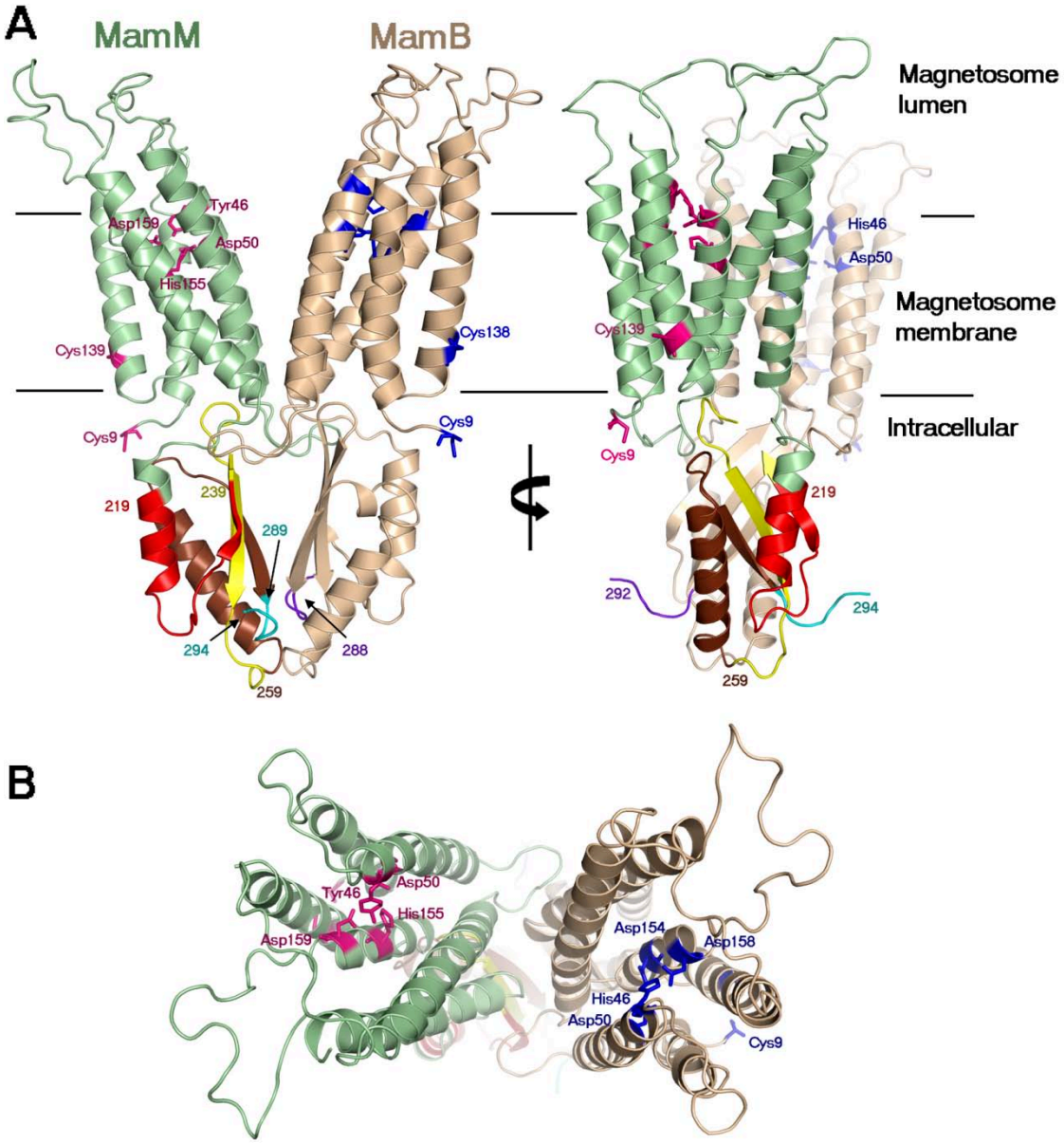

FIG. S3-5. Model representation of MamB and MamM. A) Ribbon representation of MamB (light brown) and MamM (light green) in two perpendicular angles, mutated residues are represented as sticks (blue and pink respectively). Deletions are represented as unique colors, MamB 288-297 (purple), MamM 289-318 (cyan), 259-318 (brown + cyan), 239-318 (yellow + brown + cyan) and 219-318 (red + yellow + brown + cyan). B) Top view of MamB and MamM, color scheme as in A.

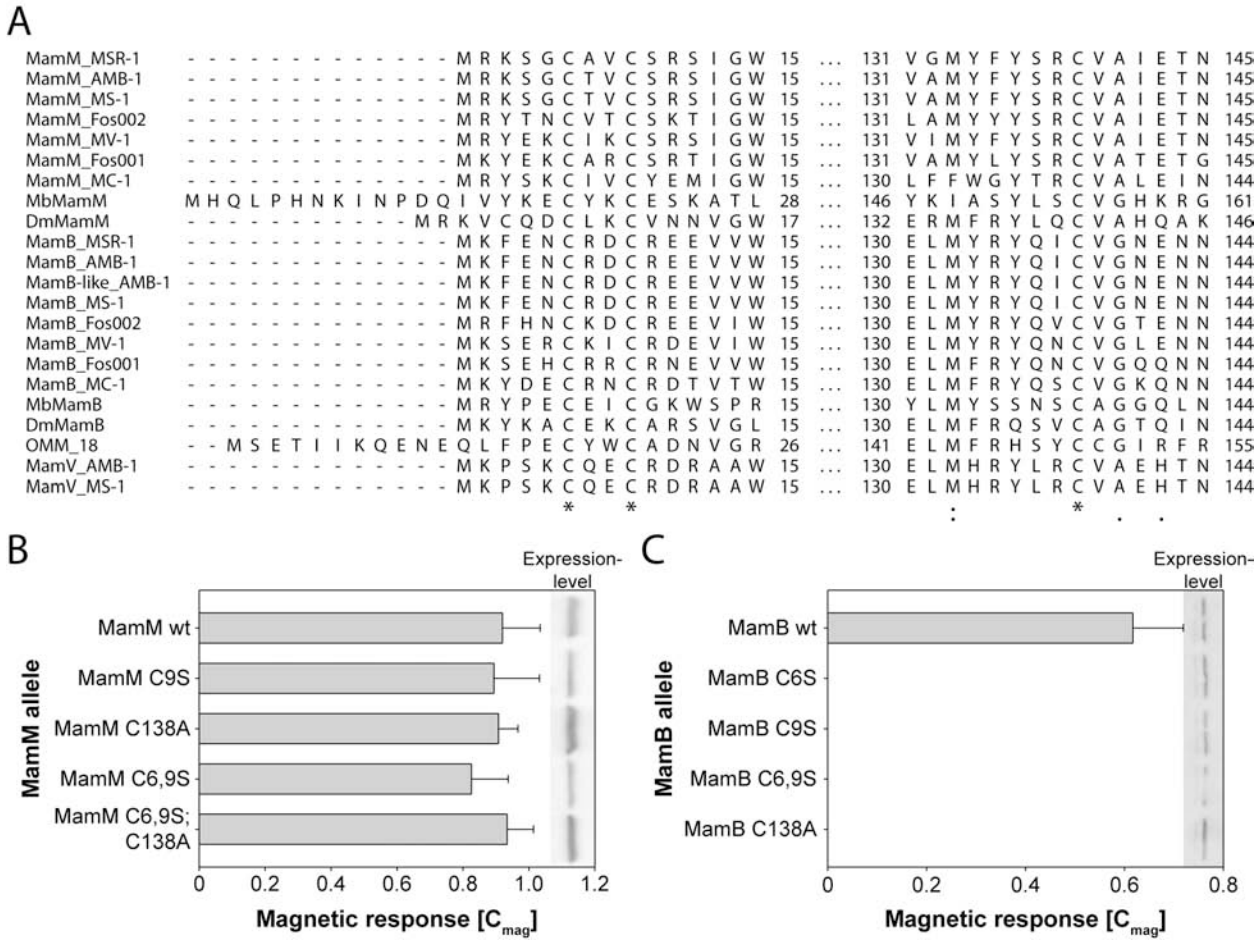

FIG. S3-6. A) ClustalW sequence alignment of all MTB-CDF proteins showing the N-terminal region with a conserved CxxC-motif and the region surrounding a third conserved cysteine residue. B) Magnetic response and expression level of Δ*mamM* transcomplemented with MamM cysteine exchange and wild type proteins. C) Magnetic response and expression level of Δ*mamB* transcomplemented with MamB cysteine exchange and wild type proteins.

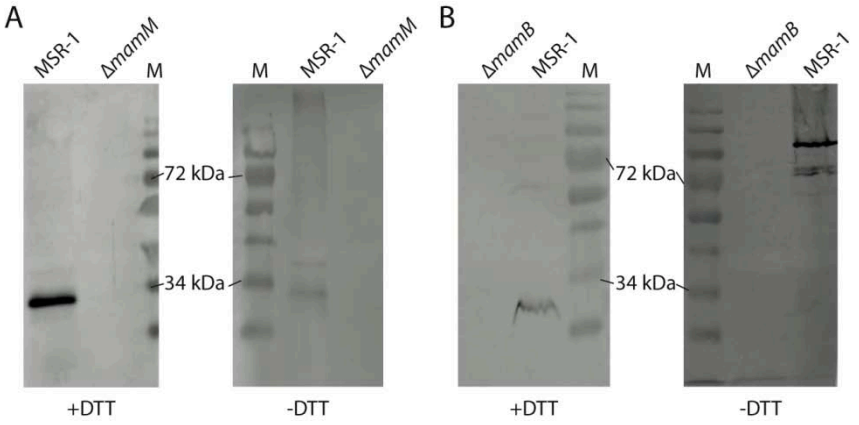

FIG S3-7. A) Immunudetection of MamM in total membrane extracts of the wild type (MSR-1) after reducing SDS-PAGE (+DTT) or nonreducing SDS-PAGE (-DTT) B) Immunudetection of MamB in total membrane extracts of the wild type (MSR-1) after reducing SDS-PAGE (+DTT) or nonreducing SDS-PAGE (-DTT).

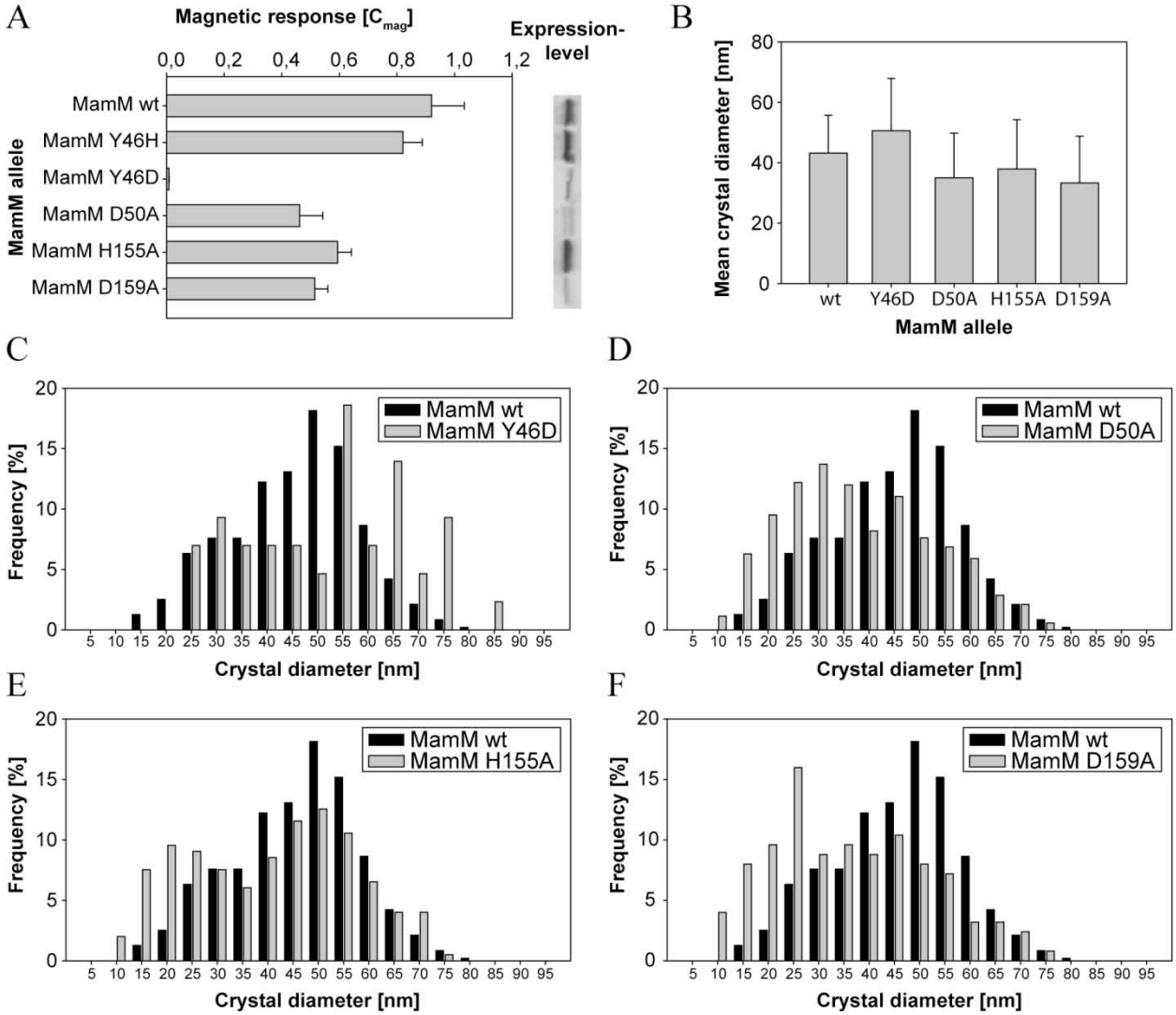

FIG. S3-8. Magnetic response (A), mean crystal size (B) and crystal size distribution of Δ*mamM* expressing wild type and mutant MamM (C-F). Values of (A) are given as means ± standard deviations (SD) from three independent transconjugants. Magnetite crystal size was determined from 474 (MamM wt), 43 (MamM Y46D), 525 (MamM D50A), 199 (MamM H155A) and 125 (MamM D159A) magnetosomes by TEM after growth at 1% O_2 at 23°C for 72 h, respectively.

3.8.3 Supplemetary Tables

Table S3-1. Comparative sequence analysis of MamB and MamM from different MTB.

Organism / Fosmid clone	Similarity / Identity (%)		
	MamB	MamM	MamB/M
	against MSR-1 proteins		within each MTB
M. gryphiswaldense MSR-1	100 / 100	100 / 100	48.1 / 26.1
M. magneticum AMB-1	97.6 / 94.6	97.8 / 93.7	47.7 / 25.8
M. magnetotacticum MS-1	97.6 / 94.6	97.8 / 93.7	47.7 / 25.8
Fos002	82.5 / 69.0	87.0 / 73.4	47.5 / 27.1
Fos001	74.7 / 53.6	69.9 / 53.6	50.5 / 28.1
magnetic vibrio MV-1	72.4 / 54.9	68.2 / 52.8	48.9 / 28
Magnetococcus sp. MC-1	69.0 / 45.2	60.7 / 42.5	54.2 / 29.5
D. magneticus RS-1	51.5 / 29.2	48.8 / 30.7	46 / 23.4
Cand. *M. bavaricum*	51.9 / 29.6	51.2 / 33.9	50.3 / 26.7

Table S3-2. Membrane topology prediction of MamM and MamB using different prediction programs.

TMD prediction program	number of predicted TMDs		aa position of TMDs	
	MamM	MamB	MamM	MamB
TMHMM	3	3	13-35; 81-103; 115-137	13-35; 82-104; 165-187
Toppred	5	4	12-32; 50-70; 81-101; 114-134; 160-180	22-42; 82-102; 112-132; 159-179
DAS	6	5	16-31; 54-60; 82-103; 118-129; 167-171; 193-199	30-34; 85-100; 120-125; 164-176; 184-191
Tmpred	4	4	12-30; 79-100; 117-133; 157-176	12-30; 82-104; 113-133; 159-179
Topcons	6	6	14-34; 42-62; 81-101; 116-136; 156-176; 181-201	16-36; 41-61; 81-101; 115-135; 154-174; 179-199
SPLIT	6	5	10-41; 50-63; 80-106; 116-137; 162-178; 185-205	15-43; 82-106; 114-132; 161-175; 177-201
PSORT	3	5	79-95; 117-133; 185-201	26-42; 82-98; 116-132; 163-179; 182-198
Memsat	6	6	13-37; 40-63; 76-100; 115-138; 157-180; 183-207	13-37; 40-63; 79-102; 113-136; 156-174; 177-198
SOSUI	6	4	15-37; 45-66; 82-104; 114-136; 163-185; 187-209	12-34; 84-106; 115-137; 161-191

Table S3-3. Positions of predicted PDZ-binding motifs within MamM and MamB (according to ELM server; http://elm.eu.org/about.html)

Predicted motif	Amino acid position in	
	MamM	MamB
PDZ class II binding	-	294-297
PDZ class III binding	49-52	10-13
	79-82	11-14
	108-111	42-45
	188-191	49-52
	191-194	157-160
	214-217	179-182
	225-228	196-199
	248-251	213-216
	267-270	241-244
	281-284	265-268
	308-311	273-276

Table S3-4. Magnetic response of various Δ*mamM* and Δ*mamB* strains before and after transcomplementation. Values are given as means (± standard deviations) from three independant transconjugants after growth at 30°C and 1.5% O_2 for 24 h.

Strain	Plasmid	Magnetic response (C_{mag})
Δ*mamM*	-	0 (± 0)
	pRU1-mamMwt	0.92 (± 0.114)
	pRU1-mamMC9S	0.89 (± 0.138)
	pRU1-mamMC6,9S	0.83 (± 0.111)
	pRU1-mamMC139A	0.91 (± 0.059)
	pRU1-mamMC6,9SC139A	0.93 (± 0.08)
	pRU1-mamMY46H	0.82 (± 0.067)
	pRU1-mamMY46D	0.01 (± 0.001)
	pRU1-mamMD50A	0.46 (± 0.081)
	pRU1-mamMH155A	0.59 (± 0.048)
	pRU1-mamMD159A	0.52 (± 0.045)
	pRU1-mamMΔ10ct	0.80 (± 0.051)
	pRU1-mamMΔ30ct	0.85 (± 0.023)
	pRU1-mamMΔ60ct	0 (± 0)
	pRU1-mamMΔ80ct	0 (± 0)
	pRU1-mamMΔ100ct	0 (± 0)
	pRU1-mamMΔTM	0 (± 0)
Δ*mamB*	-	0 (± 0)
	pRU1-mamBwt	0.617 (± 0.102)
	pRU1-mamBC6S	0 (± 0)
	pRU1-mamBC9S	0 (± 0)
	pRU1-mamBC6,9S	0 (± 0)
	pRU1-mamBC138A	0 (± 0)
	pRU1-mamBH46A	0 (± 0)
	pRU1-mamBD50A	0 (± 0)
	pRU1-mamBD50E	0 (± 0)
	pRU1-mamBD154A	0 (± 0)
	pRU1-mamBD159A	0 (± 0)
	pRU1-mamBΔ5ct	0.405 (± 0.03)
	pRU1-mamBΔ10ct	0.241 (± 0.014)
	pRU1-mamBΔ20ct	0 (± 0)
	pRU1-mamBΔ30ct	0 (± 0)
	pRU1-mamBΔ40ct	0 (± 0)

Table S3-5. Bacterial strains and plasmids used in this study

Strain or plasmid	Important features	Source or reference
Strains		
E. coli		
DH5α	F' Φ80d*lac* ΔM15 Δ(*lacZYA-argF*)U169 *deo*R *rec*A1 *end*A1	Invitogen
BW29427	*thrB1004 pro thi rpsL hsdS lacZ*ΔM15 RP4-1360 Δ(*araBAD*)567 Δ*dapA1341::[erm pir* (wt)]	Datsenko, K. and Wanner B. L. (unpublished)
Rosetta(DE3)	F^- *ompT hsdS*$_B$(r_B^- m_B^-) *gal dcm* (DE3) pRARE *(*Cam^R)	Novagen
M. gryphiswaldense		
MSR-1 R3/S1	Rif^r, Sm^r spontaneous mutant, wild type	(Schultheiss *et al.*, 2005)
MSR-1B	spontaneous non-magnetic mutant of MSR-1	(Schübbe *et al.*, 2003)
Δ*mamJ*	R3/S1 but Δ*mamJ*	(Scheffel *et al.*, 2006)
Δ*mamB*	R3/S1 but Δ*mamB*	this study
Δ*mamM*	R3/S1 but Δ*mamM*	this study
A. tumefaciens		
C58	wild type, containing the nopaline-type Ti plasmid pTiC58	(Wood *et al.*, 2001)
Plasmids		
pGEM-T easy	Cloning vector; Amp^r	Promega
pJET1.2/blunt	Cloning vector; Amp^r	Fermentas
pCM184	Broad-host-range allelic exchange vector, Km^r, Tet^r, Amp^r	(Marx and Lidstrom, 2002)
pCM184ΔmamM	pCM184 with *mamM* flanking regions	this study
pCM184ΔmamB	pCM184 with *mamB* flanking regions	this study
pCM157	Cre expression vector, Tet^r	(Marx and Lidstrom, 2002)
pBBR1MCS-2	Mobilizable broad-host-range vector; Km^r	(Kovach *et al.*, 1995)
pBBR1MCS-5	Mobilizable broad-host-range vector; Gm^r	(Kovach *et al.*, 1995)
pBBR1MCS-5-mamB	pBBR1MCS-5 + *mamB*	this study
pBBR1MCS-5-mamB	pBBR1MCS-5 + *mamM*	this study
pBBR1MCS-5-mamBM	pBBR1MCS-5 + *mamB* + *mamM*	this study
pRU1	pBBR1MCS-2with P_{mamAB}	this study
pRU1-mamMwt	pRU-1 + *mamM*	this study
pRU1-mamBwt	pRU-1 + *mamB*	this study
pRU1-mamMY46D	pRU-1 + *mamM Y46D*	this study
pRU1-mamMY46H	pRU-1 + *mamM Y46H*	this study
pRU1-mamMD50A	pRU-1 + *mamM D50A*	this study
pRU1-mamMH155A	pRU-1 + *mamM H155A*	this study
pRU1-mamMD159A	pRU-1 + *mamM D159A*	this study
pRU1-mamBH46A	pRU-1 + *mamB H46A*	this study
pRU1-mamBD50A	pRU-1 + *mamB D50A*	this study
pRU1-mamBD50E	pRU-1 + *mamB D50E*	this study
pRU1-mamBD154A	pRU-1 + *mamB D154A*	this study
pRU1-mamBD159A	pRU-1 + *mamB D159A*	this study
pRU1-mamMΔ10ct	pRU-1 + *mamM* Δ309-318	this study
pRU1-mamMΔ30ct	pRU-1 + *mamM* Δ289-318	this study
pRU1-mamMΔ60ct	pRU-1 + *mamM* Δ259-318	this study
pRU1-mamMΔ80ct	pRU-1 + *mamM* Δ239-318	this study
pRU1-mamMΔ100ct	pRU-1 + *mamM* Δ219-318	this study
pRU1-mamMΔTM	pRU-1 + *mamM* Δ1-210	this study
pRU1-mamBΔ5ct	pRU-1 + *mamB* Δ293-297	this study
pRU1-mamBΔ10ct	pRU-1 + *mamB* Δ288-297	this study

Plasmid	Important features	Source or reference
pRU1-mamMC6S	pRU-1 + *mamM C6S*	this study
pRU1-mamMC9S	pRU-1 + *mamM C9S*	this study
pRU1-mamMC6,9S	pRU-1 + *mamM C6,9S*	this study
pRU1-mamMC139A	pRU-1 + *mamM C139A*	this study
pRU1-mamMC6,9SC139A	pRU-1 + *mamM C6,9S; C139A*	this study
pRU1-mamBC6S	pRU-1 + *mamB C6S*	this study
pRU1-mamBC9S	pRU-1 + *mamB C9S*	this study
pRU1-mamBC6,9S	pRU-1 + *mamB C6,9S*	this study
pRU1-mamBC138A	pRU-1 + *mamB C138A*	this study
pBBR1MCS-2-mamBMS-1	pBBR1MCS-2 + *mamB* from *M. magnetotacticum* MS-1	this study
pBBR1MCS-2-mamBMV-1	pBBR1MCS-2 + *mamB* from magnetic vibrio strain MV-1	this study
pBBR1MCS-2-mamBFos001	pBBR1MCS-2 + *mamB* from metagenomic fosmid clone Fos001	this study
pBBR1MCS-2-mamBMC-1	pBBR1MCS-2 + *mamB* from *Magnetococcus* sp. MC-1	this study
pCL5	pBBR1MCS2 + *egfp*	(Lang and Schüler, 2008)
pCL6	pCL5 + *mamC*	(Lang and Schüler, 2008)
pCL5-mamB	pCL5 + *mamB*	this study
pCL5-mamM	pCL5 + *mamM*	this study
pRU1-mamBGFP	pRU1 + mamBGFP from pCL5	this study
pBT	Cm^r, Two-hybrid bait fusion expression vector	Stratagene
pBT*	pBT + TCGGATAAT insertion between BamHI and XhoI restriction sites	this study
pBT-mamB	pBT* + *mamB*	this study
pBT-mamMCTD	pBT* + *mamM* Δ1-210	this study
pBT-mamBCTD	pBT* + *mamB* Δ1-208	this study
pBT-mamPPDZ	pBT* + *mamP* 82-188	this study
pBT-mamEPDZ1	pBT* + *mamE* 551-663	this study
pBT-mamEPDZ2	pBT* + *mamE* Δ1-676	this study
pTRG	Tet^r, Two-hybrid target fusion expression vector	Stratagene
pTRG-mamB	pTRG + *mamB*	this study
pTRG-mamMCTD	pTRG + *mamM* Δ1-210	this study
pTRG-mamBCTD	pTRG + *mamB* Δ1-208	this study
pET51b(+)	T7-Promotor, *lacI*, Ap^R, Strep-Tag, His10-Tag	Novagen
pET51-mamBStrep-mamM	pET51b(+) + *mamB*-strep + *mamM*	this study

Table S3-6. Primers used during this study. Included restriction sites are shown in bold.

Name	Sequence (5'→3')
dM_up_f	**CCATGG**AGCCATCAGGGTTGAACTGG
dM_up_r	**GCGGCCGC**CATCCTTACCTACTCCAA
dM_do_f	**GGGCCC**TTAAGGTGGATAACTAGGTGG
dM_do_r	**ACCGGT**TGATCTGAGTGGTCCCCA
mamB3pCM_rw	**GAGCTC**TAACGATCATTGACCCGTC
mamB3pCM_fw	**GGGCCC**CCACACGCCCGAGATAT
mamB5pCMpK_fw	**GAATTC**GCTTGAGCGCTCCATC
mamB5pCM_rw3	**GGTACC**CGGCGGTGAATGCCCA
mamB-MC1fw	**CTCGAG**CCGCTTGAGGGACAGAAA
mamB-MC1rw	**TCTAGA**TTTTTAAGCTACGTCACA
mamB-MS1fw3	**CTCGAG**ATTATCGTATCCTGGGCTCCAA
mamB-MS1_rw3	**TCTAGA**TCAGGCCCGTGCCGCGGC
mamBFos001_fw	**CTCGAG**CATCGGGTACTTCAATCAATGA
mamBFos001_rw	**TCTAGA**TCAGGCCTTAACGCCGGAG
mamB(wt)_for	CGGC**GGTACC**ATGAAGTTCGAAAATTGC
mamB(wt)_rev	ATTA**GAGCTC**TCAGACCCGGACCGTCACG
mamM(wt)_for	ATTA**GGTACC**ATGAGGAAGAGCGGTTGCG
mamM(wt)_rev	CGGC**GAGCTC**CTAGTTATCCACCTTGGA
mamBgfpC_fw	**CTCGAG**GTGGAATACATGAACCGA
mamBgfpC_ rw	**CATATG**GACCCGGACCGTCACTGC
mamMgfpC_fw	**CTCGAG**TTGGAGTAGGTAAGGATGA
mamMgfpC_rw	**CATATG**GTTATCCACCTTGGACAGC
mamBTand_rw	**GGATCC**TTAGACCCGGACCGTCACT
mamMTandRBS_fw	**GGATCC**AAGAAGGAGATATACCATGAGGAAGAGCGGTTGCGCGGTCTG
mamMΔ1-201_for	**CATATG**GATGCCTATCGTGGGCTG
mamMCTD-10_rev	**GAGCTC**AGAAACTCAGCGGCTGATC
mamMCTD-30_rev	**GAGCTC**ATGCGCTGACATGCAGGGA
mamMCTD-60_rev	**GAGCTC**AGTTCTCGGGATCGACGCC
mamMCTD-80_rev	**GAGCTC**ACCGCAGATGGATGACGCC
mamMCTD-100_rev	**GAGCTC**ACTGCACCGCCTCACCCGC
mamM_C6S_for	**GGTACC**ATGAGGAAGAGCGGTTCCGCGGT
mamM_C9S_for	**GGTACC**ATGAGGAAGAGCGGTTGCGCGGTCTCCAGCA
mamM_C6,9S_for	**GGTACC**ATGAGGAAGAGCGGTTCCGCGGTCTCCAGCA
mamMY46H_for	GCCGATGCCATGCATTCGCTGAA
mamMY46D_for	GCCGATGCCATGGATTCGCTGAAG
mamMD50A_for	TGAAGGCCATGCTGAACGCCCTGATGGTGATTAT
mamMD50A_rev	ATAATCACCATCAGGGCGTTCAGCATGGCCTTCA
mamMD50E_for	GCTGAAGGAAATGCTGAACGCCCTGATGGTGATT
mamMD50E_rev	GATCACCATCAGGGAGTTCAGCATTTCCTTCAGC
mamMC139A_for	TATTCCCGCGCTGTCGCCATTGAGACT
mamMC139A_rev	GAAATACATGCCCACATTGACGCCGATG
mamMH155A_for	AAGGCTCACCATGGCGACGCCACC
mamMH155A_rev	GGCCATGGTCTTGATGAGGGGGCTG
mamMD159A_for	AAGCATCACCATGGCGCCGCCAC
mamB_C6S_for	**GGATCC**AAGTTCGAAAATTCCAGAGACTGCCG
mamB_C9S_for	**GGATCC**AAGTTCGAAAATTGCAGAGACTCCCGGG
mamB_C6,9S_for	**GGATCC**AAGTTCGAAAATTCCAGAGACTCCCGGG
mamBH46A_for	TCGCTGGCTTCGGGTGCCGATG
mamBH46A_rev	ATCGGCCACCAGAGCGACGCTGC
mamBD50A_for	GCATTCGGGTGCCGCTGTGGTTG
mamBD50A_rev	CAACCACAGCGGCACCCGAATGC
mamBD50E_for	CTGCATTCGGGTGCCGAAGTGGTTG

Name	Sequence (5'→3')
mamBD50E_rev	CAACCACTTCGGCACCCGAATGCAG
mamBC138A_for	CAGATCGCTGTTGGCAACGAAAAT
mamBC138A_rev	GTAGCGATACATCAGCTCGTTGACGAT
mamBD154A_for	TGGGCCAACCGTTCGGACGCC
mamBD154A_rev	GGCATTGGCGATGATGGCCGGG
mamBD158A_for	TGGGACAACCGTTCGGCCGCCTCGG
mamBΔ1-208_for	G**GGATCC**AGCTCCGTGGATACCGAA
mamMΔ1-210_for	**GGATCC**CACACCGCGGGTGAGGCG
mamE_PDZ1_for	**GGATCC**ACCCCCTTGACCCAGCGT
mamE_PDZ1_rev	**CTCGAG**TGGGCCGGTGACAAGAGA
mamE_PDZ2_for	**GGATCC**CCCACGGTTCCTGGCGTT
mamE_PDZ2_rev	**CTCGAG**TCAAAGAACAATCCAGAACTCTTGGC
mamP_PDZ_for	**GGATCC**CCGCGCAATCTCAAGGTC
mamP_PDZ_rev	**CTCGAG**GCGCAAAACCACGGTCAG
pBT_BamHI_rev	CGA**GGATCC**CCGGGAATTCGA
pBT_XhoI_rev	GATAAT**CTCGAG**TGAGCCGGATCTGCATCGCAGGA

Table S3-7. Organism, locus tag/protein identifier and accession numbers of proteins used for phylogenetic analyses during this study.

Organism	Locus tag/Identifier	Accession number	Database
Agrobacterium tumefaciens	Atu2274	NP_355230.2	NCBI
Arabidopsis thaliana	AtMTP6	NP_182304.2	NCBI
Arabidopsis thaliana	AtMTP3	NP_191440.2	NCBI
Arabidopsis thaliana	AtMTP1	NP_182203.1	NCBI
Arabidopsis thaliana	AtMTP2	NP_191753.1	NCBI
Arabidopsis thaliana	AtMTP4	NP_180502.2	NCBI
Arabidopsis thaliana	AtMTP5	NP_187817.2	NCBI
Arabidopsis thaliana	AtMTP12	Q9SI03.1	Swiss Prot
Arabidopsis thaliana	AtMTP8	NP_191365.2	NCBI
Arabidopsis thaliana	AtMTP11	NP_181477.1	NCBI
Arabidopsis thaliana	AtMTP10	NP_173081.2	NCBI
Arabidopsis thaliana	AtMTP9	NP_178070.2	NCBI
Arabidopsis thaliana	AtMTP7	NP_564594.1	NCBI
Ashbya gossypii	AgAFL128Cp	AAS53246	GenBank
Aspergillus fumigatus	Af5g09830	XP_753657	NCBI
Aspergillus nidulans	AN8791.2	AN8791.2	Broad Institute, v. 2
Bacillus amyloliquefaciens	BaYdfM	YP_001419916.1	NCBI
Bacillus amyloliquefaciens	BaYeaB	YP_001420288.1	NCBI
Bacillus cereus	BC_4404	AAP11317.1	GenBank
Bacillus cereus	BC_2261	AAP09225.1	GenBank
Bacillus subtilis	BsYeaB	P46348	Swiss Prot
Bacillus subtilis	BsYdfM	BAA19381.1	GenBank
Bacillus subtilis	BsCzcD	NP_390542.1	NCBI
Botrytis cinerea	BC1G_04719.1	BC1G_04719.1	Broad Institute, v. 1
Candidatus Magnetobacterium bavaricum	MbMamM	FQ377626.1	GenBank
Candidatus Magnetobacterium bavaricum	MbMamB	FQ377626.1	GenBank
Candidatus Magnetoglobus multicellularis	OMM_18	ADV17392.1	GenBank
Chromobacterium violaceum	CV_1005	AAQ58679.1	GenBank
Clostridium tetani	CTC_01013	AAO35599.1	GenBank
Clostridium tetani	CtCzcD	NP_782986.1	NCBI
Cupriavidus metallidurans	CmFieF	YP_585547.1	NCBI
Cupriavidus metallidurans CH34	CmCzcD	YP_145596.1	NCBI
Danio rerio	DrZnT10	NP_001121706.1	NCBI
Danio rerio	DrZnT6	NP_991214.1	NCBI
Deinococcus radiodurans	DR_1236	Q9RUZ4	Swiss Prot
Desulfovibrio desulfuricans	Dde_1511	YP_388005.1	NCBI
Desulfovibrio magneticus	DmMamM	YP_002955479.1	NCBI
Desulfovibrio magneticus	DmMamB	YP_002955488.1	NCBI
Enterococcus faecalis	EfEF0859	Q837I0	Swiss Prot
Escherichia coli	EcFieF	P69380	Swiss Prot
Escherichia coli	EcZitB	NP_415273.1	NCBI
Fusarium gramineaum	FG05506.1	FG05506.1	Broad Institute, v. 1
Gallus gallus	GgZnT9	XP_420731.2	NCBI
Geobacter sulfurreducens	GSU2613	AAR35985.1	GenBank
Homo sapiens	HsZnT4	O14863.2	Swiss Prot
Homo sapiens	HsZnT8	NP_776250.2	NCBI
Homo sapiens	HSZnT3	NP_003450.2	NCBI
Homo sapiens	HsZnT1	NP_067017.2	NCBI
Homo sapiens	HsZnT10	NP_061183.2	NCBI
Homo sapiens	HsZnT7	NP_598003.2	NCBI

Organism	Locus tag/Identifier	Accession number	Database
Homo sapiens	HsZnT5	NP_075053.2	NCBI
Homo sapiens	HsZnT9	EAW92998.1	GenBank
Klebsiella pneumoniae	KpFieF	Q8RR17	Swiss Prot
Magnaporthe grisea	MGG_06247	MG06247.4	Broad Institute, v. 4
magnetite containing vibrio strain MV-1	MamM_MV-1	CAV30814.1	GenBank
magnetite containing vibrio strain MV-1	MamB_MV-1	CAV30807.1	GenBank
Magnetococcus sp. MC-1	MamM_MC-1	YP_866163.1	NCBI
Magnetococcus sp. MC-1	MamB_MC-1	YP_866157.1	NCBI
Magnetospirillum gryphiswaldense	MgMamB	CAJ30127.1	GenBank
Magnetospirillum gryphiswaldense	MamM_MSR-1	CAE12036.1	GenBank
Magnetospirillum gryphiswaldense	MamB_MSR-1	AAL09999.1	GenBank
Magnetospirillum magneticum	MamM_AMB-1	YP_420330.1	NCBI
Magnetospirillum magneticum	MamV_AMB-1	YP_420341.1	NCBI
Magnetospirillum magneticum	MamB_AMB-1	YP_420337.1	NCBI
Magnetospirillum magneticum	MamB-like_AMB-1	YP_420370.1	NCBI
Magnetospirillum magnetotacticum	MamM_MS-1	ZP_00054406.2	NCBI
Magnetospirillum magnetotacticum	MamV_MS-1	ZP_00054417.2	NCBI
Magnetospirillum magnetotacticum	MamB_MS-1	ZP_00054413.1	NCBI
metagenomic sequence Fos001	MamM_Fos001	CAX83793	GenBank
metagenomic sequence Fos001	MamB_Fos001	CAX83800.1	GenBank
metagenomic sequence Fos002	MamM_Fos002	CAX84223.1	GenBank
metagenomic sequence Fos002	MamB_Fos002	CAX84216.1	GenBank
Methanocaldococcus jannaschii	Mj0449	Q57891	Swiss Prot
Methanosarcina acetivorans	MA4394	AAM07736.1	GenBank
Methanosarcina acetivorans	MA3366	AAM06735.1	GenBank
Methanosarcina acetivorans	MA0617	AAM04061.1	GenBank
Methanosarcina acetivorans	MA0549	AAM03993.1	GenBank
Methanosarcina mazei	MM1076	AAM30772.1	GenBank
Methanosarcina mazei	MM2778	AAM32474.1	GenBank
Methanosarcina mazei	MM1778	AAM31474.1	GenBank
Methanosarcina mazei	MM1711	AAM31407.1	GenBank
Mus musculus	MmZnT4	O35149.1	Swiss Prot
Mus musculus	MmZnT8	NP_766404.1	NCBI
Mus musculus	MmZnT2	NP_001034766.1	NCBI
Mus musculus	MmZnT3	NP_035903.2	NCBI
Mus musculus	MmZnT1	NP_033605.1	NCBI
Mus musculus	MmZnT6	NP_659047.2	NCBI
Mus musculus	MmZnT7	NP_075703.1	NCBI
Mus musculus	MmZnT5	NP_075023.2	NCBI
Neurospora crassa	NCU07879.2	NCU07879.2	Broad Institute, v. 2
Nostoc punctiforme	NpF0707	ZP_00109054	NCBI
Nostoc punctiforme	Npun_F2455	YP_001865959.1	NCBI
Oryza sativa	Os03g22550	Os03g22550	TIGR
Oryza sativa	OsMTP2	NP_001050094.2	NCBI
Paxillus involutus	PiMnT1	ABF74686.1	GenBank
Pectobacterium atrosepticum	PaFIEF	Q6CZ45	Swiss Prot
Populus trichocarpa	PtrMTP6	FGENESH4_PM.C_LG_X000667	DOE Joint Genome Institute

Organism	Locus tag/Identifier	Accession number	Database
Populus trichocarpa	PtrMTP3.2	XP_002317658.1	NCBI
Populus trichocarpa	PtrMTP3.1	XP_002298977.1	NCBI
Populus trichocarpa	PtrMTP4.1	XP_002299844.1	NCBI
Populus trichocarpa	PtrMTP4.2	XP_002339166.1	NCBI
Populus trichocarpa	PtrMTP12	XP_002327739.1	NCBI
Populus trichocarpa	PtrMTP8.1	XP_002304880.1	NCBI
Populus trichocarpa	PtrMTP8.2	XP_002299137.1	NCBI
Populus trichocarpa	PtrMTP11.1	XP_002315247.1	NCBI
Populus trichocarpa	PtrMTP11.2	XP_002312066.1	NCBI
Populus trichocarpa	PtrMTP9	XP_002312234.1	NCBI
Populus trichocarpa	PtrMTP10	XP_002315072.1	NCBI
Populus trichocarpa	PtrMTP7	XP_002315378.1	NCBI
Ralstonia solanacearum	RSc3077	CAD16786.1	GenBank
Rhodopseudomonas palustris	RPA1939	CAE27380.1	GenBank
Rickettsia felis	RF_1320	YP_247336.1	NCBI
Rickettsia prowazekii	RP832	Q9ZCC5	Swiss Prot
Rickettsia rickettsii	A1G_07070	P21559	Swiss Prot
Saccharomyces cerevisiae	ScMMT1	NP_013902	NCBI
Saccharomyces cerevisiae	ScMMT2	NP_015100.2	NCBI
Saccharomyces cerevisiae	ScCOT1	NP_014961.1	NCBI
Saccharomyces cerevisiae	ScZRC1	NP_013970.1	NCBI
Saccharomyces cerevisiae	ScCOT1	NP_014961.1	NCBI
Saccharomyces cerevisiae	ScZRC1	NP_013970.1	NCBI
Saccharomyces cerevisiae	ScMSC2	NP_010491.2	NCBI
Saccharomyces cerevisiae	ScZRG17	NP_014437.1	NCBI
Salmonella typhi	StiFieF	Q8Z2W4	Swiss Prot
Salmonella typhimurium	StyFieF	Q8ZKR4	Swiss Prot
Sclerotinia sclerotiorum	SS1G_07340.1	SS1G_07340.1	Broad Institute, v. 1
Shigella flexneri	SfFieF	YP_690915.1	NCBI
Streptococcus agalactiae	SAK_1232	YP_329849.1	NCBI
Synechococcus elongatus	Synpcc7942_1989	YP_401006.1	NCBI
Synechococcus sp. CC9605	Syncc9605_1040	YP_381353.1	NCBI
Synechocystis sp. PCC 6803	sll1263	P74068	Swiss Prot
Thermus scotoductus	TsCzrB	YP_004202101.1	NCBI
Thermus thermophilus	TtCzrB	CAC83722.1	GenBank
Thiomicrospira crunogena	Tcr_0241	YP_390511.1	NCBI
Ustilago maydis	UM00151.1	UM00151.1	Broad Institute, v. 1
Yersinia pseudotuberculosis	YpsFieF	Q66GA9	Swiss Prot
Zygosaccharomyces rouxii	ZrMSC2	XP_002495859.1	NCBI
Zygosaccharomyces rouxii	ZrZRG17	CAQ43236.1	GenBank

3.8.4 Supplementary references

Arnold, K., Bordoli, L., Kopp, J. and Schwede, T. (2006). The SWISS-MODEL workspace: a web-based environment for protein structure homology modelling. *Bioinformatics* **22**: 195-201.

Kovach, M. E., Elzer, P. H., Hill, D. S., Robertson, G. T., Farris, M. A., Roop, R. M. and Peterson, K. M. (1995). Four new derivatives of the broad-host-range cloning vector pBBR1MCS, carrying different antibiotic-resistance cassettes. *Gene* **166**: 175-176.

Lang, C. and Schüler, D. (2008). Expression of green fluorescent protein fused to magnetosome proteins in microaerophilic magnetotactic bacteria. *Appl. Environ. Microbiol.* **74**: 4944-4953.

Marx, C. and Lidstrom, M. (2002). Broad-Host-Range *cre-lox* system for antibiotic marker recycling in gram-negative bacteria. *Biotechniques* **33**: 1062-1067.

Montanini, B., Blaudez, D., Jeandroz, S., Sanders, D. and Chalot, M. (2007). Phylogenetic and functional analysis of the Cation Diffusion Facilitator (CDF) family: improved signature and prediction of substrate specificity. *BMC Genomics* **8**: 107.

Scheffel, A., Gruska, M., Faivre, D., Linaroudis, A., Graumann, P. L., Plitzko, J. and Schüler, D. (2006). An acidic protein aligns magnetosomes along a filamentous structure in magnetotactic bacteria. *Nature* **440**: 110-114.

Schübbe, S., Kube, M., Scheffel, A., Wawer, C., Heyen, U., Meyerdierks, A., Madkour, M. H., Mayer, F., Reinhardt, R. and Schüler, D. (2003). Characterization of a spontaneous nonmagnetic mutant of *Magnetospirillum gryphiswaldense* reveals a large deletion comprising a putative magnetosome island. *J. Bacteriol.* **185**: 5779-5790.

Schultheiss, D., Handrick, R., Jendrossek, D., Hanzlik, M. and Schüler, D. (2005). The presumptive magnetosome protein Mms16 is a poly(3-hydroxybutyrate) granule-bound protein (phasin) in *Magnetospirillum gryphiswaldense*. *J. Bacteriol.* **187**: 2416-2425.

Wood, D. W., Setubal, J. C., Kaul, R., Monks, D. E., Kitajima, J. P., Okura, V. K., Zhou, Y., Chen, L., Wood, G. E., Almeida, N. F., Woo, L., Chen, Y., Paulsen, I. T., Eisen, J. A.*, et al.* (2001). The Genome of the Natural Genetic Engineer Agrobacterium tumefaciens C58. *Science* **294**: 2317-2323.

CHAPTER 4

The MagA protein of magnetospirilla is not involved in bacterial magnetite biomineralization

4.1 Abstract

Magnetotactic bacteria have the ability to orient along geomagnetic field lines based on the formation of magnetosomes, which are intracellular nanometer-sized, membrane-enclosed magnetic iron minerals. The formation of these unique bacterial organelles involves several processes like cytoplasmic membrane invagination and magnetosome vesicle formation, accumulation of iron in the vesicles, and crystallization of magnetite. Previous studies suggested that the *magA* gene may encode a magnetosome-directed ferrous iron transporter with a supposedly essential function for magnetosome formation in *Magnetospirillum magneticum* AMB-1, and which may cause magnetite biomineralization if expressed in mammalian cells. However, more recent studies failed to detect the MagA protein among polypeptides associated with the magnetosome membrane and did not identify *magA* within the magnetosome island, a conserved genomic region essential for magnetosome formation in magnetotactic bacteria. This raised increasing doubts about the presumptive role of *magA* in bacterial magnetosome formation, which prompted us to reassess MagA function by targeted deletion in *Magnetospirillum magneticum* AMB-1 and *Magnetospirillum gryphiswaldense* MSR-1. Contrary to previous reports *magA* mutants of both strains were still able to form wild type-like magnetosomes and had no obvious growth defects. This unambiguously shows that *magA* is not involved in magnetosome formation in magnetotactic bacteria.

4.2 Introduction

Magnetotactic bacteria (MTB) form magnetosomes, which are organelles for orientation along geomagnetic field lines to facilitate the navigation of MTB within aquatic habitats (Frankel *et al.*, 2007). In magnetospirilla and other MTB, magnetosomes consist of membrane enveloped single-domain magnetite (Fe_3O_4) crystals, which are aligned in chains by cytoskeletal structures (Faivre and Schüler, 2008).

Their lifestyle adapted to chemical gradients, their fastidiousness and the lack of genetically tractable lab strains for many years hampered molecular analysis of magnetosome formation. In the first report on successful gene transfer to MTB Matsunaga and colleagues isolated five Tn5 mutants of the α-proteobacterium *Magnetospirillum magneticum* AMB-1 (AMB-1), which had lost the ability to synthesize magnetosomes. Two of these mutants (NM3 and NM5) showed Tn5-insertion into the same genomic region (Matsunaga *et al.*, 1992). Subsequent studies by the same authors showed that the non-magnetic NM5 and NM3 mutants had insertions in the *magA* gene encoding a protein with weak similarity to the *Escherichia coli* potassium efflux protein KefC. Based on results of promoter fusion to firefly luciferase the authors also reported that *magA* transcription was enhanced by low iron concentrations (Nakamura *et al.*, 1995b). Consistent with its putative function in magnetosome formation it was also shown by luciferase gene fusion assays that MagA localized to the cytoplasmic as well as to the magnetosome membrane (Nakamura *et al.*, 1995b). In addition, inverted vesicles prepared from fragmented membranes of *Escherichia coli* DH5α expressing *magA* exhibited ATP-dependent iron accumulation ability, from which it was concluded that MagA is a magnetosome-directed iron transporter (Nakamura *et al.*, 1995a). MagA was also suggested for use as an anchor protein to display foreign polypeptides on the surface of bacterial magnetosomes by genetic fusions (Matsunaga *et al.*, 1999).

A more recent study by a different lab, in which the targeted deletion of *magA* in AMB-1 supposedly resulted in the loss of the ability to form magnetosomes, seemed to confirm the reported essential function of *magA* (Smith *et al.*, 2006). However, there is still missing evidence that the observed non-magnetic phenotypes in fact were caused by the loss of *magA* function, since neither this mutant as well as the original transposon mutant (Matsunaga *et al.*, 1992) have been shown to be complemented by a wild type-copy of *magA*.

Results of more recent studies on AMB-1 and the closely related *Magnetospirillum gryphiswaldense* MSR-1 (MSR-1) seemed also to be inconsistent with an

involvement of MagA in magnetosome synthesis. Several independent proteomic studies for example failed to identify MagA in the magnetosome membrane of AMB-1 (Tanaka *et al.*, 2006) and MSR-1 (Grünberg *et al.*, 2001; Grünberg *et al.*, 2004; Lohße *et al.*, 2011). In addition, MagA-luciferase protein fusions revealed 1,000-fold lower magnetosome-associated luminescence compared to luciferase fusions with the well-studied magnetosome membrane protein MamC (also known as Mms13) (Yoshino and Matsunaga, 2006). Furthermore, comparative genome analyses of MTB did not identify *magA* among the conserved signature genes for magnetotaxis (Richter *et al.*, 2007), and showed that *magA* is not located within the genomic magnetosome island (MAI). This region is now assumed to harbor most if not all genes essential for magnetosome formation (Ullrich *et al.*, 2005; Fukuda *et al.*, 2006; Murat *et al.*, 2010; Lohße *et al.*, 2011), and has been found to be more or less conserved in all MTB (Jogler *et al.*, 2009a; Jogler *et al.*, 2009b; Abreu *et al.*, 2011; Jogler *et al.*, 2011). Although these observations increasingly questioned the proposed role of MagA, MagA is still being widely discussed as an essential determinant of magnetosome synthesis (Matsunaga *et al.*, 2009; Baumgartner and Faivre, 2011; Hsu and Chan, 2011; Komeili, 2011).

Most recently, further ambiguity was caused by two studies, which suggested using *magA* as a reporter gene for *in vivo* cellular and molecular imaging in mammalian cell lines by magnetic resonance imaging (MRI) because of its putative iron transport activity (Zurkiya *et al.*, 2008; Goldhawk *et al.*, 2009). Goldhawk *et al.* (2009) described that expression of *magA* in N2A mouse neuroblastoma cell lines resulted in elevated intracellular MRI contrast due to increased iron load of the cells. Even more intriguingly, Zurkiya *et al.* (2008) reported that expression of *magA* alone in human 293 FTcell lines was sufficient to cause the biomineralization of small magnetite particles.

In order to resolve these conflicting observations, we reassessed MagA function by targeted deletion of *magA* in MSR-1 and AMB-1. *magA* mutants of both strains showed no phenotypic effects and were still able to produce wild type-like magnetosomes. This indicates that, contrary to previous assumptions, MagA is not involved in bacterial magnetosome formation.

4.3 Materials & Methods

4.3.1 Bacterial strains and growth conditions

Bacterial strains and plasmids are described in Table 4-1. *E. coli* BW29427 was grown in lysogeny broth (LB) supplemented with 1 mM DL-α,ε-diaminopimelic acid and gentamicin (15 μg ml^{-1}), kanamycin (25 μg ml^{-1}), or tetracyclin (50 μg ml^{-1}) at 37°C with vigorous shaking (200 rpm). MSR-1 and AMB-1 strains were grown in modified flask standard medium (FSM) with 50 μM ferric citrate as described (Uebe *et al.*, 2010).

Table 4-1. Bacterial strains and plasmids used in this study.

Strain or plasmid	Important features	Source or reference
Strains		
E. coli		
BW29427	*thrB1004 pro thi rpsL hsdS lacZ*ΔM15 RP4-1360 Δ(*araBAD*)567 Δ*dapA1341::[erm pir* (wt)]	Datsenko, K. and Wanner B. L. (unpublished)
M. gryphiswaldense		
MSR-1 R3/S1	wild type but Rif^r, Sm^r	(Schultheiss and Schüler, 2003)
RU-2	R3/S1::pMagAup	this study
RU-3	R3/S1::pMagAup::pMagAdo	this study
RU-4	R3/S1 but Δ*magA*	this study
M. magneticum		
AMB-1	wild type	(Kawaguchi *et al.*, 1992)
ARU-1	AMB-1::pAMB_MagAup	this study
ARU-2	AMB-1::pAMB_MagAup::pAMB_MagAdo	this study
ARU-3	AMB-1 but Δ*magA*	this study
Plasmids		
pAL01	suicide vector, Kan^r, *lox71*	(Lohße *et al.*, 2011)
pAL02/2	suicide vector, Gm^r, *lox66*	(Lohße *et al.*, 2011)
pCM157	Cre expression vector, Tet^r	(Marx and Lidstrom, 2002)
pMagAup	pAL01 + 450 bp fragment of MSR-1 *magA* upstream flanking region	this study
pMagAdo	pAL02/2 + 2 kb fragment of MSR-1 *magA* downstream flanking region	this study
pAMB_MagAup	pAL01 + 1.25 kb fragment of AMB-1 *magA* upstream flanking region	this study
pAMB_MagAdo	pAL02/2 + 1.25 kb fragment of AMB-1 *magA* downstream flanking region	this study

4.3.2 Molecular and genetic techniques

Unless specified otherwise, molecular techniques were performed using standard protocols (Sambrook and Russel, 2001). DNA was sequenced using BigDye terminator v3.1 chemistry on an ABI 3700 capillary sequencer (Applied Biosystems, Darmstadt, Germany). Sequence data were analyzed using 4Peaks software (http://mekentosj.com/4peaks). All oligonucleotide primers (see Table S4-1 in the supplemental material) were purchased from Sigma-Aldrich (Steinheim, Germany).

4.3.3 Generation of *magA* deletions in MSR-1 and AMB-1

An in-frame *magA* deletion mutant of MSR-1 was generated by a three step Cre-*lox*-based method (Ullrich and Schüler, 2010). Therefore, a 450 bp PCR-fragment of the *magA* upstream flanking region was inserted into the NotI/EcoRI restriction sites of pAL01. The resulting vector pMagAup was then transferred to MSR-1 by conjugation using *Escherichia coli* BW29427 as a donor strain to yield strain RU-2. After verification of correct single crossover insertion of pMagAup, a second integration vector pMagAdo, containing a 2 kb SacI/SacII-digested PCR fragment of the *magA* downstream flanking region was transferred to strain RU-2 to generate strain RU-3. The Cre recombinase-encoding plasmid pCM157 was transferred to strain RU-3 to induce Cre recombinase-mediated excision of *magA* by site-specific recombination between the *lox66* and *lox71* sites located on the integration vectors. Exconjugants were screened for *magA* excision by PCR and cured from pCM157 by repeated passaging in fresh FSM.

For generation of an AMB-1 in-frame *magA* mutant 1.25 kb of the *magA* flanking regions were amplified and inserted into pAL01 and pAL02/2, respectively, to generate the integration vectors pAMB_magAup and pAMB_magAdo. Using *E. coli* BW29427 as a donor strain plasmid pAMB_magAup was transferred to AMB-1 to generate strain ARU-1. Strain ARU-2 was generated by insertion of pAMB_magAdo. After transfer of pCM157 into strain ARU-2, the resulting exconjugants were screened for Cre-mediated deletion of *magA* and cured from pCM157 by repeated passaging in fresh FSM.

4.3.4 Southern blotting

Approximately 10 µg of MSR-1 genomic DNA was digested with ClaI. The DNA fragments were resolved in a 1% agarose gel and blotted onto a nylon membrane (Protran supercharge, Whatman) using standard procedures. A PCR-amplified *magA* probe was labeled using an [α^{32}P]dATP HexaLabel DNA labeling kit (Fermentas). Prehybridization of the nylon membrane was carried out in 20 ml of Church's phosphate buffer (0.25 M Na_2HPO_4/ NaH_2PO_4, 1 mM EDTA, 7% sodium dodecyl sulfate (w/v), 1% bovine serum albumin (w/v), pH 7.2) at 53°C over night. Subsequently, the hybridization was performed at 53°C over night in Church's buffer containing the labeled probe. Washing was done twice at 53°C in wash buffer (5% SDS (w/v), 1% BSA (w/v), 1 mM EDTA, 40 mM Na_2HPO_4/NaH_2PO_4, pH 7,2) for 5 min followed by two additional wash steps in 40 mM Na_2HPO_4/NaH_2PO_4, 1% SDS (w/v), 1 mM EDTA, pH 7,2 for 10 min. After the membranes were washed, they were exposed to a phosphor screen (Kodak storage phosphor screen; Molecular Dynamics, Krefeld, Germany) for 1 d, and the hybridized signals were captured as image files by using a Storm 840 Scanner (Molecular Dynamics, Krefeld).

4.3.5 Analytical methods

Transmission electron microscopy (TEM) analyses were performed as described previously (Katzmann *et al.*, 2010).

The average magnetic response of MSR-1 or AMB-1 cell suspensions (C_{mag}) was assayed by a light scattering method in which cells were aligned at different angles relative to a light beam by means of an external magnetic field (Schüler *et al.*, 1995). The ratio of the resulting maximum and minimum scattering intensities (C_{mag}) is correlated with the average number of magnetic particles and can be used for a qualitative assessment of magnetite formation.

4.3.6 Bioinformatic analyses

Multiple sequence alignments and the similarity trees were generated with MEGA4 software (Tamura *et al.*, 2007). Sequences were aligned by ClustalW (default settings) and the similarity trees were constructed using the Neighbor-Joining (NJ) method and the bootstrap (1000 replicates) phylogeny test.

4.4 Results & Discussion

MagA is encoded by the first gene of a putative bicistronic operon that is conserved in *Magnetospirillum* species. The *magA* gene overlaps the following second ORF encoding a putative RNase HII by 8 bp (MSR-1) or 26 bp (AMB-1 and *Magnetospirillum magnetotacticum* MS-1 (MS-1)). The genomic context of the small *magA* operon, however, is not conserved, except for a putative DNA methylase located downstream of the *magA* operon in all three *Magnetospirillum* species. Based on sequence similarity MagA groups within the ubiquitous monovalent cation:proton antiporter (CPA) subfamily CPA2 (Fig. 4-1).

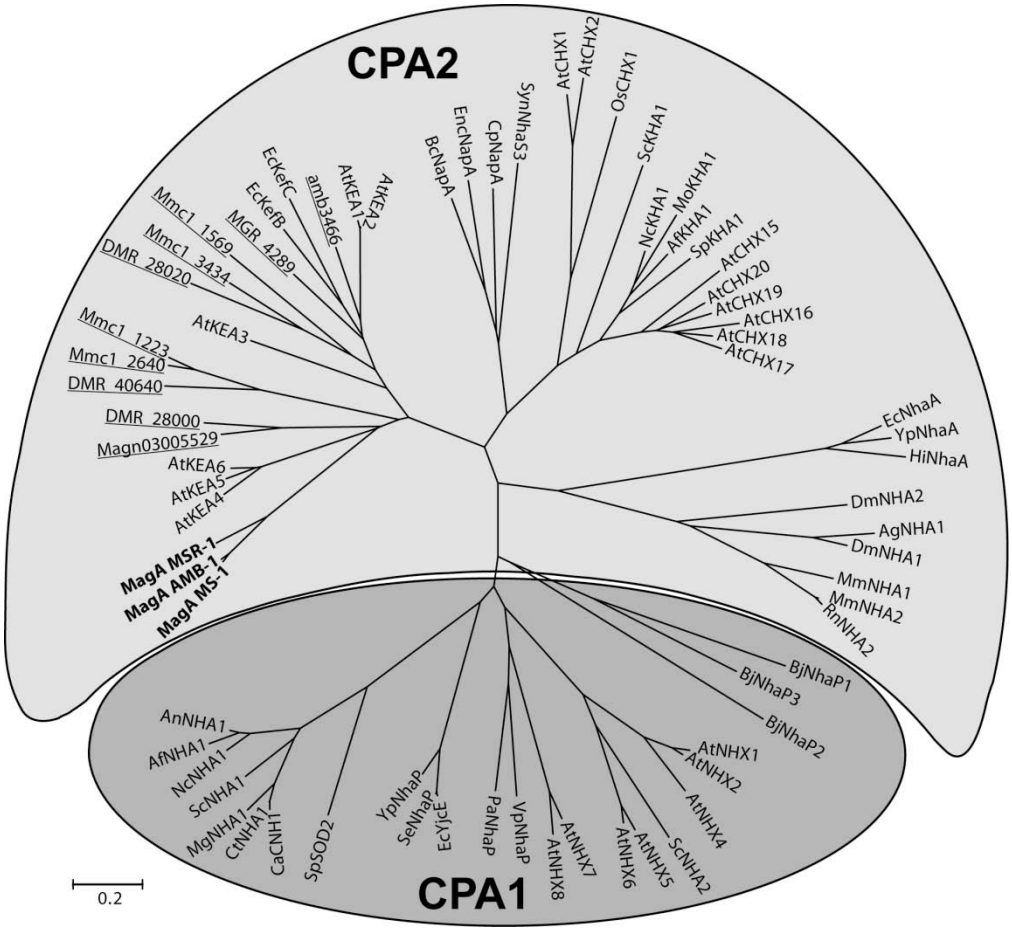

FIG. 4-1. MagA is member of the CPA2 subfamily of the monovalent cation:proton antiporter family (CPA). Bold letters represent MagA proteins of MSR-1, AMB-1 and MS-1. Underlined proteins represent MTB sequences comprising Blastp hits with an expectation value of E <1e-05 to MagA of AMB-1. The scale bar indicates an evolutionary distance of 0.2 amino acid substitutions per site. Accession numbers and origin of proteins used to generate the tree are given in Table S4-2.

The affiliation of MagA with this protein family seems to question previously observed ATP-dependent ferrous iron transport activity of MagA (Nakamura *et al.*, 1995b), since members of the CPA2 subfamily have been shown to exclusively transport monovalent cations (e.g. K^+, Na^+ or NH_4^+) in exchange for protons (Chang *et al.*, 2004) to regulate alkali resistance,

electrophile resistance, osmoregulation, and endospore germination (Booth, 1985; Ferguson *et al.*, 1997; Thackray *et al.*, 2001; Padan *et al.*, 2005). Further sequence analyses revealed that the MagA proteins of the magnetospirilla lack a putative Rossmann-fold $NAD(P)^+$-binding domain, which, however, is present in all other CPA2 proteins of MTB. These analyses showed that MagA is confined to strains of *Magnetospirillum*, but absent from the genomes of other MTB (FIG. 4-1), arguing against a universal role in magnetosome formation.

To analyze its putative function, we constructed an unmarked in frame deletion mutant of *magA* in our model organism MSR-1 (FIG. 4-2A and B). All 24 examined MSR-1 Δ*magA* clones were still mag^+, i.e. they aligned along magnetic field lines with wild type-like C_{mag} values in magnetic response assays. In addition, under standard conditions no obvious growth defects of the mutation were observed. Transmission electron microscopic (TEM) analyses of one randomly picked $magA^-$ clone (strain RU-4, FIG. 4-2A) confirmed the presence of magnetosome crystals, which were indistinguishable from the WT with respect to size, shape, and alignment (FIG. 4-2C and D).

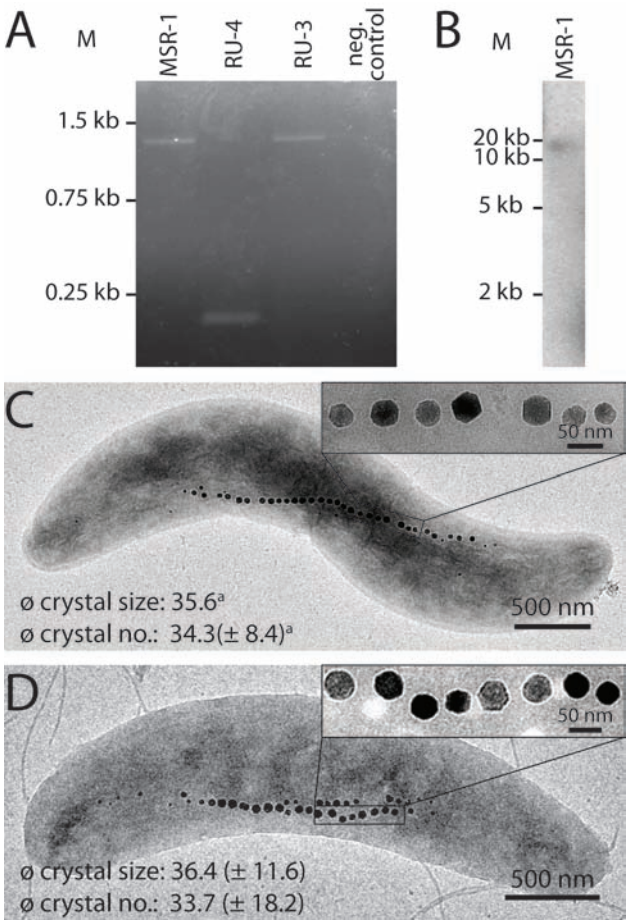

FIG. 4-2. A) Agarose gel electrophoresis of PCR products using primer for the amplification of *magA* (primer MSR-1_magA_for/rev) in strains MSR-1, RU-3 and RU-4 (see FIG. S4-1 for schematic representation of the genomic organization). Negative control: genomic DNA omitted. M, DNA size marker. B) Southern blot analysis of ClaI-digested MSR-1 genomic DNA hybridized with a 1.3 kb PCR-amplified *magA* probe. Digestion of MSR-1 gDNA should result in a single fragment of >12 kb when *magA* is present in a single copy in MSR-1. M, DNA size marker. C) Representative TEM micrograph of *M. gryphiswaldense* wild-type strain MSR-1. [a], average magnetosome number and sizes were taken from (Lohße *et al.*, 2011). D) Representative TEM micrograph of *M. gryphiswaldense* Δ*magA* strain RU-4. Insets in C) and D) show a higher magnification view of the boxed areas. Average magnetosome numbers and sizes were calculated from 886 magnetosomes.

To exclude the possibility that further, potentially redundant homologs of *magA* might be present within the incompletely assembled genome of MSR-1 (Richter *et al.*, 2007), we performed Southern blot analysis of digested genomic DNA from MSR-1. Using *magA* as a probe this indicated that as in AMB-1 *magA* is present only in a single copy in the genome of MSR-1 (FIG. 4-2B).

In contrast to most other essential magnetosome proteins, e.g. MamB or MamM (Uebe *et al.*, 2011) which generally have similarities of 89 to 98% between AMB-1 and MSR-1, MagA is rather poorly conserved and shows a comparably high sequence divergence between MagA of MSR-1 and AMB-1 or MS-1 (78 and 77% similarity, respectively) (Table 4-2), leaving the possibility that the function of MagA of MSR-1 might be distinct from MagA of AMB-1.

Table 4-2. Similarity divergence between MagA homologs of *M. gryphiswaldense* MSR-1, *M. magneticum* AMB-1, *M. magnetotacticum* MS-1, *Magnetospirillum magneticum* MGT-1 and *E. coli* CPA family proteins KefB, KefC, YbaL, NhaA and YcjE.

No.	Organism	Protein	% Similarity with protein							
			1	2	3	4	5	6	7	8
1	MSR-1	MagA	100	77.2	78.4	32.9	32.2	36.4	30.4	27.9
2	AMB-1	MagA		100	97.9	31.2	30.7	36.9	28.5	27.9
3	MS-1	MagA			100	31.7	30.5	36.6	28.3	28.2
4		KefB				100	58.8	42.1	22.0	28.7
5		KefC					100	38.7	20.1	30.7
6	*E. coli*	YbaL						100	25.6	32.6
7		NhaA							100	22.6
8		YcjE								100

Therefore, deletion of *magA* was also performed in AMB-1. Like in MSR-1, all tested AMB-1 *magA*$^-$ clones were still able to align along magnetic field lines in magnetic response-assays. TEM analyses of one AMB-1 Δ*magA* clone (strain ARU-3, FIG. 4-3A) confirmed the presence of wild-type-like magnetosomes (Fig. 4-3B and C). Hence, it can be concluded that MagA is not involved in the magnetosome formation in AMB-1 as well.

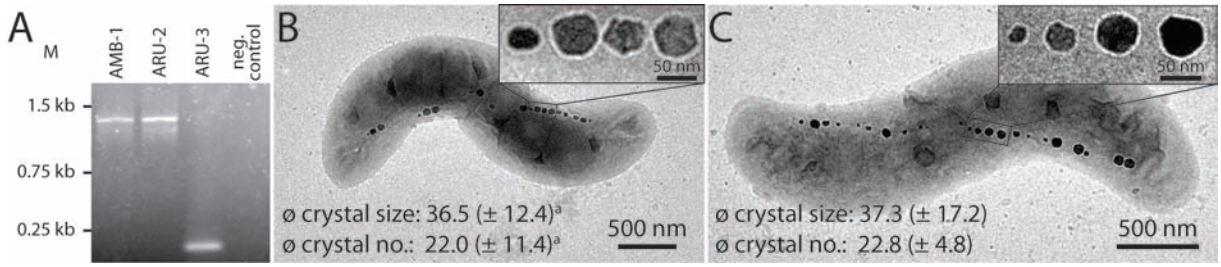

FIG. 4-3. A) Agarose gel electrophoresis of PCR products using primer for the amplification of *magA* (primer AMB-1_magA_for/rev) in strains AMB-1, ARU-2 and ARU-3 (see FIG. S4-1 for schematic representation of the genomic organization). Neg. control with genomic DNA omitted. M, DNA size marker. B) Representative TEM micrograph of *M. magneticum* wild-type strain AMB-1. [a], average magnetosome number and sizes were taken from (Wang *et al.*, 2008). C) Representative TEM micrograph of *M. magneticum* Δ*magA* strain ARU-3. Insets in B) and C) show a higher magnification view of the boxed areas. Average magnetosome numbers and sizes were calculated from 454 magnetosomes.

The magnetic phenotypes of the MSR-1 and AMB-1 *magA* mutants constructed during this study together with the *magA* localization outside the MAI, its poor conservation among MTB, and the affiliation of MagA with the CPA2 subfamily clearly contradict the results of previous studies (Matsunaga *et al.*, 1992; Smith *et al.*, 2006). However, as mentioned above all previous genetic studies were lacking appropriate experimental controls, i.e. they failed to demonstrate that wild type-like phenotypes could be restored by re-introduction of *magA* (Matsunaga *et al.*, 1992; Smith *et al.*, 2006). Thus, it can be speculated that the previously observed non-magnetic phenotypes were likely due to the accidental isolation of clones

coincidentally harboring an undetected spontaneous second-site mutation, leading then to the wrongful conclusion of a role of MagA in magnetosome formation. It has been well established that spontaneous non-magnetic mutations may arise at high frequencies in cultures of various MTB including AMB-1, which are due to RecA-dependent rearrangements within the MAI, causing extended deletions of the essential *mamAB* operon of AMB-1 and MSR-1 (Ullrich *et al.*, 2005; Fukuda *et al.*, 2006; Kolinko *et al.*, 2011). This has been already described to potentially obscure genetic analysis in the absence of appropriate controls (Komeili *et al.*, 2004; Nash, 2008; Jogler and Schüler, 2009).

The lack of any obvious phenotypic effects also argues against an essential role of MagA in metabolism and thus, the real function of MagA remains to be identified. Although beyond the scope of our study, it might be speculated that MagA might have a function in the homeostasis of monovalent cations such as sodium or potassium under certain, yet unexplored growth conditions.

In apparent contrast to lack of function in bacterial magnetite biomineralization, heterologous expression of *magA* in mammalian cell lines reportedly caused rather drastic effects, resulting in a seven-fold increased intracellular iron content or formation of small magnetite particles (Zurkiya *et al.*, 2008; Goldhawk *et al.*, 2009). However, the disparity of these observations argues against effects associated with the genuine function of MagA, and could be possibly explained by pathological consequences of gene expression, or artificially high iron levels used in these studies.

In conclusion, the findings of this study that MagA is not involved in magnetosome formation as previously supposed, and lend further support to the assumption that the MAI might contain all essential genes required for magnetosome formation, and which might have been distributed by HGT (Jogler *et al.*, 2009a; Murat *et al.*, 2010; Ullrich and Schüler, 2010).

4.5 Acknowledgements

We thank Gabriele Poxleitner for valuable input to the study. This work was supported by the Deutsche Forschungsgemeinschaft (DFG Schu1080/13-1).

4.6 References

Abreu, F., Cantão, M. E., Nicolás, M. F., Barcellos, F. G., Morillo, V., Almeida, L. G. P., do Nascimento, F. F., Lefèvre, C. T., Bazylinski, D. A., R de Vasconcelos, A. T. and Lins, U. (2011). Common ancestry of iron oxide- and iron-sulfide-based biomineralization in magnetotactic bacteria. *ISME J.* **5**: 1634-1640.

Baumgartner, J. and Faivre, D. (2011). Magnetite biomineralization in bacteria. In: *Molecular biomineralization: Aquatic organisms forming extraordinary materials*. W. E. G. Müller (ed.). Springer, Heidelberg.

Booth, I. R. (1985). Regulation of cytoplasmic pH in bacteria. *Microbiol. Rev.* **49**: 359-378.

Chang, A. B., Lin, R., Studley, W. K., Tran, C. V. and Saier Jr., M. H. (2004). Phylogeny as a guide to structure and function of membrane transport proteins. *Mol. Membr. Biol.* **21**: 171-181.

Faivre, D. and Schüler, D. (2008). Magnetotactic bacteria and magnetosomes. *Chem. Rev.* **108**: 4875-4898.

Ferguson, G., Nikolaev, Y., McLaggan, D., Maclean, M. and Booth, I. (1997). Survival during exposure to the electrophilic reagent N-ethylmaleimide in *Escherichia coli*: role of KefB and KefC potassium channels. *J. Bacteriol.* **179**: 1007-1012.

Frankel, R., Williams, T. and Bazylinski, D. (2007). Magneto-aerotaxis. In: *Magnetoreception and Magnetosomes in Bacteria*. D. Schüler (ed.). Springer, Berlin, Heidelberg.

Fukuda, Y., Okamura, Y., Takeyama, H. and Matsunaga, T. (2006). Dynamic analysis of a genomic island in *Magnetospirillum sp.* strain AMB-1 reveals how magnetosome synthesis developed. *FEBS Lett.* **580**: 801-812.

Goldhawk, D. E., Lemaire, C., McCreary, C. R., McGirr, R., Dhanvantari, S., Thompson, R. T., Figueredo, R., Koropatnick, J., Foster, P. and Prato, F. S. (2009). Magnetic resonance imaging of cells overexpressing MagA, an endogenous contrast agent for live cell imaging. *Mol. Imaging* **8**: 129-139.

Grünberg, K., Müller, E. C., Otto, A., Reszka, R., Linder, D., Kube, M., Reinhardt, R. and Schüler, D. (2004). Biochemical and proteomic analysis of the magnetosome membrane in *Magnetospirillum gryphiswaldense*. *Appl. Environ. Microbiol.* **70**: 1040-1050.

Grünberg, K., Wawer, C., Tebo, B. M. and Schüler, D. (2001). A large gene cluster encoding several magnetosome proteins is conserved in different species of magnetotactic bacteria. *Appl. Environ. Microbiol.* **67**: 4573-4582.

Hsu, C.-Y. and Chan, Y.-P. (2011). Identification and localization of proteins associated with biomineralization in the iron deposition vesicles of honeybees (*Apis mellifera*). *PLoS One* **6**: e19088.

Jogler, C., Kube, M., Schübbe, S., Ullrich, S., Teeling, H., Bazylinski, D., Reinhardt, R. and Schüler, D. (2009a). Comparative analysis of magnetosome gene clusters in magnetotactic bacteria provides further evidence for horizontal gene transfer. *Environ. Microbiol.* **11**: 1267–1277.

Jogler, C., Lin, W., Meyerdierks, A., Kube, M., Katzmann, E., Flies, C., Pan, Y., Amann, R., Reinhardt, R. and Schüler, D. (2009b). Toward cloning of the magnetotactic metagenome: Identification of magnetosome island gene clusters in uncultivated magnetotactic bacteria from different aquatic sediments. *Appl. Environ. Microbiol.* **75**: 3972-3979.

Jogler, C. and Schüler, D. (2009). Genomics, genetics, and cell biology of magnetosome formation. *Annu. Rev. Microbiol.* **63**: 501-521.

Jogler, C., Wanner, G., Kolinko, S., Niebler, M., Amann, R., Petersen, N., Kube, M., Reinhardt, R. and Schüler, D. (2011). Conservation of proteobacterial magnetosome genes and structures in an uncultivated member of the deep-branching *Nitrospira* phylum. *Proc. Natl. Acad. Sci. U.S.A.* **108**: 1134-1139.

Katzmann, E., Scheffel, A., Gruska, M., Plitzko, J. M. and Schüler, D. (2010). Loss of the actin-like protein MamK has pleiotropic effects on magnetosome formation and chain assembly in *Magnetospirillum gryphiswaldense*. *Mol. Microbiol.* **77**: 208-224.

Kawaguchi, R., Burgess, J. and Matsunaga, T. (1992). Phylogeny and 16S rRNA sequence of *Magnetospirillum* sp. AMB-1, an aerobic magnetic bacterium. *Nucl. Acid Res.* **20**: 1140.

Kolinko, I., Jogler, C., Katzmann, E. and Schüler, D. (2011). Frequent mutations within the genomic magnetosome island of *Magnetospirillum gryphiswaldense* are mediated by RecA. *J. Bacteriol.* **193**: 5328–5334.

Komeili, A. (2011). Molecular mechanisms of compartmentalization and biomineralization in magnetotactic bacteria. *FEMS Microbiol. Rev.* doi: 10.1111/j.1574-6976.2011.00315.x.

Komeili, A., Vali, H., Beveridge, T. J. and Newman, D. K. (2004). Magnetosome vesicles are present before magnetite formation, and MamA is required for their activation. *Proc. Natl. Acad. Sci. U.S.A.* **101**: 3839-3844.

Lohße, A., Ullrich, S., Katzmann, E., Borg, S., Wanner, G., Richter, M., Voigt, B., Schweder, T. and Schüler, D. (2011). Functional analysis of the magnetosome island in *Magnetospirillum gryphiswaldense*: The *mamAB* operon is sufficient for magnetite biomineralization. *PLoS One.* **6**: e25561.

Marx, C. and Lidstrom, M. (2002). Broad-Host-Range *cre-lox* system for antibiotic marker recycling in gram-negative bacteria. *Biotechniques* **33**: 1062-1067.

Matsunaga, T., Nakamura, C., Burgess, J. G. and Sode, K. (1992). Gene transfer in magnetic bacteria: transposon mutagenesis and cloning of genomic DNA fragments required for magnetosome synthesis. *J. Bacteriol.* **174**: 2748-2753.

Matsunaga, T., Nemoto, M., Arakaki, A. and Tanaka, M. (2009). Proteomic analysis of irregular, bullet-shaped magnetosomes in the sulphate-reducing magnetotactic bacterium *Desulfovibrio magneticus* RS-1. *Proteomics* **9**: 3341-3352.

Matsunaga, T., Sato, R., Kamiya, S., Tanaka, T. and Takeyama, H. (1999). Chemiluminescence enzyme immunoassay using ProteinA-bacterial magnetite complex. *J. Magn. Magn. Mater.* **194**: 126-131.

Murat, D., Quinlan, A., Vali, H. and Komeili, A. (2010). Comprehensive genetic dissection of the magnetosome gene island reveals the step-wise assembly of a prokaryotic organelle. *Proc. Natl. Acad. Sci. U.S.A.* **107**: 5593-5598.

Nakamura, C., Burgess, J. G., Sode, K. and Matsunaga, T. (1995a). An iron-regulated gene, *magA*, encoding an iron transport protein of *Magnetospirillum* sp. strain AMB-1. *J. Biol. Chem.* **270**: 28392-28396.

Nakamura, C., Kikuchi, T., Burgess, J. G. and Matsunaga, T. (1995b). Iron-regulated expression and membrane localization of the MagA protein in *Magnetospirillum* sp. Strain AMB-1. *J. Biochem.* **118**: 23-27.

Nash, C. Z. (2008). *Ph.D. thesis*: Mechanisms and evolution of magnetotactic bacteria. California Institute of Technology, Pasadena, CA.

Padan, E., Bibi, E., Ito, M. and Krulwich, T. A. (2005). Alkaline pH homeostasis in bacteria: New insights. *Biochim. Biophys. Acta Biomembr.* **1717**: 67-88.

Richter, M., Kube, M., Bazylinski, D., Lombardot, T., Glöckner, F., Reinhardt, R. and Schüler, D. (2007). Comparative genome analysis of four magnetotactic bacteria

reveals a complex set of group-specific genes implicated in magnetosome biomineralization and function. *J. Bacteriol.* **189**: 4899-4910.

Sambrook, J. and Russel, D. (2001). *Molecular cloning: A laboratory manual*. Cold Spring Harbor Laboratory Press, Cold Spring Harbor, New York.

Schüler, D., Uhl, R. and Baeuerlein, E. (1995). A simple light scattering method to assay magnetism in *Magnetospirillum gryphiswaldense*. *FEMS Microbiol. Lett.* **132**: 139-145.

Schultheiss, D. and Schüler, D. (2003). Development of a genetic system for *Magnetospirillum gryphiswaldense*. *Arch. Microbiol.* **179**: 89-94.

Smith, M. J., Sheehan, P. E., Perry, L. L., O'Connor, K., Csonka, L. N., Applegate, B. M. and Whitman, L. J. (2006). Quantifying the magnetic advantage in magnetotaxis. *Biophys. J.* **91**: 1098-1107.

Tamura, K., Dudley, J., Nei, M. and Kumar, S. (2007). MEGA4: Molecular evolutionary genetics analysis (MEGA) software version 4.0. *Mol. Biol. Evol.* **24**: 1596-1599.

Tanaka, M., Okamura, Y., Arakaki, A., Tanaka, T., Takeyama, H. and Matsunaga, T. (2006). Origin of magnetosome membrane: Proteomic analysis of magnetosome membrane and comparison with cytoplasmic membrane. *Proteomics* **6**: 5234-5247.

Thackray, P. D., Behravan, J., Southworth, T. W. and Moir, A. (2001). GerN, an antiporter homologue important in germination of *Bacillus cereus* endospores. *J. Bacteriol.* **183**: 476-482.

Uebe, R., Junge, K., Henn, V., Poxleitner, G., Katzmann, E., Plitzko, J. M., Zarivach, R., Kasama, T., Wanner, G., Pósfai, M., Böttger, L., Matzanke, B. and Schüler, D. (2011). The cation diffusion facilitator proteins MamB and MamM of *Magnetospirillum gryphiswaldense* have distinct and complex functions, and are involved in magnetite biomineralization and magnetosome membrane assembly. *Mol. Microbiol.* **82**: 818–835.

Uebe, R., Voigt, B., Schweder, T., Albrecht, D., Katzmann, E., Lang, C., Böttger, L., Matzanke, B. and Schüler, D. (2010). Deletion of a *fur*-like gene affects iron homeostasis and magnetosome formation in *Magnetospirillum gryphiswaldense*. *J. Bacteriol.* **192**: 4192-4204.

Ullrich, S., Kube, M., Schübbe, S., Reinhardt, R. and Schüler, D. (2005). A hypervariable 130-kilobase genomic region of *Magnetospirillum gryphiswaldense* comprises a magnetosome island which undergoes frequent rearrangements during stationary growth. *J. Bacteriol.* **187**: 7176-7184.

Ullrich, S. and Schüler, D. (2010). Cre-*lox*-based method for generation of large deletions within the genomic magnetosome island of *Magnetospirillum gryphiswaldense*. *Appl. Environ. Microbiol.* **76**: 2439-2444.

Wang, X., Ma, Q., Jiang, W., Lv, J., Pan, W., Song, T. and Wu, L. (2008). Effects of hypomagnetic field on magnetosome formation of *Magnetospirillum magneticum* AMB-1. *Geomicrobiol. J.* **25**: 296-303.

Yoshino, T. and Matsunaga, T. (2006). Efficient and stable display of functional proteins on bacterial magnetic particles using Mms13 as a novel anchor molecule. *Appl. Environ. Microbiol.* **72**: 465-471.

Zurkiya, O., Chan, A. W. S. and Hu, X. (2008). MagA is sufficient for producing magnetic nanoparticles in mammalian cells, making it an MRI reporter. *Magn. Reson. Med.* **59**: 1225-1231.

4.7 Supplementary information

4.7.1 Supplementary tables

Table S4-1. Primers used during this study. Included restriction sites are shown in bold.

Name	Sequence (5'→3')
magA_MSRup_for	**GCGGCCGC**TTCGGGGTGATGCAGTTCCA
magA_MSRup_rev	CCCGC**GAATTC**CACGCCGAG
magA_MSRdo_for	**GAGCTC**GGTGTCGTTGACCTTCTTGAAGC
magA_MSRdo_rev	**CCGCGG**ATCCAGCGCAAGAGGTCC
magA_AMBup_for	**GCGGCCGC**TTCGGGATGATGCAGTTCCAT
magA_AMBup_rev	**AAGCTT**CGACAGTTCCTCCGACGCCG
magA_AMBdo_for	**GAGCTC**CGGCATTCCTCAGGCG
magA_AMBdo_rev	**GGGCCC**ATCGGACCTGGCTCTGGAATTTGA
MSR_magA_for	ATGGAACTGCATCACCCCGA
MSR_magA_rev	GTTTCCAGCGACAGGTCAGG
AMB_magA_for	**CATATG**GAACTGCATCATCCCGAA
AMB_magA_rev	**GGATCC**AATTCCAGAGCCAGGTCCGGC

Table S4-2. NCBI/SwissProt accession numbers of proteins used for bioinformatic analyses during this study

Protein identifier	NCBI/SwissProt accession number	Organism
AfKHA1	XP_002372705.1	*Aspergillus flavus* NRRL3357
AfNHA1	XP_756051.1	*Aspergillus fumigatus* Af293
AgNHA1	XP_320946.3	*Anopheles gambiae* str. PEST
AnNHA1	XP_680519.1	*Aspergillus nidulans* FGSC A4
AtCHX1	NP_173088.1	*Arabidopsis thaliana*
AtCHX15	NP_178985.1	*Arabidopsis thaliana*
AtCHX16	NP_176599.2	*Arabidopsis thaliana*
AtCHX17	NP_194101.1	*Arabidopsis thaliana*
AtCHX18	NP_198976.3	*Arabidopsis thaliana*
AtCHX19	NP_188390.2	*Arabidopsis thaliana*
AtCHX2	NP_178058.1	*Arabidopsis thaliana*
AtCHX20	NP_190940.1	*Arabidopsis thaliana*
AtKEA1	NP_171684.2	*Arabidopsis thaliana*
AtKEA2	NP_191972.6	*Arabidopsis thaliana*
AtKEA3	NP_567272.4	*Arabidopsis thaliana*
AtKEA4	NP_849990.1	*Arabidopsis thaliana*
AtKEA5	NP_001119415.1	*Arabidopsis thaliana*
AtKEA6	NP_196741.2	*Arabidopsis thaliana*
AtNHX1	NP_198067.1	*Arabidopsis thaliana*
AtNHX2	NP_187154.1	*Arabidopsis thaliana*
AtNHX4	NP_200358.1	*Arabidopsis thaliana*
AtNHX5	NP_175839.2	*Arabidopsis thaliana*
AtNHX6	NP_178079.2	*Arabidopsis thaliana*
AtNHX7	NP_178307.2	*Arabidopsis thaliana*
AtNHX8	NP_172918.2	*Arabidopsis thaliana*
BcNapA	ZP_04256037.1	*Bacillus cereus* BDRD-Cer4
BjNhaP1	NP_767580.1	*Bradyrhizobium japonicum* USDA 110
BjNhaP2	NP_774808.1	*Bradyrhizobium japonicum* USDA 110
BjNhaP3	NP_767946.1	*Bradyrhizobium japonicum* USDA 110
CaCNH1	AAF72041.1	*Candida albicans*
CpNapA	NP_561153.1	*Clostridium perfringens* str. 13
CtNHA1	XP_002545336.1	*Candida tropicalis* MYA-3404
DMR_28000	YP_002954177.1	*Desulfovibrio magneticus* RS-1
DMR_28020	YP_002954179.1	*Desulfovibrio magneticus* RS-1
DMR_40640	YP_002955441.1	*Desulfovibrio magneticus* RS-1
DmNHA1	NP_723224.2	*Drosophila melanogaster*
DmNHA2	NP_732807.1	*Drosophila melanogaster*
EcKefB	ZP_06664075.1	*Escherichia coli* B088
EcKefC	NP_414589.1	*Escherichia coli* str. K-12 substr. MG1655
EcNhaA	NP_414560.1	*Escherichia coli* str. K-12 substr. MG1655
EcYjcjE	NP_418489.1	*Escherichia coli* str. K-12 substr. MG1655
EncNapA	ZP_08145304.1	*Enterococcus casseliflavus* ATCC 12755
HiNhaA	NP_438397.1	*Haemophilus influenzae* Rd KW20
Mmc1_1223	ABK43734.1	*Magnetococcus sp.* MC-1
Mmc1_1569	ABK44078.1	*Magnetococcus sp.* MC-1

Protein identifier	NCBI/SwissProt accession number	Organism
Mmc1_2640	ABK45136.1	*Magnetococcus sp.* MC-1
Mmc1_3434	ABK45920.1	*Magnetococcus sp.* MC-1
amb3466	YP_422829.1	*Magnetospirillum magneticum* AMB-1
MagA AMB-1	YP_423353.1	*Magnetospirillum magneticum* AMB-1
MagA MS-1	AAK21849.1	*Magnetospirillum magnetotacticum* MS-1
Magn03005529	ZP_00051390	*Magnetospirillum magnetotacticum* MS-1
MagA MSR-1	CAM76236.1	*Magnetospirillum gryphiswaldense* MSR-1
MGR_4289	CAM78221.1	*Magnetospirillum gryphiswaldense* MSR-1
MgNHA1	EDK37276.2	*Meyerozyma guilliermondii* ATCC 6260
MmNHA1	Q8C0X2.1	*Mus musculus*
MmNHA2	NP_849208.4	*Mus musculus*
MoKHA1	XP_367750.1	*Magnaporthe oryzae* 70-15
NcKHA1	XP_960333.1	*Neurospora crassa* OR74A
NcNHA1	XP_956694.2	*Neurospora crassa* OR74A
OsCHX1	NP_001048636.1	*Oryza sativa* Japonica Group
PaNhaP	NP_252576.1	*Pseudomonas aeruginosa* PAO1
RnNHA2	NP_001102855	*Rattus norvegicus*
ScKHA1	NP_012441.1	*Saccharomyces cerevisiae* S288c
ScNHA1	NP_013239.1	*Saccharomyces cerevisiae* S288c
ScNHA2	NP_010744.1	*Saccharomyces cerevisiae* S288c
SeNhaP	ZP_03080174.1	*Salmonella enterica*
SpKHA1	NP_593465.1	*Schizosaccharomyces pombe* 972h-
SpSOD2	NP_592782.1	*Schizosaccharomyces pombe* 972h-
SynNhaS3	YP_001735605.1	*Synechococcus* sp. PCC 7002
VpNhaP	ZP_01992733.1	*Vibrio parahaemolyticus* AQ3810
YpNhaA	NP_671001.1	*Yersinia pestis* KIM 10
YpNhaP	NP_667581.1	*Yersinia pestis* KIM 10

4.7.2 Supplementary figures

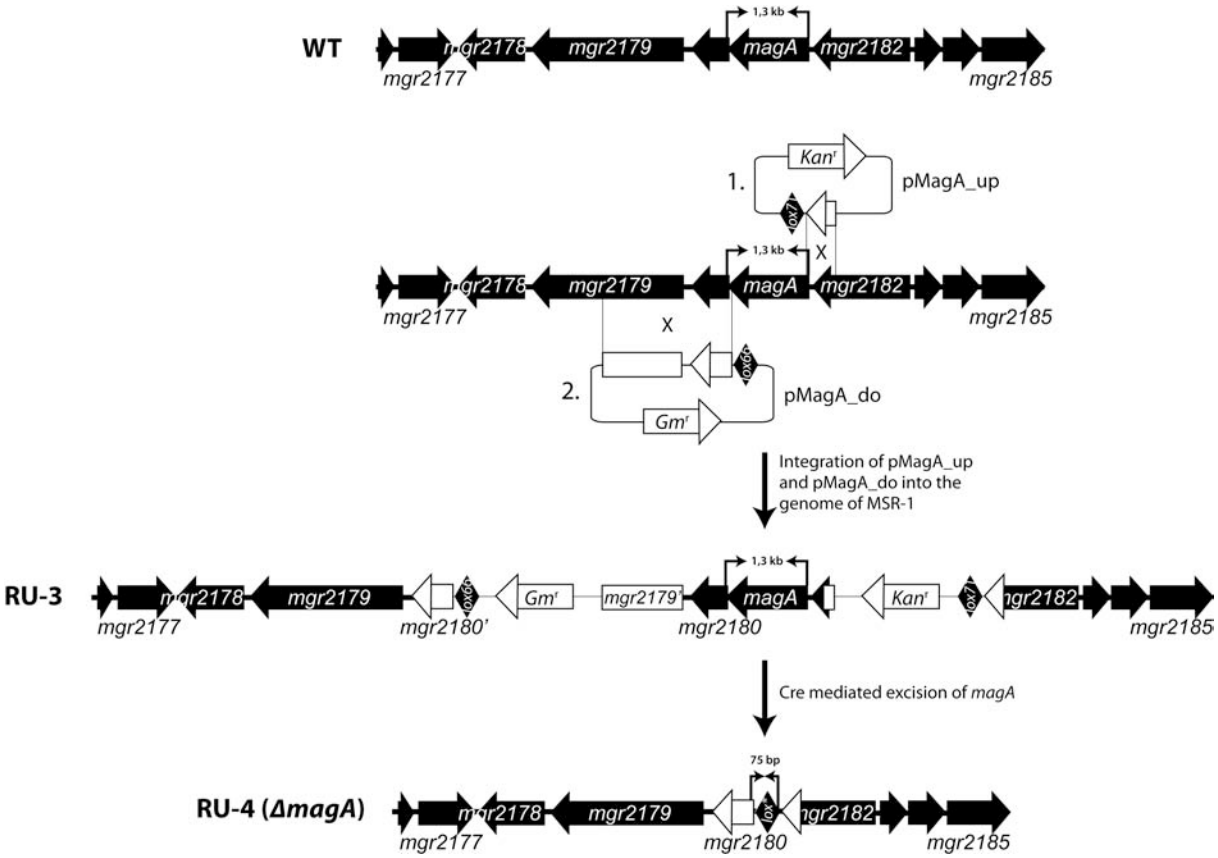

FIG. S4-1. Schematic representation of the generation of a Cre-*loxP*-mediated *magA* deletion in MSR-1. *magA* deletion was done, by a similar strategy. Position of primers MSR_magA_for and MSR_magA_rev are indicated by vertical marks. The expected sizes of PCR products are indicated between the arrows.

CHAPTER 5

Discussion

Magnetotactic bacteria (MTB) are a unique group of organisms with respect to their need for iron. In addition to their biochemical iron demand, these bacteria require huge amounts of iron for the synthesis of magnetosomes. The formation of these intracellular organelles involves several specific processes like magnetosome vesicle formation, uptake of iron, its intracellular sequestration, and crystallization of magnetite (Faivre and Schüler, 2008). In the present thesis, deletion mutagenesis, physiological experiments, several electron microscopic, and biochemical methods as well as fluorescence microscopy were applied to analyze several aspects of the iron metabolism and magnetite biomineralization in *M. gryphiswaldense*.

5.1 Regulation of magnetosome formation and intracellular iron homeostasis

Magnetotactic bacteria accumulate several orders of magnitude more iron than non-magnetotactic species (they consist of up to 4% iron as measured by dry weight) (Schüler and Baeuerlein, 1998; Bazylinski and Frankel, 2004). However, large concentrations of free intracellular iron can cause severe damage to cells due to the generation of radical oxygen species via the Fenton reaction (Imlay and Linn, 1988; Winterbourn, 1995). Thus, MTB need a precise regulation for the opposing requirements of iron accumulation for magnetite formation, biochemical pathways, and the risk of iron-mediated cell damage. In many other bacteria this is controlled by the iron-responsive transcriptional Ferric uptake regulator (Fur) (Andrews *et al.*, 2003).

Genome analysis within this thesis showed that *M. gryphiswaldense* contains an exceptionally large number (five) of genes encoding for proteins of the Fur superfamily. Based on phylogenetic analyses and identification of conserved functional residues four of these Fur-like proteins are putative iron-responsive regulators. Whereas three genes likely encode proteins of the heme-dependent Iron responsive regulator (Irr) subfamily, only one (*mgr1314*) encodes a genuine ferrous iron-responsive Fur. Consistent with its predicted role Mgr1314 was able to transcomplement an *Escherichia coli fur* mutant in an iron-responsive manner.

Furthermore, proteomic analyses in an *mgr1314* deletion mutant and the wild type grown under iron-replete and -deplete conditions showed that the abundance of several proteins implicated in iron transport (FeoB1, FeoA2, FeoB2, Mgr0081, Mgr0236; see chapter 1.3) was significantly altered in the *mgr1314* mutant, and thus confirmed that Mgr1314 is a genuine ferric uptake regulator. However, in contrast to the large Fur regulon of *E. coli*, which contains up to 100 genes (Hantke, 2001; McHugh *et al.*, 2003), the regulon of *Mg*Fur seems to be rather small since only 14 proteins were found differentially expressed in the *fur* mutant and the wild type. One possible explanation for the minor role of Fur in *M. gryphiswaldense* would be that proteins of the Irr subfamily (Mgr1305, Mgr 1399, and Mgr3480) are also involved in iron-responsive regulatory networks and might have taken over functions from *Mg*Fur. For example, in *Bradyrhizobium japonicum* and *Agrobacterium tumefaciens* it was shown that Irr and not Fur controls several genes involved in heme synthesis and iron uptake (Small *et al.*, 2009; Hibbing and Fuqua, 2011).

Consistent with the experimentally identified small Fur regulon of *M. gryphiswaldense*, *in silco* prediction of the Fur regulons of the closely related *Magnetospirillum magneticum* and *Magetospirillum magnetotacticum* revealed also only 17 and 14 putative Fur binding sites in the genome of these MTB, respectively (Rodionov *et al.*, 2006). Interestingly, the *mamGFDC* and *mms6* magnetosome gene operons were also part of the predicted Fur regulons, and it was suggested that Fur might be involved in the regulation of magnetosome formation (Rodionov *et al.*, 2006). In agreement with this, magnetosome genes of *M. gryphiswaldense* showed an iron-responsive transcription (Schübbe *et al.*, 2006), and *fur* homologues were found in close proximity of magnetosome genes in *M. magneticum*, *M. magnetotacticum* and a metagenomic gene cluster (Jogler *et al.*, 2009b; Uebe *et al.*, 2010). However, although the presence of a putative Fur binding site in the *mamGFDC*/*mms6* promoter of *M. gryphiswaldense* was confirmed by the Fur titration assay during this thesis, with the exception of Mms6, the abundance of all detected magnetosome membrane proteins was not affected by deletion of *fur* or changes of extracellular iron concentrations. One possible explanation for the observed differences between the iron-responsive transcription of magnetosome genes (Schübbe *et al.*, 2006), and the almost unaffected expression pattern of their products might be the presence of posttranscriptional regulation processes. Recently, several studies reported that protein abundance is not generally correlated with changes in mRNA abundance because of posttranscriptional regulation (Nakanishi *et al.*, 2010; Smith *et al.*, 2010; Foss *et al.*, 2011).

Although the proteomic approach revealed virtually identical abundance of the magnetosome proteins in the wild type and the *fur* deletion mutant, the *fur* mutant produced fewer and

smaller magnetite crystals than the wild type, resulting in 50% lower intracellular iron accumulation. Further analyses by transmission Mössbauer spectroscopy (TMS) and iron measurements of different cellular fractions indicated that the intracellular iron metabolism of the *fur* mutant was disturbed. The iron-to-protein ratio of the intracellular, soluble, non-magnetic fraction of the *fur* deletion mutant was 2.4-fold increased compared to the wild type. According to TMS measurements large proportions of the Δ*fur* intracellular iron (76 to 90%) were bound to an as-yet unidentified ferritin-like metabolite, whereas in the wild type this metabolite accounted for only 50% of the accumulated iron. Since deletion of *fur* in other bacteria like *Helicobacter pylori* caused derepression of ferritin (Pfr) (Bereswill *et al.*, 2000), the TMS results may indicate a similar effect in the *M. gryphiswaldense fur* mutant. However, the abundance of two putative bacterioferritins (Mgr0532 and Mgr0533) was not found to be significantly affected by deletion of *fur* (1.1 to 1.4-fold decreased abundance in Δ*fur* in the proteomic analyses), suggesting that these proteins may not be identical with the ferritin-like metabolite that caused the increased signal in TMS. Alternatively, the increased ferritin-like pool in Δ*fur* might result from an increased formation of holobacterioferritin due to higher cytoplasmic iron concentrations. Besides an increased pool of a ferritin-like metabolite in the *fur* mutant strain, TMS analyses also revealed a significantly increased proportion of free ferrous iron in Δ*fur* (4.6 to 5.7-fold increased). Since ferrous iron promotes the generation of radical oxygen species via the Fenton reaction (Imlay and Linn, 1988; Winterbourn, 1995), the increased ferrous iron pool might explain the observed sensitivity of the *fur* mutant against oxidative stress.

In summary, the results indicate that *Mg*Fur is a genuine ferric uptake regulator that is involved in intracellular iron homeostasis but not in direct regulation of magnetosome formation. Based on the proteomic analyses, the iron measurements and TMS analysis it is likely that deletion of *fur* in *M. gryphiswaldense* indirectly affected magnetosome formation by deregulation of the intracellular iron metabolism. It is possible that the increased sequestration of iron by cytoplasmic proteins caused a decreased pool of iron available for magnetite biomineralization in the *fur* mutant. Thus, the delay of magnetite synthesis in iron-induced Δ*fur* cells grown under microaerobic conditions might be the result of an increased pool of cytoplasmic iron-binding proteins, which has to be saturated first before iron becomes available for magnetite biomineralization. However, further studies including the identification and biochemical characterization of individual iron-sequestering cellular constituents and examination of the iron transport route into the magnetosomes are required to provide deeper insights into the regulation of biomineralization.

5.2 Transport of iron into magnetosome vesicles and magnetite biomineralization

In a Mössbauer study on magnetosome formation in *M. magnetotacticum* it was proposed that in a first step iron is taken up into the cytoplasm and subsequently transported into the magnetosomes (Frankel *et al.*, 1983). According to this model, iron-translocating proteins have to be present in the magnetosome membrane. Previous studies, however, attributed this function to different proteins. In order to resolve the conflicting data, in this thesis several putative magnetosome-directed iron transporter were analyzed by deletion mutagenesis, genetic and biochemical methods.

Early studies implicated MagA of *M. magneticum* in magnetosome-directed iron transport. This was concluded from the isolation of *magA* Tn5-transposon or deletion mutants that were unable to synthesize magnetite, analysis of the subcellular localization of MagA-luciferase fusion proteins as well as iron transport experiments into inverted membrane vesicles (Matsunaga *et al.*, 1992; Nakamura *et al.*, 1995a; Nakamura *et al.*, 1995b; Smith *et al.*, 2006). Apparently consistent with its putative iron transport function Goldhawk *et al.* (2009) described that expression of *magA* in N2A mouse neuroblastoma cell lines resulted in elevated intracellular iron concentrations. Even more intriguingly, Zurkiya *et al.* (2008) reported that expression of *magA* in human 293FT cell lines was sufficient to cause the biomineralization of small magnetite particles. However, despite these reports, ambiguity about the role of MagA during magnetosome formation remained. There is still no evidence that the observed non-magnetic phenotypes in fact were caused by the loss of *magA* function since neither original *M. magneticum* transposon mutant (Matsunaga *et al.*, 1992) nor the deletions mutant (Smith *et al.*, 2006) have been shown to be complemented by a wild type-copy of *magA*.

Reassessment of the role of the presumptive magnetosomal iron transporter MagA in this thesis revealed that, contrary to previous studies, *magA* deletion mutant strains of *M. magneticum* and *M. gryphiswaldense* were still able to form magnetite crystals. In addition, the magnetosomes of the *magA* deletion strains were shown to be indistinguishable from that produced by the wild type strains with respect to size, morphology, and intracellular arrangement. Consistent with these observations, several independent proteomic studies failed to identify MagA as a constituent of the magnetosome membrane of *M. magneticum* or *M. gryphiswaldense* (Grünberg *et al.*, 2001; Grünberg *et al.*, 2004; Tanaka *et al.*, 2006; Lohße *et al.*, 2011). Furthermore, the affiliation of MagA with the ubiquitous monovalent cation:proton antiporter (CPA) subfamily CPA2 (Uebe, 2011b) does not support the

previously observed ATP-dependent ferrous iron transport activity of MagA (Nakamura *et al.*, 1995b). Members of the CPA2 subfamily have been shown to exclusively transport monovalent cations (e.g. K^+, Na^+ or NH_4^+) in exchange for protons (Chang *et al.*, 2004) to regulate alkali resistance, electrophile resistance, osmoregulation, and endospore germination (Booth, 1985; Ferguson *et al.*, 1997; Thackray *et al.*, 2001; Padan *et al.*, 2005). Additionally, comparative genome analyses of MTB did not identify *magA* among the conserved signature genes for magnetotaxis (Richter *et al.*, 2007). In this thesis it was further shown that *magA* is only confined to strains of *Magnetospirillum*, and that the gene is not located within the genomic magnetosome island. This region is now assumed to harbor most if not all genes essential for magnetosome formation (Ullrich *et al.*, 2005; Fukuda *et al.*, 2006; Murat *et al.*, 2010; Lohße *et al.*, 2011), and has been found to be more or less conserved in all MTB (Jogler *et al.*, 2009a; Jogler *et al.*, 2009b; Abreu *et al.*, 2011; Jogler *et al.*, 2011).

In conclusion, these results show that MagA is not involved in bacterial magnetite biomineralization. Therefore, it can be assumed that the previously observed non-magnetic *magA* mutant phenotypes were likely due to the accidental isolation of clones coincidentally harboring an undetected spontaneous second-site mutation. It is well established that spontaneous non-magnetic mutations arise at high frequencies in cultures of *M. magneticum* and other MTB, which are due to RecA-dependent rearrangements within the MAI (Ullrich *et al.*, 2005; Fukuda *et al.*, 2006; Kolinko *et al.*, 2011), and which have been already described to obscure genetic analysis in the absence of appropriate controls (Komeili *et al.*, 2004; Nash, 2008; Jogler and Schüler, 2009).

Among the proteins encoded within the MAI of *M. gryphiswaldense* MamB and MamM, two of the most abundant proteins of the magnetosome membrane (Grünberg *et al.*, 2004), share the highest similarity to known metal transporting protein families. Based on phylogenetic analyses both magnetosome membrane proteins are members of the divalent metal ion transporting cation diffusion facilitator protein family (CDF), and were therefore proposed to catalyze magnetosome-directed ferrous iron transport (Grünberg *et al.*, 2001; Nies, 2003; Grünberg *et al.*, 2004). Consistent with their proposed iron-translocating function, MamB and MamM belong to the Fe/Zn-transporting subfamily of CDF transporter, are localized in the magnetosome membrane, and deletion of either *mamB* or *mamM* caused the loss of magnetite biomineralization as shown by TEM and TMS analyses (Uebe *et al.*, 2011). However, so far all attempts to directly confirm iron transport activity of MamB or MamM by *in vitro* (e.g. reconstituted proteoliposomes of recombinantly overexpressed proteins) or *in vivo* (e.g. serial dilution spot assays) methods failed because of unsolved technical challenges (e.g. low iron

specificity of the transport indicator, oxidation of phospholipids, or poor expression on MamM and MamB in *E. coli*) (Junge, 2008; Grass, Nies, Uebe, unpublished results). Nevertheless, during this study support for iron transport was obtained by a genetic approach. Transcomplementation of the Δ*mamM* strain with MamM proteins carrying amino acid substitutions within the putative active site (metal binding site A) strongly affected magnetite biomineralization. In addition to significantly increased amounts of small magnetite crystals (20 – 25 nm), amino acid substitutions within MamM caused a drastic increase of magnetite particles that were composed of multiple grains. Whereas more than 80% of the magnetite crystals produced by Δ*mamM* strains that were trans-complemented with the wild type MamM consisted of monocrystalline (single-grained) magnetite particles, only 10 to 24% of the crystals were monocrystalline in strains expressing mutated *mamM*. These effects on magnetosome crystal size and morphology might be caused by a reduced iron transport rate into the magnetosome vesicles since Δ*mamM* strains that expressed the mutant protein MamM D50A showed a delayed biomineralization during iron-induction experiments compared to Δ*mamM* (pRU1-mamMwt) strains. In addition, the formation of poorly crystalline iron-oxide particles during iron-induction experiments with Δ*mamM* (pRU1-mamMD50A), but not Δ*mamM* (pRU1-mamMwt) indicates that an exchange of MamM D50A leads to reduced iron concentrations within magnetosome vesicles because low iron concentrations were also found to induce the formation of poorly crystalline iron oxides during *in vitro* experiments (Faivre *et al.*, 2004). A further hint for a putative iron transporting function was the observation of small and poorly crystalline particles, which were composed of the ferric iron mineral hematite [α-$Fe(III)_2O_3$] rather than the mixed-valence mineral magnetite [$Fe(II)Fe(III)_2O_4$]. The formation of hematite could be the consequence of a reduced influx of ferrous iron into the magnetosome vesicles. Alternatively, the observed effects might have been caused by altered physico-chemical conditions inside the magnetosome compartment that disfavor magnetite formation. Decreased transport rates by mutated MamM proteins, for example, might also lead to an increased pH within the magnetosome vesicles since CDF transporter generally employ an H^+-antiport mechanism (Nies, 2003). Previous studies showed that magnetite is only stable in a pH range from ~7 to 14, whereas hematite depending on the redox potential is stable from pH ~1 to 14 (Bell *et al.*, 1987). Contrary to MamM, all MamB proteins carrying amino acid substitutions within the active center (metal binding site A) were not able to restore magnetite biomineralization of the *mamB* deletion mutant. Thus, MamB appears to be a highly specialized protein in which even minor deviations from the wild type structure were not tolerated.

In conclusion, the results showed that MamB and MamM are essential for magnetite biomineralization. Whereas the role of MamB for magnetosome-directed iron transport remained elusive, indirect evidence for ferrous iron transport into magnetosome vesicles was obtained for MamM. The site-directed mutagenesis approach on *mamM* caused the formation of small, poorly crystalline, electron-dense particles, which is consistent with observations during iron-limited abiotic magnetite formation. Unfortunately, direct demonstration for iron transport by MamM and MamB is still missing since several attempts to confirm iron transport failed. However, based on the localization of both proteins in the cytoplasmic as well as the magnetosome membrane it is likely that their transport activity is regulated directly at the magnetosome membrane to ensure that iron is transported into magnetosome vesicles and not into the periplasmic space. Therefore, it might be necessary to identify further proteins which interact with MamM and/or MamB to directly confirm metal transport activity. One possible interaction would be an iron-delivering metal-chaperone as previously suggested for FieF (Lu and Fu, 2007). Furthermore, the identification of a different mineral phase than magnetite in strains expressing mutated MamM provided the first experimental evidence that the chemical composition and the nature of the mineral phase within magnetosomes is genetically determined. However, the presence of hematite crystals in the absence of fully functional MamM might also suggest that additional magnetosome-directed ferric iron transport proteins are present in the magnetosome membrane. Previous studies speculated that the major facilitator superfamily (MFS) proteins MamH and MamZ could have ferric iron transport activity (Raschdorf, 2011), although MFS proteins like SIT1 from *Saccharomyces cerevisiae* have only been shown to catalyze siderophore-mediated iron transport (Lesuisse *et al.*, 1998). Alternatively, Nies (2011) proposed that the formation of hematite in Δ*mamM* (pRU1-mamMD50A) was based on the complete oxidation of ferrous iron due to lower ferrous iron concentrations within the magnetosome vesicle lumen compared to the wild type. However, further analyses are required to show if the formation of the mixed-valence mineral magnetite depends on the simultaneous magnetosome-directed transport of ferrous and ferric iron or on the precise regulation of the ferrous to ferric iron stoichiometry by redox-active processes.

5.3 Evidence for a tight protein-protein interaction network at the magnetosome membrane

As described in the previous section, MamM and MamB were initially studied because of their putative iron transport activity only. Further analyses on both proteins during this study however unexpectedly revealed that in addition to their putative iron transport function MamB and MamM have multiple roles at several distinct steps of magnetosome formation.
The first indication that MamB and MamM may have additional functions was obtained from the localization of MamC-GFP, a marker for the localization of the magnetosome chain. Whereas MamC-GFP localized as a chain-like structure centered at midcell in the wild type, localization of MamC-GFP in Δ*mamM* and Δ*mamB* was disturbed. In both strains the MamC-GFP signals mainly appeared as fluorescent foci without a clear intracellular localization. However, in contrast to Δ*mamB*, in ~2% of Δ*mamM* cells expressing MamC-GFP the arrangement of the fluorescent foci was reminiscent of short or fragmented magnetosome chains. Cryo-electron tomographic (CET) analyses on *M. gryphiswaldense* Δ*mamB* during this thesis revealed that the mislocalization of MamC-GFP was caused by the inability of this strain to form magnetosome vesicles, which is consistent with the phenotype of a *mamB* deletion mutant of *M. magneticum* (Murat *et al.*, 2010). In contrast to Δ*mamB,* CET analyses on Δ*mamM* showed that this mutant was still able to form empty magnetosome membrane vesicles, indicating that MamM might be involved in the correct targeting of other magnetosome membrane proteins, as also described for the *M. magneticum* magnetosome membrane HtrA-like protease MamE (Quinlan *et al.*, 2011). Alternatively, the localization pattern of MamC-GFP in Δ*mamM* might be the result of a decreased number of magnetosome membrane vesicles since Western immunoblot analyses showed that deletion of *mamM* also caused drastically reduced MamB levels. Furthermore, simultaneous expression of *mamB* and *mamM* in heterologous hosts confirmed that a high expression level of *mamB* depended on the coexpression of *mamM* and was independent of the presence of other magnetosome-specific factors. In addition, reciprocal co-purification of untagged MamB or MamM with MamM-Strep and MamB-Strep fusion proteins, respectively, showed that MamB and MamM physically interact with each other. Hence, MamM might protect MamB from proteolytic degradation. Similar observations were made when SecY (Akiyama *et al.*, 1996) or the ATP synthase subunit a of *E. coli* (Kihara *et al.*, 1995) were expressed in excess to their interacting subunits. Both unbound proteins were degraded by the membrane integrated FtsH protease when they are not protected by interacting subunits to avoid deleterious effects.

In order to determine how MamB and MamM interact with each other, gradually truncated MamM proteins were expressed in Δ*mamM* and their effect on MamB stability was monitored by Western immunoblot analyses. The results indicated that the MamM C-terminus is involved in the stabilization of MamB since expression of MamM proteins with C-terminal deletions of more than 30 amino acids caused a decrease in the abundance of MamB. Consistent with these observations, the C-terminal domains of MamM and MamB physically interacted with each other in a bacterial two-hybrid assay. However, although the C-terminus of MamM is required for wild type-like MamB abundance, the soluble MamM C-terminal domain (CTD) was not able to stabilize MamB to wild type levels when expressed alone. Hence, the interaction between MamM and MamB involves further, yet unidentified domains. Interestingly, the formation of a homodimer of the related CDF transporter FieF depends on intense interaction at the CTD-CTD interface, but also on dimerization contacts between an intracellular loop between transmembrane helix 2 (TMH) and TMH3 as well as formation of a salt bridge between the N-terminal part of TMH3 and a cytoplasmic loop that connects the transmembrane domain (TMD) to the soluble CTD (Lu and Fu, 2007; Lu *et al.*, 2009). Based on this model, MamB and MamM likely form a heterodimer, although Haney *et al.* (2005) initially proposed that CDF family proteins might generally form only homodimers. However, since heterodimer formation by CDF family proteins has also been reported previously (Ellis *et al.*, 2005; Ishihara *et al.*, 2006), the results of this thesis suggest that heterodimer formation within the CDF family might be more common than initially believed.

Nevertheless, the existence of a heterodimer of MamB and MamM alone is not sufficient to explain the observed difference of the Δ*mamB* and Δ*mamM* phenotypes, as loss of either component within a functional MamBM-heterodimer should lead to similar phenotypes. Therefore, a bacterial two-hybrid assay was applied to test if MamM and MamB are also able to form homodimers. Interaction between two MamM CTDs was only observed in the presence of divalent metal ions, whereas the interaction of two MamB CTDs was independent of metal cofactors. Thus, the ability of the Δ*mamM* mutant to still form magnetosome membrane vesicles together with the observed self-interaction of the MamB or MamM CTDs in bacterial two hybrid screens indicate that both proteins are also able to form homodimeric complexes. Although already suggested by several studies (Murgia *et al.*, 1999; Blaudez *et al.*, 2003), this is the first experimental evidence for CDF proteins that can either act in homo- or heterodimeric complexes. Alternatively, it might also be possible that the observed interaction between MamM and MamB depends on an interaction between a MamB homodimer and a homodimer of MamM.

The results of this thesis further suggest that, besides its interaction with MamM, MamB is involved in additional extensive protein-protein interaction networks. Using a non-reducing sodium dodecyl sulfate-polyacrylamid gel electrophoresis (SDS-PAGE) approach, dithiothreitol (DTT)-sensitive MamB complexes with sizes of ~62 kDa, ~78 kDa, ~80 kDa, and ~114 kDa were observed. The molecular masses of these complexes only partially matched homomeric MamB assemblies (the 62 kDa band approximately corresponds to a MamB dimer), indicating that MamB might also undergo heteromeric interactions. Notably, similar intermolecular disulfide bond formation has already been reported for the poplar CDF transporter MTP1 (Blaudez *et al.*, 2003). Substitution of each conserved cysteine residue (C6, C9 and C138) within MamB caused the inability of these mutant proteins to transcomplement Δ*mamB*, demonstrating their importance for MamB function. Interestingly, a MamB C138A exchange mutant protein was unable to form intermolecular complexes of 62 and 114 kDa. In non-reducing SDS-PAGE analyses (DTT omitted) MamB C138A mainly migrated like a MamB monomer during conventional reductive SDS-PAGE (DTT added) analyses, indicating that C138 is involved in the formation of intermolecular disulfide bonds. Non-reducing SDS-PAGE analyses of MamB C6S or MamB C9S showed that these mutant proteins are still able to form wild type-like MamB complexes. However, both cysteine residues might be involved in the formation of transient intermolecular disulfide bonds since non-reducing SDS-PAGE analyses with both mutant proteins revealed the formation of an additional high molecular weight MamB complex of ~260 kDa (R. Uebe, unpublished results). A mutant protein of MamB which contained a simultaneous substitution of C6,9S was able to form wild type-like MamB complexes, but not the high molecular weight complex of the C6S or C9S single cysteine mutants. Future identification of MamB interaction partners will be fundamental for the understanding of MamB function since exchange of the conserved cysteine residues not only altered the formation of MamB (hetero)oligomers, but also prevented magnetosome formation. Similar to MamB, MamM contains three highly conserved cysteine residues at position 6, 9 and 139. Thus, also for the MamM cysteine residues an essential function was suggested. However, non-reducing SDS-PAGE analyses revealed no hints for the formation of intermolecular disulfide bonds. In addition, substitution of the conserved cysteine residues of MamM had no effect on the ability to transcomplement Δ*mamM*, even if all three cysteine residues were substituted together. Therefore, the functions of the conserved cysteine residues of MamM remained elusive. Similarly, mutational analyses of cysteine residues of the poplar CDF transporter MTP1 also had only minor effects on the MTP1 Zn^{2+} transport activity, and did not affect the MTP1 intermolecular disulfide bond formation (Montanini *et al.*, 2007).

Bioinformatic analyses predicted eleven internal putative PDZ class III binding-motifs within MamB and MamM as well as a single PDZ class II binding-motif at the very C-terminal end of MamB. PDZ domains are small protein–protein interaction modules organizing protein networks on membranes (Fanning and Anderson, 1999), which have been extensively studied in eukaryotes, but are also present in bacterial proteins (Ponting, 1997). The most common mechanism of ligand binding by PDZ domains is the recognition and binding of the very carboxy-terminal end of the target proteins (Jelen *et al.*, 2003). Thus, removal of the MamB and MamM C-terminal ends should affect their ability to transcomplement the corresponding mutants if these proteins are interaction partner of PDZ domains. Whereas C-terminally truncated MamM proteins were able to transcomplement Δ*mamM* to a similar extent as wild type MamM, the ability of truncated MamB proteins to transcomplement Δ*mamB* gradually decreased with increasing extension of the C-terminal deletion. Since these results indicated that MamB interacts with PDZ domain containing proteins, a bacterial two-hybrid assay was used to directly test for an interaction between the MamB and putative interacting PDZ domains of MamE and MamP. These two magnetosome membrane proteins were found to contain three of ten PDZ domains present in the predicted proteome of *M. gryphiswaldense*. As suspected, the bacterial two-hybrid experiment indicated that the magnetosome protein MamE might interact with the MamB carboxy-terminal domain via its PDZ1 domain. However, further experiments are required to confirm the MamB-MamE interaction and co-localization of the interacting domains. Although the functional role of a MamB-MamE interaction remained unclear, one might speculate that MamE, like MamB, is involved in magnetosome membrane vesicle formation since Murat and colleagues described that the so far only proteins essential for magnetosome membrane vesicle formation, MamI, MamL, MamQ, and MamB, alone are not sufficient for vesicle formation (Murat *et al.*, 2010). This hypothesis is further substantiated by findings of Quinlan *et al.* (2011), where co-deletion of *mamE* and *limE* (a *mamE*-like gene) in *M. magneticum* lead to mislocalization of GFP-MamI, a protein that is essential for vesicle formation. An additional hint for a putative role of MamE in vesicle formation is the similar MamC-GFP localization pattern between *M. gryphiswaldense* Δ*mamB* observed during this thesis and *M. magneticum* Δ*mamE* (Quinlan *et al.*, 2011).

In conclusion, the results of this thesis provided evidence that MamB and MamM in addition to their putative iron transport activity have distinct and complex functions. Whereas MamM stabilizes MamB and is required for the initiation of magnetite nucleation, MamB is involved in the magnetosome membrane biogenesis. Thus, the results provide first functional insights

into how the two main processes of magnetosome formation, magnetosome membrane vesicle formation and magnetite biomineralization, are interconnected to each other via the two CDF transporters MamM and MamB (FIG. 5-1).

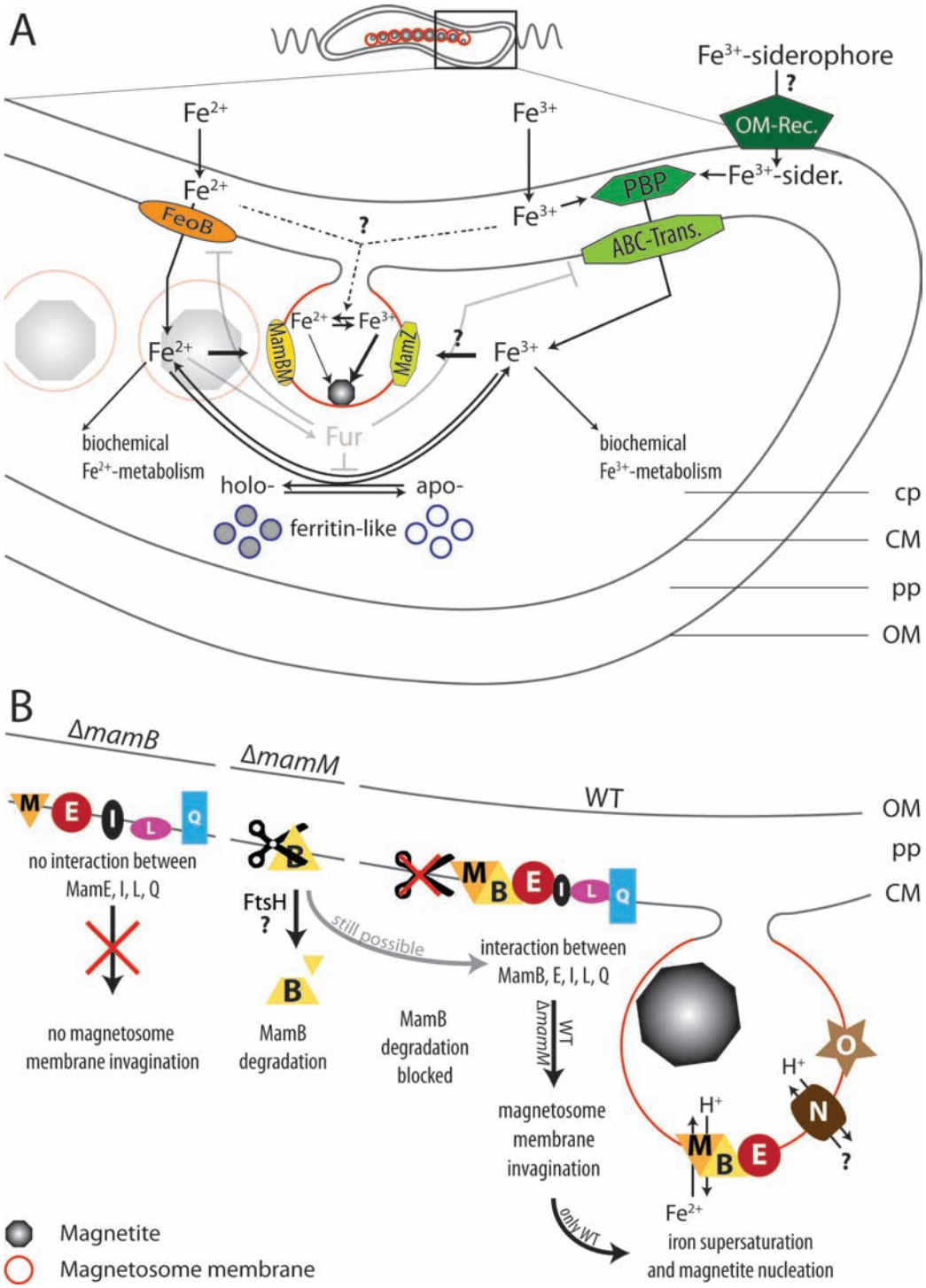

FIG. 5-1. A) Hypothetical model of the iron uptake and intracellular iron metabolism of *M. gryphiswaldense*. Ferrous iron is taken up by the high-affinity ferrous iron uptake permease FeoB (Mgr1446 or ABL14106). Ferric iron is taken up by an ATP-binding cassette (ABC) transport system, including a periplasmic binding protein (PBP, Mgr0236), a cytoplasmic ABC ATPase subunit (Mgr0235) and an ABC permease subunit (ABC-Trans., Mgr0234). Siderophore bound ferric iron is taken up via a TonB-dependent outer membrane receptor (OM-Rec., Mgr0081) and an ABC-type uptake system (Mgr0082, Mgr0083). However, so far there is no evidence for siderophore-mediated iron uptake in *M. gryphiswaldense* (Schüler and Baeuerlein, 1996; Uebe *et al.*, 2010).

Ferrous iron is transported into magnetosome vesicles via the CDF transporter heterodimer MamBM. Ferric iron is accumulated within the magnetosomes by MamZ- or MamH-mediated uptake (Raschdorf, 2011), or by oxidation of ferrous iron inside the vesicles by a so far uncharacterized redox active enzyme (Nies, 2011). Alternatively, ferrous and ferric iron might be transported into magnetosomes directly from the periplasm (dashed arrows) (Faivre *et al.*, 2007). Magnetite formation proceeds by a fast coprecipitation-like process of one ferrous (thin arrow) and two ferric (thick arrow) iron ions (Faivre *et al.*, 2007). Cytoplasmic iron is subjected to iron-dependent biochemical processes (e.g. heme synthesis, respiration, DNA synthesis) (Andrews *et al.*, 2003). Ferritin-like proteins (blue circles) store iron as insoluble ferrihydrite to prevent oxidative damage by decreasing the concentration of free cytosolic iron. The level of free cytosolic ferrous iron is sensed by the transcriptional regulator Fur (Mgr1314), which is involved in the balance of the iron uptake, storage and indirectly also in magnetosome formation. B) Hypothetical model of the different phenotypes between Δ*mamB* and Δ*mamM*. Loss of MamB might cause that MamE and the proteins essential for magnetosome membrane biogenesis, MamI, MamL and MamQ (Murat *et al.*, 2010), do not interact with each other. Therefore, in Δ*mamB* no magnetosome vesicles are formed. In the *mamM* deletion mutant, MamB is not protected from proteolytic degradation (eventually by FtsH), resulting in low MamB levels. The residual MamB however, is still able to mediate magnetosome membrane invagination by the interaction between MamB, MamE, MamI, MamL and MamQ. Lack of MamM in these magnetosome vesicles causes the inability of the deletion strain to accumulate supersaturating iron concentrations inside the magnetosome compartment and thus, no magnetite is formed. In the wild type strain (WT) MamM protects MamB from degradation by dimerization, which than interacts with MamE, MamI, MamL and MamQ to induce magnetosome membrane invagination. Accumulation of supersaturating iron concentrations and finally, magnetite nucleation, requires at least MamM (ferrous iron transport), MamN (proton export?, (Jogler and Schüler, 2009)) and MamEO (unknown protease functions, targeting of proteins to the MM, (Yang *et al.*, 2010; Quinlan *et al.*, 2011)) (Murat *et al.*, 2010).

5.4 Future directions

In order to form magnetosomes magnetotactic bacteria have to arrange and regulate several processes like magnetosome vesicle formation, uptake of iron, its intracellular sequestration, and crystallization of magnetite (Faivre and Schüler, 2008). The work detailed in this thesis provided insights into how *M. gryphiswaldense* accomplishes and regulates these processes. However, the presented results lead to a couple of new, unexpected questions, which should be addressed in the future.

The results of chapter 2 imply that iron transport into magnetosomes might proceed from the cytoplasm. To finally resolve the routes of iron into magnetosomes, deletion mutants of all identified iron uptake systems should be generated and analyzed with respect to iron uptake and magnetosome formation kinetics. If iron is transported into magnetosomes via the periplasm as proposed by (Faivre *et al.*, 2007), magnetite biomineralization should not be prevented by deletion of one or multiple iron-transport systems of the cytoplasmic membrane. Alternatively, expression of genes for the uptake and intracellular degradation of iron-charged siderophores, e.g. the enterobactin utilization genes *fepABCDG* and *fes* of *E. coli* (Payne and Mey, 2010), could help to demonstrate the iron transport pathway into the magnetosomes. During such an experiment magnetite biomineralization should only be observed if the iron transport into the magnetosomes involves the uptake into the cytoplasm.

Deletion of one or multiple putative iron-responsive transcriptional regulators (Irr-like) identified in chapter 2 would provide further insights into how magnetosome formation is integrated and regulated with the intracellular iron homeostasis and biochemical iron requirement. In addition, these analyses might help to understand the rather minor role of Fur for iron homeostasis of *M. gryphiswaldense*. Of great interest will also be the identification, isolation and characterization of the conspicuous ferritin-like metabolite detected by TMS analyses.

Despite circumstantial evidence and considerable efforts, there is still no direct evidence for magnetosome-directed iron transport by MamM and/or MamB. Besides the interaction and stabilization of MamB by MamM described in chapter 3 the presented data suggest that at least MamB is interacting with other proteins. Identification of interacting proteins is required prior to a reassessment of biochemical transport assays with MamB and MamM in their native oligomeric configuration. The identification of additional interacting proteins would also help to analyze how MamB is involved in the biogenesis of the magnetosome membrane. Additionally, *M. gryphiswaldense* strains expressing chromosomally inserted *mamB* mutant alleles should be analyzed with respect to the presence of magnetosome vesicles. These analyses will help to show which MamB domains or residues are crucial for MM formation.

Furthermore, the observation of hematite crystals within magnetosomes of strains with mutated MamM proteins indicates that it might be possible to direct the formation of modified mineral phases by "engineering" of magnetosome membrane proteins. One possible modification would be the specific insertion of "contaminating" metal ions into magnetite, to yield doped magnetosomes with altered or even enhanced magnetic properties. Since it was described previously that single amino acid exchanges within the yeast CDF transporter Zrc1 and Cot1 altered their substrate specificity (Lin *et al.*, 2008), it should be tested if site-directed mutagenesis of *mamM* also leads to changes of its substrate specificity and restores growth defects metal-sensitive yeast strains. For example, MamM proteins with the ability to restore Zn^{2+}-dependent growth defects could than be tested for the incorporation of zinc into magnetosomes.

5.5 References

Abreu, F., Cantão, M. E., Nicolás, M. F., Barcellos, F. G., Morillo, V., Almeida, L. G. P., do Nascimento, F. F., Lefèvre, C. T., Bazylinski, D. A., R de Vasconcelos, A. T. and Lins, U. (2011). Common ancestry of iron oxide- and iron-sulfide-based biomineralization in magnetotactic bacteria. *ISME J.* **5**: 1634-1640.

Akiyama, Y., Kihara, A. and Ito, K. (1996). Subunit a of proton ATPase F_0 sector is a substrate of the FtsH protease in *Escherichia coli*. *FEBS Lett.* **399**: 26-28.

Andrews, S. C., Robinson, A. K. and Rodriguez-Quinones, F. (2003). Bacterial iron homeostasis. *FEMS Microbiol. Rev.* **27**: 215-237.

Bazylinski, D. and Frankel, R. (2004). Magnetosome formation in prokaryotes. *Nature Rev.* **2**: 217-230.

Bell, P. E., Mills, A. L. and Herman, J. S. (1987). Biogeochemical conditions favoring magnetite formation during anaerobic iron reduction. *Appl. Environ. Microbiol.* **53**: 2610-2616.

Bereswill, S., Greiner, S., van Vliet, A. H. M., Waidner, B., Fassbinder, F., Schiltz, E., Kusters, J. G. and Kist, M. (2000). Regulation of ferritin-mediated cytoplasmic iron storage by the ferric uptake regulator homolog (Fur) of *Helicobacter pylori*. *J. Bacteriol.* **182**: 5948-5953.

Blaudez, D., Kohler, A., Martin, F., Sanders, D. and Chalot, M. (2003). Poplar metal tolerance protein 1 confers zinc tolerance and is an oligomeric vacuolar zinc transporter with an essential leucine zipper motif. *Plant Cell* **15**: 2911-2928.

Booth, I. R. (1985). Regulation of cytoplasmic pH in bacteria. *Microbiol. Rev.* **49**: 359-378.

Chang, A. B., Lin, R., Studley, W. K., Tran, C. V. and Saier Jr., M. H. (2004). Phylogeny as a guide to structure and function of membrane transport proteins. *Mol. Membr. Biol.* **21**: 171-181.

Ellis, C. D., MacDiarmid, C. W. and Eide, D. J. (2005). Heteromeric protein complexes mediate zinc transport into the secretory pathway of eukaryotic cells. *J. Biol. Chem.* **280**: 28811-28818.

Faivre, D., Agrinier, P., Menguy, N., Zuddas, P., Pachana, K., Gloter, A., Laval, J. and Guyot, F. (2004). Mineralogical and isotopic properties of inorganic nanocrystalline magnetites. *Geochim. Cosmochim. Acta* **68**: 4395-4403.

Faivre, D., Böttger, L. H., Matzanke, B. F. and Schüler, D. (2007). Intracellular magnetite biomineralization in bacteria proceeds by a distinct pathway involving membrane-bound ferritin and an iron(II) species. *Angew. Chem. Int. Ed. Engl.* **46**: 8495-8499.

Faivre, D. and Schüler, D. (2008). Magnetotactic bacteria and magnetosomes. *Chem. Rev.* **108**: 4875-4898.

Fanning, A. S. and Anderson, J. M. (1999). PDZ domains: fundamental building blocks in the organization of protein complexes at the plasma membrane. *J. Clin. Invest.* **103**: 767-772.

Ferguson, G., Nikolaev, Y., McLaggan, D., Maclean, M. and Booth, I. (1997). Survival during exposure to the electrophilic reagent N-ethylmaleimide in *Escherichia coli*: role of KefB and KefC potassium channels. *J. Bacteriol.* **179**: 1007-1012.

Foss, E. J., Radulovic, D., Shaffer, S. A., Goodlett, D. R., Kruglyak, L. and Bedalov, A. (2011). Genetic variation shapes protein networks mainly through non-transcriptional mechanisms. *PLoS Biol.* **9**: e1001144.

Frankel, R., Papaefthymiou, G. C., Blakemore, R. P. and O'Brian, W. (1983). Fe_3O_4 precipitation in magnetotactic bacteria. *Biochim. Biophys. Acta* **763**: 147-159.

Fukuda, Y., Okamura, Y., Takeyama, H. and Matsunaga, T. (2006). Dynamic analysis of a genomic island in *Magnetospirillum sp.* strain AMB-1 reveals how magnetosome synthesis developed. *FEBS Lett.* **580**: 801-812.

Goldhawk, D. E., Lemaire, C., McCreary, C. R., McGirr, R., Dhanvantari, S., Thompson, R. T., Figueredo, R., Koropatnick, J., Foster, P. and Prato, F. S. (2009). Magnetic resonance imaging of cells overexpressing MagA, an endogenous contrast agent for live cell imaging. *Mol. Imaging* **8**: 129-139.

Grünberg, K., Müller, E. C., Otto, A., Reszka, R., Linder, D., Kube, M., Reinhardt, R. and Schüler, D. (2004). Biochemical and proteomic analysis of the magnetosome membrane in *Magnetospirillum gryphiswaldense*. *Appl. Environ. Microbiol.* **70**: 1040-1050.

Grünberg, K., Wawer, C., Tebo, B. M. and Schüler, D. (2001). A large gene cluster encoding several magnetosome proteins is conserved in different species of magnetotactic bacteria. *Appl. Environ. Microbiol.* **67**: 4573-4582.

Haney, C. J., Grass, G., Franke, S. and Rensing, C. (2005). New developments in the understanding of the cation diffusion facilitator family. *J. Ind. Microbiol. Biotechnol.* **32**: 215-226.

Hantke, K. (2001). Iron and metal regulation in bacteria. *Curr. Opin. Microbiol.* **4**: 172-177.

Hibbing, M. E. and Fuqua, C. (2011). Antiparallel and interlinked control of cellular iron levels by the Irr and RirA regulators of *Agrobacterium tumefaciens*. *J. Bacteriol.* **193**: 3461-3472.

Imlay, J. and Linn, S. (1988). DNA damage and oxygen radical toxicity. *Science* **240**: 1302-1309.

Ishihara, K., Yamazaki, T., Ishida, Y., Suzuki, T., Oda, K., Nagao, M., Yamaguchi-Iwai, Y. and Kambe, T. (2006). Zinc transport complexes contribute to the homeostatic maintenance of secretory pathway function in vertebrate cells. *J. Biol. Chem.* **281**: 17743-17750.

Jelen, F., Oleksy, A., Smietana, K. and Otlewski, J. (2003). PDZ domains - common players in the cell signaling. *Acta Biochim. Pol.* **50**: 985-1017.

Jogler, C., Kube, M., Schübbe, S., Ullrich, S., Teeling, H., Bazylinski, D., Reinhardt, R. and Schüler, D. (2009a). Comparative analysis of magnetosome gene clusters in magnetotactic bacteria provides further evidence for horizontal gene transfer. *Environ. Microbiol.* **11**: 1267–1277.

Jogler, C., Lin, W., Meyerdierks, A., Kube, M., Katzmann, E., Flies, C., Pan, Y., Amann, R., Reinhardt, R. and Schüler, D. (2009b). Toward cloning of the magnetotactic metagenome: Identification of magnetosome island gene clusters in uncultivated magnetotactic bacteria from different aquatic sediments. *Appl. Environ. Microbiol.* **75**: 3972-3979.

Jogler, C. and Schüler, D. (2009). Genomics, genetics, and cell biology of magnetosome formation. *Annu. Rev. Microbiol.* **63**: 501-521.

Jogler, C., Wanner, G., Kolinko, S., Niebler, M., Amann, R., Petersen, N., Kube, M., Reinhardt, R. and Schüler, D. (2011). Conservation of proteobacterial magnetosome genes and structures in an uncultivated member of the deep-branching *Nitrospira* phylum. *Proc. Natl. Acad. Sci. U.S.A.* **108**: 1134-1139.

Junge, K. (2008). *Doctoral thesis*: Die Funktion der CDF-Transporter MamB und MamM beim magnetosomalen Eisentransport in *Magnetospirillum gryphiswaldense*. Universität Bremen, Bremen.

Kihara, A., Akiyama, Y. and Ito, K. (1995). FtsH is required for proteolytic elimination of uncomplexed forms of SecY, an essential protein translocase subunit. *Proc. Natl. Acad. Sci. U.S.A.* **92**: 4532-4536.

Kolinko, I., Jogler, C., Katzmann, E. and Schüler, D. (2011). Frequent mutations within the genomic magnetosome island of *Magnetospirillum gryphiswaldense* are mediated by RecA. *J. Bacteriol.* **193**: 5328–5334.

Komeili, A., Vali, H., Beveridge, T. J. and Newman, D. K. (2004). Magnetosome vesicles are present before magnetite formation, and MamA is required for their activation. *Proc. Natl. Acad. Sci. U.S.A.* **101**: 3839-3844.

Lesuisse, E., Simon-Casteras, M. and Labbe, P. (1998). Siderophore-mediated iron uptake in *Saccharomyces cerevisiae*: the SIT1 gene encodes a ferrioxamine B permease that belongs to the major facilitator superfamily. *Microbiology* **144**: 3455-3462.

Lin, H., Kumánovics, A., Nelson, J. M., Warner, D. E., Ward, D. M. and Kaplan, J. (2008). A single amino acid change in the yeast vacuolar metal transporters Zrc1 and Cot1 alters their substrate specificity. *J. Biol. Chem.* **283**: 33865-33873.

Lohße, A., Ullrich, S., Katzmann, E., Borg, S., Wanner, G., Richter, M., Voigt, B., Schweder, T. and Schüler, D. (2011). Functional analysis of the magnetosome island in *Magnetospirillum gryphiswaldense*: The *mamAB* operon is sufficient for magnetite biomineralization. *PLoS One* **6**: e25561.

Lu, M., Chai, J. and Fu, D. (2009). Structural basis for autoregulation of the zinc transporter YiiP. *Nat. Struct. Mol. Biol.* **16**: 1063-1067.

Lu, M. and Fu, D. (2007). Structure of the zinc transporter YiiP. *Science* **317**: 1746-1748.

Matsunaga, T., Nakamura, C., Burgess, J. G. and Sode, K. (1992). Gene transfer in magnetic bacteria: transposon mutagenesis and cloning of genomic DNA fragments required for magnetosome synthesis. *J. Bacteriol.* **174**: 2748-2753.

McHugh, J. P., Rodriguez-Quinones, F., Abdul-Tehrani, H., Svistunenko, D. A., Poole, R. K., Cooper, C. E. and Andrews, S. C. (2003). Global iron-dependent gene regulation in *Escherichia coli*. *J. Biol. Chem.* **278**: 29478-29486.

Montanini, B., Blaudez, D., Jeandroz, S., Sanders, D. and Chalot, M. (2007). Phylogenetic and functional analysis of the Cation Diffusion Facilitator (CDF) family: improved signature and prediction of substrate specificity. *BMC Genomics* **8**: 107.

Murat, D., Quinlan, A., Vali, H. and Komeili, A. (2010). Comprehensive genetic dissection of the magnetosome gene island reveals the step-wise assembly of a prokaryotic organelle. *Proc. Natl. Acad. Sci. U.S.A.* **107**: 5593-5598.

Murgia, C., Vespignani, I., Cerase, J., Nobili, F. and Perozzi, G. (1999). Cloning, expression, and vesicular localization of zinc transporter Dri 27/ZnT4 in intestinal tissue and cells. *Am. J. Physiol. Gastrointest. Liver Physiol.* **277**: G1231-G1239.

Nakamura, C., Burgess, J. G., Sode, K. and Matsunaga, T. (1995a). An iron-regulated gene, *magA*, encoding an iron transport protein of *Magnetospirillum* sp. strain AMB-1. *J. Biol. Chem.* **270**: 28392-28396.

Nakamura, C., Kikuchi, T., Burgess, J. G. and Matsunaga, T. (1995b). Iron-regulated expression and membrane localization of the MagA protein in *Magnetospirillum* sp. Strain AMB-1. *J. Biochem. (Tokyo)*. **118**: 23-27.

Nakanishi, Y., Fukuda, S., Chikayama, E., Kimura, Y., Ohno, H. and Kikuchi, J. (2010). Dynamic omics approach identifies nutrition-mediated microbial interactions. *J. Proteome Res.* **10**: 824-836.

Nash, C. Z. (2008). *Ph.D. thesis*: Mechanisms and evolution of magnetotactic bacteria. California Institute of Technology, Pasadena, CA.

Nies, D. (2003). Efflux-mediated heavy metal resistance in prokaryotes. *FEMS Microbiol. Rev.* **27**: 313-339.

Nies, D. (2011). How iron is transported into magnetosomes. *Mol. Microbiol.* **82**(4): 792-796.

Padan, E., Bibi, E., Ito, M. and Krulwich, T. A. (2005). Alkaline pH homeostasis in bacteria: New insights. *Biochim. Biophys. Acta Biomembr.* **1717**: 67-88.

Payne, S. M. and Mey, A. R. (2010). Iron uptake in *Shigella* and *Escherichia coli*. In: *Iron uptake and homeostasis in microorganisms.* P. Cornelis and S. C. Andrews (ed.). Caister Academic Press, Norfolk, UK

Ponting, C. P. (1997). Evidence for PDZ domains in bacteria, yeast, and plants. *Protein Sci.* **6**: 464-468.

Quinlan, A., Murat, D., Vali, H. and Komeili, A. (2011). The HtrA/DegP family protease MamE is a bifunctional protein with roles in magnetosome protein localization and magnetite biomineralization. *Mol. Microbiol.* **80**: 1075–1087.

Raschdorf, O. (2011). *Diploma thesis*: Untersuchung der Funktion des *mamXY* Operons bei der Magnetosomenformation in *Magnetospirillum gryphiswaldense*. Ludwig-Maximilians-Universität, München.

Richter, M., Kube, M., Bazylinski, D., Lombardot, T., Glöckner, F., Reinhardt, R. and Schüler, D. (2007). Comparative genome analysis of four magnetotactic bacteria reveals a complex set of group-specific genes implicated in magnetosome biomineralization and function. *J. Bacteriol.* **189**: 4899-4910.

Rodionov, D., Gelfand, M., Todd, J., Curson, A. and Johnston, A. (2006). Computational reconstruction of iron- and manganese-responsive transcriptional networks in α-proteobacteria. *PLoS Comput. Biol.* **2**: 1568-1585.

Schübbe, S., Würdemann, C., Peplies, J., Heyen, U., Wawer, C., Glöckner, F. O. and Schüler, D. (2006). Transcriptional organization and regulation of magnetosome operons in *Magnetospirillum gryphiswaldense*. *Appl. Environ. Microbiol.* **72**: 5757-5765.

Schüler, D. and Baeuerlein, E. (1996). Iron-limited growth and kinetics of iron uptake in *Magnetospirilum gryphiswaldense*. *Arch. Microbiol.* **166**: 301-307.

Schüler, D. and Baeuerlein, E. (1998). Dynamics of iron uptake and Fe_3O_4 biomineralization during aerobic and microaerobic growth of *Magnetospirillum gryphiswaldense*. *J. Bacteriol.* **180**: 159-162.

Small, S. K., Puri, S., Sangwan, I. and O'Brian, M. R. (2009). Positive control of ferric siderophore receptor gene expression by the Irr protein in *Bradyrhizobium japonicum*. *J. Bacteriol.* **191**: 1361-1368.

Smith, D. P., Kitner, J. B., Norbeck, A. D., Clauss, T. R., Lipton, M. S., Schwalbach, M. S., Steindler, L., Nicora, C. D., Smith, R. D. and Giovannoni, S. J. (2010). Transcriptional and translational regulatory responses to iron limitation in the globally distributed marine bacterium *Candidatus* Pelagibacter ubique. *PLoS One* **5**: e10487.

Smith, M. J., Sheehan, P. E., Perry, L. L., O'Connor, K., Csonka, L. N., Applegate, B. M. and Whitman, L. J. (2006). Quantifying the magnetic advantage in magnetotaxis. *Biophys. J.* **91**: 1098-1107.

Tanaka, M., Okamura, Y., Arakaki, A., Tanaka, T., Takeyama, H. and Matsunaga, T. (2006). Origin of magnetosome membrane: Proteomic analysis of magnetosome membrane and comparison with cytoplasmic membrane. *Proteomics* **6**: 5234-5247.

Thackray, P. D., Behravan, J., Southworth, T. W. and Moir, A. (2001). GerN, an antiporter homologue important in germination of *Bacillus cereus* endospores. *J. Bacteriol.* **183**: 476-482.

Uebe, R., Junge, K., Henn, V., Poxleitner, G., Katzmann, E., Plitzko, J. M., Zarivach, R., Kasama, T., Wanner, G., Pósfai, M., Böttger, L., Matzanke, B. and Schüler, D. (2011). The cation diffusion facilitator proteins MamB and MamM of *Magnetospirillum gryphiswaldense* have distinct and complex functions, and are involved in magnetite biomineralization and magnetosome membrane assembly. *Mol. Microbiol.* **82**: 818–835.

Uebe, R., Voigt, B., Schweder, T., Albrecht, D., Katzmann, E., Lang, C., Böttger, L., Matzanke, B. and Schüler, D. (2010). Deletion of a *fur*-like gene affects iron

homeostasis and magnetosome formation in *Magnetospirillum gryphiswaldense*. *J. Bacteriol.* **192**: 4192-4204.

Ullrich, S., Kube, M., Schübbe, S., Reinhardt, R. and Schüler, D. (2005). A hypervariable 130-kilobase genomic region of *Magnetospirillum gryphiswaldense* comprises a magnetosome island which undergoes frequent rearrangements during stationary growth. *J. Bacteriol.* **187**: 7176-7184.

Winterbourn, C. C. (1995). Toxicity of iron and hydrogen peroxide: the Fenton reaction. *Toxicol. Lett.* **82-83**: 969-974.

Yang, W., Li, R., Peng, T., Zhang, Y., Jiang, W., Li, Y. and Li, J. (2010). *mamO* and *mamE* genes are essential for magnetosome crystal biomineralization in *Magnetospirillum gryphiswaldense* MSR-1. *Res. Microbiol.* **161**: 701-705.

Zurkiya, O., Chan, A. W. S. and Hu, X. (2008). MagA is sufficient for producing magnetic nanoparticles in mammalian cells, making it an MRI reporter. *Magn. Reson. Med.* **59**: 1225-1231.

Acknowledgements

First of all I would like to thank my supervisor Prof. Dr. D. Schüler for giving me the opportunity to work his lab on these exciting projects. I am deeply grateful for his support, encouragement, and the trust he has put in me.

I am also very grateful to Prof. Dr. H. Jung for his interest in my work and for preparation of the evaluation.

I would like to thank Prof. Dr. B. Matzanke, Dr. L. Böttger (Universtät zu Lübeck), Dr. M. Pósfai (University of Pannonia), Dr. T. Kasama (Technical University of Denmark), Dr. R. Zarivach (Ben Gurion University of the Negev), Prof. Dr. G. Wanner (LMU), Dr. J. M. Plitzko (MPI of Biochemistry) and Prof. Dr. T. Schweder, Dr. B. Voigt and Dr. D. Albrecht (EMAU Greifswald) for fruitful collaborations.

I also have to thank all the past and present members of the “Magnetolab” for always providing assistance, sharing knowledge and for making the lab a wonderful place to work in. Special thanks to Lin, Emanuel and Claus for many fruitful scientific and nonscientific discussions at the “Kicker”.

Many thanks to “my” undergrad students Gabi, Verena, Felix, and Anja. It was really a great pleasure to work with you. I’m still impressed how you handled my occasionally confusing ideas with calm and coolness.

I am very grateful to my parents and my sister for their continuous support, trust and patience.

My deepest gratitude goes to Jana and Felicia Alizée, my wonderful family, for their love, inspiration and support during these many years.

Eidesstattliche Erklärung

Ich versichere hiermit an Eides statt, dass die vorgelegte Dissertation von mir selbständig und ohne unerlaubte Hilfe angefertigt ist. Des Weiteren erkläre ich, dass ich nicht anderweitig ohne Erfolg versucht habe, eine Dissertation einzureichen oder mich der Doktorprüfung zu unterziehen. Die vorliegende Dissertation liegt weder ganz, noch in wesentlichen Teilen einer anderen Prüfungskommission vor.

René Uebe, München